School of Civil and Mechanical Engineering

Analysis of Interstitial Saturation in and Entrainment From Gas-Liquid Separation Media

Vahid Golkar Fard

This thesis is presented for the Degree of
DOCTOR OF PHILOSOPHY
of
Curtin University

June 2020

To the best of my knowledge and belief this thesis contains no material previously published by any other person except where due acknowledgment has been made. This thesis contains no material which has been accepted for the award of any other degree or diploma in any university.

Vahid Golkar Fard
28/06/2020

"If you learn science and knowledge, you can go beyond sky and subdue it."
- Naser Khusrow

Acknowledgements

Firstly, I would like to thank my principal supervisor Dr Andrew King whom with his invaluable supports and guidance helped me during this research. His competency in numerical methods and OpenFOAM was to the level which I realised without his helps, it was impossible. Apart from his academic supports, Dr King helped me in my personal life in Australia which was beyond his duties as a supervisor.

Secondly, I would like to thank Dr Abishek Sridhar for his great ideas and also teaching me different techniques in data acquisition and analysing. Moreover, his comments were always helpful to improve all the research works before submission.

Thirdly, I appreciate Professor Ben Mullins for his guidance in the completion of this thesis. His knowledge in experiments and filtration theory was unique which was a great help during this research.

And also Dr Ryan Mead-Hunter who shared with me his extensive knowledge in coalescing filtration, and his previous works were a great help for conducting the current research.

And my recent supervisor, Dr Julien Cisonni. I would like to thank him for his helps and great insight for improving the thesis presentation.

This research was supported by funding from Department of Mechanical Engineering, Curtin University and Australian Government. Moreover, the numerical studies conducted in this research were supported by Pawsey Supercomputing Centre, Perth, Western Australia by using its advanced computing facilities and resources. Also, I would like to acknowledge the assistance of Curtin university

Electron Microscopy Facility.

I am also very thankful to my parents, Sedigheh and Saeed, for all the sacrifices they have made for me.

The last but not the least, I would like to thank Mahboubeh, my beautiful wife, who understood the time and devotion that it took to do research that took precious time away from her. Also, I would like to dedicate this thesis to my little son, Ryan, whose underlying love have enriched my soul and inspired me to pursue and complete this research.

Publications Arising from this Work

This thesis contains the following works:

V. Golkarfard , A.J.C. King, S. Abishek, R. Mead-Hunter , G. Kasper , B.J. Mullins (2019) Optimisation of wet pressure drop in nonwoven fibrous, knitted, and opencell foam filters, Separation and Purification Technology, 213, 45-55.

V. Golkarfard, R. Subramaniam, J. Broughton, A. J. C King, and B. J. Mullins (2018) Comparative Performance of 12 Crankcase Oil Mist Separators, SAE International, 12(1), 03-12-01-0001.

S. Abishek, A.J.C. King, R. Mead-Hunter, V. Golkarfard, W. Heikamp, B.J. Mullins (2017) Generation and Validation of Virtual Nonwoven, Foam and Knitted Filter (Separator/ Coalescer) Geometries for CFD Simulations, Separation and Purification Technology, 188, 493-507.

V. Golkarfard, B.J. Mullins, A.J.C. King, S. Abishek, G. Kasper, W. Heikamp (2016) Simulating Transport In And Entrainment From Nonwoven Fibrous, Knitted, And Open-Cell Foam Filters, FILTECH, Cologne, Germany.

V. Golkarfard, B.J. Mullins, A.J.C. King, S. Abishek (2016), Numerical Study of Liquid Transport in Realistic Filter Media, 20th Australasian Fluid Mechanics Conference, Perth, Australia.

V. Golkarfard , A.J.C. King, S. Abishek, R. Mead-Hunter , J. Cisonni, B.J. Mullins Investigating the local optimum in pressure drop profile of oleophilic nonwoven , knitted, and foam filters, Separation and Purification Technology,

In-Prep.

V. Golkarfard , A.J.C. King, S. Abishek, R. Mead-Hunter , J. Cisonni, B.J. Mullins Performance analysis of different oil-mist coalescing filters, Separation and Purification Technology, **In-Prep**.

Abstract

A wide range of industrial and anthropogenic systems involve multi-phase processes, which lead to generation of liquid aerosols and mists. These small liquid aerosols impose a risk to workers health and environment which need to be eliminated properly or even captured and re-used. Filtration is one of the most common treatment methods which is significantly employed in different industries for treating oil-mists and known as coalescing filtration.

The majority of previous research in aerosol removal is mainly focused on solid dust filtration which is different from coalescence filtration. Liquid aerosol filtration is much more complex compared to solid filtration, and studies in this field are mostly experimental which have resulted in some empirical models for predicting wet pressure drop, saturation profile, and efficiency in coalescing filtration. It is found that these models have a narrow applications and validity which is only applicable on the similar filter geometries and operating conditions. More importantly, majority of the studies, and all the empirical models are only developed based on fibrous filters which are only one type among different filter structures used for treating liquid-gas flows. In the present study, in addition to fibrous filter, two other types of filters such as knitted and open-cell foam media are considered in order to evaluate their performance under similar physical and operating conditions.

For the purpose of evaluating different filter performance, information about their residual saturation and pressure drop profile is required which with existing empirical models and experimental data is not possible to conduct such an investigation. Moreover, there are no studies in regard to other types of filters from performance evaluation point of view. In the present study, a methodology is developed for the systematic study of different types of filters with different structures under equivalent operating conditions. To achieve this in practice, we

need to look beyond purely experimental approaches which are limited by the filters available. This may be achieved through a numerical approach such as computational fluid dynamics (CFD), where any possible combination of filter parameters and operating conditions may be explored. It is such an approach taken in this work, with of course the requisite use of experimental data to confirm the accuracy and validity of the models used.

First, three types of coalescing filters; fibrous, knitted and open-cell foam filter media were generated virtually. The accuracy of each structural design was verified against experimental data obtained during this study, as well as established theoretical models. After confirming the validity of the filter generation methodology and accuracy of the filter media produced, initial studies on the single-phase (dry filters) were conducted as further validation and to ensure the appropriate level of mesh refinement.

In this study, the inlet velocity variation is in a higher range (compared to the literature) due to major industrial applications and contact angle variation in different types of filter media is investigated numerically. The simulation results are validated against the experimental data obtained during this study, experimental data from the literature, and empirical models. The information acquired from the CFD study provides beneficial information about the behaviour of different filter structures in different operating conditions which leads to sets of performance data for comparison. The investigations on the final stage of the filtration suggest a possible local optimum region in the pressure drop curve which has not been reported before. This local optimum in the pressure drop profile is qualitatively validated by sets of experiments in the present study. Based on this observation and the influence of the operating and physical properties on the pressure drop curve, a qualitative hypothesis is presented describing this local optimum and the influence of the filter and operating parameters on its development and location. The presence of this local optimum in pressure drop curve has a significant potential to reducing the operating and manufacturing costs of the coalescing filters.

In summary this work has:

- Developed a methodology for a systematic study of different types of coalescing filters;
- Generated different types of coalescing filter media virtually and validated

the accuracy of these compared to real filter media through rigorous experiments;

- Demonstrated a methodology for generating a quality mesh for CFD study and mesh polishing techniques in complex geometries;
- Investigated the saturation and pressure drop in different filters with different structures to evaluate the quality factors and validate the CFD results by sets of multi-phase experimental tests and existing empirical models;
- Proposed a qualitative hypothesis for estimating the local optimum in pressure drop curve.

  This thesis developed a methodology in order to compare the performance of different types of filters (fibrous, knitted, and foam media) which has not been reported in literature. Moreover, the local optimum in pressure drop curve which identified in this work is a novel contribution to the field of interfacial science and gas-liquid separation which can significantly affect the coalescence filters design in future.

Contents

List of Figures

List of Tables

Nomenclature

α_{wet}	Wet filter packing density
$\Delta\alpha$	Factiona change in the packing density of the filter
ΔP_e	Pressure drop difference between multi-phase and single-phase
ΔP_{Phobic}	Final steady state multi-phase pressure drop values in phobic media
γ	Volume fraction indicator
μ	Dynamic viscosity of the oil mist
ϕ	Particle volume fraction
ρ	Density of the gas (air)
ρ_b	Bulk density
τ	Dimensionless time
$\triangle P_s$	Steady state pressure drop
$\underline{k}$	Tensor of giving the damping coefficients
A_f	Cross sectional area of the filter
d_f	Diameter or edge-length (of strut for open-cell foam media) of the filter element
d_{fwet}	Wet fibre diameter
u	Gas flow face velocity in the filter
W	Width of the filter in perpendicular direction to the flow and gravity
β	Non-Darcy coefficient
ΔP	Pressure drop across the filter

ΔP_θ Pressure drop difference between philic and phobic media

ΔP_{max} Maximum pressure drop

ΔP_{Philic} Final steady state multi-phase pressure drop values in philic media

ΔS_θ Difference between normalised saturation in philic and phobic media

Δt Time step

λ Molecular mean free path in the air

μ' Viscosity of the pure liquid

μ Dynamic viscosity of the carrier fluid (air)

μ_b Bulk dynamic viscosity

Φ Dimensionless pressure drop

σ_{LV} Liquid-vapour interfacial tension

σ_{SL} Solid-liquid interfacial tension

θ Equilibrium contact angle

θ_{SV} Solid-vapour interfacial tension

$\triangle P_0$ Clean (dry) pressure drop of the filter

$\triangle P_c$ Pressure drop between top and bottom of the theoretical capillary

$\triangle P_w$ Wet (saturate) pressure drop

α Packing density

φ Cell face volume flux

$\vec{u}$ Average velocity field

ξ Liquid centre of mass

C_γ Compression factor

c_f Correction factor

Ca_n Capillary number

d_d Droplet diameter

E_F Single fibre efficiency

E_T Filter efficiency

$f(\alpha)$ Packing density function

f_σ Continuum surface tension force

Kn Knudsen number

m_{liq} Mass of retained liquid in the filter

N_f Total number of initial meshes

n_f Interface normal vector

P Pressure field

P_e Penetration of liquid inside the filter

Q Volumetric flow rate

r Fibre radius

r_c Capillary radius

Re_f Filter Reynolds number

S_e Saturation of the pure liquid

S_f Surface area

S_0 Iinitial saturation

S_{Philic} Normalised final steady state residual saturation in philic

S_{Phobic} Normalised final steady state residual saturation in phobic

U Velocity vector field

U_c Compression velocity

U_g Velocity vector fields of gas

U_l Velocity vector fields of liquid

V_{fibre} Fibre volume

V_{filter} Filter volume

V_{voids} Volume of void space in filter (not occupied by fibres)

x_d Distance between the centroids on the collected droplets

x_∞	Capillary rise height
Bo	Bond number
C	Courant number
Dr	Drainage rate
Eu	Euler number
f	proportion of the fibre surface which is not covered by liquid
g	Gravity accelaration
K	Permeability
k	Curvature
l	Thickness of the filter
QF	Quality factor of the filter
S	Residual saturation in the filter
t	Computational time
v	Magnitude of velcity in y direction
w	Magnitude of velcity in z direction

Chapter 1

Introduction

An aerosol can be defined as a solid or liquid particle which is suspended in a gas. Among different types of aerosols; dust, smoke, haze, mist, and fog can be mentioned as the most common types that we encounter. Based on the nature of the aerosol it may be considered desirable like its application in pharmaceutical products for delivering a medicine to the patient lungs (Rudolph et al. (2004)), or it can be detrimental like its deposition in heat exchangers (Siegel and Nazaroff (2003), Nishio et al. (1974)) by reducing the efficiency.

One of the most common types of aerosols is oil-mist. This liquid aerosol consists of oil droplets in a gas; often air. There are various processes recognised for generation and dispersion of oil-mists into environment which metal cutting, engine crankcase, and air compressors are a few to be mentioned.

Presence of oil-mists in different environments, and their adverse impacts on human health have been the topic of numerous studies. It has been shown that oil-mists have an detrimental impacts on human's skin and respiratory system (Lacent (1990)). Furthermore, investigations have proven that the presence of oil-mists in working atmosphere can be the underlying reason for lung cancers (Hendy et al. (2016), Goldstein et al. (1970)). Therefore, due to the detrimental oil-mists' serious risks to human health, many countries including Australia imposed an exposure limit of 5 mg/m^3 (Pohanish (2011)).

Apart from all the adverse health impacts of oil-mists on our life, no one is oblivious to the fact that the lubricating oil is an integral part of industry, and oil-mist are the common by-products of different processes. Oil is widely used in various industries in order to improve the functioning of various machinery or efficiencies. In metal cutting process, oil as a lubricant plays a vital role not only by its cooling properties which prevents the temperature of the tool from

rising, it also prevents the abrasion (Williams (1977)). In this process, lubricant oil usually aerosolised, and Thornburg and Leith (2000) reported that the oil mist droplets median diameters were 2.1 μm. Another main application of lubricating oil is in automotive industry, especially engine crankcases where oil reduces the friction of moving parts significantly. When an engine operates, combustion gases which are known as blow-by gases flow in the gap between the cylinder sleeves and piston rings into the crankcase (Heywood (1988)). The combustion gases are composed of various aerosols such as oil aerosol particles (0.1 to >10 μm), soot particles (0.3 to 0.5 μm), gases; CO, CO_2, NO_x, O_2, H_2O, gaseous hydrocarbons (HC), water vapour and aldehydes (Clark et al. (2006)).

Therefore, it is important that suitable methods to treat oil mists are developed and used. Common approaches include using cyclones, membranes, scrubbers and filters. However, due to the small size of the oil-mist droplets, many researchers believe that cyclones are not the best choice since their performance reduces significantly when d_p<0.1 mm (Run et al. (2015),Sauter et al. (2003)). Golkarfard et al. (2018) investigated different types of crank case filters and separators, and it was found that filters have better performance compared to cyclones significantly.

Filters with different shapes, size and properties are usually the most efficient method to remove aerosol particles from air stream since this method is comparatively low cost in addition to have high separation efficiency. Current filters are able to remove the complete size range of aerosol particles with up to 99.993% efficiency (HEPA – High Efficiency Particulate Air) (Ahn et al. (2006)), although filter efficiency is characteristically reduced for particles of the size between approximately 100 to 500 nm.

When it comes to filtration, there are two distinct subjects in this area: filtration of solid particles and filtration of liquid particles (termed as “mist” or “coalescing” filtration Mead-Hunter et al. (2014)). Although there are many studies focused on the mechanisms of dust filtration (Thomas et al. (2001), Saleem and Krammer (2007), Novick et al. (1992), Rice et al. (2006), Cheng and Tsai (1998)), there are relatively low number of studied in gas/liquid filtration and also saturated fluid filtration and associated transport mechanisms. One of the main difference between the filtration of solid particles versus liquid particles is the ability of the captured liquid droplets to coalesce into larger droplets and move through the filter by gas flow which makes the mechanisms by far more complex (Abishek et al. (2019)). Therefore, the majority of the research works conducted in this area are experimental, or based on empirical, and semi-empirical approach.

This work aims to evaluate and compare the performance of oil-mist coalescing filters with different structures. In order to achieve this, computational tools and procedures will be developed to virtually generate three types of realistic filter media (fibrous, knitted, and foam). These techniques will reduce the costs and time required for filter development in future research, and provide an opportunity to evaluate the filters before production. Also, the virtual filter design will be 3-D which enable the researchers to capture the pore-scale flow physics of different filtration problems usually studied in 2-D due to complexity of the filter structure. The validity of the filter generation methodology and generated filters in this study will be validated against experimental data and theoretical models. Moreover, Computational Fluid Dynamics (CFD) techniques by the open source modeling software (OpenFOAM) will be employed in order to model interstitial saturation and entrainment in the generated media. By analysing the virtual filters saturation and pressure drop, their performance and quality factors will be assessed in details. Another advantage of the offered simulation is that all variables such as: packing density, fibre diameter, air flow rate and saturation except the one being studied may be held constant. This idealised approach can be difficult to implement for experimental investigations. However, there is no doubt that experimental results will be used for validating the simulation results in this research.

Chapter 2

Literature Review

In this chapter, a literature review is presented on the concepts, models, techniques, and available data related to the aims of this work mentioned in Chapter 1. In the end, the gaps between the published research are identified and a series of research strategies is outlined to address them.

2.1 Aerosol Characteristics

Atmospheric aerosols are typically an air-suspended mixture of solids and liquid droplets (Hinds (1999a)) which have natural sources or are produced based on human activities. Figure 2.1 presents the most common types of particles and their size.

In 2018, the World Health Organization (WHO) reported that outdoor air pollution in both rural regions and cities was estimated to be responsible for 4.2 million premature deaths worldwide. It is revealed by WHO that 91 % of people globally live in an unsafe condition due to air pollution. Moreover, a research by WHO in 2016 found that 29 % of lung cancer deaths, 24 % of strokes, and 25 % of heart diseases were caused by air pollution (WHO (2016)). Therefore, it can be concluded that controlling and eliminating particulate matters is a must.

Although, the necessity of protecting our environment and public health is an undeniable mission, but industries still need to remain economically lucrative and viable. One of the main substances that extensively used in various industries is lubricant oil which is attributable to forming oil mists in working environments. Oil mists are defined as fine particles formed due to splashing, frictional forces, fluid shear or thermal processes. These fine droplets impose a serious risk to workers health (Decoufle (1978)).

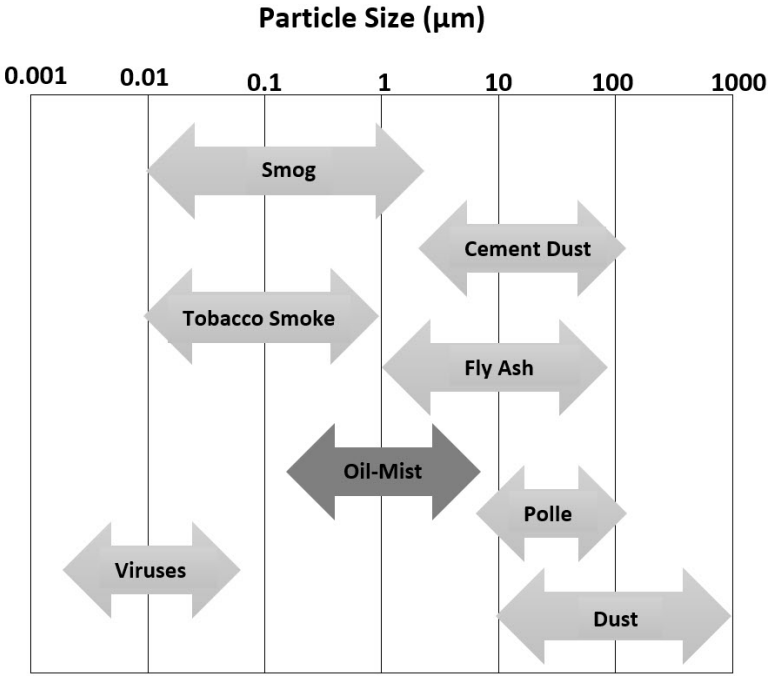

Figure 2.1: Common Types and sizes of Particulate Matter (after Hinds (1999a))

Based on different physical properties of particles and consequently different governing forces various technologies have emerged to capture and control them. Spurny (1998) grouped them into six categories: solid plate impaction (e.g. impactor), centrifugal impaction (e.g., cyclones), virtual impaction, liquid impingement (e.g., scrubbers), using external force field (e.g., electrical precipitators), and filters. Among all the mentioned categories, filtration is considered as the most economical and high efficiency method for removing fine solid and/or liquid particles from streams (Hinds (1999a)). The aim of this research is to advance our knowledge in gas-liquid filtration due to its significant role in different industries. Accordingly, filtration category will be presented in more details in the following.

2.2 Filtration

Different types of filters are applied in various industries such as food, oil and gas, health and pharmaceutical (Hinds (1999a)). Whatever the application, all filtration processes involve a medium which is permeable for one of the components of the mixture, and allow to capture of the other. Filter performance can be evaluated based on two parameters, capture efficiency (or hold-up saturation capability) and pressure drop. Ideally a filter will have a high capture efficiency

and low flow resistance. It should be mentioned that in comparison to alternative methods, filters provide sufficient capture efficiency in a wider range of particle size and flow rates. However, the main disadvantage of the filters is their periodic requirements for cleaning and the costs of replacing due to clogging and subsequent excess pressure drops (Leung et al. (2010); Podgorski et al. (2006)). This excess pressure drop leads to a critical pressure which is known as an indicator for replacing the filter. Therefore, understanding filtration mechanism, and affecting parameters on filtration behavior help us to develop high efficient filters with longer lifetime.

An increasing number of research have focused on solid particle filtration, while liquid aerosol filtration in air streams, so far, have been the subject of fewer studies. However, liquid aerosols form a considerable amount of air pollution in various industries (Frising et al. (2005); Amin et al. (2017); Hoover (2019); Gallou et al. (2011); Perry (1986)). The focus of the research presented in this thesis will be on liquid filtration in different types of filter media which will be presented in the next section.

2.2.1 Types of Filters

Due to vast variety of materials and diverse forms are used to make a filter media, different types of classifications have been presented by several authors (Purchas, D.B. (2002), Hutten (2007), Sutherland (2008), Dickenson (1995)). Generally, filters media can be classified into surface and depth media types. Surface type media are recognised by the fact that aerosols in suspension are mostly captured on the surface of the medium, with little penetration into the pores. Examples of this type are filter paper, filter cloths and wire mesh. Depth type media, used mainly for liquid filtration, are distinguished by the fact that the aerosols penetrate into the voids, where they are retained. The voids of such media are considerably larger than the sizes of the aerosols in suspension, whose concentration is generally not high enough to promote aerosol bridging across the pores; the aerosols may be captured mechanically. It should be mentioned that some media function simultaneously as depth and surface filter types and do not fit readily into this mode of classification. In liquid filtration, the most common filter types are woven filter, non-woven filter and open-cell foam filter.

In the case of **woven filters**, although a wide range of materials for manufacturing the fibers themselves are used, the construction and filtration characteristics of a filter are determined by the type of yarn, the weave or fabric construction and properties. The main application of woven media is in cleanable/regenerable

filter systems where the integrity of the filter plays an important role (Brown and Cox (2017)). Knitted filters which are special class of this category and known for their significant mechanical strength are mainly used in mist separation process (Brunazzi and Paglianti (2000), Choi and Lo (2003)). It is worth mentioning that knitted filters are generally highly extensible and anisotropic when it comes to filtration, so their applications is mainly limited to mist separation in specific industries like fume hoods, metalworking fluid mist collectors and petrochemical process mist eliminators (Brown and Cox (2017)). There has been relatively little previous study on this type of filters and most of the research focused on the physical properties (Yuksekkaya et al. (2010),Ka Fai Choi and Tin Yee Lo (2006),Anand and Lawton (1991)) and pressure drop and efficiency (Mullins et al. (2011),Dehkordi et al. (2017),Mullins et al. (2017)) of such filters. Figure 2.2 shows a knitted media.

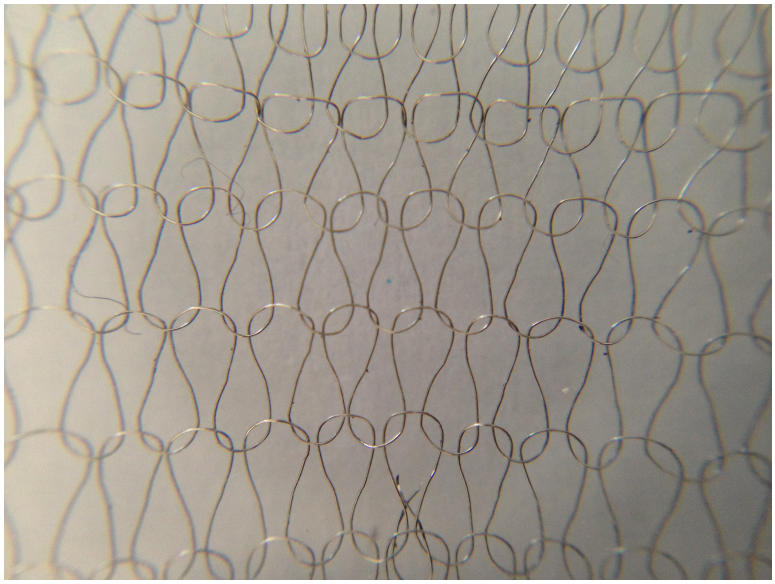

Figure 2.2: Knitted filter media (single layer)

There has been some research into developing knitted filter virtually in regards to conduct numerical studies. Anand and Lawton (1991) presented the mathematical structure of knitted fabrics based on the several years of research on textiles. A mathematical model to describe plain knitted fabric accounting for deformation was proposed by Ka Fai Choi and Tin Yee Lo (2006); Choi and Lo (2003). Recently, Mullins et al. (2017) reported a methodology for the generation and validation of a knitted media for filtration applications.

Non-Woven filters are typically composed of (near) randomly packed arrays of fibres, which may be composed of molten plastic, stainless steel, glass fibre, or

various polymers, and typically have very low packing densities. They are flat or tufted porous sheets and they are not made by weaving or knitting and do not require converting the fibres to yarn. Generally they are called fibrous filters (Abishek et al. (2017), Mead-Hunter et al. (2014)), and Figure 2.3 shows a typical fibrous filter.

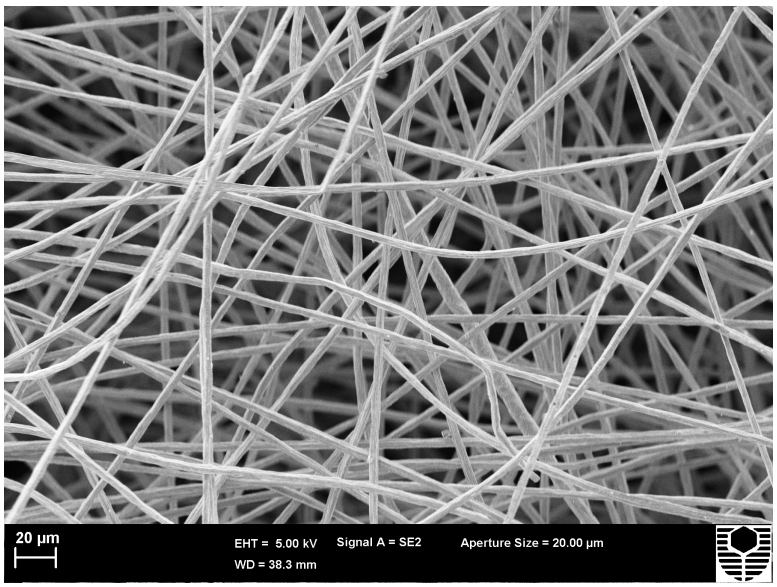

Figure 2.3: A Scanning Electron Microscope (SEM) image of a fibrous filter (Curtin University Electron Microscopy Facility)

Fibrous filters have diverse application in air, gas and liquid filtration. Air and gas filtration consume approximately 65% of the non-woven filtration media, and the rest of 35% belongs to liquid filtration (Gregor (2009)). There are different industries that use non-woven filters such as pharmaceutical, medical, water purification, oil and gas industry as oil-mist eliminators in gas stream and automative industry for eliminating oil-mists from crank case (Golkarfard et al. (2018)).

Open-cell Foam filters are a class of porous media that contains voids in the range from $10\mu m$ to 5 mm. The cell edges are named struts, and this combination forms an interconnected structure (open-cell foam). These filters have numerous industrial applications due to their special structure which are of high stiffness, high permeability and low density (Gibson and Ashby (1989); Aitken et al. (1993)), and reported has an acceptable efficiency (Ray et al. (2005), Ardekhani and Raiszadeh (2012)). Figure 2.4 shows an open-cell foam media.

Since the advent of open-cell foam filters, there has been extensive research conducting into various aspects of these filter geometries such as heat transfer

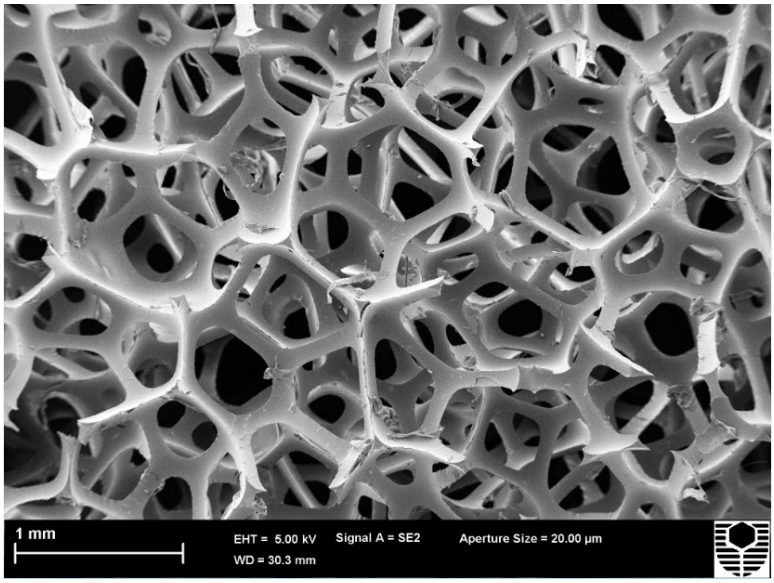

Figure 2.4: Open-cell foam filter media (SEM) image of a foam filter (Curtin University Electron Microscopy Facility)

(De Schampheleire et al. (2016); Billiet et al. (2015); Diani et al. (2015)) which mainly used MRI, CT scan or other imaging techniques to produce the filter media for the studies.

2.2.2 Properties of Filter Media

Filter media are characterised by many different mechanical properties. Researchers divide these properties into two main categories detailed in this section: mechanical properties and application oriented properties.

Mechanical Properties

These properties are rigidity, packing density, strength, resistance to creep/stretch, stability of edges, resistance to abrasion, stability to vibration, dimensions of available supplies, ability to be fabricated, sealing/gasketing function.

Due to importance and extensive application of packing density in the research, this characteristic will be explained in more details.

Packing density or solidity of a filter is the ratio of the fibre volume (V_{fibre}) to filter volume (V_{filter}).

$$\alpha = \frac{V_{fibre}}{V_{filter}} \tag{2.1}$$

where in Equation 2.1, $V_{filter} = V_{fibre} + V_{voids}$. V_{voids} is the volume inside the filter not occupied by fibres.

Application-Orientated Properties

These properties are related to the compatibility of a medium with the process environment. These properties are: chemical and thermal stability, dynamic stability, adsorptive characteristics, wettability, health and safety aspects, static characteristics, and disposability. Since the surface wettability characteristics plays an important role in liquid filtration and scope of this research, in the following this will be explained in more details.

Wettability

One of the main characteristics of a fibre surface is its properties against a liquid which divides it into philic (wettable), or phobic (non-wettable) category. When a liquid aerosol is captured by a philic filter fibre, due to the physical properties of the fibre surface it can spread out to "wet" the fibre. This phenomena has been the subject of numerous studies (Degennes (1987), Semal et al. (1999), Seveno et al. (2009)). It should be mentioned that the majority of previous works focused on flat surfaces rather than a cylindrical shape like in filter fibre.

The contact angle of a droplet on a flat surface is defined by Young's Equation (McHale et al. (2001)):

$$cos\theta = \frac{(\sigma_{SV} - \sigma_{SL})}{\sigma_{LV}} \tag{2.2}$$

where in Equation 2.2, θ is the equilibrium contact angle, θ_{SG} is the solid-gas interfacial tension, σ_{SL} is the solid-liquid interfacial tension and σ_{LG} is the liquid-gas interfacial tension (2.5). As it can be deduced from Equation 2.2, this Equation is not applicable for the case in which droplet forms a thin layer on the surface or in other word, it is valid where $\theta > 0$.

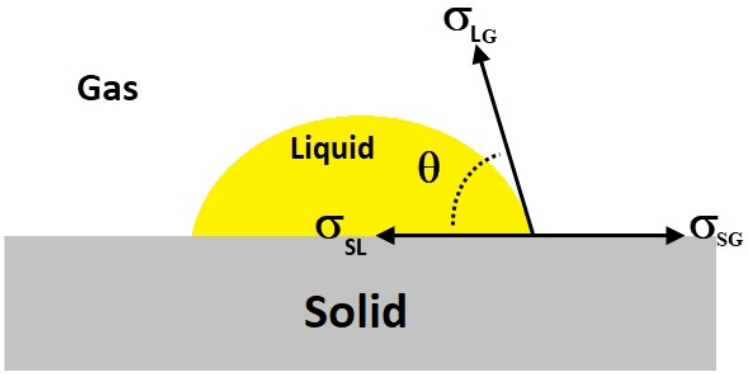

Figure 2.5: Schematic illustration of an oil-mist droplet on a solid surface as described by Young's equation (after Soleimani-Gorgani and Karami (2016)).

Fibre Wetting

Roe (1975) indicated that collected droplets on the fibres are categorised into two groups (based on their shape) which mainly depends on fibre surface properties and collected liquid droplet properties. One group named Clamshell having contact angle $\geq 90°$ and the other is barrel droplet which the contact angle is $< 90°$.

In wettable fibres, the liquid spread out along the fibre and wet the fibre which leads to a thin film around the fibre (Mead-Hunter et al. (2014)), then due to the Plateau-Rayleigh instability the droplets divide into separate barrel shapes on the fibre (Mullins and Kasper, 2006). On the other hand, in non-wettable fibre the droplets do not wet the fibre and remain as a clamshell shaped on the fibres. These droplets growths by coalescing with other near droplets and can be detached by the velocity of air stream. Figure 2.6 shows the diagrammatic presentation of the clamshell and barrel shaped droplets on the oleophobic (non-wettable) and oleophilic (wettable) fibre.

Super-phobic and super-philic which are the extreme wetting behavior of a fibre have applications in various industry fields such as oil-water separation (Guo et al. (2014)), corrosion resistance property (Kang et al. (2011)), and self-cleaning surface applications (Zhou et al. (2015)).

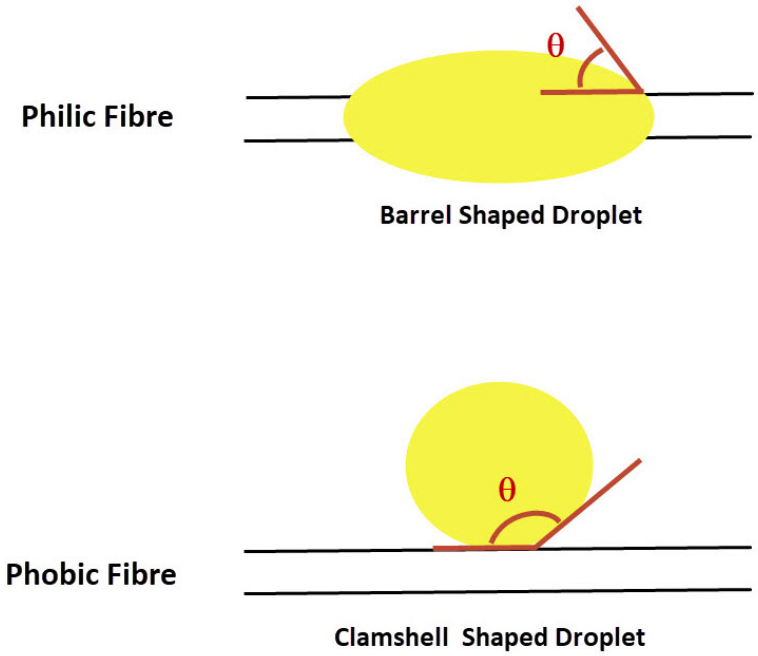

Figure 2.6: Diagrammatic presentation of clamshell and barrel shaped droplets on non-wettable (phobic) and wettable (philic) fibres.

2.2.3 Filtration Theory

The underlying objective of filtration is to surely remove one compound from another. In particle filtration, the aim is to capture suspended aerosol deposited on a unit length of a fibre depending on flow velocity (which mostly expressed in the non-dimensional form of Reynolds number), fibre diameter, filter packing density, and filter thickness. In the following, filter Reynolds number and aerosol capture mechanisms as the principals of filtration will be explained.

Reynolds Number

Reynolds number (Re) is an important dimensionless quantity which indicates the ratio between inertial and viscous forces. The flow pattern in the system mainly depends on the value of Reynolds number. In the case of filtration, Re_f is known as filter Reynolds number which can be calculated by Equation 2.3.

$$Re_f = \frac{\rho u d_f}{\mu} \tag{2.3}$$

where ρ is the density of the gas in our study, u is the gas flow face velocity in the filter, μ is dynamic viscosity of the carrier fluid, and d_f is diameter (of strut

for open-cell foam media) of the filter element (Abishek et al. (2017, 2018).

Aerosol Droplet/Particle Capture Mechanisms

When it comes to filtration of aerosol droplet/particles, understanding aerosols capture mechanism is important. According to Hinds (1999a), there are five different capture mechanisms as: interception, impaction, diffusion, gravitational settling and electrostatic attraction which are presented by Figure 2.7.

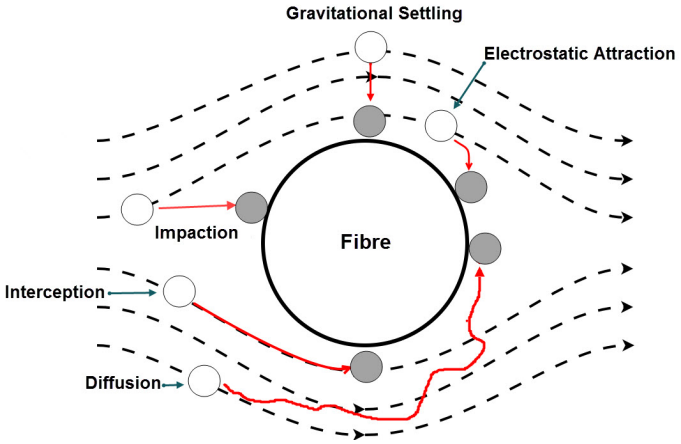

Figure 2.7: Diagrammatic presentation of aerosol droplet/particle capture mechanisms (after Mead-Hunter et al., 2014).

Interception occurs when a particle/droplet is following a streamline which has a particle/droplet radius distance from the fibre. In this circumstance, the particle/droplet will touch the fibre and be captured (Hinds (1999a)), so in other words, based on particle/droplet size there is specific streamline which leads to deposition on the fibre. It is worth mentioning that particle/droplet does not have enough inertia to deviate from the streamline and it is large enough to not to be affected by diffusion (Hutten (2007)). In general, particles/droplets ranging from 0.1 to 1 μm can be captured by interception mechanism (Zhang et al. (2018)).

Impaction occurs when a particle/droplet is not able to follow the streamline (which changes near in vicinity of the fibre) due to its inertia and deviate from the streamline and finally hits the fibre then captured (Hinds (1999a)). This type of capture mechanism is more predominant in high velocity gas filtration or in high packing density filters. This mechanism plays a significant role in capturing

particles/droplets larger than 0.3-1 μm (Zhang et al. (2018)).

In order to describe diffusion mechanism first the kinetic theory of gases should be reviewed. According to Kennard (1938), gas molecules travels in a straight line while not bumping to each other which resulted in a random or zigzag path motion of gas molecules (molecules act as a rigid sphere). This random motion of gas molecules is known as Brownian motion which was observed by Brown in 1827. The diffusion mechanism of capture in particle/droplet occurs due to the Brownian motion of gas molecules which hit the droplet/particle and causes random motion of it. According to Bagheri et al. (2012) diffusion will be effective for droplet/particles smaller than $10nm$. Therefore, this mechanism is more predominant in low velocity gas filtration and small particle/droplet size.

Gravitational settling occurs due to the mass of a droplet/particle. This mechanism is more predominant for droplet/particles greater than $10\mu m$ (Bagheri et al. (2012)). According to Hinds (1999a), this mechanism is less significant than impaction or interception. It is also notable that gravitational settling mainly depends on filter orientation and face velocity (Mead-Hunter et al. (2014)).

Electrostatic Attraction occur when electrical charges are present on the filter medium or on the droplet/particles. The capture may occur due to the attractive forces between different charges on the filter and the droplet/particle (Hinds (1999a)). It is note worthy that this mechanism is not usual in oil-mist filters since the filter is often wet and oils are poor conductors (Mead-Hunter et al. (2014)).

Figure 2.8 presents all the filtration mechanisms discussed above and their influence on filter capture efficiency by particle size. In Figure 2.8, MPPS stands for the maximum penetrating particle size.

Recently, Abishek et al. (2019) have identified some new capture mechanisms. They studied the effects of dynamic contact angle on fibre capturing efficiency in both philic and phobic media in their research. It was found that advancing contact angle, the capillary stage, advancing and receding contact angles are the key factors in collision regimes. Their findings indicate that there are at least four regimes which are : likely capture in philic media, likely droplet re-entrainment with minimal or no capture in phobic media, partial or full capture with receding contact angle assisted in sticky-phobic mechanism, partial or full re-entrainment with advancing contact angle in roll-off-philic mechanism.

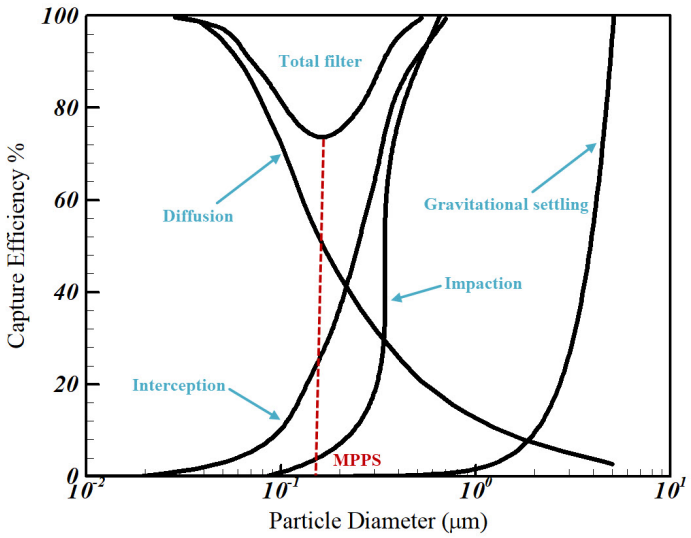

Figure 2.8: Capture efficiency for particles with different diameter size (after Hinds (1999b)).

2.3 Liquid Aerosol Filtration

As mentioned in previous sections, the main difference between liquid aerosol and solid particles filtration is the fact that liquid aerosols coalesce into larger droplets (Yarin et al. (2006)) after being collected by filter. This results in wetting of the fibres and formation of a liquid film on the surface of the fibres (Mullins et al. (2004)). The film and larger droplets form a liquid bridge at fibre intersections and between fibers (Liew and Conder (1985)). These bridges remain equalised under capillary forces (Kampa et al. (2009)). Finally the drainage rate or re-entrainment equals the accumulation (Contal et al. (2004)). In opposite, solid particles remain stationary after hitting the fibre in filtration process (Spielman (1977)).

2.3.1 Mist Filter Loading

Loading of oil-mist filters has been characterised to different stages by some researchers (Charvet et al. (2010); Contal et al. (2004)), but it is worth mentioning that all theses stages are valid while the flow velocity is not changing over time.

Stage 1: Charvet et al. (2010) named this stage as 'static' stage as it is assumed that the captured oil in the filter remain stationary. Contal et al. (2004) showed that deposition of captured droplets on the fibers lead to increase in fric-

tional area and consequently increase in pressure drop. Furthermore, collected droplets occupy the fiber, so reduces the collection surface resulted in droplets penetration through the filter.

Stage 2: In this stage, a change occurs in pressure profile and filter penetration increases. Contal et al. (2004) justified it by reduction in collecting area and re-distribution of collected liquid within the filter.

Stage 3: In this stage, the captured liquid droplets increase the flow resistance which lead to increase the pressure drop exponentially. Furthermore, increased flow resistance causes an increase in interstitial velocity which consequently decrease the penetration through the filter (Contal et al. (2004)). Charvet et al. (2010) named this stage (combination of stages 2 and 3) as 'dynamic' stage which assumes that collected droplets do not remain stationary and form liquid bridges.

Stage 4: This stage is the final stage and known as "pseudo"-steady state which means collection and drainage rate are the same. In this stage, the pressure drop and penetration remain constant.

To have a better understanding of discussed stages, Figure 2.9 shows these stages for philic (four stages are separated with vertical solid lines and labeled accordingly) and phobic filter media.

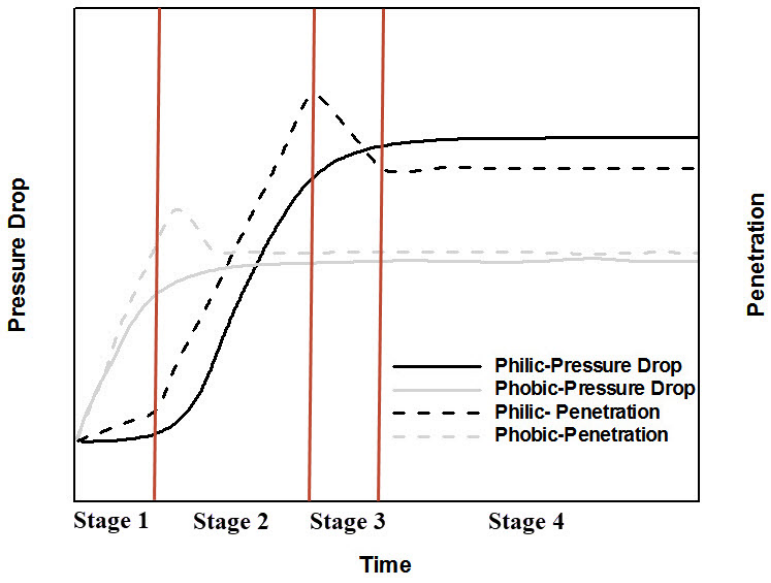

Figure 2.9: Pressure drop and penetration versus time for philic and phobic media (after Mead-Hunter et al., 2014).

As it can be seen from Figure 2.9, phobic media dose not have stage 1 in comparison with philic media. So, it can be concluded that there are three stages for phobic media, while 4 stages for philic.

2.3.2 Efficiency, Penetration, and Quality Factor in Coalescence Filters

The interaction between the filter structure and the droplet in the flow stream results in different capture mechanisms explained in 2.2.3. Each of these mechanisms associated to an individual efficiency which can be resulted in the global collection efficiency of the filter Mead-Hunter et al. (2014). Due to the complexity of the filter structure, it is very difficult to develop a comprehensive model for calculating the filter efficiency. Therefore, many authors (Chen (1955); Hinds (1999b); Lee and Liu (1982); Liu and Rubow (1990); Stechkina et al. (1969); Yeh and Liu (1974)) considered a single fibre perpendicular to the flow stream and developed the efficiency model (semi-empirical equations) based on that which is known as Single Fibre Efficiency (SFE) theory. It has bee documented that these models have very limited applications due to their empirical origins, and the influence of trapped particles on flow stream in the filters which cause deviation from these models predictions.

In regard to total efficiency calculation in filters, some authors conducted a series of research on this, and developed some models to predict the total efficiency of a filter which will be presented in the following. Raynor and Leith (2000) developed an efficiency model based on assuming constant saturation ratio through the filter. The proposed model can be defined by Equation 2.4:

$$E_T = 1 - exp\left[\frac{-4\alpha E_F l f}{\pi(1-\alpha)(1-S)d_f}\right] \tag{2.4}$$

where α is packing density, E_F is the single fibre efficiency, l is the thickness of the filter, S is the saturation in the filter and d_f is the fibre diameter. f is the proportion of the fibre surface which is not covered by liquid, and can be defined as following:

$$f = 1 - \frac{d_d}{x_d} \tag{2.5}$$

d_d is the droplet diameter and can be calculated by:

$$d_d = \left[\frac{3S(1-\alpha)d_f^2 x_d}{2\alpha}\right]^{\frac{1}{3}} \tag{2.6}$$

x_d is the distance between the centroids on the collected droplets which calculated by:

$$x_d = 5\left[\frac{S(1-\alpha)}{\alpha} + 1\right] \tag{2.7}$$

Another assumption that Raynor and Leith (2000) considered for developing their model was that the coalesced droplets' diameter is significantly larger than the fibre diameter, and no further coalescence happening in the filter Raynor and Leith (2000). The other point about this model is that this model is only applicable in steady state regime, where no further change occurs in filter pressure drop. It seems this model is wrong at least for diffusional collection as the single fibre efficiency term used in Equation 2.4. It is reported by Mead-Hunter et al. (2014) that this model has a poor agreement with microfibre media where the saturation in the filter is high, and captured droplets affect the aerosol in flow stream. Another drawback of the Raynor and Leith (2000)'s model is assuming equal saturation with distance in the filter which is not realistic, and more importantly it may not be available for efficiency measurement. Hinds (1999b) tired to tackle this issue by presenting a model without any saturation term. This model is defined as:

$$E_T = 1 - exp\left[\frac{-4\alpha E_F l}{\pi d_f}\right] \tag{2.8}$$

In regard to the Hinds (1999b) model, it should first be noted that this model is based on the dust filtration data, therefore dose not deal with mist filters. Moreover, it is seen that this model still has the single efficiency term, which should be calculated based on the predominating mechanisms in the specific application.

Zhang et al. (2017) proposed an efficiency model for entire filtration process based on a set of experiments. Their model is defined by the Equation 2.9:

$$E_T = 1 - exp\left[-\frac{4E_f\alpha(1 - S_e(\mu/\mu'(1-\alpha))l)}{\pi\big[1-\alpha(1-S_e(\mu/\mu'(1-\alpha))\big]d_f}\right] \tag{2.9}$$

where S_e is the saturation of the pure liquid, μ is the dynamic viscosity of the oil mist, μ' is the viscosity of the pure liquid. The relationship between the two viscosities can be defined as (Murshed et al. (2008)):

$$\mu' = \mu\left(1 - \frac{\phi}{0.64}\right)^{-1.6} \tag{2.10}$$

where ϕ is the particle volume fraction. It is assumed that all fibres throughout the filter thickness operated as a unified layer. Moreover their model is based on the fibrous filter with only horizontal and vertical fibres in the filter for simplifying the calculation. Their model underestimate the efficiency values for particle sizes less than 700 nm, and overestimate the efficiency in larger particles.

Another important parameter in coalescence filters is penetration which can be defined as the number of particles passing through a filter over the total number of particles introduced to the filter. In other word, penetration can be presented as the following equation (Sanchez et al. (1997); Mead-Hunter et al. (2014)):

$$P_e = 1 - E_T \tag{2.11}$$

where E_T is the total (global) filter efficiency. There are different semi-empirical models (Raynor and Leith (2000); Liew and Conder (1985); Payet et al. (1992); Gougeon et al. (1994)) for predicting the penetration of a filter (all developed for fibrous media), but all of them have application limitations (limited to specific packing density range), and mainly applicable to the same filter range that the experiments were conducted. These models are fully reviewed and explained in the research of Mead-Hunter et al. (2014).

A parameter which describes filter performance based on the most important criteria is called quality factor or index criteria (Sanchez et al. (1997); Mead-Hunter et al. (2014)). This parameter originally introduced by Chen (1955), and also called filtration index by McFee and Sedlet (1968). The two important filter variables which quality factor is defined based on them are penetration (P_e) and pressure drop. Therefore, the quality factor is defined by (Hinds (1999b); Sanchez et al. (1997); Mead-Hunter et al. (2014)):

$$QF = \frac{-ln(P_e)}{\Delta P} \tag{2.12}$$

Quality factor is the parameter which has been established by several authors (Mead-Hunter et al. (2014); Chen (1955); Hinds (1999a); Pich (2017); Matteson and Ward (2018)) in order to compare filters. The higher the quality factor, the better the filter performs. It is worth mentioning that for comparing filters performance based on quality factor, the measurements should be taken at the same inlet velocity.

2.3.3 Pressure Drop Models in Coalescence Filters

There are number of models for predicting pressure drop through the filter, but they are mostly based on empirical or semi-empirical approach which extensively depends on experimental condition and applies to very limited applications. Theoretical models mostly developed from cell model proposed by Kuwabara (1959) or semi-empirical by Davies (1953). It is worth mentioning that these theories are only applicable for dry (clean) fibrous filters. In the following these theories will be discussed.

Davies Equation (Davies (1953)) for calculating pressure drop is:

$$\triangle P_0 = \frac{\mu Q l}{{d_f}^2 A_f}[64\alpha^{1.5}(1 + 56\alpha^3)] \tag{2.13}$$

where $\triangle P_0$ is clean pressure drop of the filter, d_f is fibre diameter, A_f is cross-sectional area of the filter, μ is dynamic viscosity of the gas, Q is volumetric flow rate, l is filter thickness and α is packing density of the filter. It should be mentioned that the term in square bracket is known as $f(\alpha)$ which is an empirical correction to account for non-perpendicular fibres. This correlation is valid for fibrous filters with packing density ranging $0.006 \leq \alpha \leq 0.3$.

In regards to saturated filter in steady state, Liew and Conder (1985) Equation is applicable:

$$\triangle P_s = \triangle P\left[1.09\left(\alpha\frac{l}{d_f}\right)^{-0.561}\left(\frac{u\mu}{\sigma_{LV}\cos\theta}\right)^{-0.477}\right] \tag{2.14}$$

where $\triangle P_s$ is steady state pressure drop, $\triangle P$ is dry (clean) pressure drop,α is clean packing density, l is filter thickness, d_f is fibre diameter, u is filtration velocity, μ is dynamic viscosity, σ_{LV} is liquid surface tension and θ is contact angle. It should be emphasised that this correlation applies only to fibrous filters with packing density ranging $0.075 \leq \alpha \leq 0.142$.

Davies (1953) modified his original pressure drop model, and it has been shown that it provides satisfactory results for early loading filtration stage (Frising et al. (2005)). In the modified model, Davies considered the effects of retained liquid in the filter and replaced the fibre diameter d_f and filter packing density α with wet fibre diameter d_{fwet} and wet filter packing density α_{wet}, respectively. So, the model becomes:

$$\triangle P = u\mu l \frac{64\alpha_{wet}^2(1+56\alpha^3)}{{d_{fwet}}^2}, \tag{2.15}$$

$$\alpha_{wet} = \alpha + \frac{m_{liq}}{A_f l \rho_l}, \tag{2.16}$$

$$d_{fwet} = d_f \sqrt{1 + \frac{m_{liq}}{A_f l \rho_l \alpha_f}} \tag{2.17}$$

where u is face velocity. In Equations 2.16 and 2.17, m_{liq} is the mass of retained liquid in the filter and A_f is cross sectional area of the filter. Frising et al. (2005) reported that this model is accurate when the liquid wet the fibres perfectly and distributed uniformly throughout the filter.

Spielman and Goren (1968) developed a theoretical model based on the proposed Brinkman (1949) flow model. The essence of the Spielman and Goren (1968) model is to considering damping force proportional to the velocity in addition to pressure and viscous forces. The Equation of motion becomes:

$$\nabla P = \mu \nabla^2 \vec{u} - \mu \underline{k}.\vec{u} \tag{2.18}$$

where P is the average pressure field, $\vec{u}$ is average velocity field, and $\underline{k}$ is considered as a tensor giving the damping coefficients. The coefficient $\underline{k}$ is taken to be the Darcy resistance coefficient (Spielman and Goren (1968)). They calculated $\underline{k}$ theoretically based on different geometries by relating the selected geometry (circular elements) to Darcy coefficient. The model covers four orientation distribution which are:

(1) Fibres randomly distributed with various angels in planes which are all perpendicular to the superficial velocity.

(2) Fibers are in parallel direction to the superficial velocity.

(3) Fibres with random and various angle in planes in parallel to the superficial velocity direction.

(4) Fibers are all oriented randomly in different directions.

Figure 2.10 presents the calculated non-dimensional pressure drop versus filter packing density based on Spielman and Goren (1968) proposed model.

In Figure 2.10, Φ is dimensionless pressure drop which is calculated as below:

$$\Phi = \frac{\triangle P r^2}{4\alpha\mu u l} \tag{2.19}$$

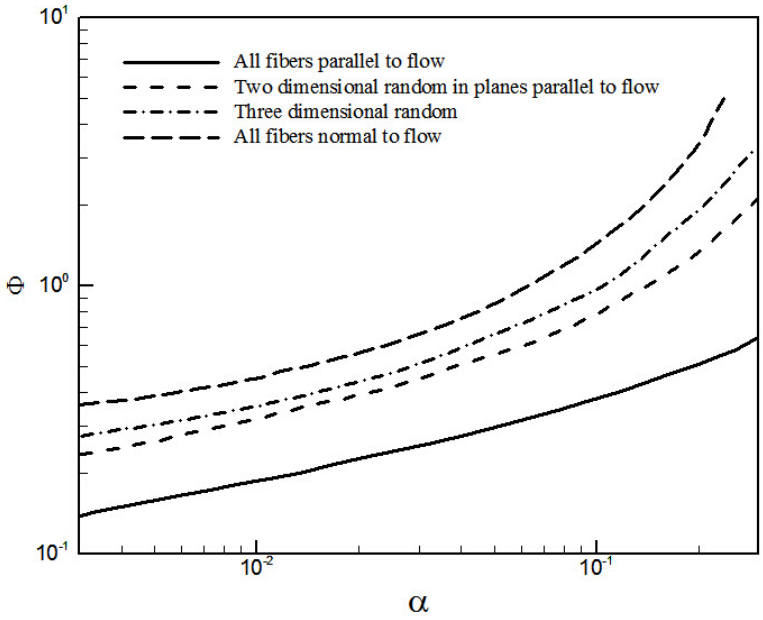

Figure 2.10: Theoretical non-dimensional pressure drop versus packing density (after Spielman and Goren (1968))

where r is fibre radius.

Mead-Hunter et al. (2014) reviewed Spielman and Goren (1968) results in their work and compared them against several experimental results. Their research results show that this theoretical model like empirical ones has application limitations due to considering limited parameters. It was found that the best agreement occur in Kn values for the experimental works range from 0.0049 to 0.2129.

Kn is Knudsen number and defined as:

$$Kn = \frac{2\lambda}{d_f} \tag{2.20}$$

where in Equation 2.20, λ is the molecular mean free path in the air.

Schweers and Löffler (1994) applied Kuwabara (1959) model (for calculating permeability) to develop a theoretical pressure model which covered angle between fibers, slip flow and directional permeability. Andan et al. (2008) used Brown (1993) modified pressure Equations (which were based on some empirical coefficients extracted from experiments) for $kn < 0.25$ and combined them with a linear saturation profile. So, the application of the model is limited to the original experiments conducted by Brown (1993).

Kampa et al. (2014) proposed a phenomenological model named 'jump and channel'. They conducted an experimental study on phobic and philic media to investigate the pressure drop increase inside the filter in liquid filtration problems. The results indicated two distinct features in both philic and phobic media pressure drop curves which called $\triangle P$ *jump* and *channel* $\triangle P$.

$\triangle P$ *jump* : is defined as the equivalent to the capillary entry or exit pressure, which drives liquid in to phobic media or push out liquid from a philic media filter.

channel $\triangle P$: is defined as the pressure of the airflow which moves captured liquid droplets through distinct parallel channels inside or between layers of filters. In philic media, the film on the back of the filter is fed by these channels, while in phobic media droplet formation occurs at the end of these channels.

All the proposed models are either theoretical or empirical which all have application limits such as certain range of packing density, or a valid range of Knudsen number. In the following, a comprehensive review on the coalescing filtration will be presented. Likewise most of the research fields which studies divided into experimental and theoretical (numerical), there are extensive studies in coalescence filtration as well, but only the most related studies to this research will be presented and discussed here.

2.3.4 Saturation Models in Coalescence Filters

In regards to saturation model for oil-mist filters, there are number of researchers who proposed some equations and models, but two of them have reliable outcome. In the following a brief review of these models will be presented.

Liew and Conder (1985) developed a simple power law expression for calculating the saturation in mist filters. In their work, they considered filters with packing density, α, ranging from 0.076 to 0.142, filter thickness, l, between 7.1 and 7.8 mm and fibre diameter equal to 4, 8, 12, and 22 μm. Equations 2.21 and 2.22 show the expression.

$$S = 0.0829\left(\frac{\alpha l}{d_f}\right)^{-0.321} Ca_n^{-0.431} \tag{2.21}$$

where Ca_n is capillary number and calculated by;

$$Ca_n = \left(\frac{Q\mu}{A_f \sigma \cos\theta}\right)\left(\frac{\triangle P_w}{\triangle P_0}\right) \tag{2.22}$$

θ is contact angle which Liew and Conder (1985) assumed zero, Q is the volumetric flow rate, $\triangle P_w$ is wet (saturate) pressure drop, and $\triangle P_0$ is dry (clean) pressure drop. Mead-Hunter et al. (2014) investigated the accuracy of this model, and it was shown it predicts acceptable saturation values if the ratio of $\frac{\alpha l}{d_f}$ is similar for selected filters to ones used in Liew and Conder (1985) research. Furthermore, it should be noted this model is only applicable for fibrous type filters.

Raynor and Leith (2000) combined Bond number (Bo), capillary number(Ca) and drainage rate (Dr) to develop an expression for predicting saturation in mist filters.Bond number (Bo) is a ratio of gravitational forces to surface tension forces. While the gravitational forces pull the captured liquid down, the surface tension resists deformation of the drop that may cause movement. So, Bond number is used to describe the liquid transport through the filter and is calculated by:

$$Bo = \left(\frac{\rho g d_f^2}{\sigma}\right) \times 10^5 \tag{2.23}$$

where ρ is fluid density, g is the acceleration due to gravity, d_f is fibre diameter, σ is liquid surface tension, and 10^5 is a multiplier used to drive Bo to a value close to one for empirical model construction.

Raynor and Leith (2000) employed capillary number to explain the re-entrainment mathematically from a filter which compares air drag forces to surface tension forces. The expression is given by:

$$Ca = \left(\frac{\mu u}{\sigma}\right) \times 10^5 \tag{2.24}$$

where μ is liquid dynamic viscosity, u is face velocity, σ is liquid surface tension, and a multiplier of 10^5 is used as in Equation 2.23. As it can be seen from comparison of capillary equations 2.24 (proposed by Raynor and Leith (2000)) and 2.22 (proposed by Liew and Conder (1985)) there is a difference between expressions. In this case, if the θ assumed to be zero and neglect the wet to clean pressure drop ratio, the two expressions come to similar equation except for the 10^5-multiplier. It should be mentioned that 10^5-multiplier is used in both Equations 2.24 and 2.23 in order to aid the construction of empirical expressions (Raynor and Leith (2000)).

Raynor and Leith (2000) define their drainage rate term (Dr) as:

$$Dr = \frac{\mu D}{\sigma l W} \tag{2.25}$$

where μ is liquid dynamic viscosity, D is drainage rate, σ is liquid surface tension, l is filter thickness, and W is the width of the filter in perpendicular direction to the flow and gravity. The equilibrium saturation ratio developed by Raynor and Leith (2000) is as below:

$$S_e = \frac{\alpha^{0.39\pm0.09}}{Bo^{[(0.47\pm0.06)+(0.24\pm0.07)\ln(Bo)]}Ca^{0.11\pm0.04}} \times \exp\left[\big(0.04\pm0.06\big)+\big(6.6\pm1.5\big)\times10^5 Dr\right] \tag{2.26}$$

Raynor and Leith (2000) used diethyl-hexyl sebacte (DEHS) as the liquid in their experiment in order to develop the model. The physical properties of the filters for developing the model are given as: thickness equal to $88mm$, fibre diameter ranging from 2.9 to 8.5 μm, and packing density between 0.026 and 0.035.

Mead-Hunter et al. (2013) developed a capillary based model. In their research, based on the filter face velocity, some empirical relationships between pressure drop and saturation proposed. Then, they developed a theoretical model based on modified Washburn (Reed and Wilson (1993)) by incorporating pressure drop term into capillary rise expression:

$$x_\infty = \frac{-\triangle P_c r_c + 2\sigma\cos\theta}{r_c \rho g} \tag{2.27}$$

where x_∞ is capillary rise height, $\triangle P_c$ is the pressure drop between top and bottom of the theoretical capillary which can be calculated by:

$$\triangle P_c = \frac{(\pi+1)}{\pi}\frac{r}{r_c} \tag{2.28}$$

In equation 2.28, r is fibre radius, and r_c is capillary radius. r_c is calculated based on the expression given by Mullins et al. (2007) as:

$$r_c = \left(- A\log_e\big(\frac{\alpha}{r_f}\big) - B\right)c_f \tag{2.29}$$

where A and B are material specific constants, and c_f is a correction factor. After calculating capillary rise height, filter saturation may be determined based on a simple geometric relation (Mead-Hunter et al. (2013)). One of the main limitations of the capillary based model is depending on input pressure drop which means the value of pressure drop needs to be measured experimentally in order to use the model for predicting the saturation.

In summary, choosing the saturation models depends on the availability of the pressure drop values and also the physical properties information of the filters. In the case the the pressure drop is available, the Liew and Conder (1985) model can be used, but there is still some limitations based on the $\frac{\alpha l}{d_f}$ ratios. In the absence of the pressure drop values, capillary number can be calculated by 2.24, but it causes an over prediction on the saturation level (Mead-Hunter et al. (2014)). Given the empirical nature of the models, there is a possibility that the saturation in a certain filter-liquid combination may not be able to be approximated accurately. Moreover, it worth mentioning that all the discussed saturation models are applicable to fibrous filters only, and there is no investigations on their accuracy on saturation level prediction in other types of filter media.

2.4 Experimental Studies on Operating Condition and Optimising Coalescing Filters

Coalescence filters operating condition has been the subject of some research so far (Kolb et al. (2017); Frising et al. (2005); Penner et al. (2019); Contal et al. (2004); Chen et al. (2018); Charvet et al. (2008)). Operating condition of a filter is a decisive factor in order to improve the filter efficiency and reduce the pressure drop to the system. It is reported by Nassif (2012) that 1 Pa increase in filter pressure drop will resulted in 1.8-3.2 kWh power consumption enhancement. Therefore, reducing the pressure drop through the filters and keeping or even increasing the filter efficiency of the filters is the ultimate goal of many researchers in this field. A number of research have examined the whole filters experimentally in order to evaluate filter behaviour. Their tests generally involve loading the filters with oil-mists and measuring the pressure drop, saturation, drainage, and efficiency of the filter. In the following, the most related works to this study (gas-liquid (oil-mist) coalescence filters with different structures and evaluating their performance) are divided into three sections: studies focused on pressure drop and saturation profile in filters, studies focused on quality factor and performance of filters, and studies focused on the effects of wettability on filtration . For better comparison, the experimental case information related to each study are summarised in Table 2.1.

Table 2.1: Summary of experimental works in coalescence filtration related to this study

Author(s)	Wettability	α	l (mm)	d_f (μm)	u (m/s)	Filter Type
Agranovski and Braddock (1998b)	philic	0.03	5	8	1-4	fibrous
Agranovski et al. (2001)	philic	0.03	6	8	0.16-0.64	fibrous
	phobic	0.08	3	30	0.32	fibrous
Charvet et al. (2008)	-	0.05	0.68	-	0.5	fibrous
	-	0.05	0.68	-	0.42	fibrous
Charvet et al. (2011)	-	0.28	0.34	-	0.11-0.42	fibrous
Frising et al. (2005)	-	0.079	0.409	1.21	0.058	fibrous
Frising et al. (2005)	-	0.078	0.409	1.21	0.058-0.25	fibrous
Jankowski (2009)	-	0.0525	4.32	54.77	1-1.75	fibrous
		0.0349	6.49	18.06		fibrous
		0.1924	2.08	16.52		fibrous
Letts et al. (2003)	philic/phobic	0.047	8.8	8.5	0.105	fibrous
Mead-Hunter et al. (2013)	philic	0.016-0.022	5.08-6.9	4-6.4	0.267-0.928	fibrous
Mullins et al. (2014)	philic	0.05	0.6	0.67	0.248	fibrous
	philic	0.06	0.6	0.66	0.248	fibrous
	phobic	0.073	0.46	3.4	0.248	fibrous
Raynor and Leith (2000)	philic	0.016-0.054	8.8	2.9,8.5	0.05-0.25	fibrous
Patel et al. (2013)	philic	-	14	2-5	0.6	fibrous
Vasudevan and Chase (2004)	-	0.9-0.95	0.41-0.47	2-6	10	fibrous
Manzo et al. (2016)	-	0.012-0.037	2	2, 6.5	0.1	fibrous
Zhang et al. (2017)	philic	0.09	0.35	2	0.101	fibrous

Author(s)	Wettability	α	l (mm)	d_f (μm)	u (m/s)	Filter Type
Chen et al. (2018)	phobic	0.078	0.49	3.55	0.12	fibrous
	phobic	0.069	0.42	1.80	0.12	fibrous
	phobic	0.079	0.38	1.29	0.12	fibrous
	philic	0.072	0.41	4.08	0.12	
	philic	0.067	0.46	3.07	0.12	
	philic	0.070	0.46	2.33	0.12	fibrous
	philic	0.071	0.45	1.92	0.12	fibrous
Kolb et al. (2017)	philic	0.05	0.5	-	0.05-0.7	fibrous
Chang et al. (2018)	Phobic	0.066	0.42	1.75	0.1	fibrous
	phobic	0.190	1.89	19	0.1	fibrous
	Philic	0.188	1.88	18.60	0.1	fibrous
Chen et al. (2019b)	philic	0.074	0.52	2.20	0.12	fibrous
	philic	0.070	0.46	3.18	0.12	fibrous
	phobic	0.071	0.42	1.78	0.12	fibrous
	phobic	0.070	0.54	3.46	0.12	fibrous
Wurster et al. (2015)	phobic	0.05	2.5	1.5	0.25	fibrous
	philic	0.05	2.5	1.5	0.25	fibrous
Chen et al. (2019a)	philic	0.070	0.46	3.18	0.12	fibrous
	phobic	0.070	0.54	3.46	0.12	fibrous
Liu et al. (2020)	phobic	-	0.56-2.24	5	0.1	fibrous
	philic	-	0.56-2.24	15	0.1	fibrous
Brunazzi and Paglianti (1998)	-	-	0.02	150	1-2	knitted

Author(s)	Wettability	α	l (mm)	d_f (μm)	u (m/s)	Filter Type
	-	-	0.025	150	1-2	knitted
	-	-	0.026	65	1-2	knitted
	-	-	0.022	150	1-2	knitted
	-	-	0.025	65	1-2	knitted
Sheng et al. (2020)	-	0.207	0.42	-	1-2.5	knitted
	-	0.011	2.30	-	1-2.5	knitted
	-	0.0107	0.28	-	1-2.5	knitted
	-	0.032	3	24	1-2.5	fibrous
El-Dessouky et al. (2000)	-	-	1000-2000	200-320	0.98-7.5	knitted

2.4.1 Experimental Studies on Pressure Drop and Saturation

Studies in Nonwoven Fibrous Media

Fairs (1958) indicated that captured liquid in filter media causes 80-85 % of the total pressure drop in the system. Raynor and Leith (2000) developed a set of equations for describing the filtration, drainage, evaporation, and re-entrainment from a philic fibrous filter. A pressure drop correlation was developed based on the experimental tests which predicts the pressure drop based on packing density and the final steady saturation level. The drawback of the proposed model was its application limit where the thickness of the filter should be 0.88 mm, otherwise the prediction is not accurate. Frising et al. (2005) investigated the effect of interruption in oil-mist loading to the fibrous filters on pressure drop. Their findings showed 20 % increase in the filter pressure drop when the aerosol loading interrupted, but it did not have any influence on the filter penetration. Frising et al. (2005) studied the influence of inlet velocity on fibrous filter pressure drop and penetration. It was shown that higher velocity resulted in lower penetration of liquid in the filter. They presented a phenomenological model for pressure drop in fibrous filters based on their experimental results. Their model is applicable to all filtration stages explained before, although some discrepancies can be seen for the jump pressure drop modeling results.

Charvet et al. (2008) studied filtration efficiency and pressure drop in liquid capture mechanisms using fibrous coalescence filter. Their results demonstrated the advantage of operating coalescence fibrous filters at high velocities. Moreover, there was no effect of aerosol concentration variation on pressure drop increase in the system. Charvet et al. (2011) employed synchrotron X-ray holotomography in order to determine the behaviour of fibrous filters during filtration. They used the resulted images for analysis of droplet formation in filters to calculate local packing density and consequently a pressure drop model for the filter. They addressed the point that their results probably do not provide actual distribution of the liquid in filters due to re-distribution may occurred during stopping the tests for imaging. Mead-Hunter et al. (2013) investigated the relationship between pressure drop and saturation in coalescence filters by conducting set of experiments. They proposed a capillary-based saturation model by a data fitting technique. Their model is able to predict the saturation in the filter for similar filter properties, although for applying that to a new media, some experiments required in order to calibrate the model coefficients.

Zhang et al. (2017) developed a model to access the oil content influence on pressure drop in filters. It was shown that the oil content increase attributed

to pressure drop decrease and efficiency improvement. The proposed model was able to explain the relationship between the oil content level and filter efficiency, but it should be emphasized that their model was developed based on one filter only, which cannot be generalised. Kolb et al. (2017) investigated the dependence of pressure drop in oleophilic fibrous media and saturation on air flow velocity experimentally. Their results indicated that (in the filters studied) the difference between filter wet and dry pressure drops is independent of inlet air velocity. They reasoned that increase in inlet velocity was compensated for by a downward adjustment in saturation, instead of causing an increase in pressure drop. Chang et al. (2018) studied the influence of a drainage layer on saturation profile and liquid distribution of phobic coalescence filters. The results showed that total wetting regions enlarged and the saturation level increased by assembling a drainage layer in the filter.

Studies in Woven Knitted Media

Most studies in knitted media focused on physical properties and generation of these media (Anand and Lawton (1991); Jeddi and Dabiryan (2008); Yip and Ng (2008); Yuksekkaya et al. (2010); Rakhimov et al. (2018); Ince and Yildirim (2019)), and there have been relatively very limited number of studied in knitted media pressure drop or efficiency evaluation. Helsor et al. (2005) investigated knitted media characteristics on pressure drop in this media. They have tested 4 different packed knitted filter with packing densities $0.02 < \alpha < 0.46$. It should be mentioned that their results were not sufficient enough to present a practical model for pressure drop in knitted media.

Mullins et al. (2017) stated that knitted media follow the classical pressure drop and efficiency theory approximately, although a deviation from those theories is reported. Lorimier et al. (2008) reported that the knitted media produced 77 % higher pressure drop compared to a nonwoven filter, while the efficiency of the knitted media was 18.5 % lower. Mullins et al. (2011) found 47 % higher pressure drop produced by knitted media against Davies equation (Davies (1953)) and 37 % higher in efficiency calculation compared to Sing Fibre Efficiency (S.F.E) theory (Mead-Hunter et al. (2014)). Diedericks et al. (1998) proposed a model for predicting the pressure drop in knitted media, but it required large number of parameters and dimensionless terms in order to predict a reasonable value. Zhu et al. (2015) conducted research on wire-mesh mist eliminators. Their results indicated that pressure drop raised by increasing in filter packing density, inlet velocity and filter thickness. They found the optimum layer spacing in demister varies from 1-1.15 mm under experimental conditions.

Studies in Open-cell Foam Media

Several authors studied the clean pressure drop in open-cell foam media (Dietrich et al. (2009); Inayat et al. (2011); Bonnet et al. (2008); Liu et al. (2006); Topin et al. (2006); Dukhan (2006); Madani et al. (2007)) just by measuring the difference between the inlet and outlet pressure. Skibinski et al. (2015) studied the effect of pore size variation on pressure drop in foam media. The results revealed a strong correlation between the distribution of the pore volume and pressure drop in the filter. In the case of pressure drop correlation models in open-cell foam media, many researchers (Incera Garrido et al. (2008); Kumar and Topin (2014); Lacroix et al. (2007); Innocentini et al. (1999); Richardson et al. (2000)) proposed their models based on Ergun and Orning (1949). The point about all the mentioned studies and models is that they are all only applicable to single-phase condition. The other problem with open-cell foam media theoretical models is that they cannot be used on every arbitrary selected open-cell foam media. Furthermore, oversimplification of strut shape and sizing, definition of Reynolds number discrepancies for measuring morphological properties causes more limitations to validity of these models (Xu et al. (2008)).

Lammermann et al. (2016) studied the liquid distribution in a 100 mm diameter column filled with periodic open-cell foam filters. Their results confirmed that there is a potential in foam media to have a higher performance compared to random particle beds.

2.4.2 Experimental Studies on Quality Factor and filter Performance

In the following, some of the research works similar to this study which used quality factor for comparing the performance of the filter are presented.

Studies in Nonwoven Fibrous Media

Hajra et al. (2003) evaluated the effects of humidity, temperature, and adding polymer layer in a coalescence fibrous filter. The quality factor improved significantly by adding the polymer layer to the filter. Moreover, their results indicated a performance enhancement by increasing temperature. Vasudevan and Chase (2004) employed quality factor analysis to verify the performance of combining two types of glass media. Their results indicated an improvement in quality factor parameter. Jankowski (2009) studied the effect of structural filter parameters on fibrous coalescence filtration performance. They found that thickness, packing density, and aerosol flow rate play an important role in filtration performance.

Their results indicated that an increase in the aerosol flow rate through the fibrous filter has a significant impact on changes in flow resistance and efficiency.

Bredin and Mullins (2012) investigated the effect of flow interruption on the performance of two different fibrous filters. Their results suggested that discontinuous aerosol loading causes increase in saturation and pressure drop in both types of filters. Patel et al. (2013) studied the effects of nonwoven polypropylene fabrics as drainage sheet in a glass fibre filter media. Their results showed an improvement in quality factor of the tested filters by increasing the capture efficiency and decrease in the filter pressure drop. Liu et al. (2015) applied quality factor parameter in order to compare the performance of the fibrous filter cartridge. According to their quality factor analysis, they found out that an excess layers had no influence on improving the filtration performance.

Manzo et al. (2016) studied the influence of fibre material properties on filtration performance. They compared stainless steel fibrous filter against glass fibre. The quality factor results showed that stainless steel media has an higher quality factor compared to glass fibre filter. Wei et al. (2019) has indicated by their research that a fibrous filter after super-phobic treatment shows a significant improvement in the efficiency without increasing in pressure drop. Liu et al. (2020) conducted an experimental research on the super-phobic filters. An oil-guiding fibrous later was placed at the front face of the filter, which results indicated 20 % reduction in pressure drop.

Studies in Woven Knitted Media

Carpenter and Othmer (1955) experimentally measured the efficiency of wire-mesh separators. Their results indicated a low efficiency for lower velocities, while the efficiency improved for high velocities (5 m/s). They presented a model based on the experimental results and theory, which later evaluated by Brunazzi and Paglianti (1998). It was shown that the Carpenter and Othmer (1955) model have a good estimation for filters with thickness higher than 65 mm, while for thinner knitted filters it predicts lower value. Brunazzi and Paglianti (1998, 2000) proposed models for thinner knitted media, but it should be mentioned that these models are highly empirical.

El-Dessouky et al. (2000) conducted a set of experiments in industrial scale on knitted media. Their results indicated that the filter efficiency improved by increasing the face velocity and decreasing the knitted diameter. Recently, Sheng et al. (2020) investigated a three-dimensional knitted media used in cooking ventilation systems, and compared to a nonwoven fibrous media. Their results revealed

that the knitted media produced 1/4 of the pressure drop imposed by nonwoven to the system at velocity 2.5 m/s. Moreover, it was shown that the quality factor of knitted media is higher in all velocities tested , but the difference decreased by in increase in face velocity. In the case of this test, it is worth mentioning that the filters that have been compared in this experiment did not have any physical similarities, or in other word, the tested fibrous and knitted media were not equivalent for comparison.

Studies in Open-cell Foam Media

Belforte et al. (2011) compared the efficiency and quality factor of three cartridge filters with adding open-cell foam layer. The results indicated that polyurethane foam had a distinct improvement in filter efficiency. It should be mentioned that their research was conducted only in one face velocity of 0.4 m/s.

2.4.3 Experimental Studies on Philic and Phobic Filters

Studies in Nonwoven Fibrous Media

Agranovski et al. (2001) studied combination of philic and phobic media in a system. They found that the best arrangement is where the carrier gas passes the philic media first and then through the phobic media. They shown that philic fibrous filters are very efficient at capturing small liquid droplets, although they identified that the major drawback associated with philic media is relatively large droplets re-entrainment from the end face of the filter. Their results indicated that phobic media are more appropriate for collecting large oil droplets. Letts et al. (2003) researched on the fibre materials used in different fibrous filters in order to improve mist filtration. Their results suggested that using phobic media may result in lower levels of liquid retention in filters and consequently reduces the pressure drop in the system. Mullins et al. (2014) examined the combined philic and phobic media versus the philic media in their study. Another factor that they study was adding a mesh layer between phobic and philic media, which improved the drainage from the system, and consequently decreased the re-entrainment from the last filter layer. They reported that the optimum configuration is phobic media in the front, philic media in the rear, and a mesh between them.

Wurster et al. (2015) conducted a comparative research on philic an phobic coalescence media to investigate the mechanisms of liquid entrainment. The results showed that oil droplet re-entrainment from both filter media were formed

by bubble formation first and then bursting, instead of blow-off. Chen et al. (2018) evaluated the influence of wettability and pore size on the performance of fibrous filters. They experimentally studied three phobic glass-fibre filters and four philic media which the summary of the experiment conditions is listed in Table 2.1. They used Kampa et al. (2014) pressure drop model in order to explain their results. It was shown that excess channel pressure drop was not changed in phobic media by decreasing the pore size, while it showed a inverse proportional to the pore size in philic media. Chen et al. (2019a) investigated the influence of different liquid surface tension on wet pressure drop, saturation, liquid distribution and efficiency in philic and phobic fibrous filters. Their results revealed that liquid surface tension had a significant effect on jump pressure drop, however no influence observed on channel pressure. Moreover, they observed higher saturation decrease with increase in surface tension, especially in phobic media. Finally, the results concluded that super-phobic filters had the best overall performance among all studied filters which was attributed to lack of liquid hold-up in phobic media. Chen et al. (2019b) studied the effect of wettability on coalescence filtration performance. Their findings suggested that phobic media has a better overall performance in compare to philic media at the steady state stage of filtration. Furthermore, it was shown that the saturation level in phobic media was about the half of philic media in the final stage. It should be mentioned that their study only conducted at one face velocity and the filter properties are listed in Table 2.1.

2.5 Computational Approach to Filtration

In this thesis, numerical approach is used in order to study saturation and pressure drop profile in different types of oil-mist filters, therefor the application of computational methods in filtration will be presented in the following. In chapter 4, Computational Fluid Dynamics (CFD) will be explained in more details.

2.5.1 Application of CFD to Oil-mist Filtration

The majority of CFD simulations in filtration research area have focused on capturing solid particles (Deuschle et al. (2008); Qian et al. (2009); Hosseini and Tafreshi (2012); Yue et al. (2016); Saleh et al. (2013); Huang et al. (2016); Hosseini and Tafreshi (2010a); Bensaid et al. (2010); Maddineni et al. (2018)). There are some research conducted on fluid flow through the filters (Tafreshi et al. (2009), Fotovati et al. (2010)), focused on the structure of filters (Nakamura et al. (2018), Abishek et al. (2017), Soltani et al. (2014), Moghadam et al. (2019), Sozumert et al. (2020)), or evaluating the pressure drop in the clean filters (Chaudhuri et al.

(2019), Liu et al. (2019), Rozy et al. (2020)). There are some studies mainly carried on CFD simulations on solid-liquid particle removal by filters (Frising et al. (2005), Mead-Hunter et al. (2012), Bredin et al. (2012), Mullins et al. (2014), Mullins et al. (2004)). Moreover, CFD has been employed for single fibre geometries which are used mostly for validation, or potentially developing new models (Gac and Gradon (2012), Mead-Hunter et al. (2012), Khalili et al. (2016), Abishek et al. (2019)).

As mentioned before, all these works focused either on air flow through fibrous filters, capturing the solid particles, evaluating the mechanical structure or generating a filter, or solid-liquid particle removal. The aim of this work is to conduct a comprehensive research on liquid (oil-mist) filtration in different media type by using CFD, therefore a literature review and investigation in liquid aerosol filtration will be presented in the following separately.

CFD Application in Fibrous Filters

Jaganathan et al. (2008) applied CFD to model the permeability in fibrous filters. In their research, they used Digital Volumetric Imaging (DVI) technique to create fibrous filter and conduct simulations. Palakurthi et al. (2015) studied unidirectional capillary in fibrous media. They generated the fibrous geometry filter by using GeoDict commercial software (www.geodict.com). CFD techniques were applied in order to simulate the liquid penetration in a fibrous filter. Although their study presented some validation for the VOF solver used, the generated filter geometry was not verified against any experimental study to how if it is a true representative of the media. Palakurthi et al. (2018) employed CFD for determining the quasi-static capillary pressure-saturation relationship. In their study, VOF was used and verified against analytical solution. They indicated in their work that VOF is a robust method for solving porescale problems in compare to reduced-order modeling approach such as pore-network models.

Mead-Hunter et al. (2012) studied the Plateau-Rayleigh instability by applying CFD techniques. Their results indicated that CFD is able to resolve reentrainment of liquid droplets from fibers and mist filters. Mead-Hunter et al. (2013) used CFD to develop a model by coupling VOF and Lagrangian particle tracking algorithms to capture liquid (oil-mist) coalescence and drainage from fibrous filters. In their work, they showed that CFD is applicable to simulate aerosol dynamics which occur in coalescing/mist filters. In their research, only fibrous filter were considered and the main focus of the investigation was on the developed model and its validation by theoretical and analytical models.

CFD Application in Knitted Filters

Similar to fibrous filter studies, there are some research applying CFD to investigate the fluid flow and permeability through knitted media (Tung et al. (2002), Mezarcioz et al. (2014), Dehkordi et al. (2017), Rief et al. (2011), Puszkarz and Krucińska (2018), Okolo et al. (2019)), simulating gas-solid filtration process (Nazarboland et al. (2008)), evaluating the pressure drop (Wang et al. (2007), Rahimi and Abbaspour (2008), Luan and Sun (2010), Yoshida et al. (2015), Gurreri et al. (2016)).

Mullins et al. (2011) developed a geometric model by using Strophoid Equation. They applied CFD to evaluate the particle capture efficiency and pressure drop of knitted filters with different packing densities. To the best of our knowledge, there is no study in knitted media to cover liquid-gas separation by using CFD.

CFD Application in Open-cell Foam Filters

Xu et al. (2008) applied CFD to propose a theoretical model to predict fluid flow characteristics and permeability of the three-dimensional foam filter. They used CFD results to calculate various parameters such as permeability, inertial and friction coefficients. Their geometry was a tetrakaidecahedron structure composed of six squares and eight hexagons and only visually compared against SEM image. It is worth mentioning that although they results indicates a good agreement with experimental acquired data from SiC foam filters, but it cannot be generalised to other foam media.

Tabor et al. (2008) applied CFD to validate their novice technique of image-meshing from a realistic plastic open-cell foam media. They compared the micro structure of the foam filter with SEM image of the media, and finally evaluate the pressure drop CFD results against existing experimental data, and good agreement were achieved. It should be mentioned that they did not investigate the filtration. Diani et al. (2014) validated their micro CT scan method by comparing clean pressure drop of simulations against experimental results. In their work, they selected four metal foam with different pores per inch (PPI) and after scanning import them to another software (ScanFE module in Simpleware) for generating computational meshes. It has been stated that this method is extremely costly as it requires huge memory resource during the process, so they just modeled a very small part of their real filters. Their final results show a good agreement between numerical and experimental results, although they did not conduct any research on filtration characteristics of these media.

Della Torre et al. (2014) employed CFD in order to investigate the underlying physical phenomena which affect the pressure drop in open-cell foams. In the case of geometry creating, they used micro CT and imaged based modeling techniques for modeling foam filters. The research focused only on clean pressure drop through foam filters, and the results indicated that reduction in pore size causes an increase in pressure drop through the filter. Skibinski et al. (2015) produced virtual foam filter with Laguerre–Voronoi tessellations (LVT) algorithm and conduct CFD analysis on the domain to investigate the relation between the pore size variation and pressure drop. They only modeled single phase flow through the filters then validate their results by conducting experiments on the foam filter media created by laser melting techniques. It was found that there is a strong relation between pore volume variation coefficient and permeability, but driving an exact correlation between them was not achievable due to differences in porosity of the designed structures.

Nie et al. (2018) carried out CFD simulations on gas-liquid separation in open-cell foam media. They used filters with packing density of 0.25, 0.15, and 0.05 at a velocity of 5 - 50 m/s. It should be noted that these authors utilised a Discrete Phase Model (DPM) instead of VOF (as per the current work). This means that deformation of liquid droplet and also accumulation of liquid was ignored in the Nie et al. (2018) study. The rational for this simplification was that VOF was claimed to be time consuming and/or computationally expensive.

Recently, Abishek et al. (2018) studied the effects of filter (non-woven and foam) representative domain size on the accuracy of the results. In the research, both two-phase flow and single phase flow were investigated by using CFD techniques. The results indicated that two-phase flow is more dependent on mesh resolution and the structure of the filter than the domain size. Furthermore, they found that the uncertainties can be reduced 10% when increasing the domain size from $50d_f$ to $100d_f$.

2.6 Summary

Although there has been much attention toward oil-mist filtration, still significant gaps in liquid-gas filtration remained to be filled by further investigations. As it was discussed in section 2.3, all proposed models are based on experimental data which are only applicable to limited conditions, so further study is required in this field.

Based on the presented review, the key gaps in literature are:

- Most of the previous research resulted in empirical and semi-empirical correlations which are limited to specific geometries and operating conditions;
- There is no study to provide comparison of different types of filters such as fibrous, knitted and foam media;
- Very limited studies on contact angle effects (research mostly focused on single fibre analysis);
- Wet pressure drop models are based on experimental data fitting which have application limitation. Moreover, there are limited models which work on single-phase condition and only works for fibrous filter media;
- The majority of the works focused on fibrous media (both numerical and experimental). Further research required in other types of filters such as:Open-cell foam and knitted media;
- The comparison between different coalescence filter structure performance is rare and significant portion of the published research is limited to on type of media, and evaluating the effect of some operating parameters on the performance;
- In experimental studies, the comparison for evaluating the parameters conducted in filter media which are not ideally equivalent;
- Majority of the published research focused in the global efficiency or performance enhancement, while there is no study in local optimising of the coalescence filters;
- There have been fewer studies on phobic media;
- The majority of CFD studies are limited to narrow range of inlet velocities;
- In numerical studies, there are no significant research on evaluating the virtual filter generation and evaluating the geometry.

This work aims to fill these gaps by:

- Generating different types of filter media virtually and evaluating the generation methodology and filter geometry against theory and experiments;
- Developing and applying CFD methods to model gas/liquid interaction in a typical filter media;

- Evaluating the performance and pressure drop in different types of filter by using CFD techniques;
- Analysing other types of filter media such as open-cell foam and knitted filters;
- Provide an equivalent condition in order to compare different filters by applying CFD;
- Validating the applied CFD model against experimental data;
- Investigating other parameters affecting filtration such as inlet velocity, and contact angle in liquid/gas systems;
- Analysing the contact angle effect on filters performance, and investigate its effects with combination of different filter structure and face velocities;
- Investigating pressure drop profile in order to locate the local optimum working condition in different filters;
- Building a model for studying coalescence filtration which is less expensive compared to experiments.

Chapter 3

Research Case

In the previous chapter, the key gaps in the literature were identified. It was found that the majority of previous works were focused on the theoretical or empirical models which are limited to a narrow range specific operating conditions. Moreover, most of previous studies focus on fibrous filters, while other filter types such as knitted and open-cell foams have received comparatively less attention. Furthermore, the lack of comprehensive comparison study of different filter media is evident.

Therefore, this research project aims to add a greater understanding to liquid filtration by creating different types of realistic filter media and conducting numerical and experimental studies. In particular, the effects of filter structure, wettability and inlet velocity will be assessed during simulations. The investigations will focus on the final filtration stage, in which filters attain steady state condition. It should be mentioned that this stage is crucial to understand as filters spend majority of their lifetime at this stage. This thesis will also study the effect of retained liquid in filter media on the pressure drop profile. The finding will be compared against experimental results. A research plan was developed to address these aims and objectives. In this chapter, an overview over the original research contained in this thesis has been provided, which can be categorised by the following:

- Creating representative filter geometries virtually (fibrous filters, knitted filters and open-cell foam filters) and validating the accuracy of the simulated filters against experimental study and theoretical models.

- Applying advanced CFD techniques (mesh generation for complex geometries, applying and validating multi-phase flow model) to simulate phobic filters and investigating the effect of filter structure and inlet velocity on

saturation, pressure drop and transport of residual oil through the filters.

- Applying advanced CFD methods for philic simulations and studying the effects of inlet velocity and filter structure.

- Investigating the effect of contact angle on residual saturation, pressure drop, and performance of different filters.

Chapter 4 provides a methodology description applied in this thesis for creating fibrous, knitted and open-cell foam filters in order to conduct numerical simulations. Moreover, this chapter explains the numerical techniques and experimental methodology utilised in this study.

Chapter 5 verifies the accuracy of the created virtual filter media against experimental results and theoretical models. After validating the single-phase results, the multi-phase simulation results are validated against previous experimental and numerical studies.

Chapter 6 examines phobic filters with different structures. The saturation, pressure drop, and quality factor are presented versus Reynolds number in fibrous, knitted and open-cell foam filter media.

Chapter 7 compares philic fibrous, knitted an open-cell foam filter media. The saturation profile, multi-phase pressure drop, and quality factor are calculated and presented. Furthermore, the inlet velocity variation was considered to evaluate its effects on saturation and multi-phase pressure drop.

Chapter 8 compares phobic and philic filters in order to investigate the effects of wettability (Contact angle) on saturation profile and multi-phase pressure drop in fibrous, knitted and open-cell foam filters at different inlet velocity. Moreover, the influence of contact angle on different filters' performance is identified.

Chapter 9 explores a local optimum region observed in experimental and simulated pressure drop curves. A working hypothesis is presented to allow estimation of this local optimum.

Chapter 10 presents a recap on all findings during the numerical and experimental study . Furthermore, a series of research topics are proposed for further research works.

Chapter 4

Methodology

In this chapter the methods adopted generating realistic virtual filter media for use in simulations are discussed. As will be detailed in the following, two different approaches numerical and experimental are employed in this research. In the case of numerical method, three types of different filter media (firbous, knitted and open-cell foam) are generated by using a combination of different software such as Python, Gmsh, Blender, and Matlab. In the next step, CFD techniques are applied by using Open Field Operation And Manipulation (OpenFOAM) software to model single-phase and multi-phase flows through generated filters with different structures. Single-phase simulations are carried out to validate the accuracy of the generated filters. Multi-phase modeling are employed to study the saturation, liquid transport, and pressure drop in the filters. Moreover, multi-phase simulations provide an insight to compare the performance of different generated filters.

In order to validate both single-phase and multi-phase numerical simulations, series of experiments are conducted. In the first step, initial sample filter measurements, preparation (phobic media), and experimental rig design are completed. Next, a number of clean pressure drop tests of different types of filters with different physical properties are conducted. Finally, two fibrous filters with specific physical properties are selected carefully for conducting multi-phase flow experiments. The final (equilibrium) saturation and pressure drop of these filters are measured in multi-phase tests.

4.1 Generation of Virtual Filter Media

In order to generate different filter media structure for this study, different approaches have been applied which will be explained separately for each filter type

in the following.

4.1.1 Fibrous Filter Generation

Non-woven fibrous filter is created by combination of Python code and Blender software. This methodology was developed by supervisors of this research, but the application and evaluation of these geometries conducted during this PhD study. In the initial stage, the primary inputs such as target packing density, fibre diameter, target filter dimensions (3-D), length of fibre elements, filter cross-section resolution, and orthogonality-index (for specifying the level of generating fibre elements in parallel planes and perpendicular to the flow direction) are provided to the Python script. In the next stage, statistical von Mises distribution is used to generate successive fibres with specified angle between the fibre element and the flow direction (Z axis in this study). Next step is to randomly rotate fibre elements through a specified angle, then translate them along Z axis. In the next step, the fibre elements lines transform to cylindrical fibre elements according to specified diameter by user. The script starts to estimate the resulted packing density in the given domain size, and compares it with the target packing density value. Iterative scheme will be used in the code until the target packing density reaches with no fibre element overlap, if the packing density estimation does not meet the target value. Finally, the Python output is modified to exact domain size in Blender software in stl format. Figure 4.1 presents all the explained stages.

As it is shown by the flowchart, the final file format will be in stl which is suitable for geometry meshing in OpenFOAM and conducting CFD simulations. Figure 4.2 compares the virtually generated fibrous filter to a realistic stainless steel fibrous media (SEM image).

As it can be seen from Figure 4.2, the generated filter using presented methodology is in good qualitative agreement with SEM of a real filter media.

4.1.2 Open-cell Foam Filter Generation

To generate an Open-cell foam filter geometry, free source packages including Gmsh, OpenFOAM, and Blender are used. In the first step, a bounding box is generated by meshing software Gmsh. In the next step, a tetrahedral cells are generated and exported as .vtk mesh file. This file is imported to OpenFOAM software, and the mesh is converted to a polyhedral mesh and exported as an obj file for modifying in Blender software. In Blender, the created foam skeleton in

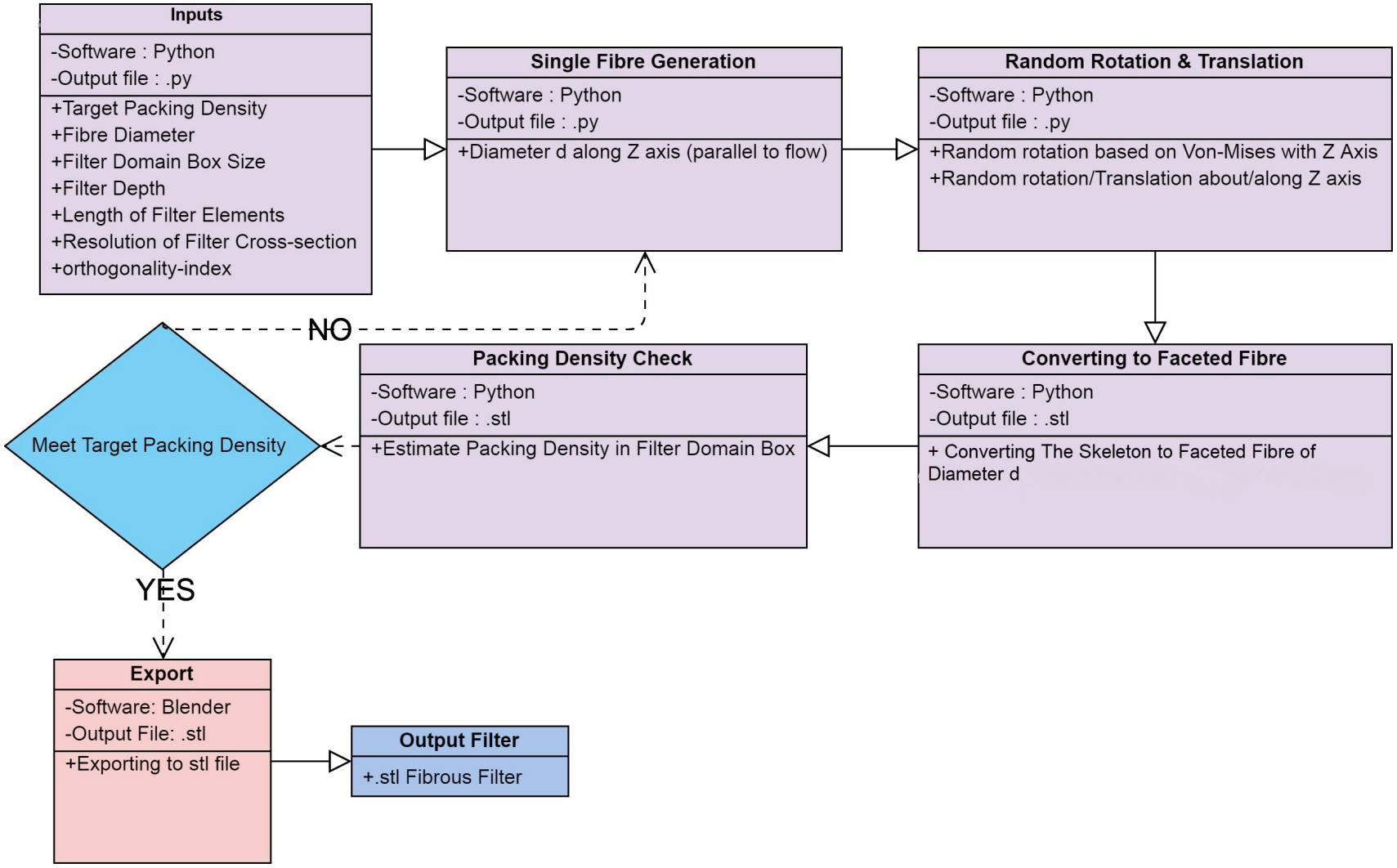

Figure 4.1: Methodology for generation of a fibrous filter

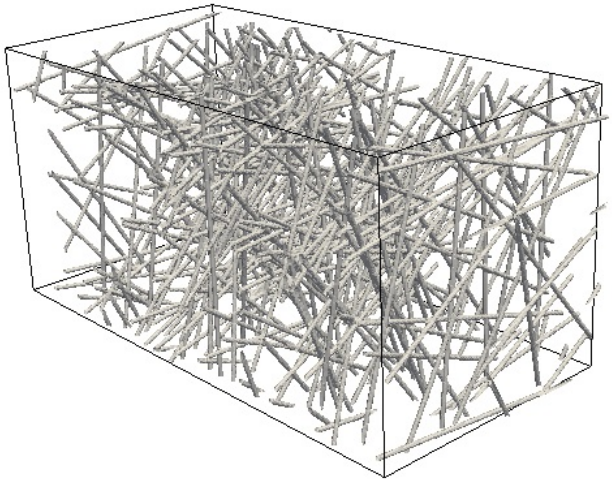

(a) Generated Fibrous Media

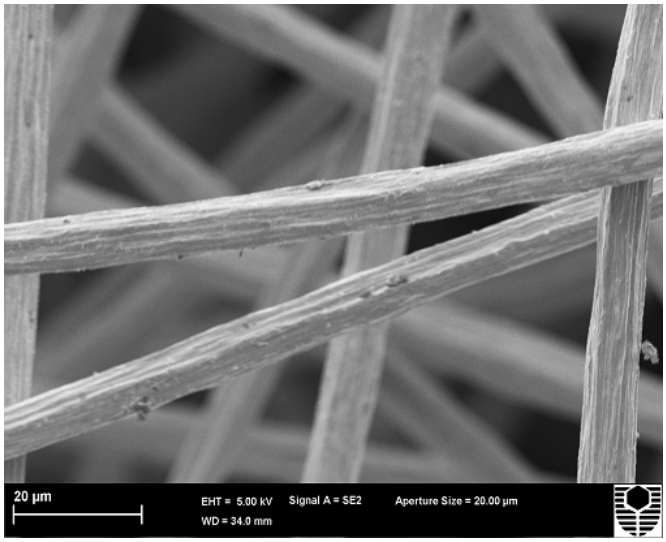

(b) SEM: Stainless Steel Fibrous

Figure 4.2: Comparison of a generated fibrous filter with SEM of a real filter media

previous step is transformed to an open-cell foam filter by creating cross-section for the elements (strut). The next step is to evaluate the resulted packing density and redoing the process if it does not meet the target packing density. Figure 4.3 represents the stages and methodology employed for generation of an open-cell foam filter.

Generated foam filter with the current method is compared against CT scan results of Diani et al. (2014), and it is presented by Figure 4.4.

An important point that should be discussed is the cross-sectional shape of the open-cell foam filters. As explained in the research by Abishek et al. (2017), the cross-sectional shape of foam filters' strut mainly depends on the packing density and material of the filters. In higher density foam filters the cross-sectional shape is circular, while relatively low density polymer foams resulted in circular-horn triangular shape. Moreover, Schmierer and Razani (2006) showed that circularity of the cross-sectional shape of a foam filter strut is a function of filter packing density where by increasing the packing density from 2 to 12 %, the circularity of the strut shape decreases linearly. In this research, a circular cross-sectional shape is considered and d_f denotes the strut diameter in foam filter discussions. It can be seen from Figure 4.4 that the generated foam filter with using the presented methodology is in good qualitative agreement with the CT Scan of a real media.

4.1.3 Knitted Filter Generation

For generating a knitted filter media, a combination of MATLAB software and Blender has been used. In the initial step, the user-controlled parameters such as: height and width of the loops, number of loops in each row, number of rows, thickness of the filter, spacing between layers, and packing density are entered to the MATLAB code. A single loop is generated in the next stage based on the given control parameters. In the following step, a row of the knitted loops is created along X axis. In the same plane, loops added above the previous created knitted row to from a knitted sheet. Based on the given knitted sheet gap, the knitted planes duplicates along the Z axis. In the next step, the packing density is estimated and compared to the target value. This process repeated until the target packing density is achieved. The generated knitted skeleton is imported to Blender software in order to generate the knitted faceted according to the target element diameter. Finally, the geometry in stl format is created and exported from Blender software. Figure 4.5 shows the flowchart of a knitted filter generation.

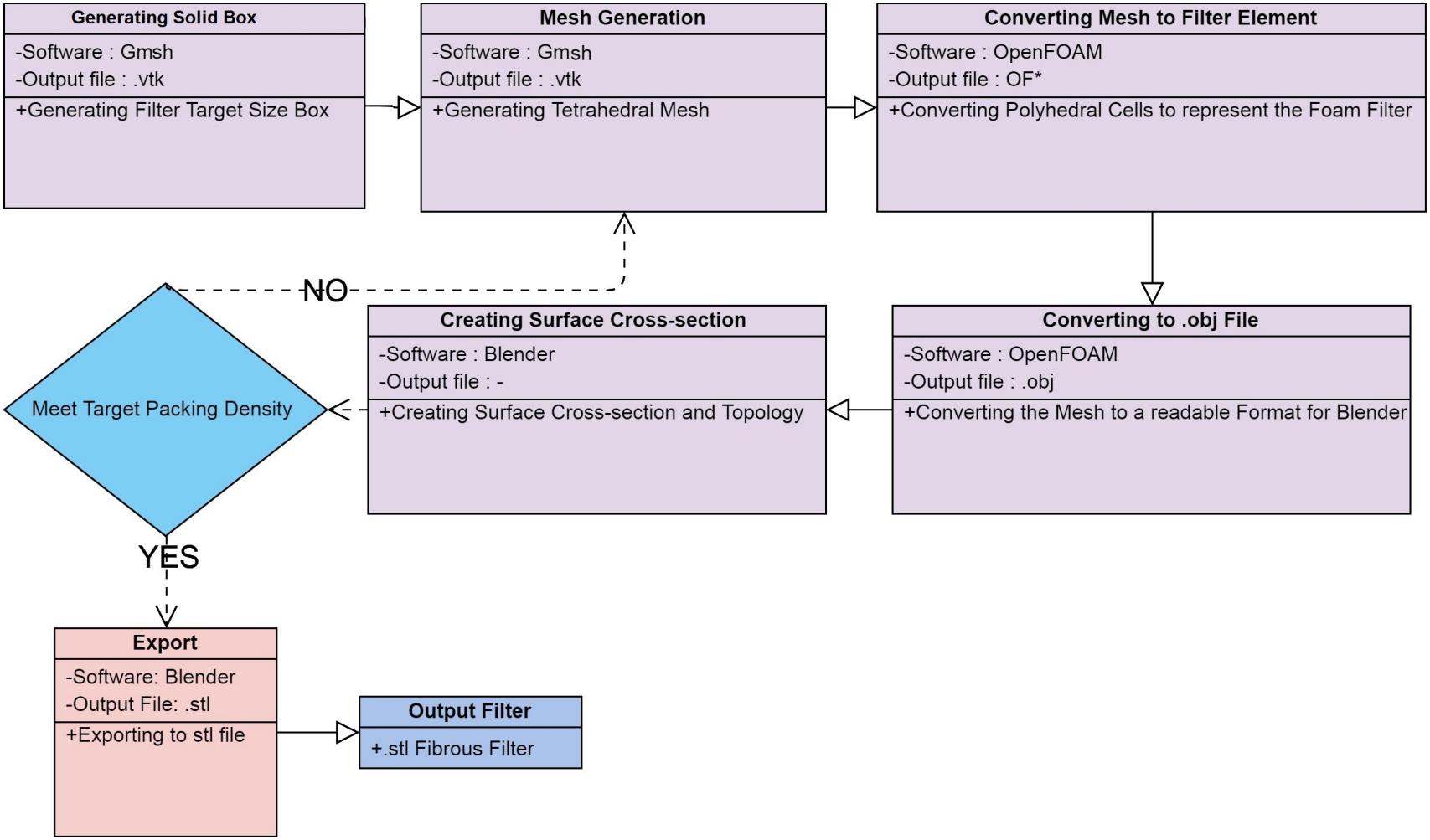

Figure 4.3: Methodology for generation of an open-cell foam filter

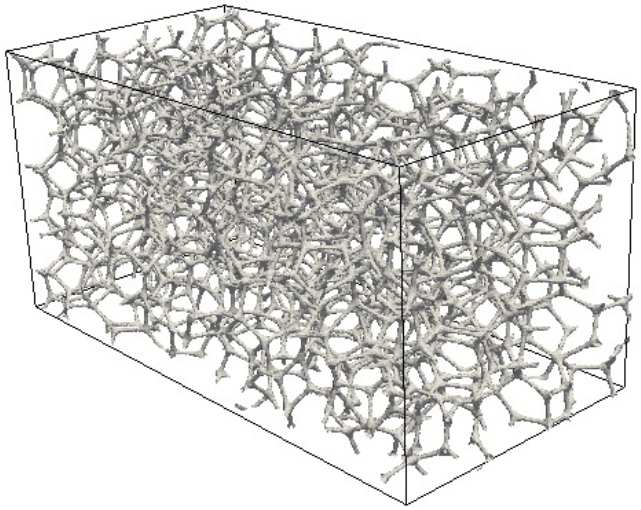

(a) Generated Open-cell Foam Media

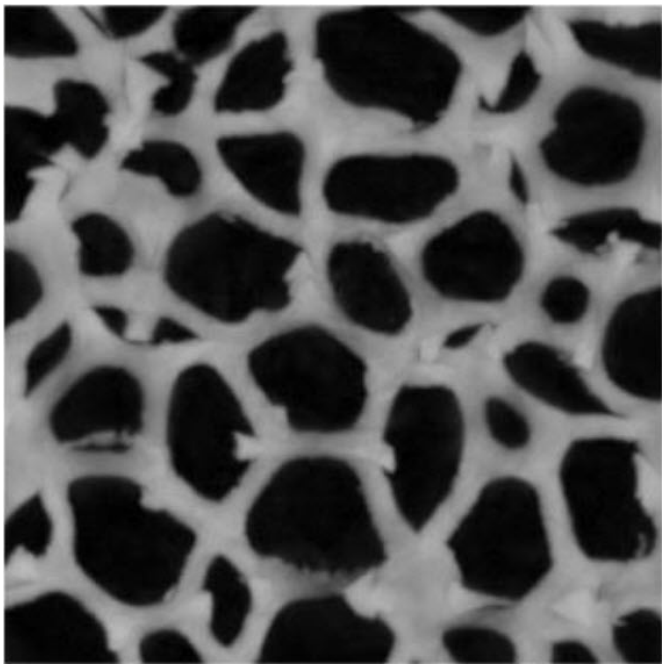

(b) CT Scan

Figure 4.4: Comparison of generated foam filter with CT scan of a real filter media (Diani et al. (2014))

Figure 4.6 indicates a good qualitative agreement between the generated knitted filter and a schematic (Ceken et al. (2012)) of the knitted structure.

4.2 Computational Methodology

Navier-Stokes equations govern the fluid mechanics part of systems like mist filters. These equations are partial differential and due to their non-linear nature, analytical solutions are only available for a limited number of highly simplified cases. Therefore, a numerical approach is required. Computational Fluid Dynamics (CFD) provides a solution to these equations for a given system by discretising the model equations, applying proper boundary conditions, initial conditions and solving the derived equations iteratively.

A number of well tried options are available to researchers, for the implementation of CFD techniques, these include commercial CFD packages (e.g. VisualCFD, SimScale, FLUENT, ANSYS-CFX), open source CFD packages like OpenFOAM, or developing their own code. Each of these options has its advantages and disadvantages. In regard to commercial packages, the main advantages are technical support, graphical user interface (GUI), and easy to pre-processing and post-processing the CFD problem. On the other hand, their notable disadvantage is that they are expensive (license fees involved), particularly if the simulations are complex and require parallel simulations. In the case of an open source software like OpenFOAM which is developed by OpenCFD Ltd, the simulations are cost effective (no license required), easy to simulate parallel cases, free to alter the software, has large user/developer base, and it is reliable and accurate. However, there are some drawbacks associated with that like limited user support, and the need for additional software for post-processing.

The CFD package choice criteria is mainly depends on the available resources, size, complexity and goals of the simulations. Due to the mentioned advantages of OpenFOAM software, it is used in this work.

4.2.1 Case Study for the Research

As discussed in Chapter 3, the research has been conducted on different filter structures both numerically and experimentally. Based on the methodology explained in section 4.1, three types of fibrous, knitted and open-cell foam filters have been generated and studied in this research. Figure 4.7 presents all three

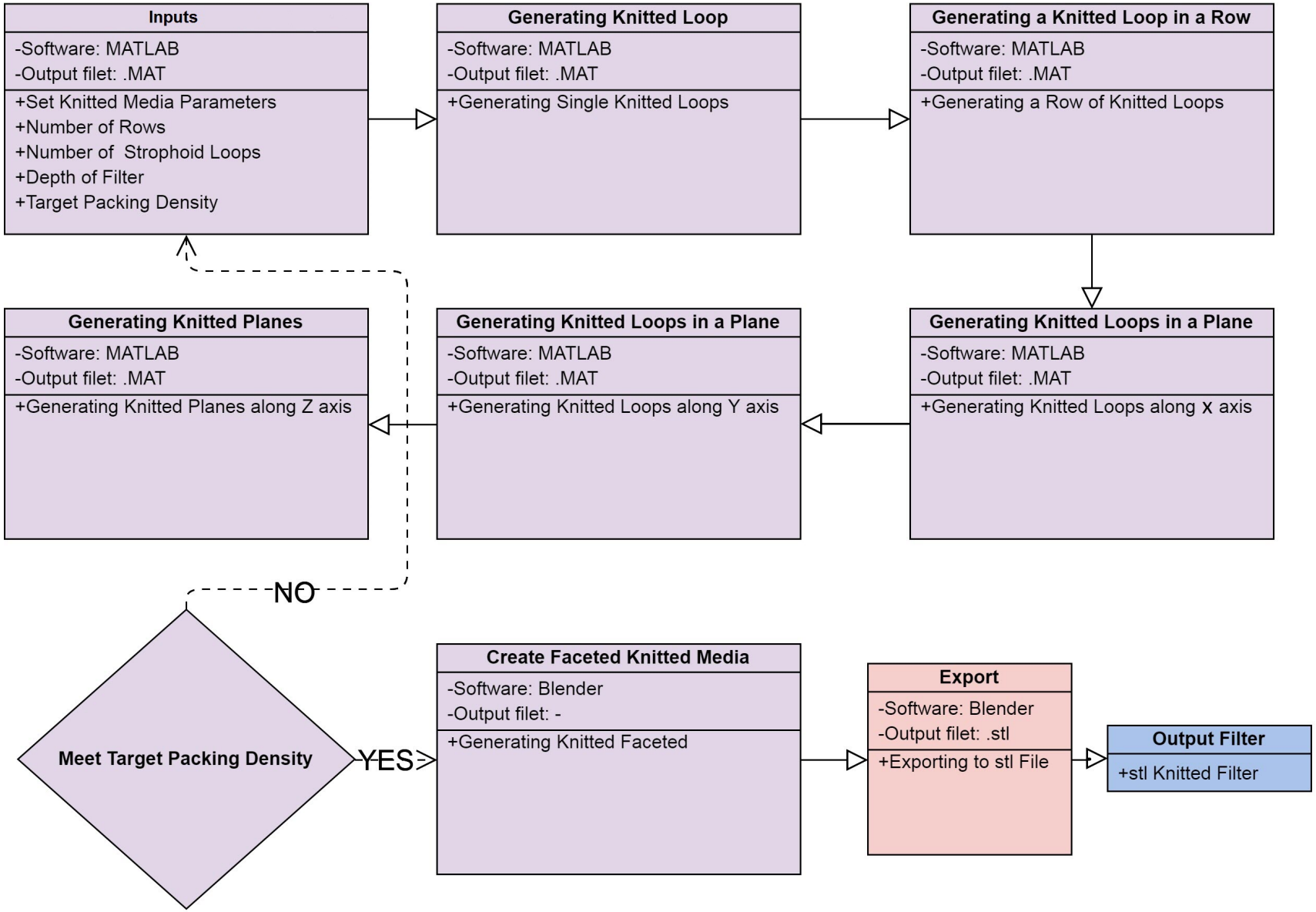

Figure 4.5: Methodology for generation of a knitted filter media

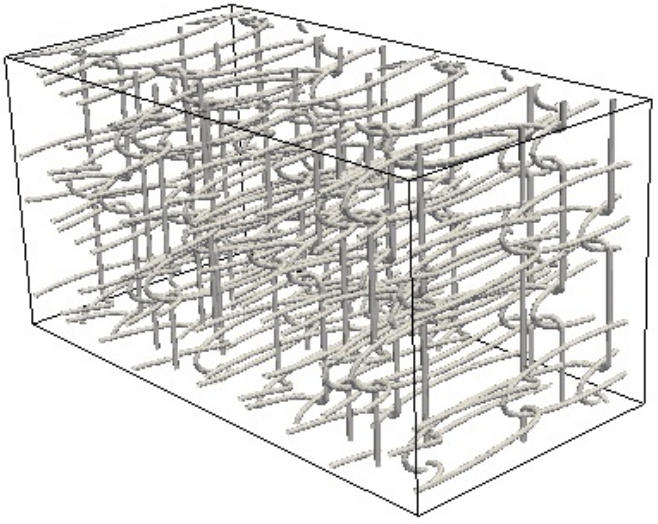

(a) Generated knitted Media

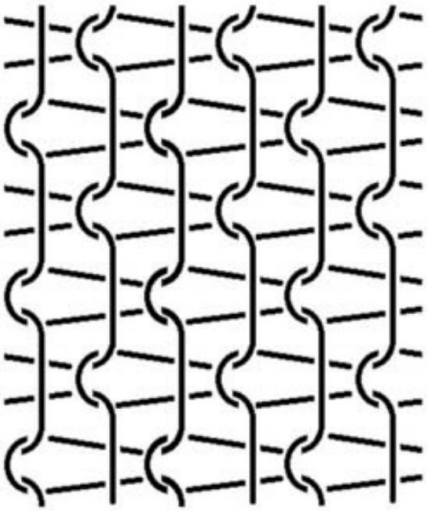

(b) Schematic

Figure 4.6: Comparison of generated knitted filter with a schematic (Ceken et al. (2012)) of the knitted structure.

generated filters used in this study.

After evaluating the generated filter geometries, the aim of this study is to compare the liquid progress, pressure drop, and performance of pre-saturated oil-mist filters in different geometric configuration, different air flow condition, and different contact angle. All the cases are pre-saturated since the simulations are time-consuming, and it would be computationally too expensive to conduct all the simulations with unloaded filter. In order to produce comparable media with different structures, all filter media have packing density of 2% with fibre element diameter of $8.5\mu m$. The filter dimensions for all the cases (both multi-phase and single-phase) are : $0.5mm(x)$, $0.5mm(y)$, and $2mm(z)$. Figure 4.8 shows the dimensions on the fibrous filter as an example. It should be noted that the aim of this study is to evaluate the virtual filter generation, CFD modeling of oil-mist filtration and re-entrainment, and comparing performance of different filter structures. Therefore, similar physical properties are considered for fibrous, knitted and foam filters. Table 4.1 summarised the generated filters physical properties.

Table 4.1: Properties of the filters used for numerical study in this research.

Filter	α (%)	l (mm)	w (mm)	d_f (μm)
Fibrous	2	2	0.5	8.5
Foam	2	2	0.5	8.5
Knitted	2	2	0.5	8.5

In regard to CFD simulations, the computational domain was extended by 1 mm from both inlet and outlet planes to be placed far from any strong gradients. The dimensions considered is $w = 58 \times d_f$ and $l = 200 \times d_f$. Selecting larger dimensions for these simulations is impractical due to the significant increase in computation costs and time. It was found by Abishek et al. (2018) that the minimum size required for simulating the flow in filter media and capturing the largest relevant scale characteristics and structures is the size between $50 \times d_f$ and $100 \times d_f$. The same work also showed that multi-phase flows are more sensitive to mesh resolution than the domain size in comparison to single-phase flows. Since the main purpose of this research is to investigate the last filtration stage, and in order to minimize the computational efforts, all the simulations were commenced by 30% of filter media as initial saturation with Di-Ethyl-Hexyl-Sebacate (DEHS). It is a mono-component, non-soluble, odourless and colourless liquid which is suitable for producing stable oil aerosol. Moreover, DEHS is a common laboratory oil with very low vapour pressure, therefore evaporation can be ignored. Also, DEHS has similar properties (at room temperature) to many oils

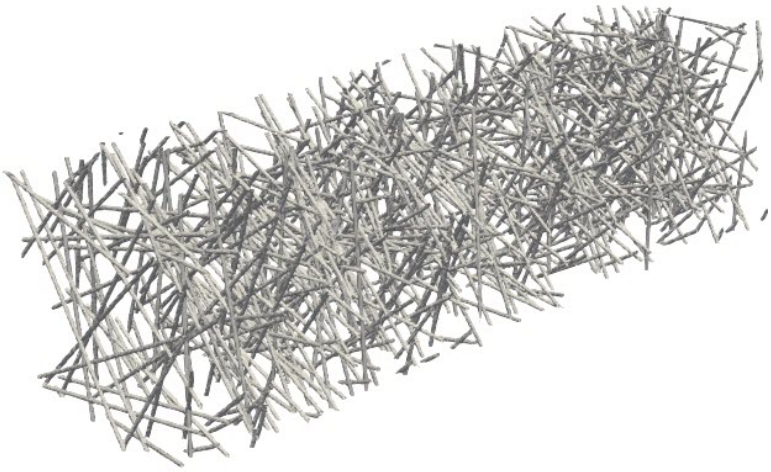

(a) Fibrous filter

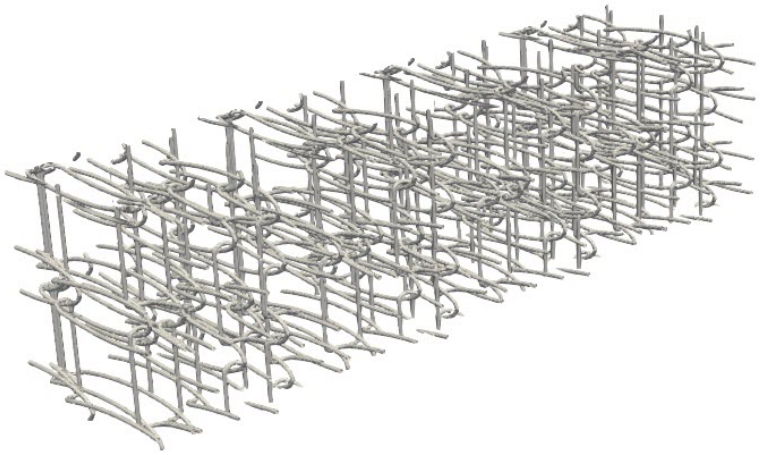

(b) Knitted filter

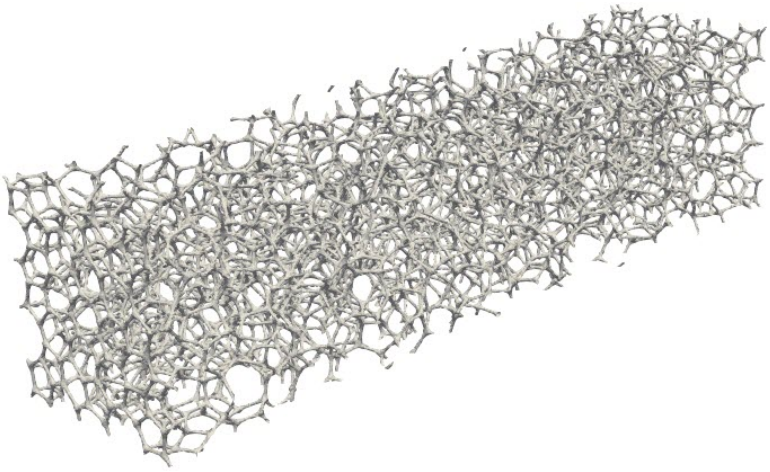

(c) Foam filter

Figure 4.7: Filter geometries generated for implementing CFD calculations.

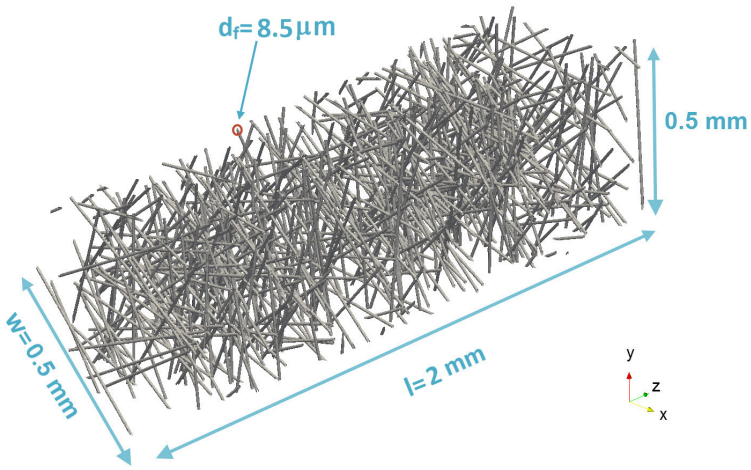

Figure 4.8: Filter dimensions for single-phase and multi-phase studies (Fibrous type as an example)

utilised industrially (Heim et al. (2008)), as typical (elevated) operating temperatures. The physical properties of DEHS and air (fluids employed in this research) are summarised in Table 4.2.The value of surface tension, σ, is between air and DEHS.

Table 4.2: Physical properties of DEHS and air employed in this study.

	$\rho(kg/m^3)$	$\mu(Pa.s)$	$\sigma(N/m)$
DEHS	914	0.025	0.0324
Air	1.1845	1.557×10^{-5}	–

Figure 4.9 shows the initial position of droplets in an open-cell foam case with 30% initial saturation as a representative.

There are number of reasons that the filters are loaded with discrete droplets instead of partially filled region by oil. First of all, there are different filters with distinct structure of elements. Therefore, presence of a big bulk of oil droplet in the center of each filter does not provide an ideal condition for comparison. By spreading the droplets (oil-mists) throughout the filters, a comparable condition is achieved as all the filters have the initial saturation throughout their domain equally and the possibility of holding droplets in the intersections of elements will be decreased. Moreover, some simulation tests have conducted on fibrous filter (as an example) to evaluate the initial droplet distribution effect on the final sat-

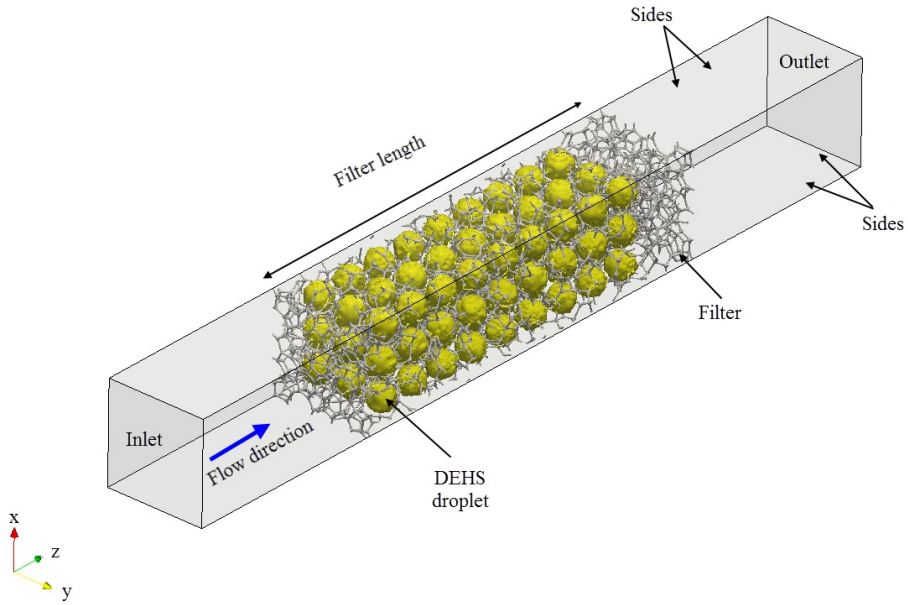

Figure 4.9: Initial position of distributed droplets

uration results. In these simulations, two inlet velocity cases (2 and 5 m/s) are selected and compared to initial zero velocity condition. In initial zero condition simulations, an initial sufficient time (30 units of dimensionless time) is given to the droplets for coalescence, then the velocity set to 2 or 5 m/s for different cases. The results of these tests are shown by the Figure 4.10. S is saturation volume fraction (saturation) which can be calculated by Equation 4.1:

$$S = \frac{V_l}{V_{void}} \tag{4.1}$$

Where S is saturation volume fraction (saturation), V_l is the volume of liquid phase (DEHS) in the filter domain, and V_{void} is the summation liquid phase and gas volume (volume inside the filter not occupied by fibres). In Figure 4.10, τ is dimensionless time described by Equation 4.2:

$$\tau = \frac{t \times u}{l} \tag{4.2}$$

Where t is time, u is inlet velocity, and l is the filter thickness.

It is evident from Figure 4.10 that the difference in final saturation in both test cases is marginal which confirms that the initial droplet distribution employed

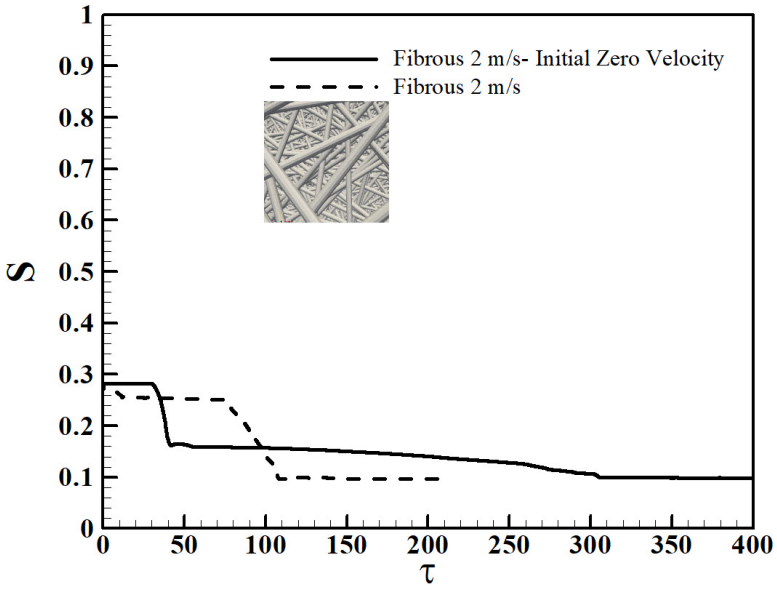

(a) 2 m/s case

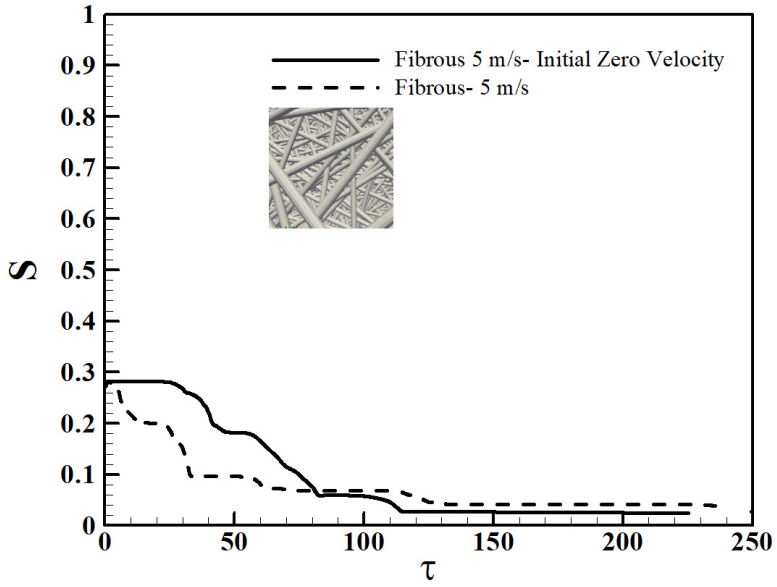

(b) 5 m/s case

Figure 4.10: Comparison of 2 and 5 m/s test cases against initial zero velocity condition.

in this study is an acceptable condition. It is worth mentioning that preliminary studies were conducted to determine the minimum saturation required for the simulation to converge to the true solution (saturation level). It was found that 30 % of the simulated filter volume filled with DEHS is needed.

There are two static contact angles considered in this study. The contact angle between fibre and liquid (oil) is considered $\theta = 120°$ for phobic (oleophobic) simulations and $\theta = 20°$ for philic (oleophilic) cases. Due to the differences of phobic and philic filters in retaining liquid ability, two ranges of inlet face velocities are prescribed at inlet boundary. For phobic simulations, 0.05, 0.1, 0.5, 1 and 2 m/s inlet face velocities are considered. In regard to philic media study, 0.1, 0.5, 1, 2, 3, and 5 m/s inlet velocities are considered. These face velocities resulted in $0.0065 \leq Re_f \leq 3.23$. Face velocities ranging from 0.05 to 1 m/s are common in the majority of filtration applications (Mead-Hunter et al. (2013); Kampa et al. (2014)) and higher velocities (2-5 m/s) can be seen in industrial filters (Poon and Liu (1999)), explosive trace detection technologies (Klouda et al. (2011)), or aerosol instrumentation abroad aircraft (McMurry (2000)) which are normally between 2 and 10 m/s.

4.2.2 Governing Equations

In this section, the numerical assumptions, mathematical formulations, initial and boundary conditions, and solution techniques for both single-phase and multiphase models will be explained.

4.2.3 Mathematical Model for Single-phase Flow

Assumptions

The general assumptions for the mathematical model developed are as follows:

- Steady state
- The working fluid, air, is incompressible and isothermal with constant properties.
- Laminar flow is assumed to prevail inside the solution domain for the face velocities considered in this study ($Re_f < 15$).

Mathematical Formulation of Single-phase flow

Based on the given assumptions, the continuity and conservation of momentum equations will be expressed as the following:

$$\nabla \cdot U = 0 \tag{4.3}$$

The conservation of momentum will be simplified to:

$$\nabla \cdot (UU) = -\nabla P + \nabla \cdot (\nu \nabla U) \tag{4.4}$$

Boundary Conditions of single-phase flow

In order to solve partial differential equations of continuity and conservation of momentum, the following boundary conditions are implemented:

- **Inlet**: for the velocity field, the *fixedValue* boundary condition is imposed. In this boundary condition, it is assumed that the velocity is constant at the inlet plane. In regard to pressure field, *fixedFluxPressure* is considered. In single-phase study, this boundary condition imposes a zero gradient condition, although its effect in multi-phase flows is different which will be explained in the related section.

- **Outlet**: for the velocity and pressure fields at outlet, *pressureInletOutletVelocity* and *totalPressure* boundary conditions are considered, respectively. *pressureInletOutletVelocity* specifies zero gradient at all times, except on the tangential velocity which is set to 0. The *totalPressure* condition specifies according to the following equation:

$$P = \begin{cases} P_0 & \text{for outflow} \\ P_0 - \frac{1}{2}|u^2| & \text{for inflow} \end{cases} \tag{4.5}$$

- **Surrounding sides**: In this research, Symmetry boundary condition is used for the surrounding sides of the computational box, even though there is no plane of symmetry in a disordered fibrous structure. This boundary condition is considered for the simulations because the flow is mainly in the through-plane direction, and lateral flows are negligible (Jaganathan et al. (2008); Hosseini and Tafreshi (2010b)).

- **Fibers**: No Slip boundary condition is considered for fibers which means the flow velocity at the stationary solid wall (fibres in this case) is equal to zero. Furthermore, according to the diameter of fibers($8.5\mu m$) and inlet velocities lead to $0.01 < Kn_f < 0.05$ which is outside of slip flow regime (Pich (1971)). For implementing this condition in OpenFOAM, *fixedValue* boundary condition with 0 value is set for the velocity field. For the pressure field *fixedFluxPressure* is considered which is described earlier.

Solution Techniques of the Single-phase Flow

After discretising the computational domain using unstructured meshes, simpleFOAM solver is used to solve incompressible single-phase flow. OpenFOAM is used in this research for conducting CFD techniques. This package uses a cell centred finite volume method in order to solve partial differential equations of continuity (4.3) and momentum(4.4) equations. In this method, all equations integrated over each control volumes (cells) on the mesh, and Gauss's theorem applies to convert surface integrals which contain divergence term to volume integrals. This approach lead to conserve the mass and momentum quantities at the discrete level. Furthermore, equations are solved in a fixed coordinate and mesh structure does not change over time even for transient simulations.

By solving momentum equation for velocity, the result should satisfy continuity as well. In order to achieve this goal, a divergence of the momentum equation should be taken and substitute in to continuity equation which resulted in Poisson equation for the pressure. In order to solve this complicated equation, simpleFoam apply the SIMPLE (Semi-Implicit Method for Pressure Linked Equations) algorithm (Patankar and Spalding (1972)). Momentum and pressure equations should be solved iteratively which the procedure is as below:

- Step 1, the momentum equation is solved to calculate intermediate velocity field.
- Step 2, a correction to pressure field is achieved by solving pressure equation.
- Step 3, velocities from step 1 are updated based on new pressure from pressure correction.
- Step 4, the fluxes at the cell faces and boundary are updated.
- Step 5, this process is repeated until the convergence is achieved. The convergence criteria was set to 10^{-6}.

To maintain the stability of the mentioned procedure some techniques should be employed. The stability is improved by using under relaxation factors between 0 and 1. For all the equations under relaxation factor is considered 0.7, while for the pressure equation it is set to 0.3. In regard to the numerical schemes, second order Gaussian finite volume integration using linear interpolation is employed for gradients of pressure and velocity fields. Gaussian finite volume integration interpolates the values from cell centers to face centers, and it is the most common scheme (Greenshields (2011)). Linear-upwind divergence scheme is used for diversion terms. This scheme is second order which is derived from upwind and returns upwind weighting factors and also uses a gradient-based explicit correction.

4.2.4 Mathematical Model for Multi-phase Flow

Assumptions

The general assumptions for the mathematical model developed are as follows:

- The carrier fluid, air, is incompressible and isothermal with constant properties.
- The liquid phase considered is DEHS with constant properties (given by Table 4.2).
- Laminar flow is assumed to prevail inside the solution domain for the face velocities considered in this study ($Re_f < 15$).
- Contact angle between the liquid phase and solids in the study assumed to be static in both philic and phobic media.

Mathematical Formulation of the Multi-phase Flow

Multi-phase flows where two immiscible fluids present, additional algorithm compared to single-phase will be required to capture the interfaces between them. There are two computational methods for calculating the interfaces named surface methods and volume methods.

Surface Methods

There are different ways to mark the interface which are: particles on interface developed by Daly (1967), Height functions developed by Nichols and Hirt (1973), Level set method presented by Osher and Sethian (1988), and Surface fitted methods which developed and modified by many researchers (Dervieux and Thomasset (1980); Takizawa et al. (1992) and Clarke and Issa (1997)). The extensive review of all these methods are discussed in Ubbink and Issa (1999) work.

Volume Methods

In volume methods, the fluid on the both sides of the interface will be marked. So, as it can be deduced the exact location of the interface is not explicitly defined, therefore special technique required. The majority of these methods use the calculation of the surface tension forces presented by Brackbill et al. (1992) which is known as continuum surface force (CSF). Volume of fluid is a volume method which uses a scaler indicator function between 0 and 1 for each fluid. Every cell occupied by fluid 1 assigned 0 and each cell filled with fluid 2 assigned indicator 1, and cells with value between 0 and 1 means contain the interface. For a better demonstration, Figure 4.11 shows volume fraction on a discrete mesh. This method has some advantages in compare to particle marker method like less computations needed because it only store a scaler number for each cell and solve only one extra transport equation (for the indicator) to calculate its propagation through the domain. However, there is a drawback associated with this method like smearing the step profile of interface over several cells in convective differencing schemes (Ubbink (1997)).

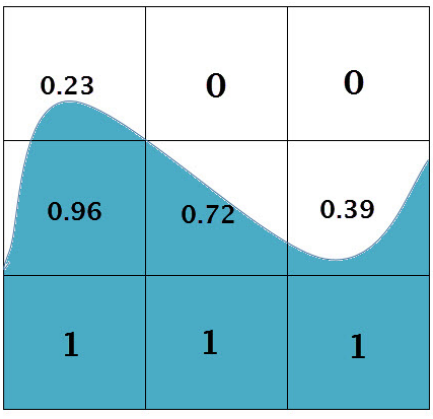

Figure 4.11: Volume fractions on a discrete mesh

VOF is the most widely used method in modeling multi-phase flows and cat-

egorised into two variants:

(1) Geometric VOF methods, which uses geometric operations to a sub-cell representation of the interface and then compute the volume fluxes by a Lagrangian sense. There are some disadvantages associated with this approach such as increased computational expenses and difficulty to be implemented in higher dimensions (Xiao et al. (2011)).

(2) Algebraic VOF methods, which eliminates the reconstruction step and instead combines first and higher order schemes in order to preserve the sharpness of the interface (Ubbink and Issa (1999)).

When it comes to comparison of these two methods, it should be noted that geometric VOF schemes have more accurate results, although at an extensive cost of computations. Moreover, geometric VOF is restricted to be used in specific mesh type, like hexahedral meshes, and it is substantially complicated to implement. On the other hand, algebraic VOF schemes are faster, although less accurate. Furthermore, they can be easily implement and developed for different general mesh types (Deshpande and Anumolu (2012)).

In this work, the algebraic approach is used to simulate multi-phase flow. Among different numerical methods, the open source VOF methodology (proposed by Ubbink and Issa (1999)) named interFoam which was implemented in OpenFOAM CFD package as reported by Deshpande and Anumolu (2012). Several works have used interFOAM in their research, and it is well documented (Abishek et al. (2017); Monfared et al. (2016); Hasan and Raisul (2016); Paik and Shin (2015); Oggiano et al. (2017); Basha (2016); Mead-Hunter et al. (2017); Orlov et al. (2015)).

Three-dimensional simulation of multi-phase flow is performed by using Volume of Fluid (VOF) method. In VOF a volume fraction parameter, γ, is used to indicate the presence of each phase in different locations of the computational domain. In this study for the phase 1 (air) the $\gamma = 0$ and for phase 2 (oil) $\gamma = 1$. Based on the given assumptions the governing equations are continuity , momentum , and phase fraction equation which are:

$$\nabla \cdot U = 0 \tag{4.6}$$

$$\frac{\partial \rho_b U}{\partial t} + \nabla \cdot (\rho_b U U) = -\nabla P + \nabla \cdot (\mu_b \nabla U) + \rho_b g + f_\sigma \tag{4.7}$$

$$\frac{\partial \gamma}{\partial t} + \nabla \cdot (\gamma U) = 0 \tag{4.8}$$

In equations 4.6 - 4.7, U is the velocity vector field, P is the pressure field, and g is gravitational acceleration. Parameters ρ_b and μ_b are bulk density and bulk dynamic viscosity calculated based on weighted of phase distribution as below:

$$\mu_b = \gamma \mu_g + (1 - \gamma)\mu_l \tag{4.9}$$

$$\rho_b = \gamma \rho_g + (1 - \gamma)\rho_l \tag{4.10}$$

Where in Equations 4.9 and 4.10, g and l stand for gas (air) and liquid (oil) phases, respectively. The last term on the right-hand side of the Equation 4.7, f_σ is the interfacial surface tension force density known as continuum surface tension force (CSF) presented by Brackbill et al. (1992). This force term defined as:

$$f_\sigma = -\sigma k(\nabla \gamma) \tag{4.11}$$

Where in Equation 4.11, σ is the surface tension of the liquid-air interface, and k is curvature ($k = \nabla \cdot (\frac{\nabla \gamma}{|\nabla \gamma|})$). It should be noted that this force is only presents just at the interface (where $0 < \gamma_l < 1$), and it is zero elsewhere in the domain. The main purpose of adding this term to the momentum equation (4.7) is to alleviate the computational issues associated with a sharp pressure jump that exists cross the liquid-gas interface.

Initial and Boundary Conditions of Multi-phase Flow

The boundary conditions applied in multi-phase simulations are the same as conditions presented in single phase boundary conditions with extra initial condition and volume fraction boundary condition as below:

- **Initial condition**: The computational domain is loaded with 30 % of the filter void volume. The embedded utility called setFields is used for specifying the regions inside the computational domain filled with DEHS. The oil droplets distributed through the filter with zero initial velocity.

- **Volume fraction**: The contact angle between fibre and liquid (oil) is imposed by using *constantContactAngle* condition which allows to consider a

constant angle at the corresponding boundary. $\theta = 120^\circ$ is set for phobic simulations and $\theta = 20^\circ$ for philic cases as static. At the inlet boundary, fixed value equal to zero is assigned for the volume fraction. At the outlet boundary, the *inletOutlet* boundary condition is employed. This is a condition which assumes a zero gradient condition for outflow and a constant value of 0, representing air, for inflow. Symmetry condition is used for surrounding sides boundaries.

fixedFluxPressure, the pressure field boundary condition, is imposed to inlet and outlet boundaries in multi-phase flow (similar to single-phase flow simulations). The main difference of this boundary condition in multi-phase flows compared to single-phase flows is the effect of body forces like surface tension which is present in multi-phase simulations. This condition adjusts the pressure gradient according to this body force.

Solution Techniques of Multi-phase Flow

In VOF method, volume fraction equation in conjunction with momentum and continuity is solved simultaneously. For solving the coupled equations of momentum and continuity, a combination of PISO and SIMPLE algorithms known as PIMPLE is used. The principle of this algorithm is as follow: within one time step, a steady state solution with under relaxation is searched. After finding the solution, the calculations proceed on time. In this algorithm an outer correction loop is used to ensure that the explicit parts of the equations are converged. In the next step, the answers evaluated against pre-defined convergence criteria, and if meets, the calculation move on in time. This procedure continues until the solution reaches the final time. Once the velocity field is found, the Equation 4.8 is solved to acquire the volume fraction. Although the velocity and volume fraction gained by solving Equations 4.6 - 4.8 at every cell in the domain, the location of the interface still need to be identified with high resolution. To achieve this, two fluid formulation technique is employed where the contribution of each phase in velocity can be calculated:

$$\frac{\partial \gamma}{\partial t} + \nabla \cdot (\gamma U_g) = 0 \tag{4.12}$$

$$\frac{\partial (1-\gamma)}{\partial t} + \nabla \cdot ((1-\gamma) U_l) = 0 \tag{4.13}$$

Where U_g and U_l are velocity vector fields of gas and liquid phase, respectively. To proceed the methodology, it is assumed that the both phases have contribution

to the convection of interface in the domain according to their volume fraction, therefore:

$$U = \gamma U_g + (1-\gamma)U_l \tag{4.14}$$

The equation 4.8 can be rearranged to the following equation:

$$\frac{\partial \gamma}{\partial t} + \nabla \cdot (\gamma U) - \nabla \cdot (\gamma(1-\gamma)U_c) = 0 \tag{4.15}$$

Where $U_c = U_g - U_l$ is compression velocity (Deshpande and Anumolu (2012)). By comparing equations 4.8 and 4.15, it can be seen that a convection term is added to Equation 4.15. By close attention, it can be deduced that this term is only nonzero at the interface, and it will be zero in both pure phases(gas or liquid), as the γ is either 0 or 1. The main advantage of the compression velocity is to compress the interface and make it thinner, so it ensures to have a sharp interface. The compression velocity is give by:

$$U_c = n_f \min\left[C_\gamma \left|\frac{\varphi}{S_f}\right|, max\left(\frac{|\ \varphi\ |}{|\ S_f\ |}\right)\right] \tag{4.16}$$

n_f is the interface normal vector, φ and S_f are the cell face volume flux and surface area, respectively. $\left(\frac{|\varphi|}{|S_f|}\right)$ is the magnitude of velocity. C_γ is the compression factor specified by user, and it can be between 0 to 4. The higher compression factor resulted in thinner interface, but it causes errors in interfacial curvature and interfacial smearing (Deshpande and Anumolu (2012)). In all the simulations, $C_\gamma = 1$ is considered which has shown to achieve the most reliable solution (Deshpande and Anumolu (2012)).

There are two main concerns associated with free surface which are diffusion and spurious currents. As explained before, using compression velocity technique is the main way to overcome false and artificial diffusion through the domain. In regard to spurious currents it should be noted that these are unphysical flows in vicinity of interface due to numerical errors (Deshpande and Anumolu (2012)). There are two mechanisms responsible for development of the spurious currents which are:

- Inaccurate Interface Capture: when the interface captured approximately in a numerical mesh with a step-shape rather than smooth, this discontinuity results in spurious currents. Therefore, the spurious currents increase by decreasing local cell size (Deshpande and Anumolu (2012)).

- Neglecting viscosity in momentum equation (4.7): this leads to failure in achieving force balance between pressure gradient and surface tension force on the right hand side of the momentum equation which causes the acceleration of flow velocity and development of spurious currents.

Deshpande and Anumolu (2012) proposed a max time step as a constraint to control the solution and prevents from spurious currents development.

$$\Delta t = \frac{1}{2}\big[C2\tau_\mu + \sqrt{(C_2\tau_\mu)^2 + 4C_1\tau_\rho^2}\big] \tag{4.17}$$

Where;

$$\tau_\mu = \frac{\mu\Delta x}{\sigma} \tag{4.18}$$

$$\tau_\rho = \sqrt{\frac{\rho\Delta x^3}{\sigma}} \tag{4.19}$$

In Equation 4.17, C_1 and C_2 are user specified constants which based on the investigations of Deshpande and Anumolu (2012) should be set to $C_1 = 0.01$ and $C_2 = 10$ to achieve a stable solution.

Furthermore, in order to improve the stability of the solution, an adaptive time step has been used. The adaptive time step works based on calculation of Courant number (4.20). A brief description of Courant number will be provided in the following.

Courant–Friedrichs–Lewy (CFL) is a condition that states for solving certain partial differential equations, the time step should be less than certain time, otherwise the simulation results are not valid (Courant et al. (1928)). The general CFL condition form is:

$$C = \triangle t \sum_{i=1}^{n} \frac{u_{x_i}}{\triangle x_i} \leq C_{max} \tag{4.20}$$

for the three dimensional case it becomes:

$$C = \frac{u\triangle t}{\triangle x} + \frac{v\triangle t}{\triangle y} + \frac{w\triangle t}{\triangle z} \leq C_{max} \tag{4.21}$$

Where the dimensionless number,C, is called the Courant number, u, v and w are the magnitude of the velocity in x, y and z directions, respectively. $\triangle t$ is the time step, and $\triangle x, y, z$ are the the length interval. The Courant number basically indicates the number of meshes advanced during the time-step. According

to equation 4.20, $C_{max} = 1$ is the stability criteria for 1-D problems, while in 2-D and 3-D cases, Courant number should not be greater than 0.5 and 0.3, respectively. As it can be deduced form Courant number equation (equation 4.20), the mesh size and time-step size are dependent on each other, and they should be considered before starting the simulations to achieve a stable and valid results. Therefore, based on specified Courant number, a new time step size is calculated to maintain the limit imposed by Courant number.

To implement all the CFD techniques, interFOAM solver from OpenFOAM package is used for this study. It is worth mentioning that the boundedness of the volume fraction parameter is preserved by using Total Variation Diminishing (TVD) method implemented in OpenFOAM called MULES, Multidimensional Universal Limiter with Explicit Solution, (Deshpande and Anumolu (2012)).

All computational simulations are carried out using 96 cores on supercomputing facility Magnus, at Pawsey Supercomputer Centre, Perth, Australia. Magnus is a petascale supercomputer with 1.097 TeraFLOPS computing power, 93 Terabytes memory with 35712 processor cores. This facility provides an oportunity for all researchers across Australia to tackle large simulations which previously was not possible.

4.3 Experimental Methodology and Design Approach

The general approach used for designing of the tests are as following:

(i) Identification of the desired experimental variables and governing condition to acquire them.

(ii) Identification of proper devices and instruments for measuring the identified variables.

(iii) Designing the flow loop to meet the test goal and variable measurements.

(iv) Procurement of materials for experiments.

(v) Fabrication of all devices and instrument and integration into experimental apparatus.

In this study, both Single-phase and multi-phase experiments carried out to verify virtually generated filters, validation of numerical schemes, equilibrium

saturation of filter and evaluating dry and wet pressure drop. The experimental facilities used for both single phase and multi-phase tests are predominantly the same with some minor changes.

4.3.1 Single-phase Experiments for Evaluating Virtual Filters and CFD Solver

In order to evaluate the simulated different filter media and simpleFOAM solver, sets of experiments conducted in this study. The Figure 4.12 indicates the desirable variables, measuring systems and devices used in these tests.

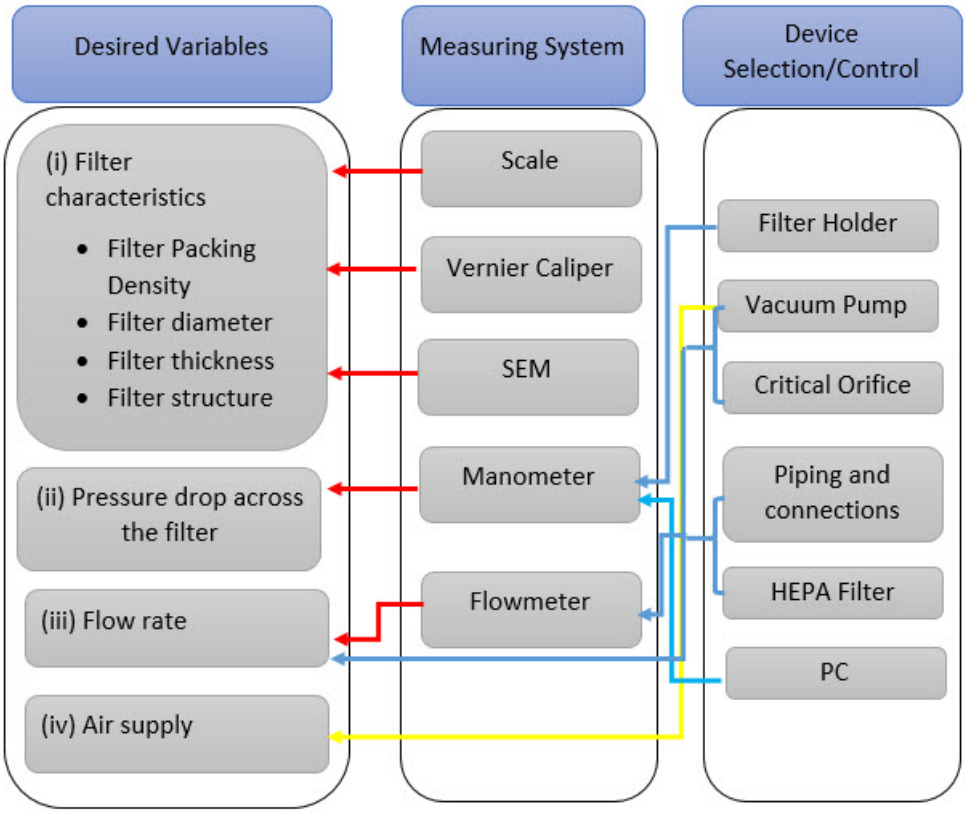

Figure 4.12: Identification of desirable variables, measuring systems and used devices in single-phase tests (after Abishek (2013))

In the following sections different aspects of experimental studies for single-phase flow will be explained.

Experimental Apparatus and Flow Loop

In order to conduct single-phase experimental study, an apparatus was designed to enable us for holding the filters and measuring the pressure drop across the filters. Figure 4.13 shows the designed apparatus. The material chosen for this filter holder was acrylic since it was clear for visual checks and also resistant to oil which used in multi-phase tests.

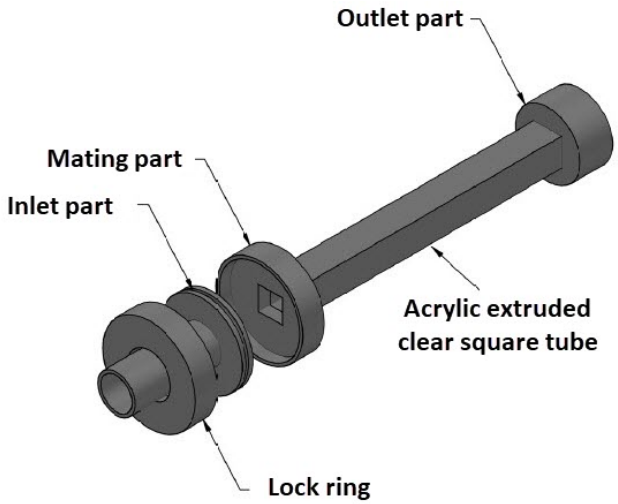

Figure 4.13: Designed apparatus for holding filters

The flow loop that designed based on the information provided from Figure 4.12 is presented by the Figure 4.14.

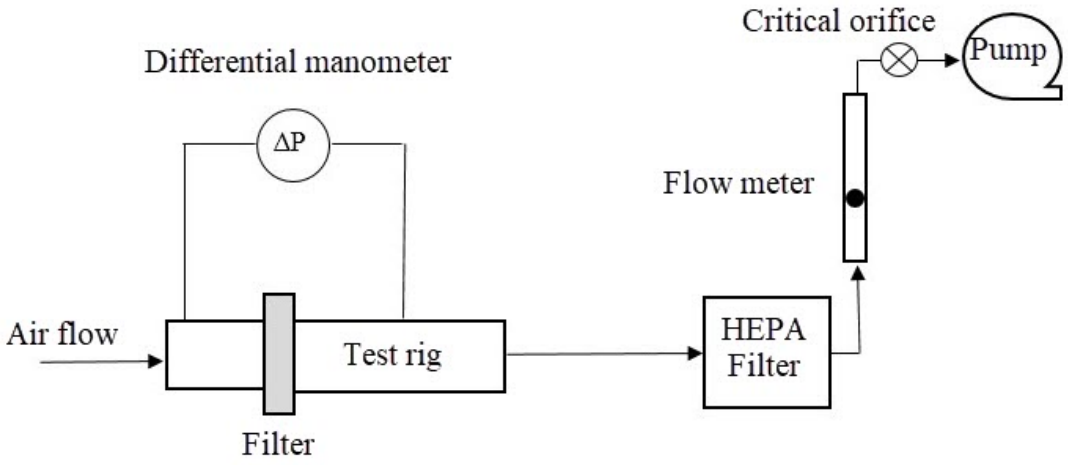

Figure 4.14: Flow Loop for Single Phase Experiments

Description of Experimental Facility

As it can be seen from Figure 4.14, there are five devices that have been used for conducting single-phase experiments which will be explained in more detail.

- Manometer (TSI,9555-P) provided on-line measurements of pressure drop across the filter. As indicated in the apparatus, the probes were located two sides of filters (front and back). The test results were saved on the device and transfered to the PC by a USB cable.
- High Efficiency Particulate Air (HEPA) filter was used in front of flow meter in order to protect the flow meter from any possible particles in the flow stream.
- Digital mass flow meter (TSI, 4045) was used to monitor and measure the system flow rate in-line. This device was used in order to improve the accuracy of the measurements, and ensure that the flow rate was correctly set.
- A critical orifice was applied at the pump suction in order to control and adjust the flow rate through the filters and maintain the steady state conditions.
- A vacuum pump (Sogevac, SV40 B) was employed to run air through the system.

Characterisation of Filter Media

Three types of filter structure fibrous, foam and knitted have been selected and prepared for experimental tests. The properties of filter media used are shown in Table 4.3. With regard to the filter selection criteria for validating the single-phase study, it should be mentioned that for every filter structure type (fibrous, knitted, and foam), two experimental sample filters with similar structures were considered. For validating the virtual generation filter methodology and the filter structures used in this research, experimental sample filters were selected with different physical characteristics in order to prove the generality of the filter generation approach which was utilised in this research (further detailed in Abishek et al. (2017)). In the validation process, all the physical properties of different filters were non-dimensionalised by Eu number which includes the effects of diameter, material properties, and thickness. Moreover, the diversity and variation of the filters with different structures are countless in the market. As the main objective of this research was to conduct numerical studies on virtually generated

filters, the main focus was on optimising the physical properties of the numerically generated filters for computation purposes. Therefore, filters structurally similar to the numerical validation cases were used for the experimental validation. In table 4.3, α is packing density, l is filter thickness, and d_f is fibre diameter.

Table 4.3: properties of the filters examined for the single-phase experimental study

Filter	Materials	α (%)	l (mm)	d_f (μm)
Fibrous-E1	Stainless steel	1 ± 0.04	3.3 ± 0.2	7.8 ± 0.5
Fibrous-E2	Polyester	20 ± 0.07	1.65 ± 0.17	15.4 ± 0.7
Foam-E1	Polyurethane	2.05 ± 0.05	4.48 ± 0.2	71.07 ± 0.67
Foam-E2	Polyurethane	1.9 ± 0.08	4.6 ± 0.25	102 ± 3.15
Knitted-E1	Stainless steel	1.9 ± 0.07	19.46 ± 0.24	137.3 ± 0.6
Knitted-E2	Copper	6.2 ± 0.08	24 ± 0.15	283 ± 4

Single-Phase Experimental Procedure

In the first step all samples (except knitted filters which were folded) were cut in a circular shape with a size of 60 mm diameter. All the filter samples dimensions were measured by digital vernier caliper and weighted by a scale. In order to calculate packing density of filters, Equation 2.1 was used. Each measurement wa repeated 20 times to confirm repeatability of the measurements and decrease uncertainty in the results.

A critical orifice was used to control the flow rate, which ranged from 0 LPM to 150 LPM producing face velocities ranging between $0 - 2m/s$. Before conducting tests with different filters, a test was carried out with all setup, but without a filter to measure the effect of apparatus on pressure drop. This apparatus head loss was deducted from filter pressure drop measurements which eliminated any affect of apparatus head loss from final results. The apparatus pressure drop results showed to be $\Delta p < 10\%$ of ΔP with filter for the same range of flow rate tested.

Scanning Electron Microscopy (SEM) was employed to evaluate the pore structure of filters and measuring filter diameters and pore diameter (for foam filter). For the nonmetallic fibrous and foam media, platinum particles were used to coat the filters with a thin layer ($< 50nm$) to enhance the electrical conductivity required for SEM. All the images from SEM were analysed digitally

by ImageJ software (Rueden et al. (2017)) to measure the fibre element diameter.

As it can be seen from filter holder (4.14), all the filters were oriented vertically with the air flowing horizontally. A minimum of 3 replicate experiments were performed for the face velocity ranging $0 - 2m/s$. At each flow rate the pressure drop across the filter were stored in the TSI manometer and waited for 3 minuets to make sure the trend shows steady state condition.

4.3.2 Multi-phase Experiments for Measuring Multi-phase Pressure Drop and Saturation

The same apparatus and flow loop were used to perform multi-phase tests. The only extra variable were measured was initial and equilibrium saturation which have been measured by scale and it will be explained in more details in experimental procedure section.

Characterisation of Filter Media

Two phobic and philic media were used for multi-phase experimental tests. The following table shows these filters properties.

Table 4.4: Filter properties examined for multi-phase experiments

Filter	Materials	Contact Angle	α (%)	l (mm)	d_f (μm)
Fibrous-ME1	Polyester	$109^\circ \pm 2^\circ$	20 ± 0.07	1.65 ± 0.17	15.4 ± 0.7
Fibrous-ME2	Stainless steel	$< 1^\circ$	1 ± 0.04	3.3 ± 0.25	7.9 ± 0.5

Preparation of Phobic Media

For preparation of phobic media, a procedure have been employed to convert an philic media to phobic. To achieve this, Polytetrauoroethylene (PTFE) was used to coat the surface of philic media. After fully saturating the philic filter with 5% of PTFE, the filter were removed from the solution and placed in an oven for polymerization with 100° for 35 minutes. It is to be noted that single-phase pressure drop examination was conducted after treating the filter surface. The results showed a small difference (less than 8% increase in pressure drop), which suggests that the fibre diameters and subsequently the filter's packing density was increased slightly. On the other hand, the contact angle increased significantly

as it was expected which the Figure 4.15 shows the sample treated filter.

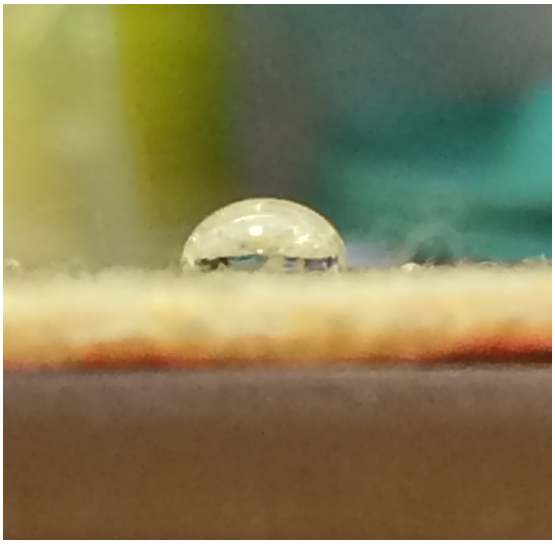

Figure 4.15: Droplet on media rendered phobic through procedure described above

As it can be seen from Figure 4.15, oil droplet (DEHS) makes a clamshell shape droplet which by digital measurement technique shows a contact angle equal to $109^\circ \pm 2^\circ$.

Pre-Saturation

In order to carry out the multi-phase experiments, DEHS was used in this research. The properties of this oil is summarised in table 4.2. The main purpose of the multi-phase experiments are to measure the equilibrium saturation and corresponding pressure drop at different face velocities. There are two ways to reach this equilibrium. One is to generate oil mist droplets and load the inlet air. The filter will collect the droplets and gain the equilibrium slowly. It was found that it is much quicker to over saturate the filter in DEHS container, and drain the excess oil (Bredin (2012)). This method not only saves experimental time significantly, it also provided more consistent results over repetition of tests. Therefore, in this research all the filters were dipped in a DEHS container for 30 minutes to become supersaturated and then allowed 5 minutes for dripping the excess oil. In regard to phobic filter, it is not possible to pre-saturate it with dipping in DEHS container as the contact angle between the oil and treated fibre surface do not allow the oil to penetrate into the filter. To overcome this issue, a vacuum pressure chamber with -94 kpa below atmospheric pressure was used.

The Figure 4.16 shows the vacuum chamber employed in this study.

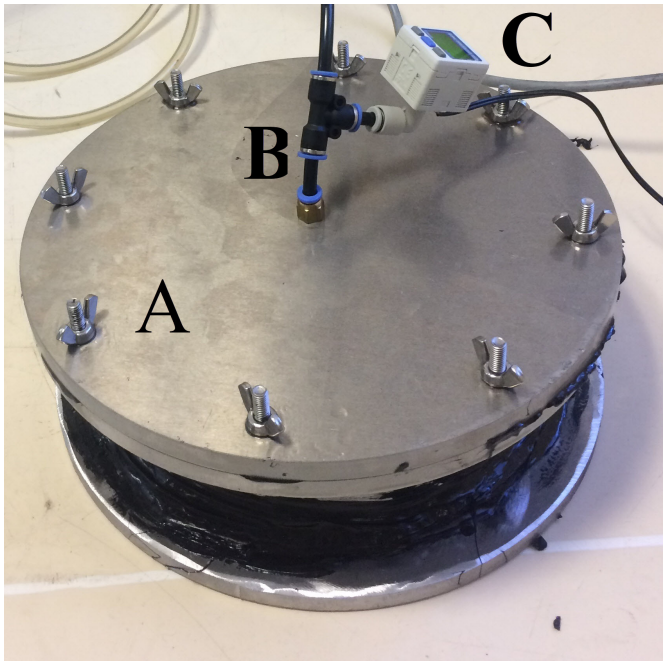

Figure 4.16: Vacuum chamber for saturating phobic media where A: The chamber, B: Vacuum line, C: Digital manometer

The saturation level was calculated before each test in order to ensure that the filter is fully saturated.

Multi-Phase Experimental Procedure

In the first step, similarly to single phase tests, all the filter properties such as weight, dimensions, packing density and contact angle measurements were carried out before conducting the experimental tests. Since the main objective of multi-phase experimental tests were to measure equilibrium saturation and corresponding wet pressure drop, a further calculations added to the procedure compared to the single-phase tests.

At the beginning, the filters were saturated by DEHS (according to the described methods earlier). Filter saturation were measured by the following equation:

$$S = \frac{(\frac{m_l}{\rho_l})}{V_{void}} \tag{4.22}$$

Where m_l and ρ_l are mass and density of liquid (DEHS), respectively. V_{void} is the volume not occupied by fibre which is air in our test, and it can be calculated by the following equation:

$$V_{void} = (\frac{m_l}{\rho_f}) \times (\frac{1-\alpha}{\alpha}) \tag{4.23}$$

After saturating filters and confirming the initial saturation level by given equations (4.22 and 4.23), different face velocities ranging 0.05 to 2.1 m/s were employed in experiments. At each velocity, sufficient amount of time was given for the test to reach steady state and monitoring pressure drop curve confirmed that. Then the test was stopped and the filter was weighed for equilibrium saturation calculation. This process repeated until that last velocity point. To provide a better demonstration, Figure 4.17 shows a pressure drop versus time for the fully saturated philic media at velocity equal to 1.3 m/s.

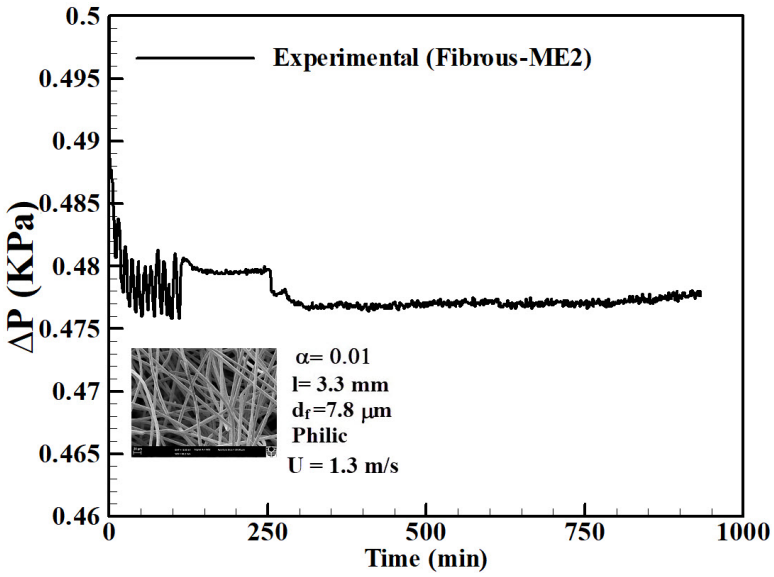

Figure 4.17: Pressure drop versus velocity in experimental philic media at U= 1.3 m/s.

4.3.3 Data Extraction, Calibration and Uncertainty Analysis

Using the experimental methodology described in the proceeding sections, single-phase pressure drop, multi-phase (wet) pressure drop, equilibrium saturation at different velocities, and filter physical properties were measured. In the case of pressure drop results, as they were used for validation and comparing with other

theoretical results, the data extraction was different. The effect of apparatus should be considered in the pressure drop results, so a polynomial curve was fitted to both measured and apparatus pressure drop in order to acquire the net pressure drop across the filter. Figure 4.18 shows the result for one of the sample filters as an example.

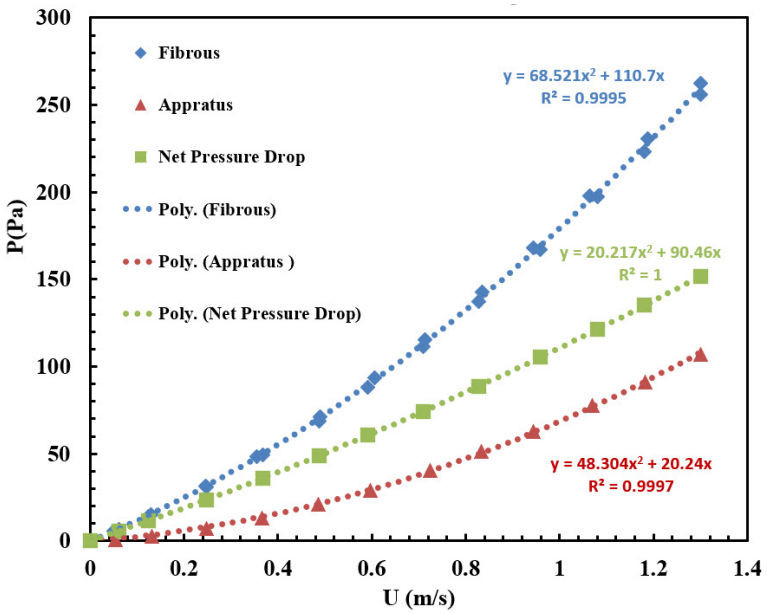

Figure 4.18: Data extraction and curve fit for an experimental fibrous filter case.

The flow meter and manometer used in this research were both factory calibrated in the range of research conducted. In regards to uncertainty calculations, Bell (2001) methodology was followed for the measured parameters. The reported expanded uncertainty was based on a standard uncertainty multiplied by a coverage factor k = 2, providing a level of confidence of approximately 95 %. The reported diameters were the mean of 40 repeated measurements of horizontal, vertical, and inclined elements in the fibrous, knitted and foam filters from SEM images. The ImageJ software was used for extracting the data from SEM images. The results were corrected for the estimated effect of possible mistake in picking measurement points, and effects of deviation from 90 degrees angle (between fibre element wall and drawing line as diameter by ImageJ software) when measured. The uncertainty of the measured contact angles, packing density, thickness and diameters were determined based on errors in predicted slope, error in distance (or geometry). In the case of flow rates and pressure drops, the precision errors were included in uncertainty calculations as well.

Table 4.5: Uncertainty estimates of different filters used in this study

Filters	$d_f(\pm\%)$	$\alpha(\pm\%)$	l $(\pm\%)$	θ°	$P_{single-phase}(\pm\%)$	$P_{multi-phase}(\pm\%)$	$S(\pm\%)$
Fibrous-E1	6.4	4	6.06	-	4.43	-	-
Fibrous-E2	4.54	0.35	10.34	-	4.65	-	-
Knitted-E1	0.43	3.68	1.23	-	5.2	-	-
Knitted-E2	1.41	1.29	0.62	-	4.9	-	-
Foam-E1	0.94	2.43	4.46	-	1.6	-	-
Foam-E2	2.3	4.21	5.43	-	1.03	-	-
Fibrous-ME1	4.54	0.35	10.3	2	4.43	5.1	8.9
Fibrous-ME2	6.32	4	7.57	1	4.65	6.3	7.4

Chapter 5

Mesh Generation Techniques, Virtual Filter Media and Simulation Validations

5.1 Introduction

As mentioned in the proceeding sections, the aim of this work is to compare the performance and investigate the pressure drop profile of three different filter media structures (fibrous, knitted, and foam) with equivalent physical properties such as packing density, cross section area, fibre element diameter, contact angle, and thickness. Therefore, rigorous validation of the media generated against classical single-phase permeability relationships, and multi-phase pressure drop and saturation profile are crucial. This chapter discusses the computational mesh generation and improvement techniques, reliability of the computational simulations using the generated virtual media in the current research (explained in Section 4.1), and also validation of the solver used for single-phase and multi-phase simulations (explained in Sections 4.2.3 and 4.2.4, respectively).

In order to achieve this, the mesh generation techniques used in this research by applying in-built functions in OpenFOAM are presented and a procedure for reducing poor quality cells is explained. In the next step, the mesh sensitivity analysis is conducted to verify the independency of the pressure drop results from mesh size in single-phase flows as the results will be used for validating the accuracy of the generated filter media. As such, sets of numerical simulations have been conducted to compare dimensionless pressure drop across different filter media to the conducted experiments (explained in section 4.3.1) and results in literature. It is worth mentioning that a collaborative study on validation of the

methodology of generating different realistic virtual filters (Abishek et al. (2017)) was done which the experimental research and validation conducted as a part of this PhD research. As stated before, the aim of this research is not validating the methodology of filter generation, but validating the accuracy of the designed filters for this particular study, and demonstrating that the filters are equivalent and realistic. In addition to CFD simulations conducted in this study, some of the numerical results from (Abishek et al. (2017)) is presented here in order to re-enforce the validations. Accordingly, the experimental cases considered for this part are listed in the Table 4.3.

There are two factors that should be evaluated to ensure the virtual filter media is a valid representative of a realistic media. The first one is the effect of packing density on pressure drop, and the second is the effect of Reynolds number (R_f) on the pressure drop. In the following sections both factors will be evaluated and discussed for the generated filters in this work and the research by Abishek et al. (2017).

In this chapter, the mesh sensitivity analysis is conducted on multi-phase simulations as well. It is shown that the multi-phase results are more sensitive to mesh resolution compared to single-phase (Abishek et al. (2017)). Furthermore, the influence of computational box size (distance from the filter geometry end to the end of computational box) is investigated by comparing the saturation result at one specific inlet velocity in different computational geometry length sizes. Finally, the saturation and multi-phase pressure drop results are validated against experimental data in literature and in current research for both phobic and philic media.

5.2 Mesh Generation

5.2.1 Meshing Technique and Mesh Quality Improvement

Due to the complexity of different filter structures, the generation of sufficiently refined computational meshes suitable for CFD calculations is a challenging task. In this thesis, a procedure has been employed based on available functions and tools in OpenFOAM along with an iterative refinement approach to produce a mesh meeting predefined mesh quality criteria. Figure 5.1 shows the work flow for the mesh generation process.

For better demonstration, the open-cell foam meshing process is presented in Figure 5.1. As it is seen from the meshing flow chart (different background colours

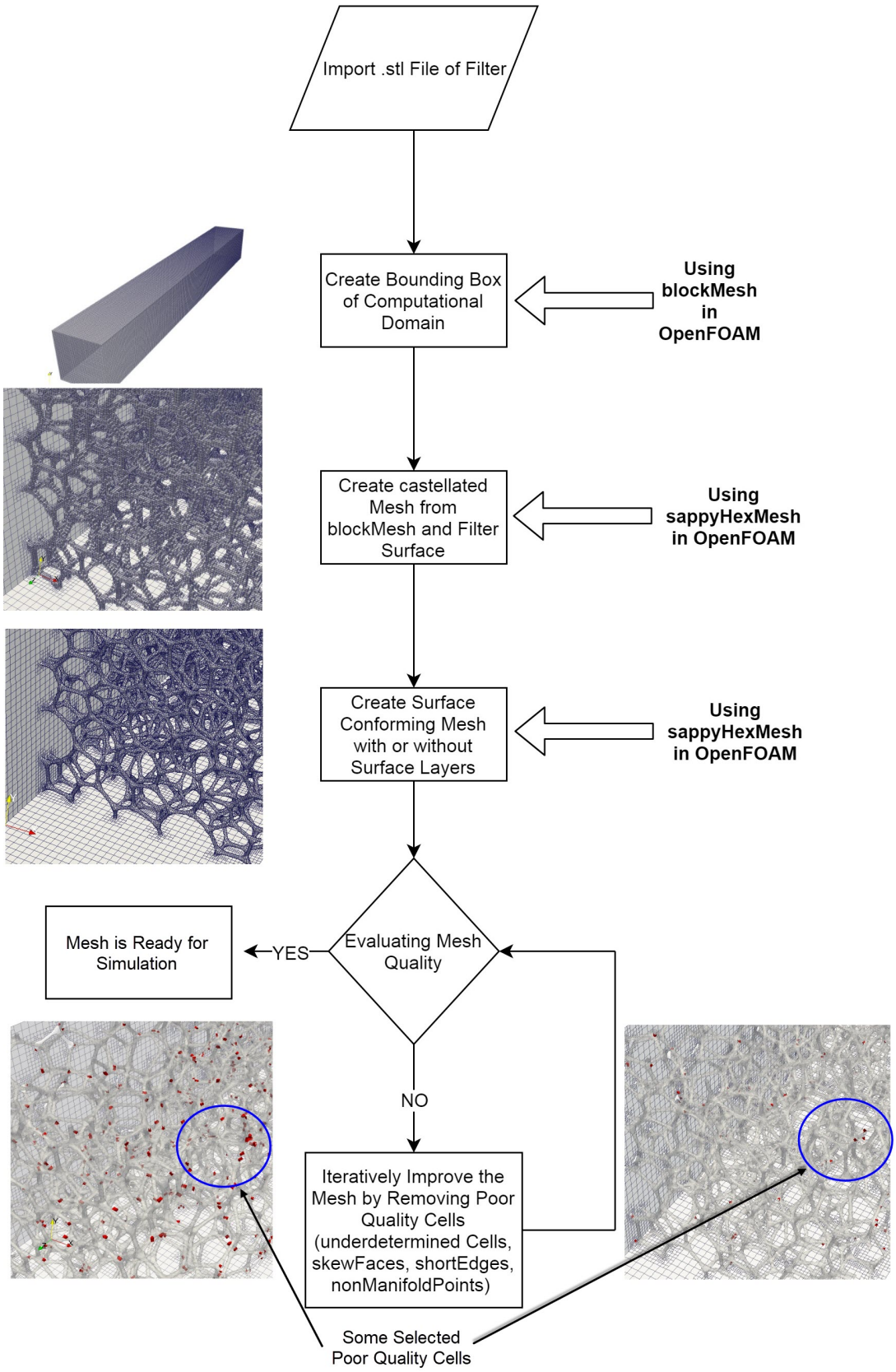

Figure 5.1: Methodology for generation of computational mesh (only surface mesh has been shown for clarity)

in the flow chart is only for better demonstration purpose), the first step is creating a simple background hexahedral mesh around the filter by using blockMesh utility in OpenFOAM. These hexahedral meshes with aspect ratio of 1 provide the base for applying the advanced and fully customizable utility, snappyHexMesh, in three main stages: (1) initial castellation in which cell splitting is performed by intersection of filter elements and background mesh. (2) snapping to surface involves moving cell vertex points to the filter element in order to remove jagged castellated surface form the mesh. (3) mesh layers is an optional stage which adds hexahedral cells aligned to the filter element. Applying this procedure provide the user with ability of creating any mesh with fully customizable size based on the CFD calculations needs.

Some authors (Lehmann et al. (2016); Gervais et al. (2012); Tafreshi et al. (2009)) have applied a voxelized grid algorithm in order to produce the computational meshes, however, this has a number of limitations. The approach used in this work has considerable advantages over such an approach, for the following reasons; first, in the present technique the mesh resolution can be increased locally rather than globally in regions where gradients are expected to be high during CFD calculations, as a result of decreasing the cubic relationship in cell size with mesh resolution. Second, voxel meshes do not contain information on local fibre surface orientations, so the contact angle cannot be studied, while in the current technique cell intersections are fitted to the filter element, and the influence of wetting can be studied for filter design.

The generated base-mesh should be checked against various quality parameters such as skewness, orthogonality, twist, under determined cells, short edges, aspect ratio and etc. Due to the nature and complexity of filter micro-structures, producing small fraction of poor quality cells (some poor cells in red colour highlighted by circles in Figure 5.1 for an open-cell foam media as a representative) are inevitable during meshing generation process. To provide a better demonstration, Figure 5.2 shows the poor quality cell in the computational domain after initial mesh.

In order to improve the accuracy of CFD results this issue should be rectified. This is carried out by using in-built function in OpenFOAM (topoSet) where all the poor quality cells are improved or ultimately removed from domain iteratively, and in each iteration a quality control performed. Figure 5.3 shows the cumulative statistics of the poor quality cell reduction by applying the present mesh-correction iterative method for fibrous, knitted and open-cell foam filter. In Figure 5.3, N_f is the total number of initial meshes, α is the packing density of the filter, $\Delta\alpha$ is the fraction change in the packing density of the filter, w

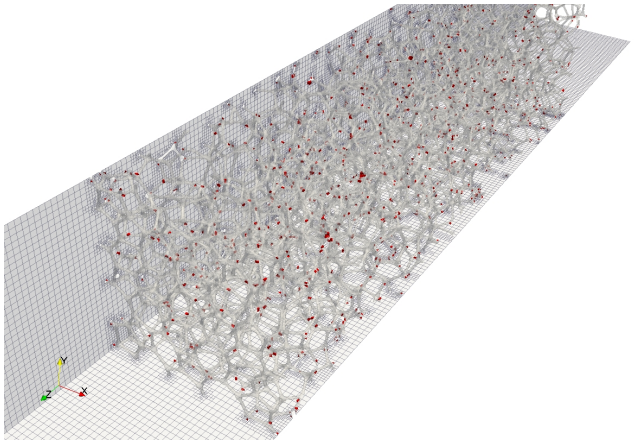

Figure 5.2: Poor quality computational cells (indicated by red colour) after generation of initial mesh (only surface mesh has been shown for better clarification).

is the width of the filter, and d_f is the diameter of a the fibre element in the filter.

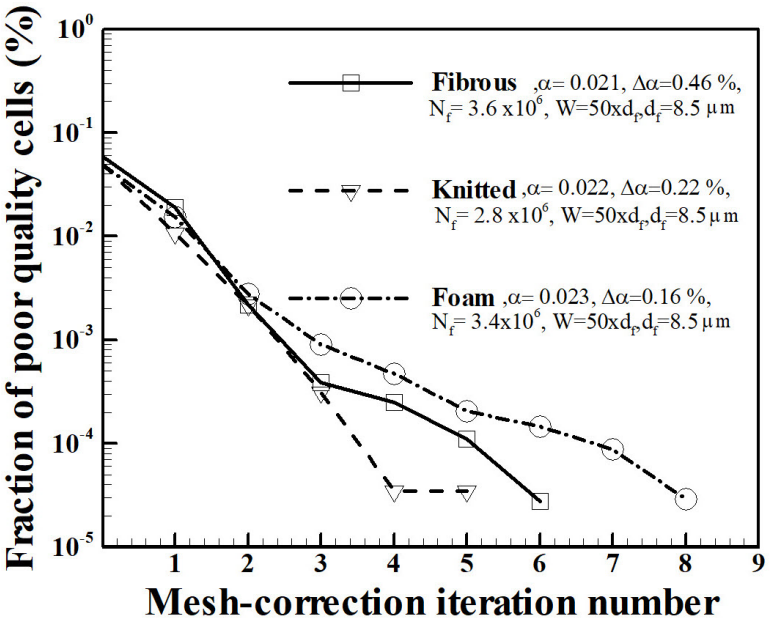

Figure 5.3: Poor quality cell reduction in various filters

It can be seen from Figure 5.3 that fractional change in packing density ($\Delta\alpha$) after cleaning all poor quality cells is less than 0.5 % in all geometries which confirms the suitability of the applied technique. Figure 5.4 presents the final computational meshes for fibrous, knitted and open-cell foam filter media.

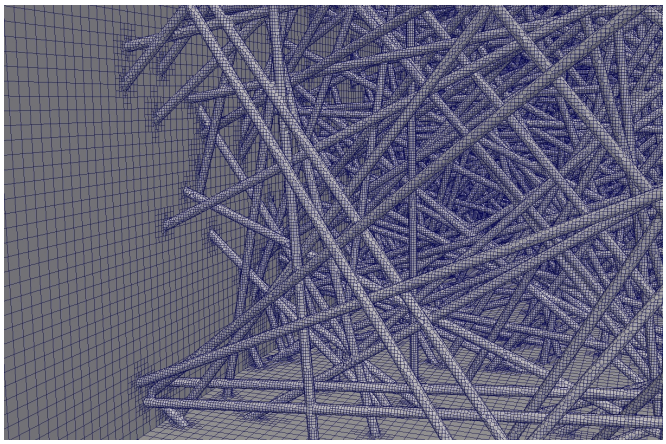

(a) fibrous

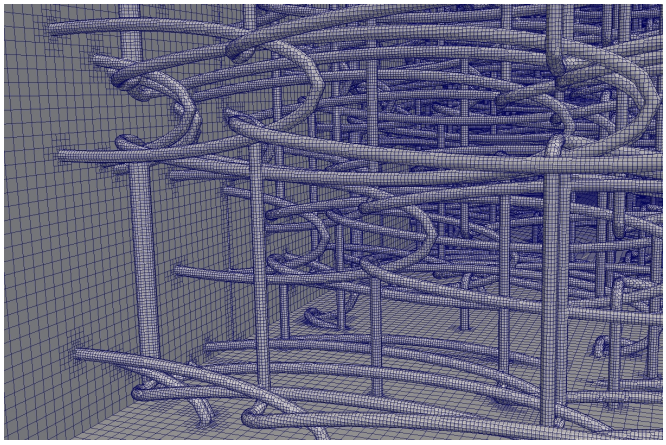

(b) knitted

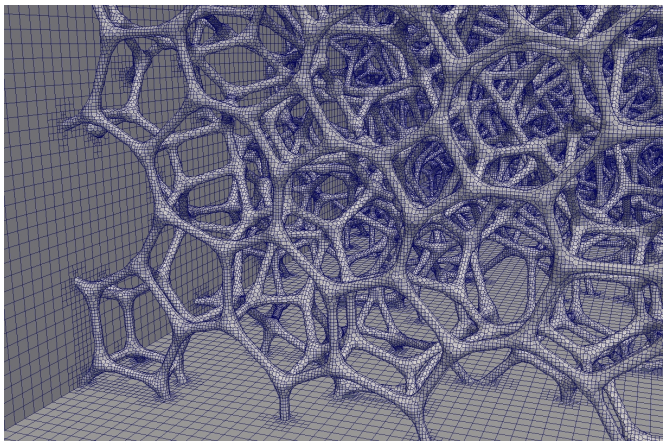

(c) foam

Figure 5.4: Representative computational mesh for fibrous, knitted and foam filter media (only surface mesh presented for clarity)

5.2.2 Filter Geometry Meshing and Packing Density Relationship

It is a standard procedure to conduct a mesh study in order to confirm the accuracy of CFD results, but it is different in filter numerical simulations as by decreasing the cell size, the packing density of the filter will change since the greater fraction of the filter element can be resolved during meshing process. Therefore, a mesh study is carried out to find the influence of mesh size on packing density, and the results are shown by Figure 5.5.

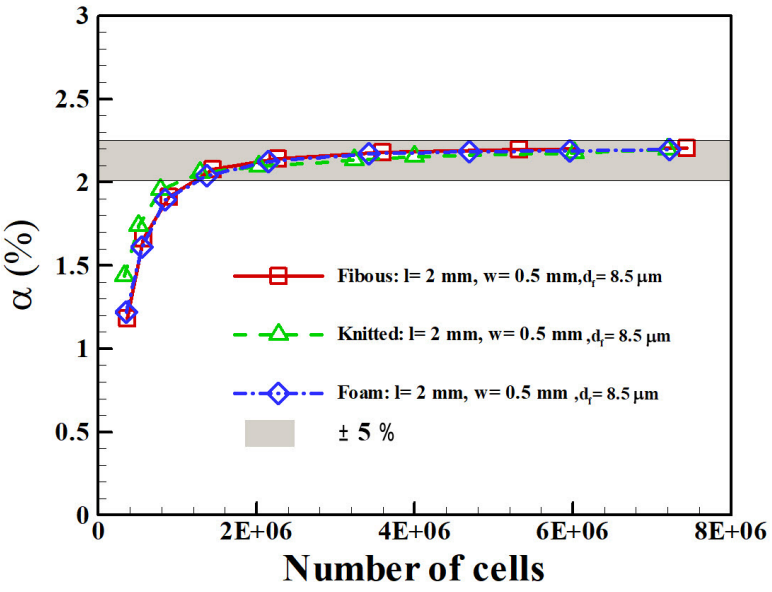

Figure 5.5: Influence of mesh refinement on packing density of virtually generated fibrous, knitted and foam media

In Figure 5.5, l is the length (thickness) of the filter, w is the width of the filter, and d_f is the packing density of the filter. It can be deduced from Figure 5.5 that the packing density becomes independent of the cell size ($< 5\%$) at about 1.6×10^6 computational cells for the presented filter media.

The meshing and quality improvement techniques presented in this research are general for any filter structure. For creating a suitable mesh, knowing the actual packing density value would be helpful as by refining the mesh, the computational packing density approaches to the actual value (as shown in Figure 5.5). After checking for low quality cells and using the proposed methodology for improving the computational mesh quality, a systematic mesh study should be conducted to ensure the results are independent from the mesh size.

5.3 Single-phase Flow Mesh Independency verification and Virtual Filter Media Validation

5.3.1 Mesh Sensitivity Analysis in Single-phase Simulations

For the purpose of mesh sensitivity analysis in single-phase flow (air flow through filter media), the pressure drop results by using the methodology explained in Section 4.2.3 is examined at 2 m/s inlet velocity in all filter media. The mesh resolution influence on dry pressure drop value in all filter media is depicted by Figure 5.6. It is worth mentioning that the single-phase pressure drop results (dry pressure drop) will be used in the next section for evaluating the accuracy of the generated filter media. Therefore, the single-phase pressure drop results are monitored carefully and the mesh independency testes by 5% variation limit is considered for achieving more precise results.

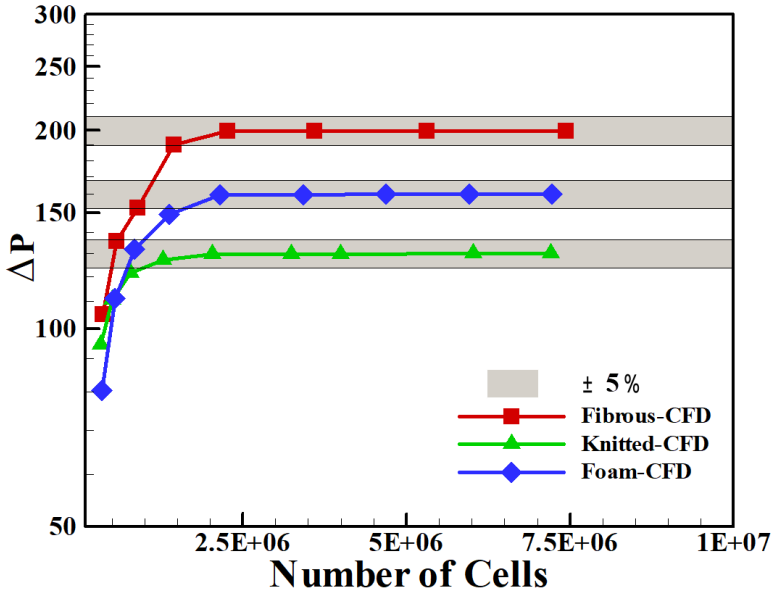

Figure 5.6: Influence of mesh refinement on dry pressure drop results in fibrous, knitted, and foam media.

It can be seen from Figure 5.6 that all filters are producing accurate pressure drop values for mesh resolutions above 2×10^6. Therefore, this mesh resolution is considered for all filter media for dry pressure drop results in order to ensure the accuracy of the results for the generated filter media verification study in next stage.

5.3.2 Virtually Generated Filter Media Validation

Verifying the Effect of Packing Density on Pressure Drop

In order to verify the effect of packing density on pressure drop, set of simulations conducted on the generated filter media (fibrous, knitted, and foam) with equal physical properties described in Section 4.2.1. Furthermore, some numerical results from Abishek et al. (2017) employed in this section for a better demonstration. Table 5.1 presents the numerical cases considered.

Table 5.1: properties of the virtual filters considered for validation of computational methodology.

Filter	α (%)	l (mm)	d_f (μm)	Source
Fibrous-N1	2	2	8.5	Present
Fibrous-N2	20.3	1.65	15	Present
Foam-N1	2	2	8.5	Present
Foam-N2	5	2	20	Abishek et al. (2017)
Foam-N3	1.9	4.6	102	Abishek et al. (2017)
Knitted-N1	2	2	8.5	Present
Knitted-N2	5	4.3	70	Abishek et al. (2017)
Knitted-N3	7	23	283	Abishek et al. (2017)

Figure 5.7 depicts the dimensionless pressure drop obtained from present simulations and numerical data from Abishek et al. (2017) against the classical models from Spielman and Goren (1968) where fully explained in Section 2.3.3. According to the methodology explained in the Section 4.2.3, the governing equations for single-phase (air) flows are solved with a constant inlet velocity of $0.6m/s$ resulting in $0.38 < Re_f < 12.91$. The acquired pressure drop results from these simulations used in the Equation 2.19 in order to calculate the dimensionless pressure drop.

It can be seen from Figure 5.7 that fibrous filter agrees perfectly with the case when all fibers are normal to the flow, with showing marginally deviation toward the case with three dimensional random. This can be justified by a closer look at the fibrous geometry (Figure 4.7- (a)) generated where some of the fibre elements have an angle < 90 with flow direction vector (3-D fibre elements). It is also seen that Fibrous-N2 case, with high packing density, agrees well with 3-D random theoretical results as generated with lower orthogonality. Open-cell foam filters are consist of partially aligned and partially perpendicular struts to the

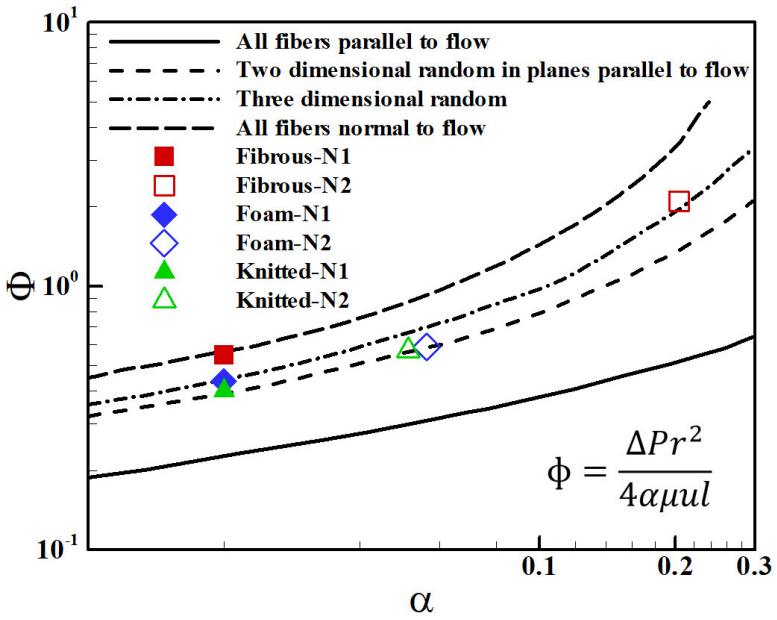

Figure 5.7: Comparison of predicted dimensionless pressure drop from different virtual filter media against Spielman and Goren (1968) research.

flow direction. It can be seen that their dimensionless pressure drop lies between theoretical predictions of Spielman and Goren (1968) where fibres are 3-D random and all fibres normal to flow. Knitted filters have an interlocking structure which some of its elements are not perpendicular to the mean flow. Furthermore, knitted filters have some void areas which reduces the resistance against the flow and causes lower pressure drop compared to fibrous filters. In spite of the different structures of the foam and knitted media compared to fibrous media, there is still a good agreement with theory of Spielman and Goren (1968), and the results show a consistent trend with increasing packing density for any considered filter geometry.

Verifying the Effect of Reynolds Number on Pressure Drop

In this section the predicted pressure drop across the generated virtual filters will be validated against a semi-empirical model and experiments. The numerical simulations conducted in the range of stokes flow where $0.1 < Re_f < 10$.

It was shown in section 2.5.1 that there have been more attention toward fibrous filters from the past compared to other types of filter media (Mead-Hunter et al. (2014)). Therefore, virtually generated fibrous media can be compared against experimental and semi-empirical correlation. Figure 5.8 presents the comparison of predicted dimensionless pressure drop (represented in terms of

Eu) with theoretical models and experimental data.

As explained in section 2.3.3, semi-empirical by Davies (1953) which is valid for the range of packing density $0.006 \leq \alpha \leq 0.3$ and presented by Equation 2.13 will be re-arranged as the following:

$$\triangle P = \frac{\mu Q l}{{d_f}^2 A_f}[64\alpha^{1.5}(1+56\alpha^3)] \Longrightarrow Eu = \frac{64}{Re_f} \times [\alpha^{1.5}(1+56\alpha^3)] \tag{5.1}$$

Where $Eu = \frac{\Delta P d_f}{\rho u^2 l}$ is the Euler number. The main purpose of this re-arrangement of the equation is to extract Euler number values for the specific filter properties ($\alpha = 0.021$) in this study according to Davies equation. Therefore, the generated fibrous filter (Fibrous-N1) in this study can be compared to Davies semi-empirical result.

It is seen form Figure 5.8 (a) that the simulation results have a perfect agreement with slope and magnitude of the dimensionless pressure drop predicted by Davies (1953). The other correlation that can be used for validating the fibrous filter is the theory of Spielman and Goren (1968). As it was explained before, this correlation is valid for $0.003 \leq \alpha \leq 0.3$, therefore the generated virtual fibrous filter media with packing density equal to 2.1 % is valid to be verified by this theoretical model. For plotting Figure 5.8 (b), the corresponding Euler number is extracted at $\alpha = 0.021$ from Equation 2.19 and the results indicate a good agreement with the theory of Spielman and Goren (1968).

Another important point which can be seen in the Figure 5.8 (b) is the deviation from Spielman and Goren (1968) theory for higher velocity cases which leads to $Re_f > 1$. To investigate the underlying reason for this occurrence, one should consider the governing laws in fluid pressure drop through a porous media. Darcy (1856) presented a fundamental law which links velocity and pressure drop of a fluid through a porous media. This law is quite general and applicable for liquids, gases, and even the mixtures. Darcy's law can be presented by the Equation 5.2 (Spielman and Goren (1968)):

$$\Delta P = -\frac{1}{K}\mu u l \tag{5.2}$$

Where ΔP is pressure drop, K is permeability, μ is gas dynamic viscosity, u is face velocity, and l is the length of the media. It is widely accepted that for $Re_f < 1$ the Darcy regime occurs and capable to correctly describe the pressure drop of a flow (Della Torre et al. (2014)). However, by increase in flow velocity,

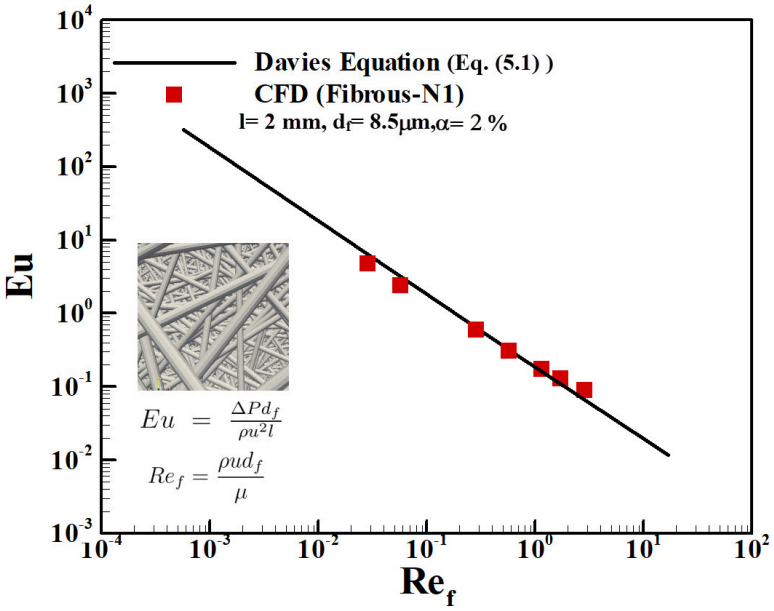

(a) Present CFD simulation (Fibrous-N1) against Davies (1953)

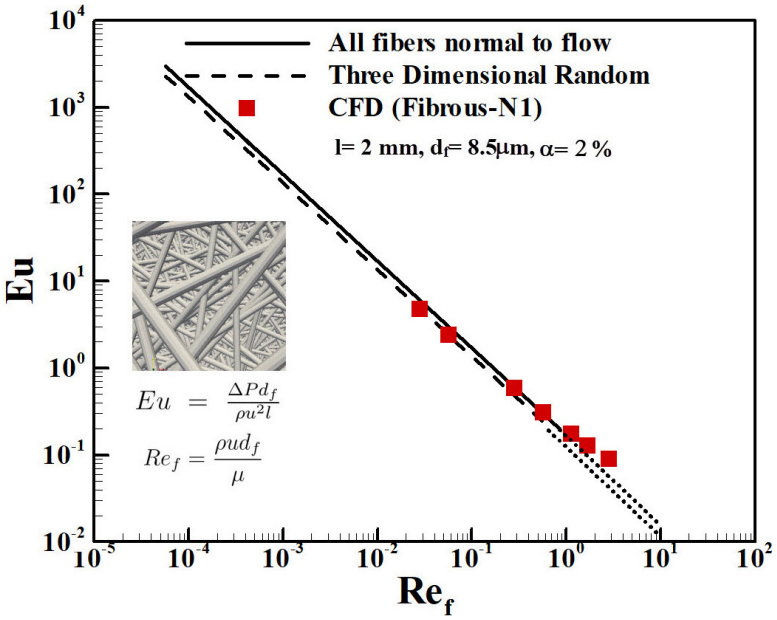

(b) Present CFD simulation (Fibrous-N1) against Spielman and Goren (1968)

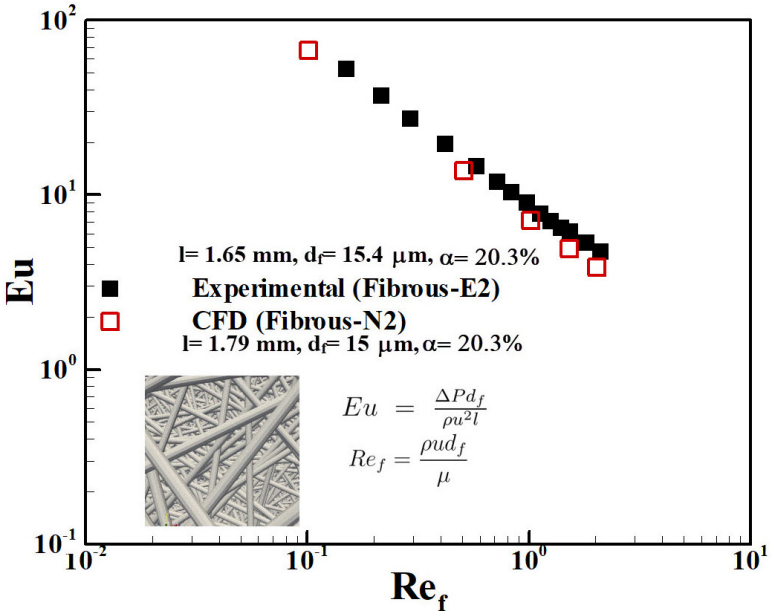

(c) Present CFD simulation (Fibrous-N2) against experimental data (Fibrous-E2).

Figure 5.8: Comparison of predicted dimensionless pressure drop for generated fibrous filter media against experimental data and theoretical model.

a discrepancy between experimental results and Darcy's law prediction develops. Forchheimer (1901) related this phenomena to inertial effects and suggested a modified version of Darcy's law with additional term which represents kinetic energy (Andrade et al. (1999); Whitaker (1996)). The Darcy-Forchheimer regime forms in $1 - 10 < Re_f < 150$ which the flow is dominated by inertial forces and the relationship between pressure drop and velocity is non-linear. The Equation 5.3 presents the Forchheimer equation (Andrade et al. (1999)):

$$\Delta P = -\frac{1}{K}\mu u l + \beta \times (\rho \times u^2) \tag{5.3}$$

Where β is non-Darcy coefficient and ρ is fluid density. It is worth mentioning that this non-linearity develops still within laminar flow regime, and it is not related to turbulence (Scheidegger (1974); Noman and Kalam (1990); Hlushkou and Tallarek (2006); Della Torre et al. (2014)). Majority of the researchers assume that $1 < Re_f < 10$ is the upper limit for Darcy's law (Chapman (1981); Della Torre et al. (2014)). As can be seen from the Figure 5.8 (b), the dimensionless pressure drop results from the present simulations adhere perfectly to the proposed equation by Darcy (which is the basis of the model presented by Spielman

and Goren (1968)) for low velocity cases (where $Re_f < 1$), while the deviation is occurred for higher velocity cases due to non-linearity of Darcy-Forchheimer regime.

Figure 5.8 (c) depicts the simulation results for a high packing density virtually generated fibrous filter (Firbous-N2) against experimental pressure drop (Fibrous-E2). This filter is generated for validation purpose, and verify the effects of Reynolds number variation in high packing density media. It is evident from Figure 5.8 (c) that the CFD results acquired in this study have a great agreement with the experimental data.

For examining the accuracy of generated foam filter media and validity of single phase simulations in foam geometry, two numerical cases (Foam-N1 and Foam-N3 which are summarised in Table 5.1) and two experimental cases (Foam-E1 and Foam-E2 which are summarised in Table 4.3) are considered in order to investigate the effects of Reynolds number on pressure drop prediction of generated foam media in this study. Figure 5.9 represents comparison of predicted dimensionless pressure drop of generated foam filter media in this study against experimental data and theoretical model.

Figure 5.9 (a) presents the simulation data of the generated virtual foam media (Foam-N1) in this study compared to experimental dimensionless pressure drop results of the case Foam-E1. It is seen that the predicted dimensionless pressure drop from the virtually generated foam media is in a good agreement with experimental data. Figure 5.9 (b) shows the CFD results of Abishek et al. (2017) work (Foam-N3) against a set of experimental pressure drop data acquired in this research (Foam-E2). A good agreement between CFD results (foam filter generated based on the methodology explained in section 4.1) and experimental data (Foam-E2) is evident from the graph which re-iterate the validity of the generated foam filter media.

Apart from experimental validation of the results, the CFD simulation results (dimensionless pressure drop) can be compared to the results from the theory of Spielman and Goren (1968). Although the origin of the Spielman and Goren (1968) is based on fibrous filters with different orientations, still it can be used to evaluate the relationship between pressure drop and Reynolds number. As explained before, the corresponding Euler number is extracted from Spielman and Goren (1968) at $\alpha = 0.021$ (generated foam filter packing density) and plotted against filter Reynolds number (Re_f). Figure 5.9 (c) indicates that the CFD results from this study (Foam-N1) follows the Spielman and Goren (1968) theory. It is clear that the generated foam filter results are similar to the case with three

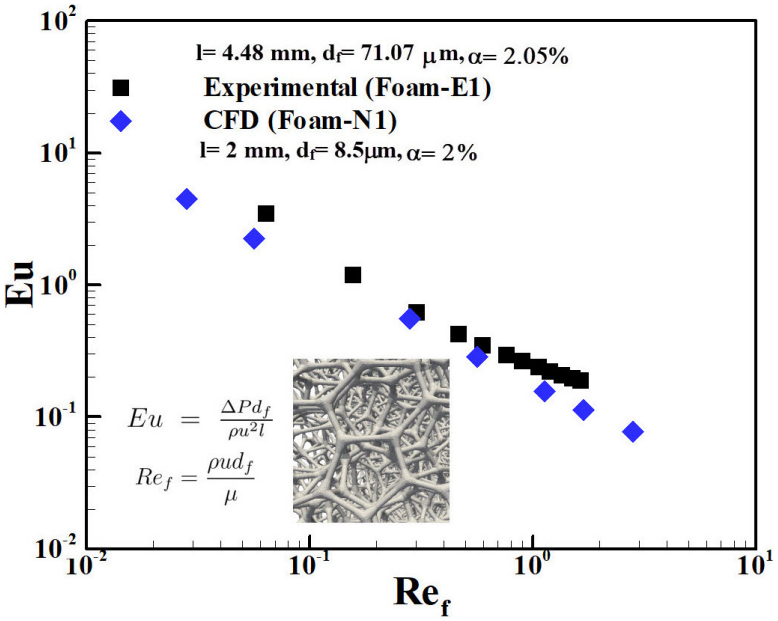

(a) Present CFD simulation (Foam-N1) against experimental data (Foam-E1).

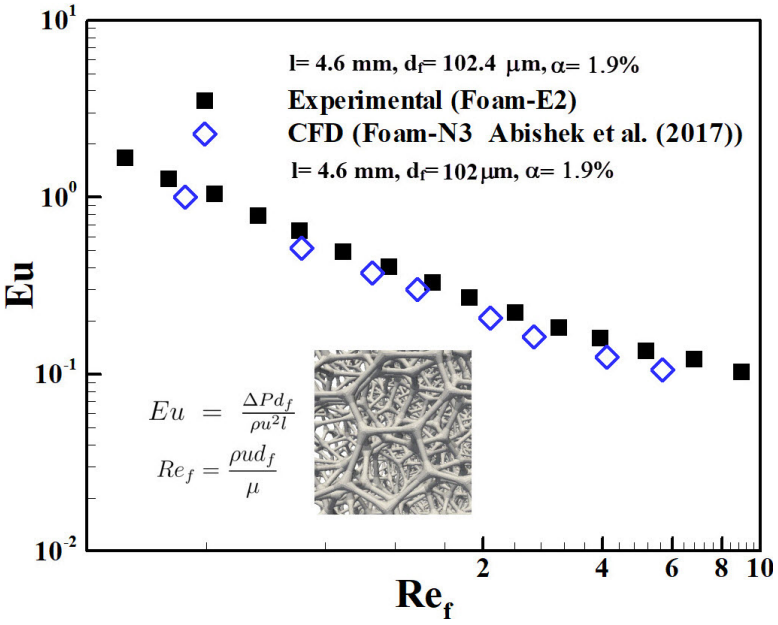

(b) Abishek et al. (2017) CFD simulation (Foam-N3) against experimental data (Foam-E2).

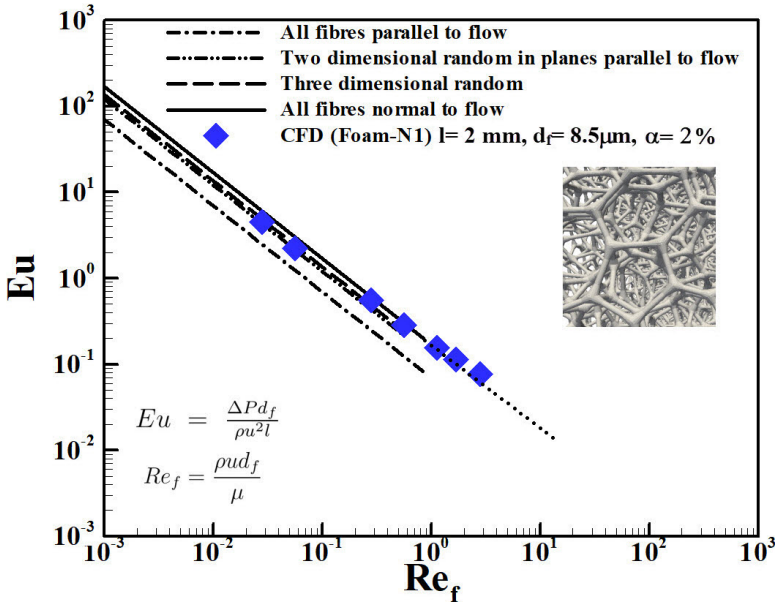

(c) Present CFD simulation (Foam-N1) against theoretical model of Spielman and Goren (1968).

Figure 5.9: Comparison of predicted dimensionless pressure drop for generated foam filter media against experimental data and theoretical model.

dimensional random fibre orientation and the case where all fibres are normal to the flow. This can be justified by the structure of foam filter elements which is different from a fibrous filter and has been addressed in detail during the packing density effect study.

In order to investigate the accuracy of the generated knitted media and computational CFD method employed in this study, two sets of numerical cases (Knitted-N1 and Knitted-N3 cases listed in Table 5.1) and two experimental cases (Knitted-E1 and Knitted-E2 listed in Table 4.3) are considered. It should be mentioned that knitted media is one of the most well defined structures which has several different structures and mathematical equations for defining the knitted loops. The knitted media used in this research (Knitted-N1 case) is developed based on the classical strophoid equation which has been extended by Jeddi and Dabiryan (2008). Figure 5.10 demonstrate the comparison of predicted dimensionless pressure drop for generated knitted filter media against experimental data and theoretical model.

It is seen from Figure 5.10 (a) that a good agreement between the predicted dimensionless pressure drop and experimental results exists. Figure 5.10 (b) evaluates the accuracy of the CFD simulations and generated knitted filter media

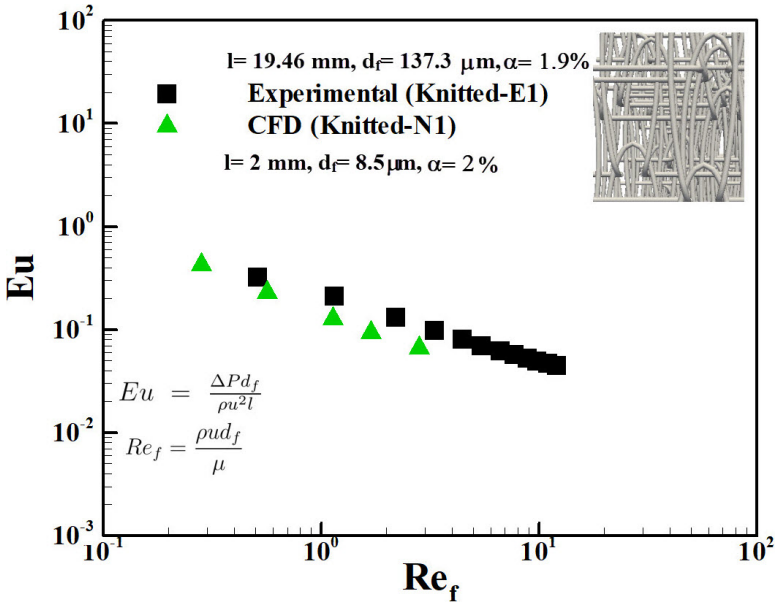

(a) Present CFD simulation (Kitted-N1) against experimental data (Knitted-E1).

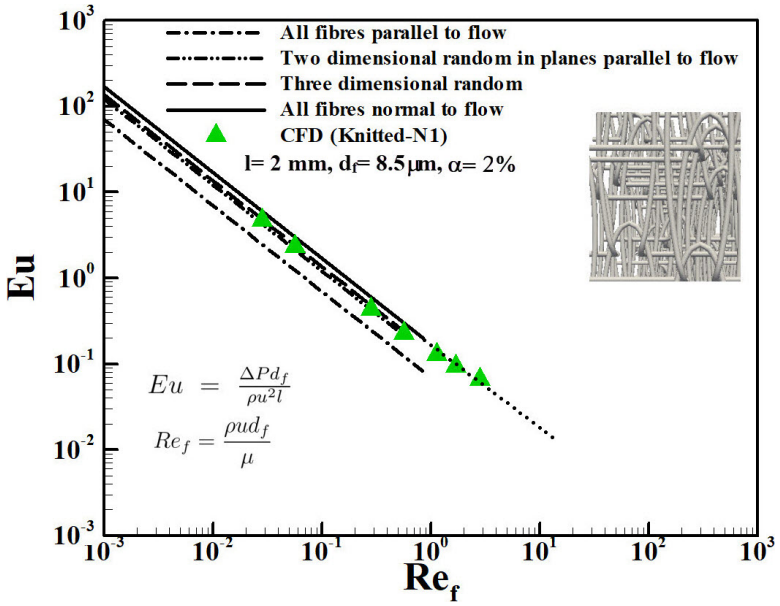

(b) Present CFD simulation (Knitted-N1) against theoretical model of Spielman and Goren (1968).

Figure 5.10: Comparison of predicted dimensionless pressure drop for generated knitted filter media against experimental data and theoretical model.

against theoretical model by Spielman and Goren (1968). It can be seen that the slope as well as the magnitude of the dimensionless pressure drop acquired from present CFD simulations are in a good agreement with the theory of Spielman and Goren (1968) which re-iterate the accuracy of the methodology employed for generating knitted filters and also CFD techniques in this study.

The knitted media generated and tested in the research work by Abishek et al. (2017) (Knitted-N3 case) was applied a different mathematical equation for defining the knitted loop (Choi and Lo (2003)) which sets of experiments were conducted for validation of this structure. The comparison results against experiments are presented in Appendix B.

5.4 Multi-phase Flow Mesh Independency and Computational Box Length verification

5.4.1 Mesh Sensitivity Analysis in Multi-phase Simulations

In order to evaluate the influence of the mesh refinement on multi-phase flow results, the transient VOF simulations (explained in Section 4.2.4) of air flow through a pre-saturated filter with 30% of DEHS is used. The final steady state residual saturation value at 1m/s inlet velocity in all filter media are tested by different mesh resolution.

It is visible from Figure 5.11 that unlike the mesh refinement influence on packing density and single-phase pressure drop, the multi-phase saturation results show a greater scatter rather converging to an asymptotic limit with mesh refinement. This occurrence indicates that unlike the single-phase flow through a filter media, contact-line in dynamics at the oil-filter interface is more sensitive to small variations in mesh configuration which can be resulted in a higher variations in steady state results. It is seen from Figure 5.11 that all filter media with mesh configuration greater than 2×10^6 exhibits an acceptable variation in steady state value which is in the range of $\pm 10\%$ and presented by the shaded regions.

It should be emphasised that applying the finest mesh for multi-phase simulations does not necessarily improve the solution or final results (Deshpande and Anumolu (2012)). As explained in Section 4.2.4, the adaptive time step is employed for VOF simulations which is controlled by Courant number (Equa-

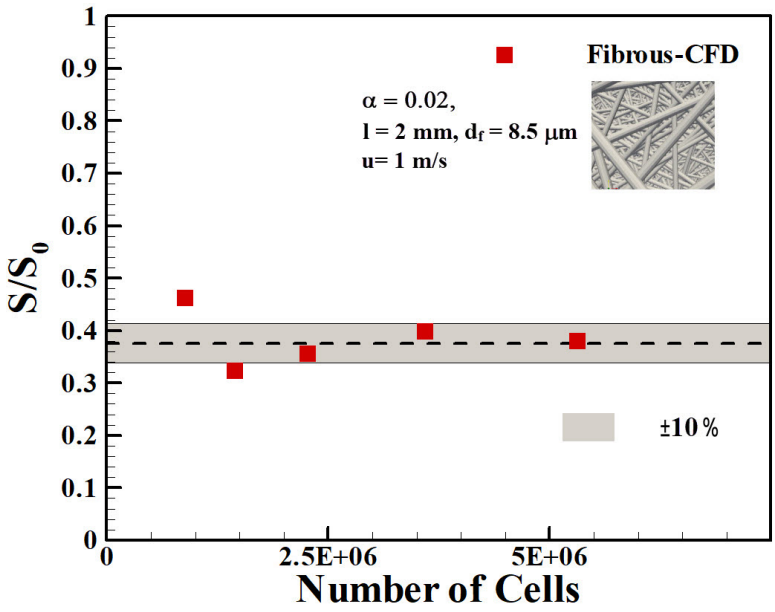

(a) Fibrous filter

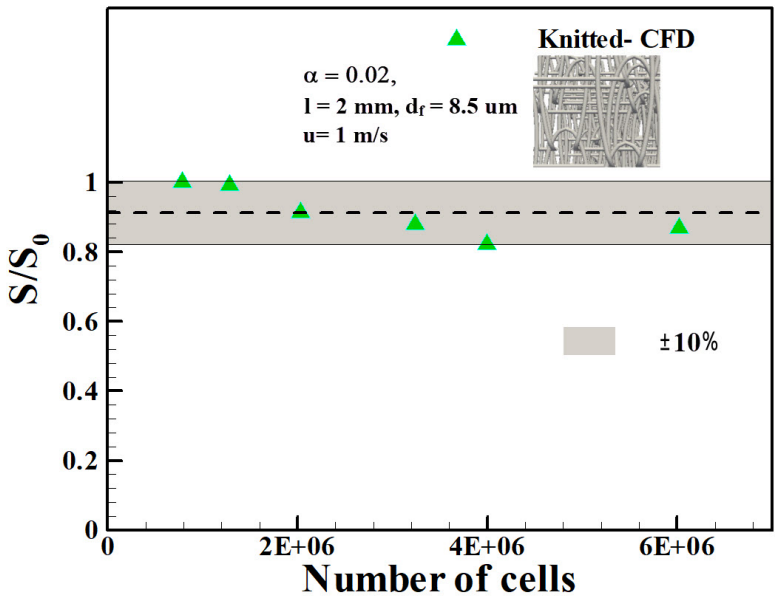

(b) Knitted filter

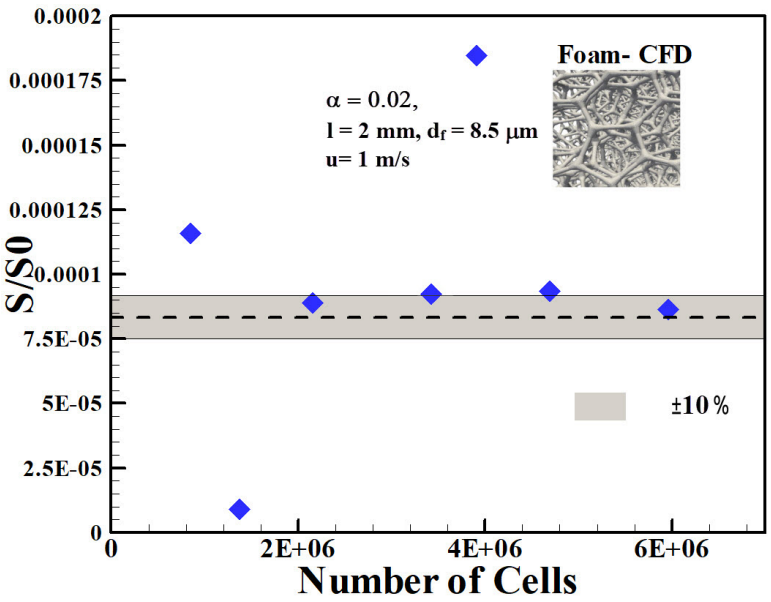

(c) Foam filter

Figure 5.11: Influence of mesh refinement on residual saturation results in phobic foam media.

tion 4.20). From the Courant number definition, it can be deduced that refining the mesh is resulted in decreasing the solution time step, which can resulted in spurious currents in the solution and also instability (Deshpande and Anumolu (2012)). Therefore, a careful mesh study should be conducted in order to prevent the mentioned problems.

5.4.2 Investigating the Effect of Computational Box Length

The other important factor which can affect the simulations is the length of the computational box compared to the thickness of the filter. Fo this purpose, Figure 5.12 presents the normalised saturation versus the fraction of computational box (Z) over the thickness of the filter (l).

It is clearly seen from Figure 5.12 that the results are independent of the computational length when the computational box is twice or larger than the filter thickness. It was seen during the simulations that in smaller dimensions, the re-entrainment droplets' diameter (especially in phobic media) can be larger than the distance between the filter rear face and computational end face which caused the stronger pressure gradient forming and extracting the oil droplet faster. Therefor, the computational box of 4 mm is considered for this research as the filter thickness is 2 mm.

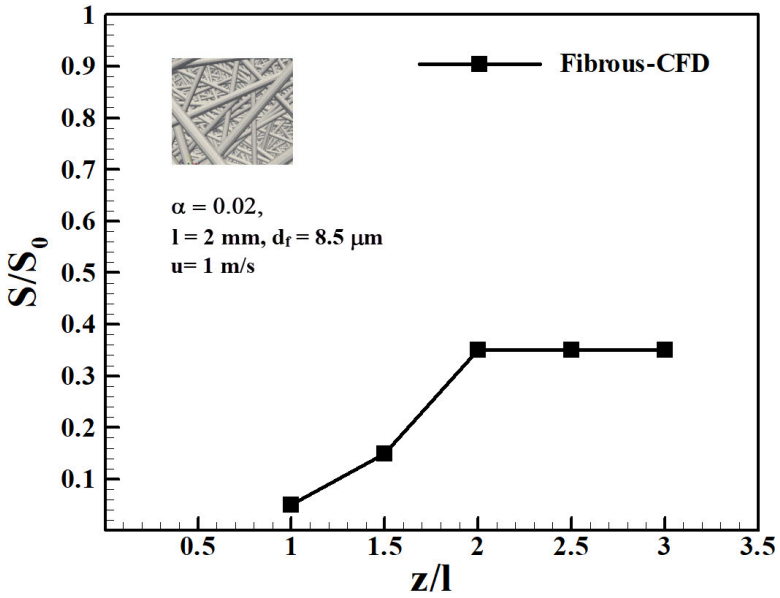

Figure 5.12: Influence of computational box length on the residual saturation results in phobic fibrous media.

5.5 Multi-phase Flow Simulations Validation

A rigorous validation for multi-phase flow simulations is carried out to make sure that the CFD methodology used, simulation setups, mesh quality and boundary conditions imposed are accurately capable of delivering reliable results. In this section, the CFD results are compared to experimental results in this research and experimental results from the literature. As the main outcome from this research is gained from pressure drop and saturation results, it is these values which are validated. It should be noted that since the present experimental tests in this work and majority of all previous experimental studies are based on fibrous media, only CFD results of fibrous case is considered for validation as a representative.

5.5.1 Multi-phase (wet) Pressure Drop Validation

In the first step, the steady state multi-phase (wet) pressure drop values of CFD from this research are compared against different published experimental studies in literature which considered phobic or philic media in their work. The list of these studies are summarised in Table 2.1. The results acquired for steady state

(equilibrium) pressure drop for both phobic and philic media are depicted in Figure 5.13.

In order to plot different pressure drop results from various authors in the same figure, the results are plotted in terms of $\frac{\Delta P}{u.l}$ versus $\frac{\alpha}{d_f^2}$. These two parameter sets are gained from Davies Equation (Eq. 2.13) assuming the constant dynamic viscosity (μ) of the carrier fluid (air) in all studies. Accordingly, only experimental works which provided sufficient information such as: packing density, fibre diameter, face velocity, and filter thickness could be plotted. In the case of filter thickness, some studies used multiple layers of the same filter were used during the experiments in these cases the filter thickness is multiplied by the number of layers used.

It can be seen from Figure 5.13-(a) that the majority of the wet pressure drop results from different experimental research in phobic media fall about a single line which is a power law fit to all experimental data (except the CFD results from this work). This regression can be explained by the following equation:

$$\frac{\Delta P}{u.l} = 2.70 \times 10^{-6} \left(\frac{\alpha}{d_f^2} \right)^{1.2495} \tag{5.4}$$

and the value of R^2 is 0.8324.

As it can be seen from the Figure 5.13-(a), there is a good agreement between the CFD results from this work (all CFD cases are considered in this part) with the experimental results published in phobic media, which verify that the pressure drop values of this work are in the range. It can be seen from the Figure 5.13-(a) that experimental wet pressure drop from this research (Fibrous-ME1 case) and Chang et al. (2018) are higher than the power law fit across all the data from previous works. This can be attributed to the packing density in theses two cases which is around 20% in both cases, and also large fibre diameter ($> 16\mu m$). In order to verify this claim, the wet pressure drop from the experiments of this work (Fibrous-ME1) and fibrous-CFD pressure results are presented in non-dimensional form ($Eu = \frac{\Delta P d_f}{\rho u^2 l}$) and divided by packing density function ($f(\alpha) = \alpha^{1.5}.(1 + 56\alpha^3)$) and plotted versus Reynolds number which is shown by Figure 5.14. A good agreement is shown in Figure 5.14 reinforcing the validity of the present computational methods and multi-phase (wet) pressure drop results in phobic media.

Figure 5.13-(b) illustrates the experiments and CFD simulation results conducted in this research work compared to previous studies with philic media. Similar to phobic media, it is seen that approximately all the studies fall about

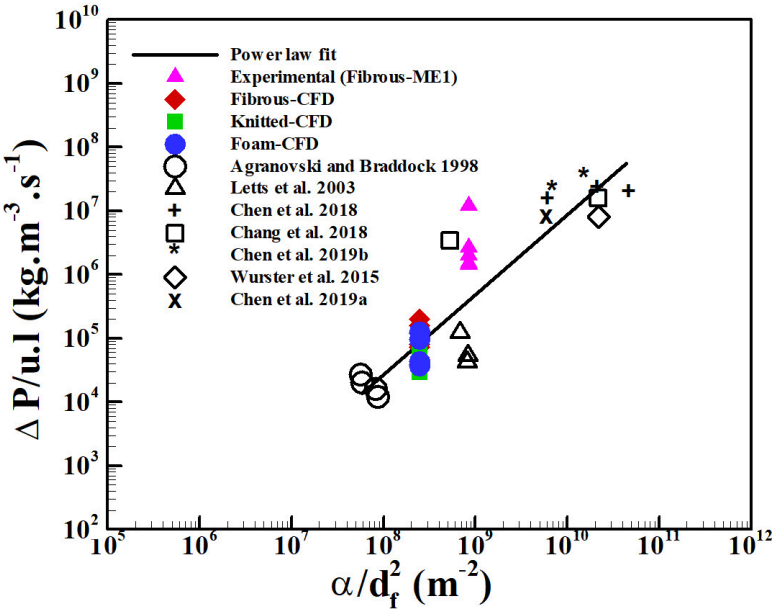

(a) Phobic media studies

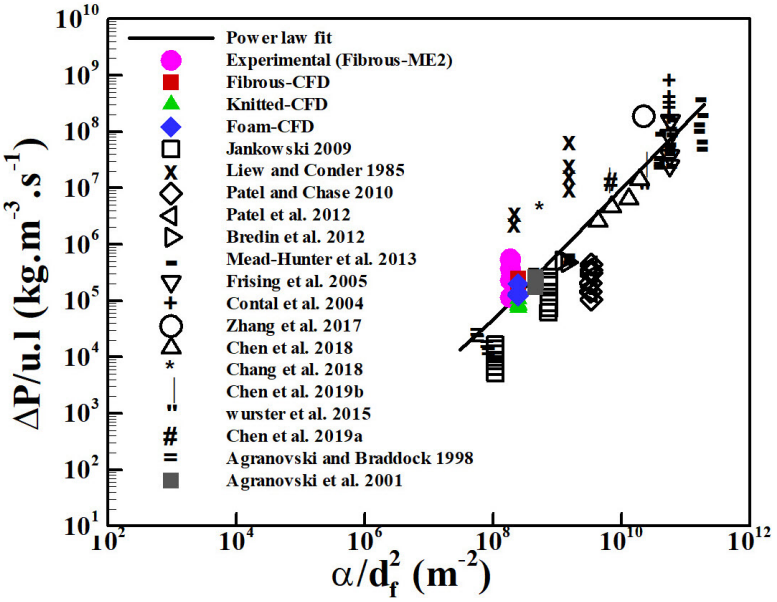

(b) Philic media studies

Figure 5.13: Comparison of multi-phase (wet) CFD pressure drop results against pressure drop values from all studies found which considered phobic and philic media with sufficient data.

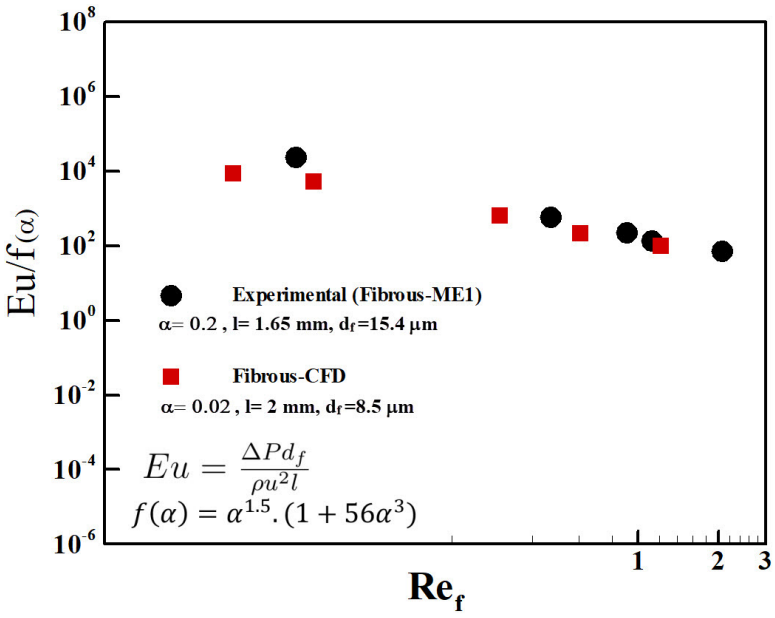

Figure 5.14: Comparison of non-dimensional multi-phase (wet) pressure drop of experimental versus CFD in phobic media.

the power law fitted line where its equation is:

$$\frac{\Delta P}{u.l} = 2.36 \times 10^{-5} \left(\frac{\alpha}{d_f^2} \right)^{1.159} \tag{5.5}$$

It is seen from Figure 5.13-(b) that the present CFD multi-phase (wet) pressure drop results (for all filter media type studied) and experimental tests (Fibrous-ME2) carried out in this research work has a good agreement with the trend of pressure drop slope from previous works. It is note worthy that it is not clear why the pressure drop results from Liew and Conder (1985) has this significant deviation from the trend line, but it should be mentioned that it is the only work that used geraniol aerosol for loading the filters studied. Furthermore, it can be seen that the wet pressure drop CFD results in this work has a good agreement with experimental test (Fibrous-ME2) and the experimental study of Agranovski et al. (2001). For a better demonstration, Figure 5.15 presents the dimensionless pressure drop (Eu) divided by packing density function versus Reynolds number.

A good agreement exists between the CFD wet pressure drop results and the data from experiments which confirms the accuracy of the predicted pressure drops in this study. In summary, both wet pressure drop results of phobic and philic media shows a good agreement with experimental results in literature and also experiments conducted in this research. This reinforce the validity of the simulations conducted in this research work.

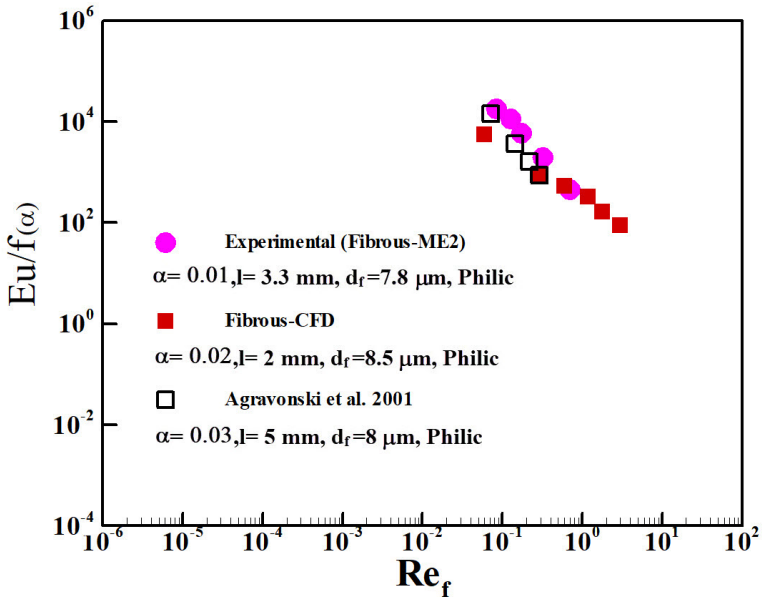

Figure 5.15: Comparison of non-dimensional multi-phase (wet) pressure drop of experimental versus CFD in philic media.

5.5.2 Residual Saturation Validation

For verifying the validity of the saturation results, two different approaches can be considered. The first approach is to use experimental test, and the second approach is applying an empirical saturation model. The validation of the residual saturation is already done by a fully detailed study of Abishek et al. (2019) which was a part of the overall research project of which this PhD forms a part. Figure 5.16 demonstrates the equilibrium saturation results against experiments.

It should be mentioned that only philic media was considered in the research work of Abishek et al. (2019) and due to difficulty of capturing the exact fibre contact angle, two low equilibrium contact angles $\theta = 5°$ and $\theta = 10°$ were considered to ensure the computational stability. It can be deduced form the Figure 5.16 that the solver is perfectly capable of predicting residual saturation compared to the experimental test.

In the case of empirical models for predicting saturation level in coalescence filters, due to applicability limitations associated with these models, it is not possible to use any of them for validating the current simulations. As explained in Section 2.3.4, empirical models are limited to a narrow range of inlet velocities and also specific filter physical properties such as packing density, fibre diameter,

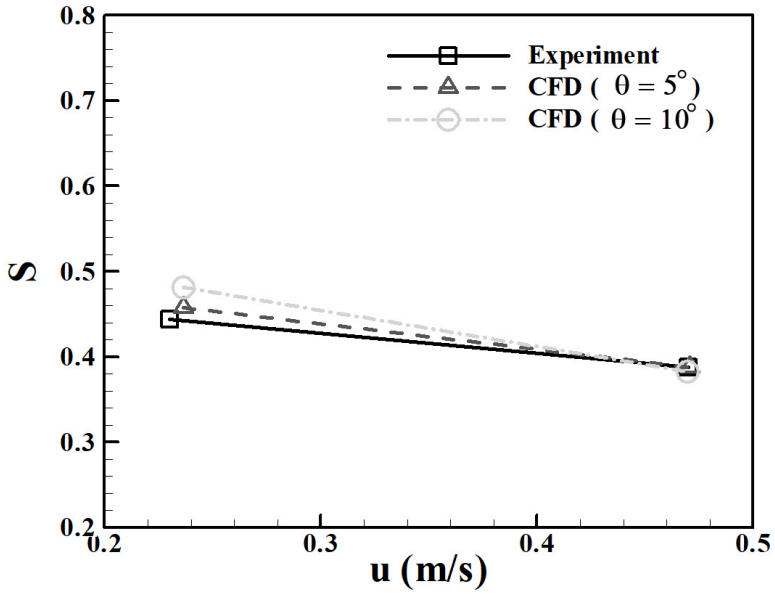

Figure 5.16: Comparison of the CFD residual saturation results against experiments (Abishek et al. (2018)).

filter thickness.

5.6 Conclusion

In this chapter, mesh generation techniques, filter media structure accuracy, mesh sensitivity analysis, single-phase and multi-phase simulation validations were presented.

It was shown that the procedure applied for reducing the poor quality mesh improved the mesh quality. After verifying the independency of the single-phase pressure drop results from the mesh resolution, accuracy of the virtually generated filter media with different structures were verified. It was shown that the virtually generated filters in this study were capable to predict the pressure drop accurately. This was verified by comparing dimensionless pressure drop results from generated filters with experimental and theoretical models. It was found that the methodology for generating virtual filter media explained in section 4.1 is corroborated by the good agreement between the predicted and theoretical or experimental results. The CFD methodology explained in section 4.2.3 was validated by comparing the CFD simulation results from this study with sets of different experimental data and theoretical results. The perfect agreement between the results assured the accuracy of the simpleFOAM solver, meshing

techniques, and also employed boundary conditions in this study. The reliability of the single-phase results is significantly important as these data will be used in future chapters in order to measure the net pressure drop caused by presence of droplets in all three media.

The mesh sensitivity analysis of multi-phase simulations indicated that the multi-phase results are more sensitive to the mesh resolution compared to the single-phase simulations. The mesh study showed that the number of cells considered in this research is sufficient in order to produce reliable results. Moreover, the influence of computational box length on the multi-phase results were studied, and it was found that the selected computational box size is capable of predicting accurate results.

Finally, the multi-phase results (pressure drop and residual saturation) were validated against experimental results from current research work and in literature. It was shown that wet pressure drop results from CFD simulations in both phobic and philic media agrees well with experimental tests which demonstrates the validity of the current multi-phase results. The validations of both wet pressure drop and saturation indicated the accuracy of the CFD methodology used (explained in Section 4.2.4) and also the numerical conditions imposed to the boundaries of the computational domain.

Chapter 6

Comparison of Equilibrium Pressure Drop, Residual Saturation, and Quality Factor in Phobic Fibrous, Knitted, and Foam Filters

6.1 Introduction

In this chapter, the performance of oil-mist coalescing filters with different structures is investigated. In order to achieve this, three different filter media (fibrous, knitted, and foam) are generated virtually, and their accuracy in resembling realistic filter media were verified in Chapter 5. As discussed in preceding Chapters , Computational Fluid Dynamics (CFD) is applied in order to carry out the investigations. The basic principles of CFD were presented in section 4.2. In terms of liquid filtration, CFD offers filter behaviour modeling which does not suffer from the drawbacks and limitations of empirical models explained in Chapter 2. It is obvious that conducting simulations are computational intensive compared to empirical modelings, but if CFD applied correctly, it will present more accurate results. To achieve accurate results, a CFD solver should be able to model the physics of the problem realistically such as pressure drop, coalescence and break up of droplets. As explained in Chapter 4, OpenFOAM software was used in this research. All the cases considered in this research, methodology applied for conducting simulations such as boundary conditions, solver settings and meshing procedures were all fully detailed in Chapter 4.

For evaluating different filter performance, the quality factor is used for comparison which was explained in Chapter 2. For the purpose of quality factor calculations, saturation and pressure drop values of the filter are required. As explained before, in this research the final stage of the filtration is considered which steady state values of pressure drop and saturation are calculated by CFD. The simulations presented are transient, and the numerical calculations were continued until the final saturation state for the given velocity was attained. This can be confirmed by observing the plateau trend in pressure drop, saturation profile, and centre of mass of oil in the filter region. This can be shown by viewing the sample results for the 2 m/s (inlet velocity) case in Figure 6.1.

As the aim of this chapter is to compare the filters in steady state, only final stage values of pressure drop, saturation, and centre of mass of retained oil are presented. The transient results can be found in Appendix A. In the beginning of this chapter, every filter is studied separately and the influence of inlet velocity variation on the saturation level, pressure drop profile, and centre of mass of retained oil in the filter, and quality factor is investigated. In the next step, all filters are compared against each other in a similar condition.

6.2 Investigating the Effect of Inlet Velocity Variation on Residual Saturation, Pressure Drop Profile, and Quality Factor of Different Phobic Media

In order to calculate the equilibrium saturation, the saturation of the filters were calculated by Equation 4.22 at every time step. To achieve this, a utility has been used to extract the saturation data from the simulations. In this section, the steady state saturation value in each velocity is normalised by the initial saturation value (30% of the void volume), and it is plotted against corresponding Reynolds number. The transient values of residual saturation and dimensionless time (calculated by Equation 4.2) for all filter media and at all velocities can be found in Appendix A.

Similarly, the pressure drop profile is plotted by using the in-built utility in OpenFOAM software to extract the pressure drop data between two inlet and outlet faces of the computational domain. The transient pressure drop values and dimensionless time are plotted and presented in Appendix A.

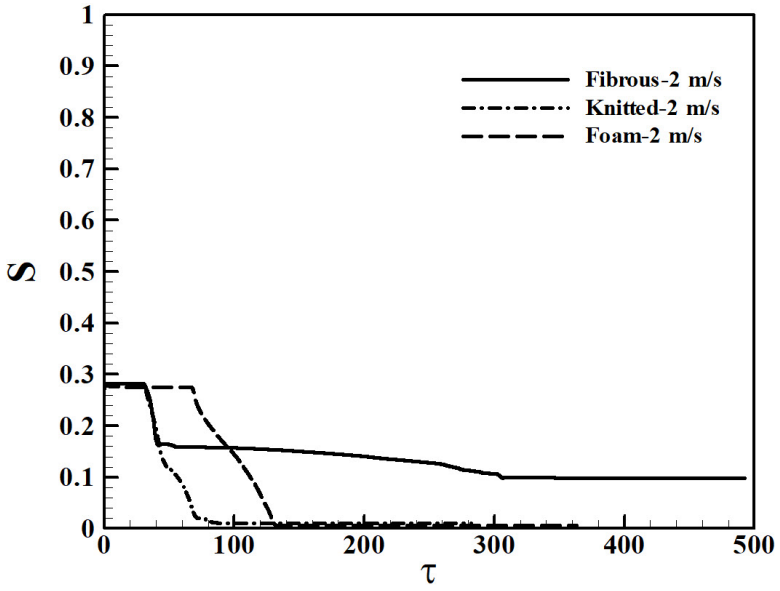

(a) Saturation profile

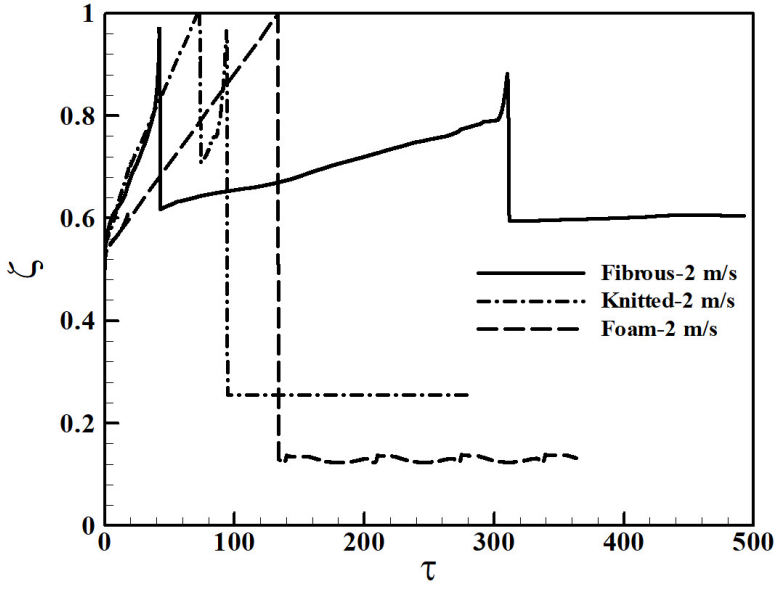

(b) Liquid Centre of Mass Vector

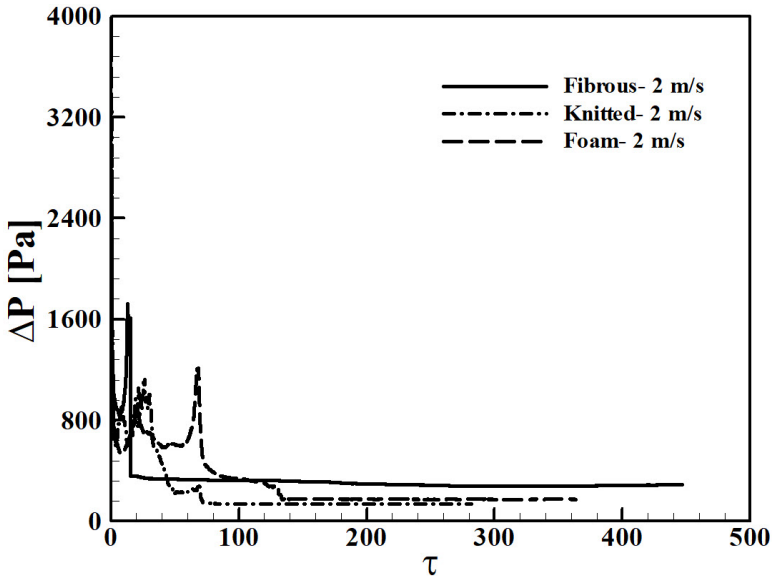

(c) Pressure Drop Profile

Figure 6.1: Transient variation in the saturation, liquid centre of mass, and pressure drop in three phobic media at 2 m/s.

Moreover, the total centre of mass of droplets are presented against dimensionless time which can be found in Appendix A. These trends are used to confirm reaching the steady condition. A utility has been employed to calculate and extract all the droplets positions in the computational domain. Summation of all these vectors were non-dimensionalaised by the filter thickness, so it shows the movement of all droplets toward the rear face of the filters, and their final steady position. It should be mentioned that in this section only the final steady position of the droplets are presented which can be helpful for understanding the trapped oil behaviour and movement inside the filter media.

In the case of performance evaluation and comparison, the quality factor is calculated base on the final steady state values of residual saturation and wet pressure drop by applying Equation 2.12 for every filter media. The quality factor results are depicted against Reynolds number to evaluate the effects of velocity change on filters performance.

6.2.1 Fibrous Filter

The dimensionless residual saturation against Reynolds number is shown by Figure 6.2. It is seen that the general trend shows a reduction in saturation by increasing in Reynolds number (due to increasing in inlet velocity as the other pa-

rameters kept constant). This occurrence has been reported by many researchers (Mead-Hunter et al. (2014); Frising et al. (2005); Contal et al. (2004)), and it can be explained by the fact that with increasing inlet velocity of filtration, the drag force on the retained oil drops within the filter enhances (Mullins et al. (2005)), which pushes them toward the downstream and resulted in a lower saturation inside the filter.

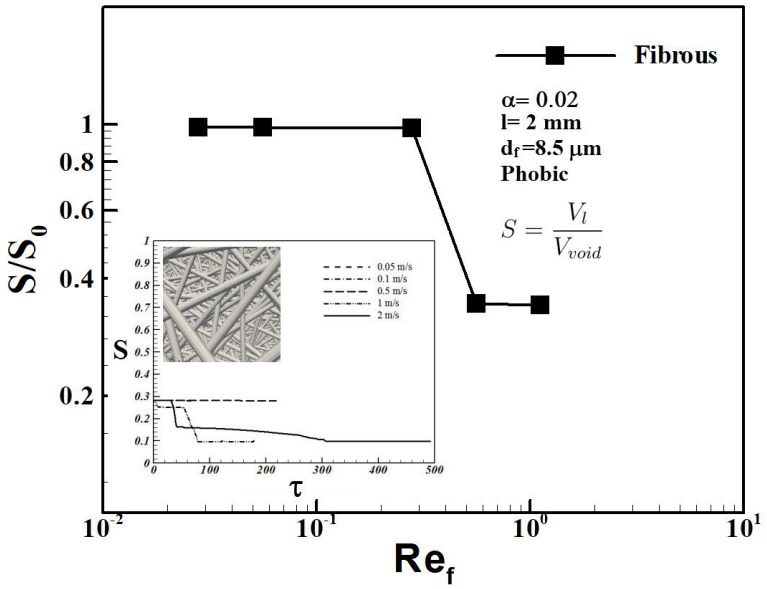

Figure 6.2: Effect of Reynolds number on equilibrium saturation in phobic fibrous filter.

By a close look at Figure 6.2, a step shape is seen in the trend line. There are two reasons for this shape: First, the number of sample points for saturation study is limited to 5 points (due to computational costs), and at the first three inlet velocities no drainage occurred which indicates that the flow was not able to provide the sufficient force to move droplets toward the rear face of the filter. Second, the intervals between the sample points is high (especially between the last three velocities). These two reasons lead to the step looking shape of the saturation graph which steady state behaviour cannot be shown completely.

The typical equilibrium distribution of retained oil droplets (their final steady state positions) are plotted by Figure 6.3 for better visualisation of saturation profile and comparison purpose. To achieve this, the snapshot of the phase $\gamma = 1$ at the final time step of each velocity case is presented.

The residual saturation reduction can be seen by comparing different velocity cases in Figure 6.3, which confirms the saturation profile in Figure 6.2. Further-

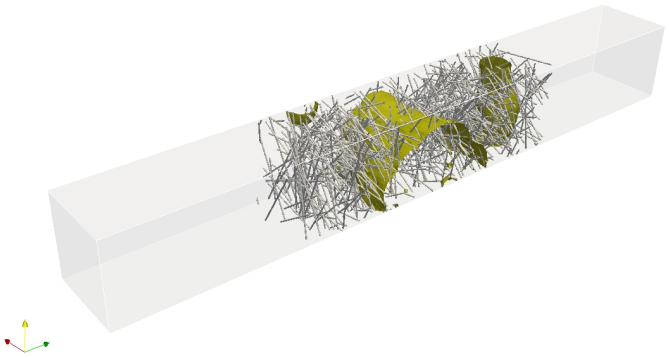

(a) 0.05 m/s

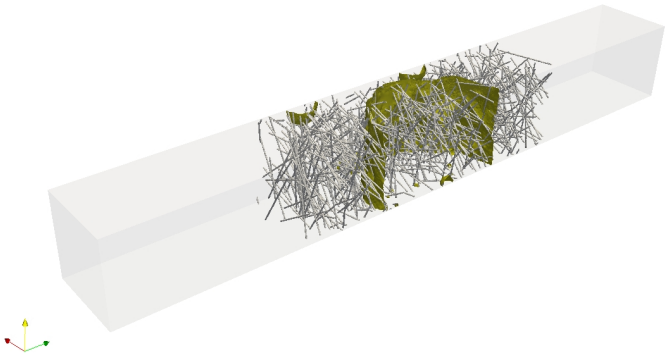

(b) 0.1 m/s

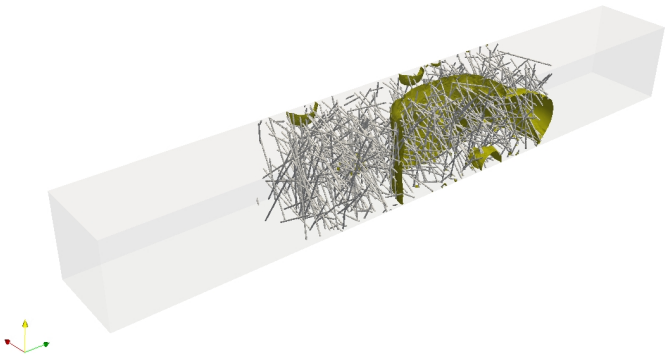

(c) 0.5 m/s

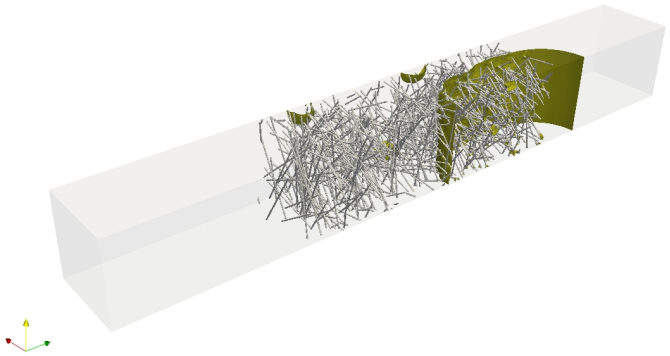

(d) 1 m/s

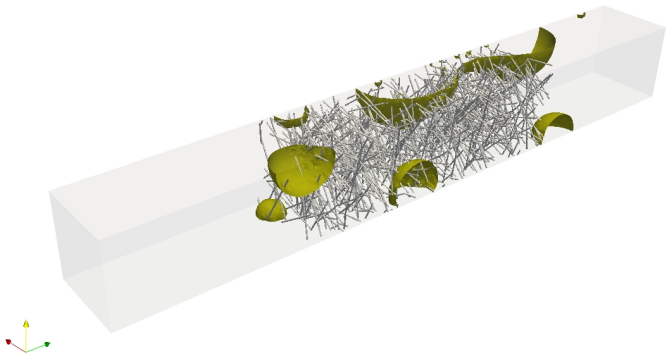

(e) 2 m/s

Figure 6.3: Retained oil droplets in phobic fibrous filter at the final steady state position.

more, it can be seen from Figure 6.3 that there is a significant difference between re-distribution of retained droplets in high Reynolds number case (2 m/s) and other cases. It is seen that at higher velocity the fluid distribution are more disperse. Charvet et al. (2008) and Contal et al. (2004) found in their experiments that filtering liquid at higher velocities causes higher re-distribution of captured liquids, reduces the penetration and ultimately will decrease the flow resistance.

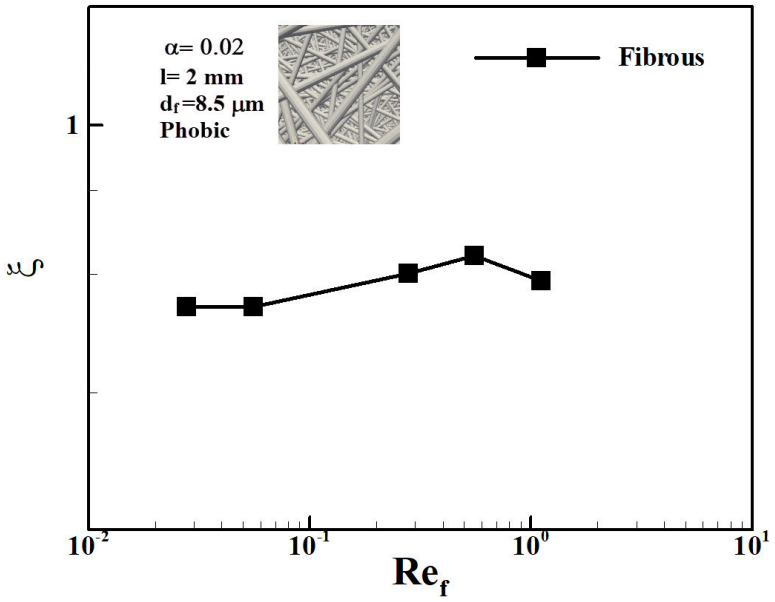

Figure 6.4: Retained oil final steady state centre of mass position at different Reynolds numbers in phobic fibrous media.

Figure 6.4 shows the final steady state position of the retained oil in the phobic fibrous filter in all study cases. This graph indicates three regions in the centre of mass graph. The first region indicates no change in centre of mass vector which suggests that with low inlet velocity flows ($Re_f < 0.1$) the residual oil does not move forward and reformation occurs. The second region in the graph which belongs to the flow rates with $0.1 < Re_f < 1$ indicates an increase in centre of mass vector. This suggests that with increasing Reynolds number (inlet velocity) the retained oil moves towards the rear face of the filter. It can be seen from Figure 6.4 that for the flow rate with $Re_f > 1$ the centre of mass of the retain oil decreases. This occurrence can be explained by two events. First, the oil droplets which are re-entrained from the back of the filter are not involved in centre of mass vector calculation. Second, higher inlet velocity reduces the penetration of the captured oil inside the filter as a result of higher dispersion rate (Charvet et al. (2008)) lead to decrease in a residual oil centre of mass vector.

The other important parameter which should be studied in filtration is the pressure distribution in the filter media. It is note worthy that the pressure drop in coalescence filters is attributed to two factors. First is the influence of the retained liquid inside the filter (oil residual saturation level) which Frising et al. (2005) found that captured liquid inside the filter media causes 80-85 % of the total pressure drop. Second, is the effect of filter structure (effect of passing flow in porous media). Figure 6.5 presents the comparison of dry and wet pressure drop in fibrous media at different Reynolds numbers.

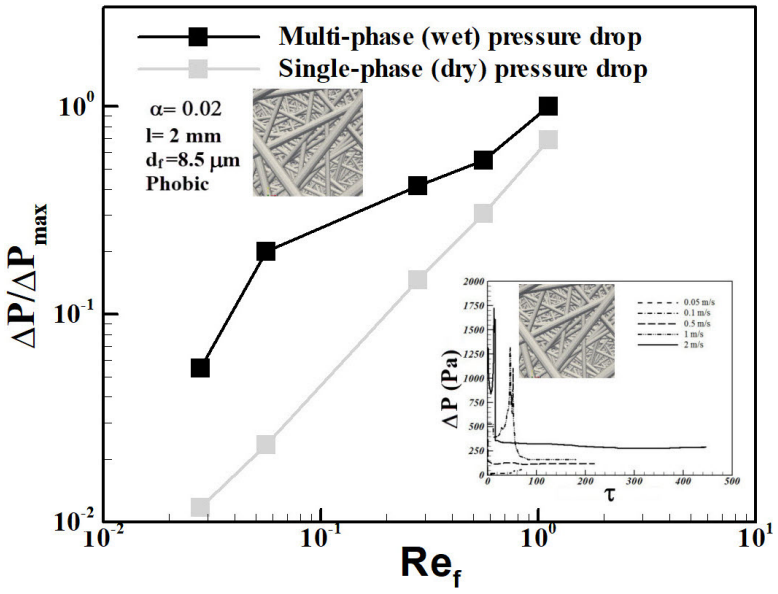

Figure 6.5: Effect of Reynolds number on multi-phase (wet) and single-phase (dry) pressure drop profile in phobic fibrous filter media.

It can be deduced form Figure 6.5 that both wet and dry pressure drop increases by increasing Reynolds number (due to increase in inlet velocity). It can be seen that dry pressure drop increases linearly in all study cases, while wet pressure drop indicates a non-linear increase in pressure drop, specially at lower Reynolds numbers. It is evident that the difference between wet and dry pressure drop values is larger at low Reynolds numbers, while the difference reduces at higher inlet velocity case. It can be calculated form the results that residual oil saturation can produce up to 88% of the total pressure drop in low Reynolds number case and reduces to 31% of total pressure drop in the highest Reynolds number. It is associated to the residual oil saturation level which reduces by increasing Reynolds number (Figure 6.2), and also decrease in flow resistance due to re-distribution of captured oil in the filter (Charvet et al. (2008); Contal et al. (2004)). The opposing effects of saturation reduction and dry filter pressure drop increase against increasing the inlet velocity suggests a possibility of having an

optimum flow velocity which results in lower pressure drop. In the case of the transient pressure drop graph presented in Figure 6.5, some oscillations are obvious in initial time steps at higher velocity cases. These correspond to events when re-distribution of captured oil in the media, partial blockage of the filter, and also detaching droplets occur which were visually observed during simulations.

In order to evaluate the performance of the fibrous filter in different Reynolds numbers, the Quality factor is calculated and presented by Figure 6.6.

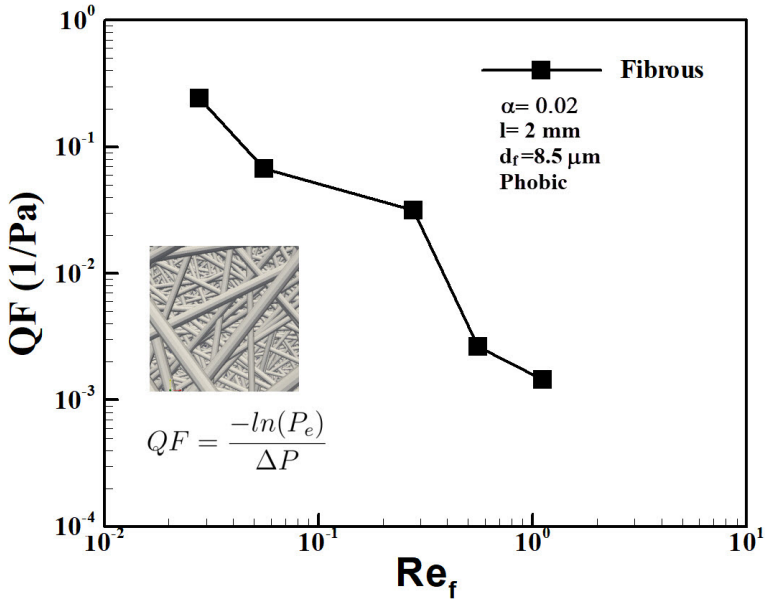

Figure 6.6: Effect of Reynolds number on quality factor in phobic fibrous filter media.

As it is seen from Figure 6.6, the quality factor decreases by increasing in Reynolds number (increasing in inlet velocity). It is worth mentioning that operating filters at higher velocities increase filter efficiency (specially in solid/gas separation), but evaluating a filter based on efficiency cannot give a proper measure to determine the filter performance. It is seen in Figure 6.6 that the quality factor is higher in lower velocities, although it has been suggested for operating coalescence filters at higher velocity to decrease the flow resistance. It can be explained by high retaining ability of fibrous filter in lower Reynolds numbers. Similar trend was found in a research on industrial crank case ventilators (Golkarfard et al. (2018)) where fibrous filters showed reduction in quality factor with increase in the gas flow rate.

6.2.2 Knitted Filter

With regard to analysing knitted filter media, the influence of Reynolds number on residual oil saturation is investigated and presented by Figure 6.7.

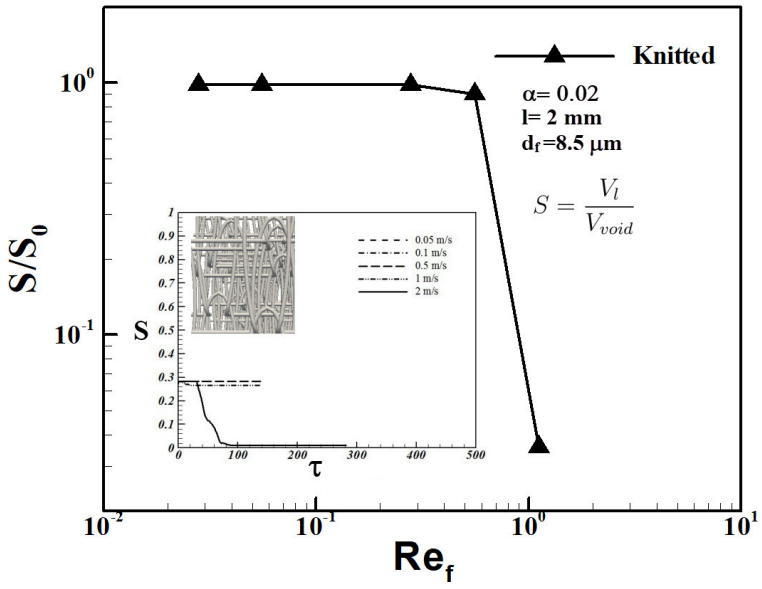

Figure 6.7: Effect of Reynolds number on equilibrium saturation in phobic knitted filter.

It is seen that similar trend to fibrous filter presents in knitted media as well which shows reduction in saturation by increasing in Reynolds number (increase in inlet flow velocity). Figure 6.7 demonstrates a gradual decreases in saturation until Reynolds 0.5 (1 m/s inlet velocity case) which the results show only 10 % reduction in residual oil saturation, and a steep decrease for higher Reynolds numbers which indicates re-entrainment of 97 % of the oil from the filter media. The results suggest that knitted media has a good self cleaning ability for inlet velocities higher than 1 m/s, which helps to reduce the flow resistance. For better demonstration, Figure 6.8 shows the final steady position of the captured oil in the phobic knitted media.

It is deduced form the Figure 6.8 that the low inlet velocity cases do not provide enough sheer forces for pushing the residual oil out of the filter. Moreover, up to inlet velocity of 1 m/s, the residual oil coalescence and form a big droplet which causes the forward progress of the oil in direction of carrier flow. It can be seen that high velocity (2 m/s) reduces the penetration of oil inside the knitted filter. It can be confirmed by holding some oil in the inlet section of the filter, although the majority of captured oil portion is pushed out by flow drag force

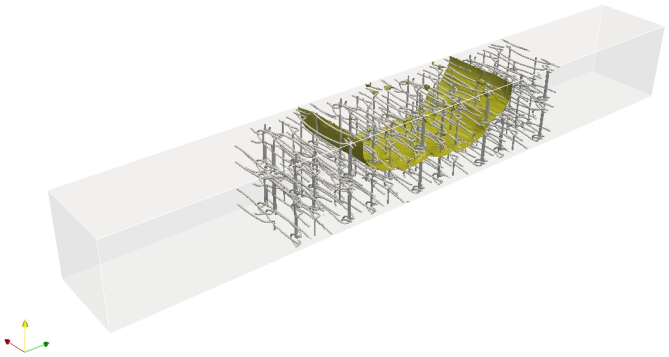

(a) 0.05 m/s

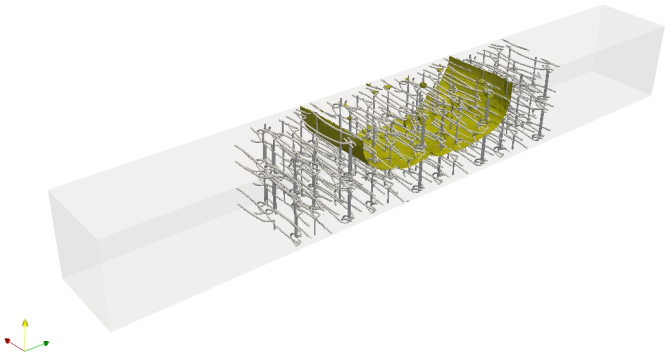

(b) 0.1 m/s

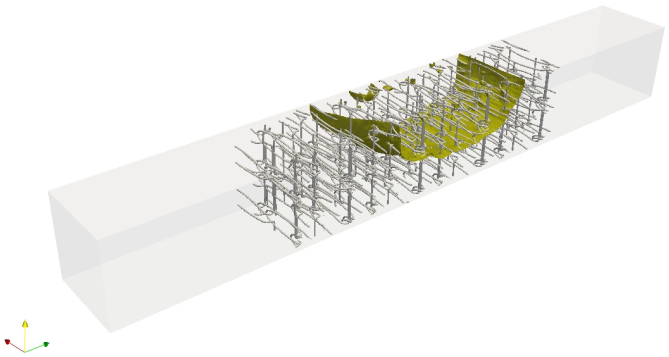

(c) 0.5 m/s

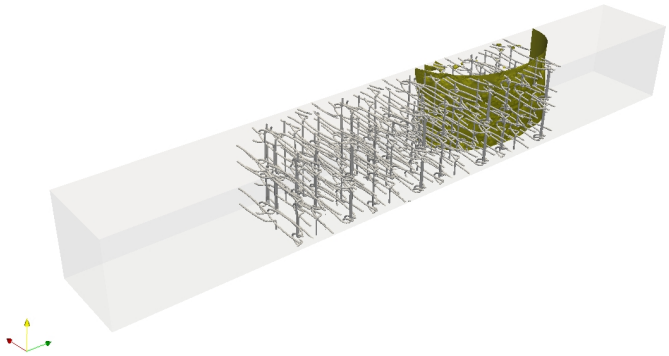

(d) 1 m/s

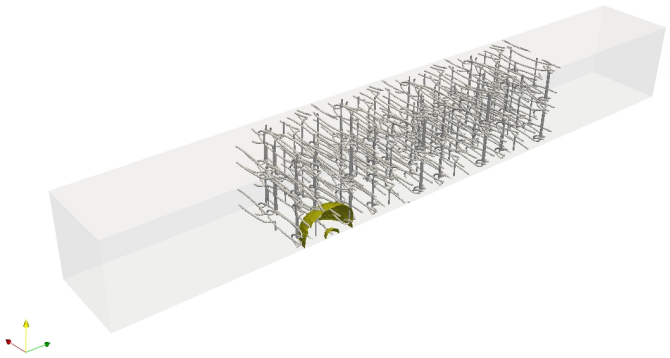

(e) 2 m/s

Figure 6.8: Retained oil droplets in phobic knitted filter at the final steady state position.

(Mullins et al. (2005, 2007)). This events can be confirmed by evaluating the final steady position of retained oil in different Reynolds number. Figure 6.9 indicates the final steady oil position vector values in knitted media.

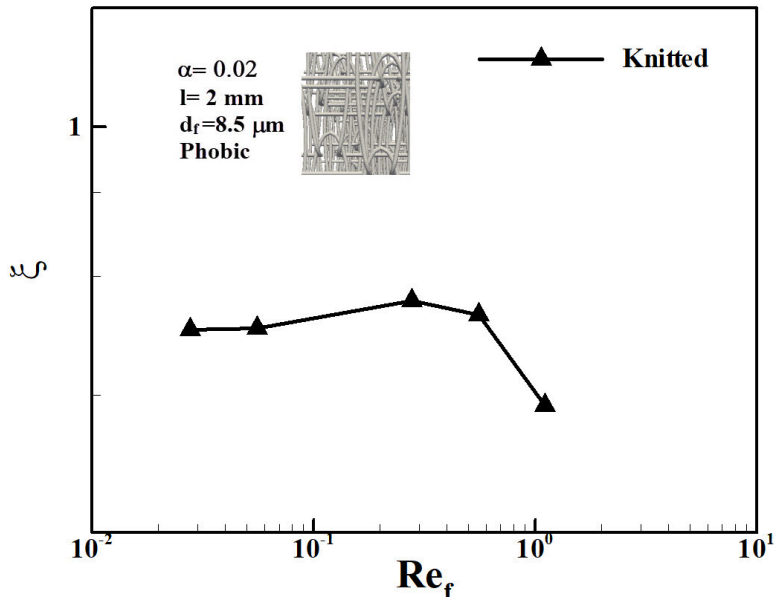

Figure 6.9: Retained oil final steady state centre of mass position at different Reynolds numbers in phobic knitted media.

A similar trend to the phobic fibrous filter can be seen in knitted media, which shows the position vector initially increases by increasing in inlet velocity (shows the progress of residual oil toward the rear face), and then decreases due to re-entrainment from the rear face of the filter and also distribution of trapped oil into smaller fluid distributions. This causes lower resistance to the flow and consequently resulted in less pressure drop to the system, and require larger drag force to be removed from the filter (Frising et al. (2005)).

Figure 6.10 presents the pressure drop across phobic knitted media against Reynolds number. As discussed earlier in this chapter, both single-phase and multi-phase pressure drop profiles are normalised and presented.

The first point that can be seen in Figure 6.10 is the increasing multi-phase (wet) pressure drop by increasing in Reynolds number. It is deduced that this enhancement is almost linear similar to the single-phase pressure drop which the presence of the residual oil in the filter attributed to 54 % in low velocity inlet case up to 65 % at higher velocity (1 m/s case). This shows that the pressure drop trend deviate gradually from the single-phase pressure drop trend. Moreover, it is seen that at the highest Reynolds number (2 m/s), the wet pressure drop value

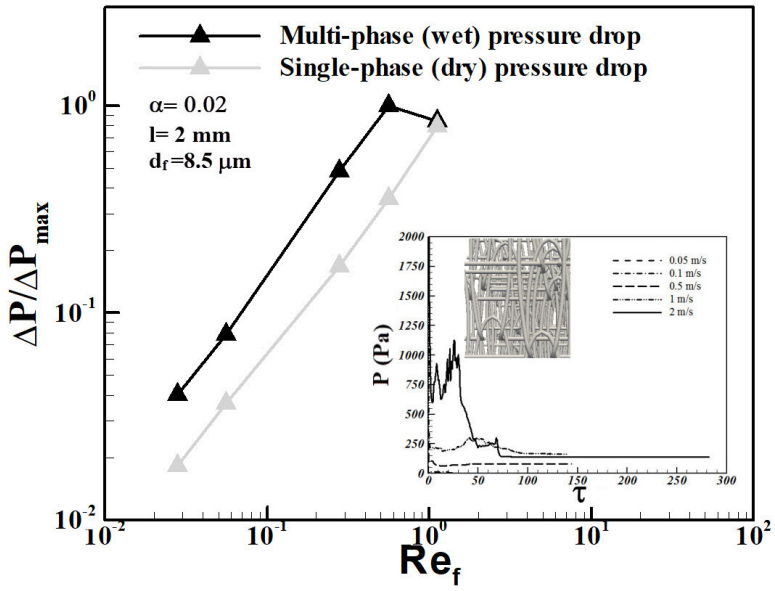

Figure 6.10: Effect of Reynolds number on multi-phase (wet) and single-phase (dry) pressure drop profile in phobic knitted filter media.

approaches the the dry pressure drop value which is mainly due to low amount of residual oil saturation (only 3 %) in the filter, and also lower wet pressure drop in higher Reynolds number case compared to lower Reynolds number. This suggests again that there is a possibility for having an optimum region in the pressure drop profile in phobic knitted media.

For the purposes of examining the performance of the phobic knitted media, its quality factor against Reynolds number is calculated according to its oil retention ability and imposing pressure drop to the system. Figure 6.11 depicts the influence of Reynolds number on quality factor in phobic knitted media.

It is noticeable from Figure 6.11 that similar to phobic fibrous media, the knitted media quality factor reduces by increasing in Reynolds number (increasing in inlet velocity). Although from the residual saturation profile it was seen that knitted media holds the captured oil for higher velocities, but it imposes higher pressure drop to the system which reduces the quality of the filtration.

6.2.3 Open-cell Foam Filter

Figure 6.12 shows the residual oil saturation profile against Reynolds number of phobic foam media to investigate this filter type in different velocity inlet conditions. From the first observations, the similar trend of the saturation reduction

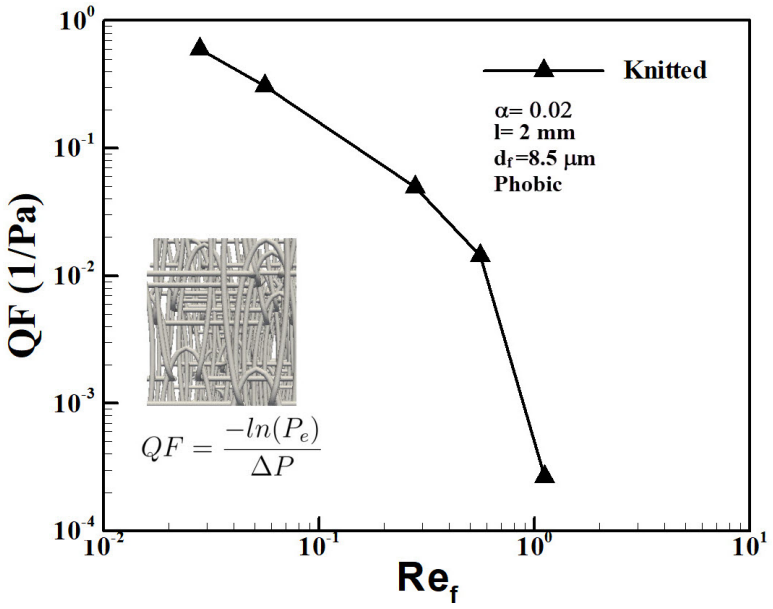

Figure 6.11: Effect of Reynolds number on quality factor in phobic knitted filter media.

with Reynolds number (which discussed earlier in other two filter media structures) presents in foam filter as well. More importantly, it can be deduced from the saturation graph for phobic foam filters that re-entrainment starts at low values of Re_f. This suggests that media structure plays a key role here with the pores in the foam filter being more connected resulting in the formation of larger droplets within the media. These droplets can cover the width of the filter and therefore impose a higher pressure drop on the system. This pressure drop acts as a strong driving force sufficient to move the residual oil to the rear face of the filter even at low inlet velocities. This is further illustrated in Figure 6.13 plotting where the final steady state position of the residual oil in the phobic foam filter is shown.

As in Figure 6.13 can be seen from the snapshots of the residual oil saturation in phobic foam media, at low Reynolds number the residual oil inside the foam filter forms a larger droplet which covers the width of the filter and gradually moves toward the rear face in the higher velocity case (0.1 m/s). By increasing in inlet flow velocity, the dispersion of the oil occurs inside the foam filter which resulted in some oil residual close to the inlet section of the filter. This event is presented in Figure 6.14 by showing the residual oil final steady centre of mass position vector value against Reynolds number.

It is evident from the Figure 6.14 that the centre of mass vector increases in

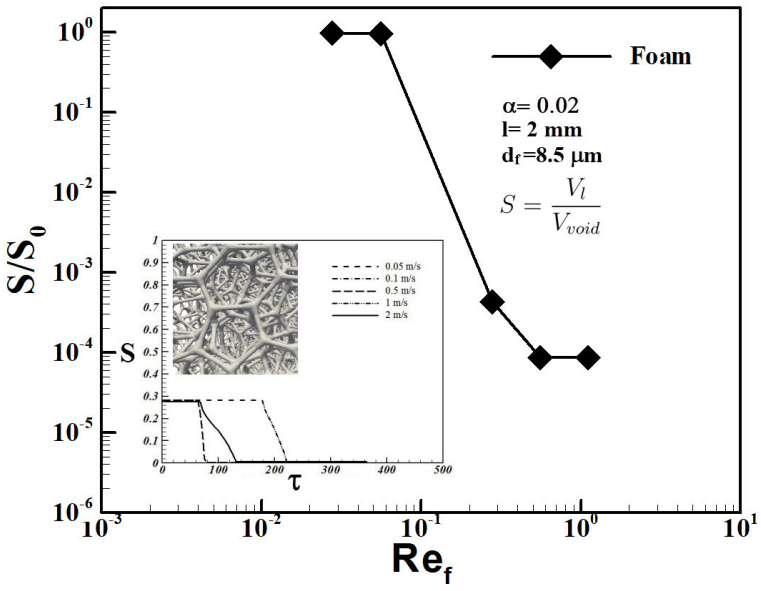

Figure 6.12: Effect of Reynolds number on equilibrium saturation in phobic foam filter.

low inlet flow velocity cases($Re_f < 0.3$) . This suggests that the residual saturation moves towards the rear face of the foam filter. In higher inlet velocity cases where $Re_f > 0.3$, the centre of mass graph shows a sharp decline which is mainly due to significant re-entrainment occurring in foam media (Figure 6.12). This portion of the saturation which left the domain is not considered in the centre of mass vector calculation. Moreover, some oil saturation are retained close to the inlet face due to higher velocity effect and dispersion effect (which was fully discussed earlier). These two events causes the sharp decline in the residual saturation centre of mass position.

For the purposes of reviewing the pressure drop in foam media, Figure 6.15 demonstrates the influence of Reynolds number on multi-phase and single-phase pressured drop values.

It is clear from Figure 6.15 that in low Re_f number cases, the multi-phase pressure drop contributes to 70 to 77 % of the total pressure drop in the system, while an increase in inlet velocity reduces this to almost 5 to 8 % of the total pressure drop. Similar to other filter structures studied so far, the opposing effects of residual oil (saturation) and pressure drop in the system suggests that an optimum region may be present. Closer examination of Figure 6.15, reveals that the last two study cases the multi-phase pressure drop deviates from the single-phase pressure drop trend. This result suggests that even low saturation level in higher inlet velocity plays a key role. This phenomena will be discussed

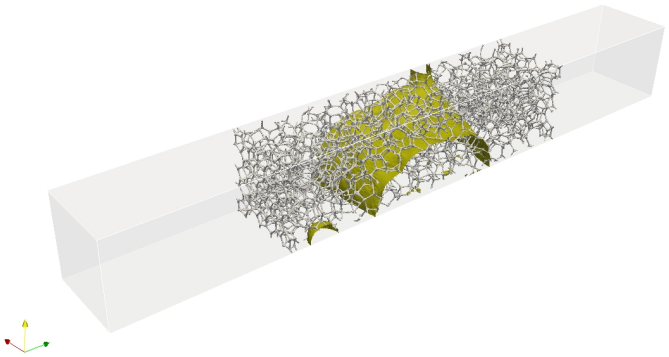

(a) 0.05 m/s

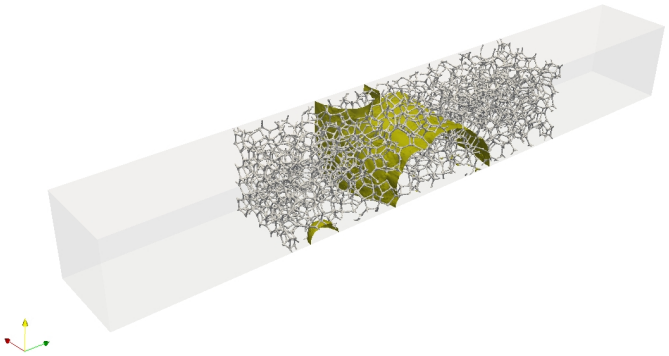

(b) 0.1 m/s

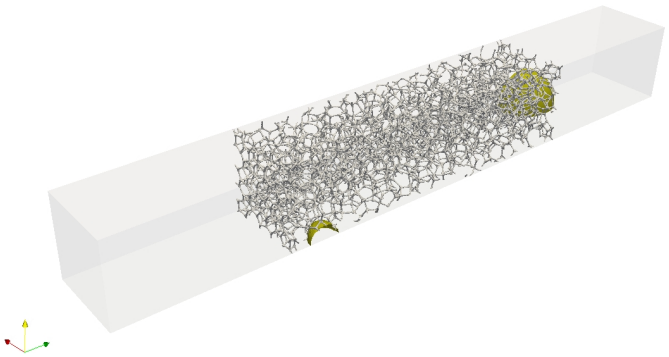

(c) 0.5 m/s

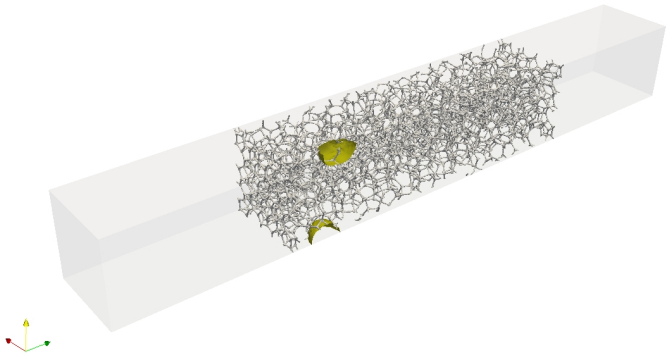

(d) 1 m/s

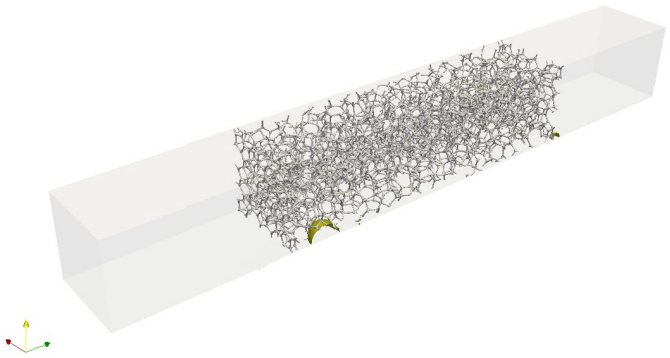

(e) 2 m/s

Figure 6.13: Retained oil droplets in phobic foam filter at the final steady state position.

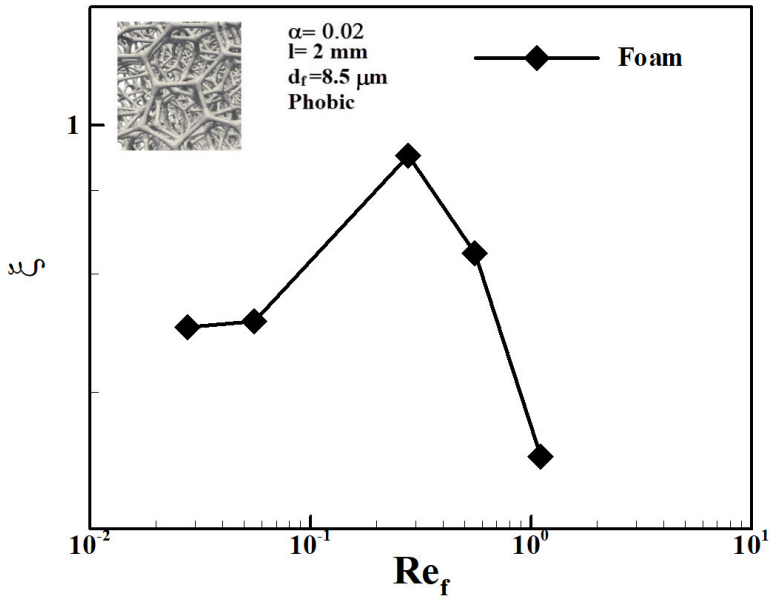

Figure 6.14: Retained oil final steady state centre of mass position at different Reynolds numbers in phobic foam media.

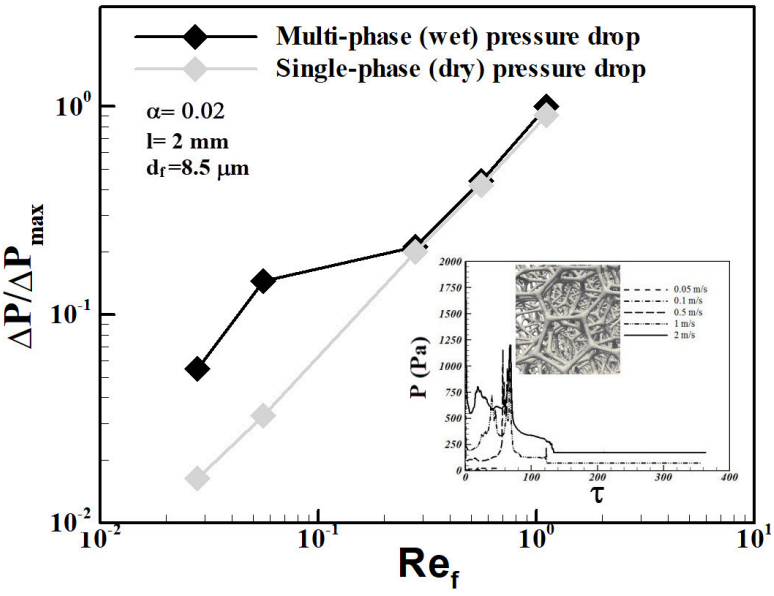

Figure 6.15: Effect of Reynolds number on multi-phase (wet) and single-phase (dry) pressure drop profile in phobic foam filter media.

in more details in Chapter 9.

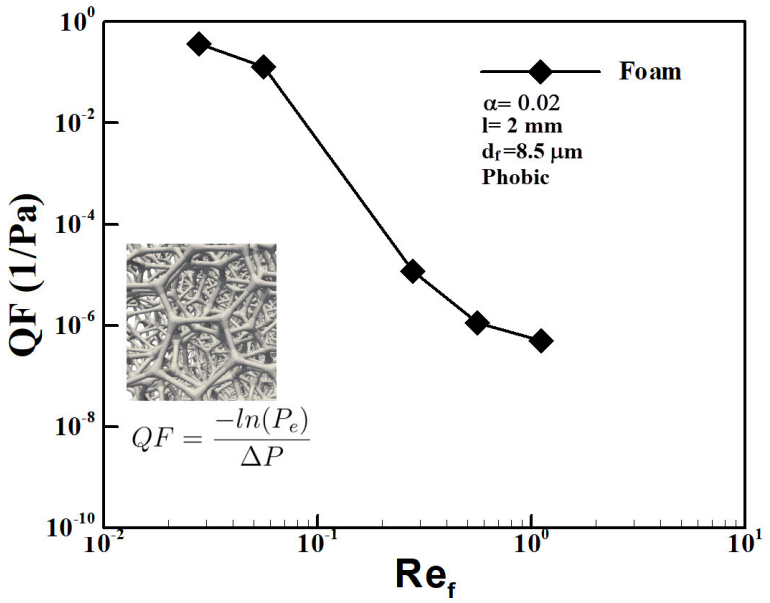

Figure 6.16: Effect of Reynolds number on quality factor in phobic foam filter media.

Figure 6.16 presents the quality factor of phobic foam media at different Reynolds number to help for verifying its performance. Similar to other studied filters, the investigation of quality factor in phobic foam media indicates that by increasing the Reynolds number (due to increase in inlet velocity), the performance of the phobic filter reduces significantly which can be explained by its poor retaining ability.

6.2.4 Comparison of Performance of Three Phobic Media With Different Structures

In this section, the quality factor calculations of all studied filter media are represented again in order to provide a better insight for comparison. At the beginning, the saturation profile of the mentioned filter media are depicted in Figure 6.17 to provide a better comparison view.

It is seen from Figure 6.17 that all filters hold the filter oil content at low Reynolds number flows (inlet velocity <0.1 m/s). Furthermore, it is clearly observable that foam filter has the lowest retaining ability among all studied phobic media filters, which its re-entrainment starts at lower Reynolds number (0.5 m/s

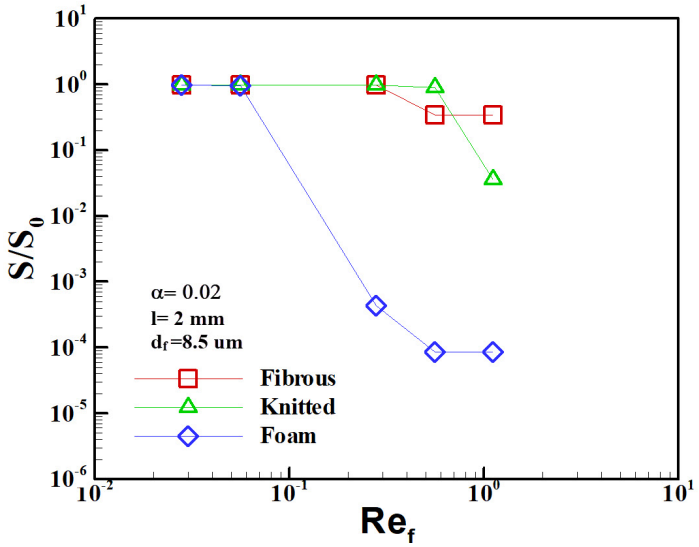

Figure 6.17: Effect of Reynolds number on residual saturation in phobic fibrous, knitted, and foam media filters.

inlet velocity). Fibrous and knitted media shows a better liquid holding ability at higher velocities, especially fibrous filter media indicates higher residual saturation level in the highest inlet velocity test case. This event can be explained by the structure of fibrous filter which the intersections of the fibre elements provides larger contact area to an oil droplet inside the filter and improves its retaining ability (Contal et al. (2004)), while in knitted media such an intersections dose not present. Moreover, it was shown that higher velocity disperse the residual oil in fibrous filter media significantly compared to other media which consequently decreases the flow resistance (Frising et al. (2005)) and resulted in lower drag force to the residual oil. On the other hand, foam media has significant pores with void space which all connected and allows residual oil to form a larger droplet (due to phobicity of the media), which causes higher pressure drop and consequently higher drag force on the droplet in the domain.

Figure 6.18 compares the multi-phase (wet) pressure drop in all studied filter media. It is worth mentioning that all pressure drop values are non-dimensionalised by the maximum pressure drop (in fibrous filter)in order to be comparable.

It is visible in Figure 6.18 that fibrous filter media produces the highest pressure drop in all Reynolds numbers. In low Reynolds number case studies (first two inlet velocity cases) which all filter media hold the oil inside the filter, knitted media imposes the least pressure drop to the system. From the pressure drop values, it can be calculated that fibrous filter produces 2.5 and 5 times higher

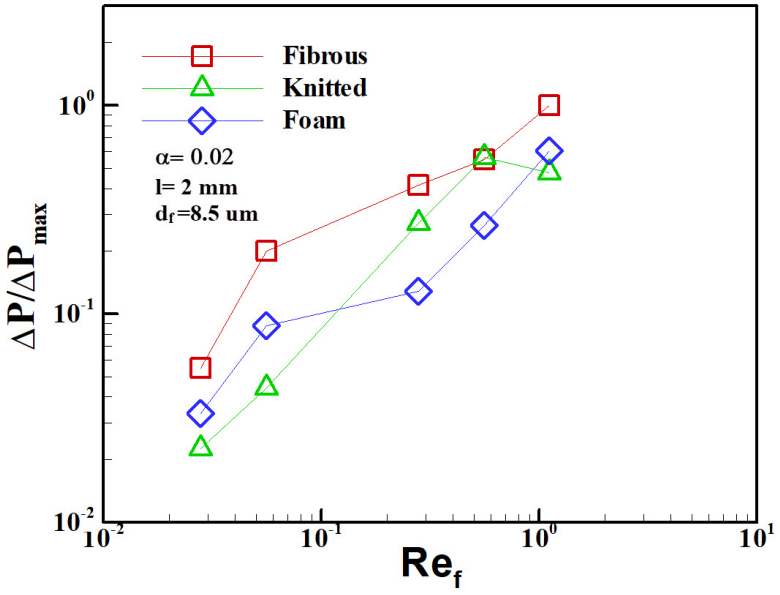

Figure 6.18: Effect of Reynolds number on multi-phase pressure drop profile in phobic fibrous, knitted, and foam media filters.

pressure drop compared to knitted media in 0.05 and 0.1 m/s inlet velocities, respectively. It is worth mentioning that the study filters produces different dry pressure drop values, but in low Reynolds numbers their difference is marginal. This can be confirmed by viewing the Figure 6.19.

An interesting point which can be seen in comparing the single and multi-phase pressure drop graphs (Figures 6.18 and 6.19) is the fact that in the first two inlet velocities, the single-phase pressure drop in all filter media is very similar (16 % difference for the lowest to the highest values), while the multi-phase pressure drop graph shows a significant difference among filters (250 % between the lowest and the highest pressure drop values). This event can be attributed to the residual oil coalesce difference in these different structures. As shown earlier, the retained oil forms larger droplets in fibrous filters covering the width of the filter and as a result of capillary and shear forces results in higher flow resistance compared to knitted media. This occurrence was also observed by Sheng et al. (2020), where comparisons between knitted and fibrous filters were made. Their results indicated that knitted media produces 1/4 of the pressure drop compared to fibrous filter at similar inlet velocities. As mentioned before, foam filter produces pressure drop close to its dry filter pressure drop values in higher Reynolds number due to re-entrainment of the oil, but fibrous and knitted filter media deviate from their dry pressure drop profile due to presence of residual oil saturation in these filters.

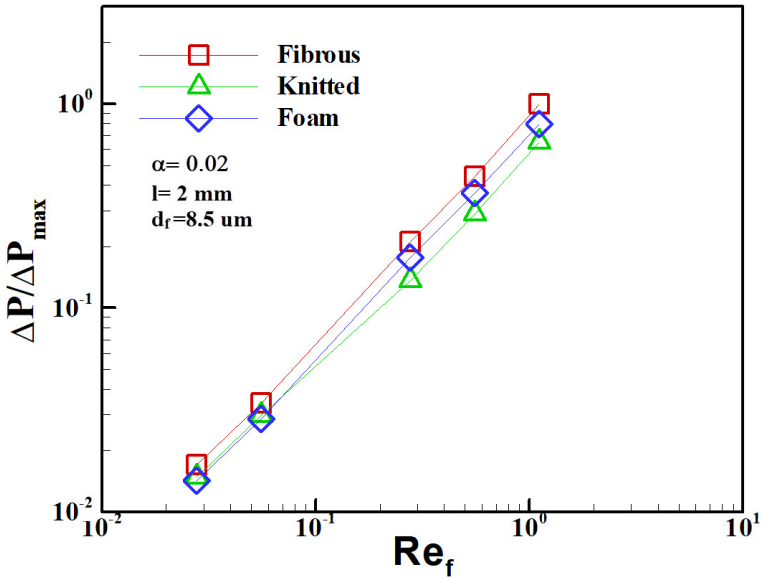

Figure 6.19: Effect of Reynolds number on single-phase pressure drop profile in fibrous, knitted, and foam media filters.

Figure 6.20 illustrates the quality factor comparison of all filter media against Reynolds number. Here in the first two low Reynolds number cases, all filers have high quality factors compared to the higher Reynolds number cases due to increasing re-entrainment at higher velocities. As can be seen, knitted media shows the best performance in the majority of flow rates mainly due to its high oil retaining ability and lower pressure drop.

These results agree well with Sheng et al. (2020) which showed that knitted media performs better than fibrous media over the range of parameters studied. It is clear that at the highest velocity, the fibrous filter performs better than other filters owing to its ability to better distribute residual oil thereby reducing the flow resistance. It is apparent that knitted media is not a proper choice for higher Reynolds number flows. Finally, it can be seen that foam media has the lowest quality factor at higher Reynolds number which is related to its comparatively poor oil retaining capability.

6.3 Conclusion

In this chapter, an extensive numerical study was conducted on multi-phase flow modeling in three different phobic filter structures (fibrous, knitted, and foam) with contact angle equal to 120° at various inlet velocities (0.05, 0.1, 0.5, 1, and

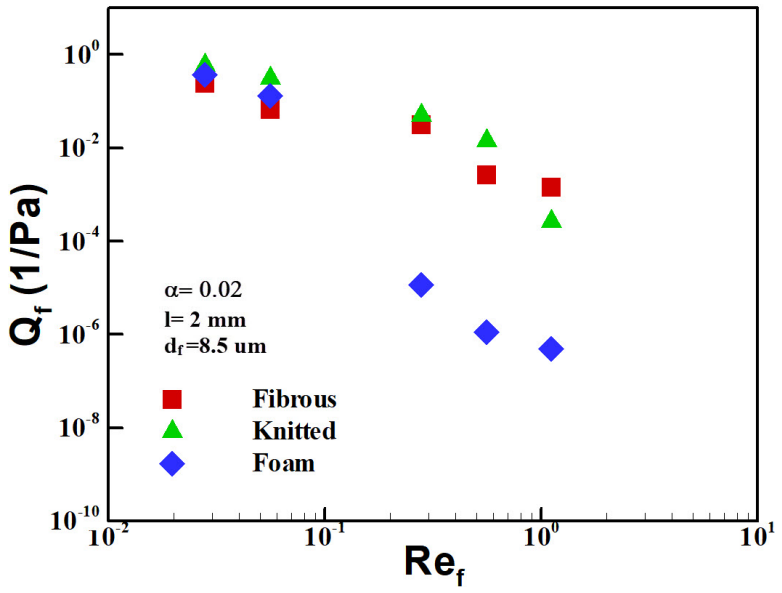

Figure 6.20: Effect of Reynolds number on quality factor in phobic fibrous, knitted, and foam media filters.

2 m/s) and equivalent pre-saturation. All filters had similar physical properties such as packing density, fibre element diameter, filter thickness, and filter cross section area. Therefore, it provides a consistent evaluation and comparison of their performance.

CFD results indicated that residual oil saturation decreases with increase in inlet velocity (due to increase in flow forces) as the general trend in all filter media. It was found that foam media has the lowest retaining capability among all phobic filters (where the onset of the re-entrainment was 0.5 m/s), while the knitted media showed higher retaining ability up to 1 m/s. It was shown that fibrous filter has the best holding ability for higher velocities due to its structure difference which causes more distribution of residual oil inside the filter and reduces the flow resistance and pressure drop.

Reviewing the multi-phase (wet) pressure drop results showed that residual oil saturation has a significant impact in low inlet velocity cases (0.05 and 0.1 m/s) and causes a strong deviation form the dry pressure drop trend, while its effect decreases by increasing in inlet flow velocity due to reduction in residual oil and also flow resistance. CFD results demonstrated that fibrous filter imposed the highest pressure drop among all studied filter media, while knitted media had the lowest pressure drop due to its interlocking with large void space structure. Furthermore, it was found that by increasing the flow velocity, the flow resistance reduces, while the filter structure imposes higher resistance and pressure drop

to the system. It was discussed that these opposing effects may resulted in an optimum region in pressure drop profile.

Finally, the quality factor analysis of three phobic media revealed that knitted media performed the best for the majority of the inlet velocities (0.05, 0.1, 0.5 and 1 m/s) due to its high liquid holding capability, while foam media showed the worst performance. It was found that fibrous filter has the highest quality factor compared to the other two media types for the highest inlet velocity (2 m/s) where the residual oil distribution occurred and reduced the flow resistance in this media.

Chapter 7

Comparison of Equilibrium Pressure Drop, Residual Saturation, and Quality Factor in Philic Fibrous, Knitted, and Foam Filters

7.1 Introduction

In this chapter, three philic media with different structure of fibrous, knitted and foam will be studied numerically by using CFD techniques described in chapter 4.2. As mentioned earlier in Boundary Conditions section (4.2.4), the contact angle in philic filters is considered as $\theta = 20°$. The rest of conditions such as packing density, fibre diameter, filter size, initial saturation, and CFD solvers are the same as used in phobic simulations. It should be noted that inlet velocity in philic media should be increased to higher range compared to phobic filters as stronger force is required for detachment of droplets in philic filters (Hotz et al.; Mullins et al.). Therefore, inlet velocity range is extended to 5 m/s which resulted in $Re_f = 2.78$.

In the following sections, the CFD results of philic filters will be presented and discussed in detail. The steady state saturation and pressure drop results are employed in order to evaluate filters performance by calculating their quality factor (Eq. 2.12). As discussed in Chapter 6, the transient graphs are used for confirming steady state of the filters at different velocity and only the steady state graphs are presented for analysis. All the transient simulation results are

in Appendix A, and in the following only 1 m/s test case is illustrated by Figure 7.1 for an example.

Initially in this chapter, every filter is studied separately and the effect of inlet velocity variation on residual saturation, pressure drop, and centre of mass of residual oil in the filter, and quality factor is investigated. In the next step, all filters are compared against each other in similar condition.

7.1.1 Investigating the Effect of Inlet Velocity Variation on Residual Saturation, Pressure Drop Profile, and Quality Factor of Different Philic Media

7.1.2 Fibrous Filter

The dimensionless saturation profile against Reynolds number for philic fibrous media is depicted by Figure 7.2.

As expected, with increasing Reynolds number (increasing velocity as other parameters kept constant) the saturation reduces. The simulations indicate a general decreasing trend in residual saturation as has been reported in the literature (Contal et al. (2004); Mullins et al. (2014); Mead-Hunter (2013)). The numerical results indicate that up to $Re_f = 1.67$, initial saturation reduces only by 8%, while in the last inlet velocity case which resulted in $Re_f = 2.78$, the re-entrainment increases to 35%.

The other important factor which should be considered in philic media is attached droplets to the rear face of the filter which is shown in Figure 7.3 for a better demonstration. The droplets are attached to the rear face of the filters in different velocities. A similar phenomenon was observed during the experimental study of Bredin and Mullins (2012), where it was found even these droplets can return to the filter by capillary force when the inlet flow is discontinued. This liquid volume is considered in saturation calculations (although they are out of the filter region itself) the oil is still on the filter and therefore impacts pressure drop. It is observed that in low inlet velocity cases, the residual oil forms a contiguous liquid structures through the filter, while in higher velocity cases the residual oil disperse inside the filter which ultimately reduces the flow resistance (Contal et al. (2004); Charvet et al. (2008)). It is visible from Figure 7.3 that by increasing in face velocity, the droplets move progressively through the filter which is confirmed by calculating residual oil centre of mass position for all velocities. This event is illustrated in Figure 7.4, where the the final steady state

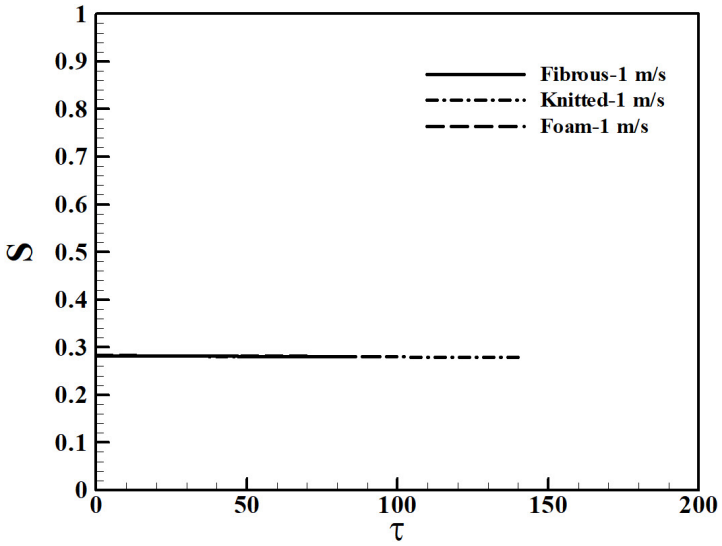

(a) Saturation profile

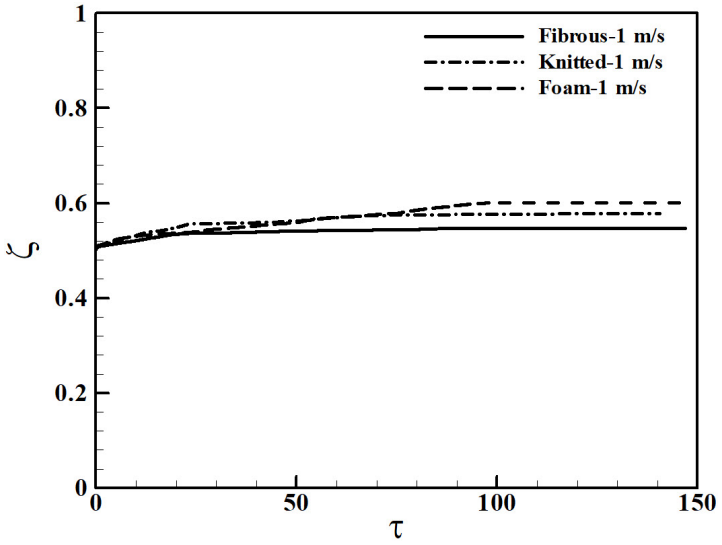

(b) Liquid Centre of Mass Vector

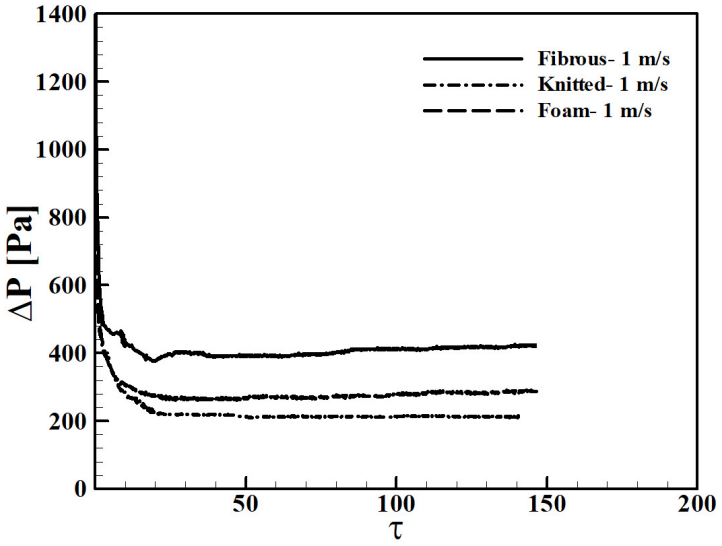

(c) Pressure Drop Profile

Figure 7.1: Comparison of saturation, liquid centre of mass, and pressure drop in three oleophilic media at 1 m/s.

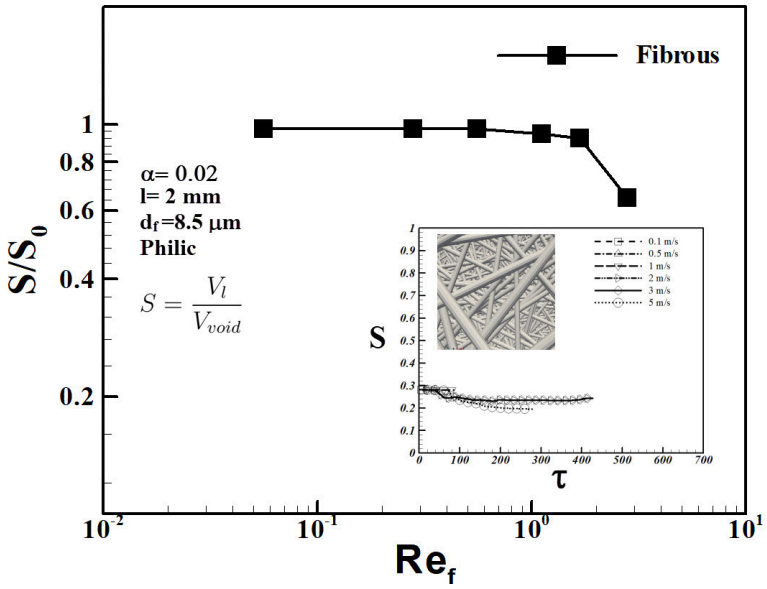

Figure 7.2: Effect of Reynolds number on equilibrium saturation in Philic fibrous filter.

position of residual oil is observable.

It is evident from Figure 7.4 that the residual oil centre of mass moves towards the rear face of the filter by increasing with Reynolds number (inlet face velocity). This can be explained by the effect of capillary and air flow forces which pushes the residual oil toward the rear face of the filter (Mullins et al. (2007)).

The other parameter evaluated in fibrous media is multi-phase (wet) pressure drop which is presented by Figure 7.5 along the dry pressure drop values in corresponding Reynolds numbers in order to isolate the effects of residual oil saturation on the wet pressure drop profile.

It can be concluded form the Figure 7.5 that both multi-phase and single-phase pressure drop rises by increasing in Reynolds number (increasing inlet velocity). It is visible from the graph that the difference between multi-phase and single-phase pressure drop values decreases by increasing in Reynolds number. The CFD results indicate that the residual oil saturation contributed to 84% of the total pressure drop at the lowest Reynolds number and drops to 62% for the highest Reynolds number. This event can be explained by reduction in residual oil saturation due to increase in Reynolds number (Figure 7.2). Moreover, reduction in flow resistance due to residual oil dispersion inside the filter media is another reason for declining the influence of residual oil on the pressure drop profile (Charvet et al. (2008); Contal et al. (2004)). Similar to phobic media which

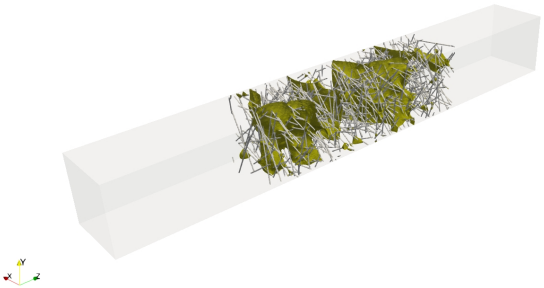

(a) 0.1 m/s

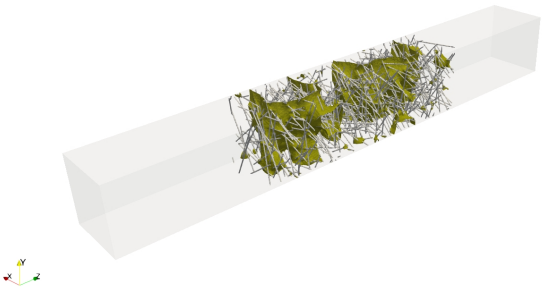

(b) 0.5 m/s

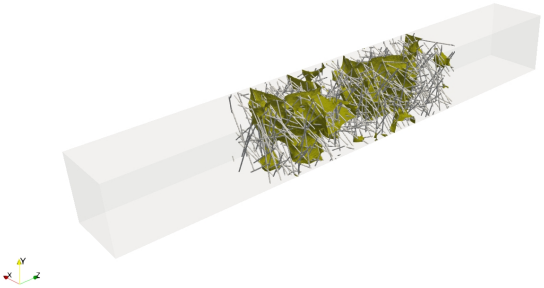

(c) 1 m/s

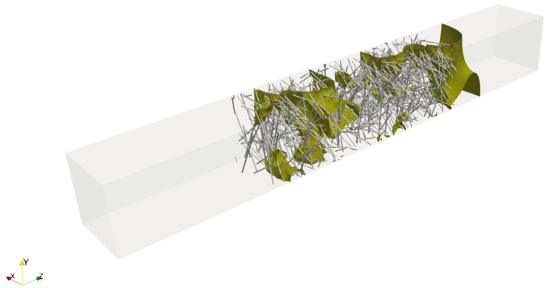

(d) 2 m/s

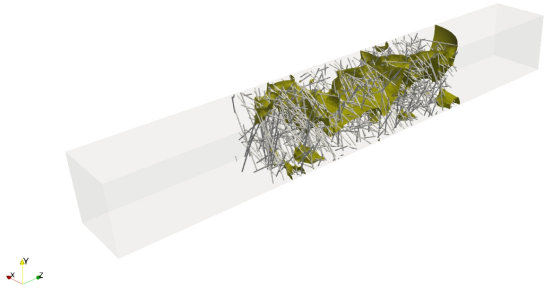

(e) 3 m/s

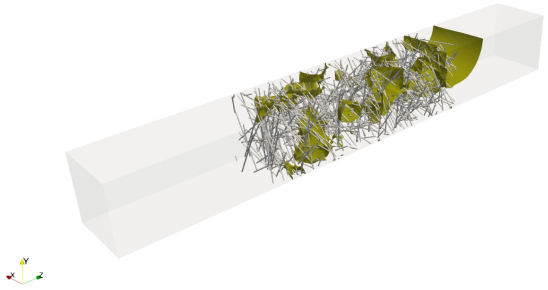

(f) 5 m/s

Figure 7.3: Retained oil droplets in philic fibrous filter at final time step.

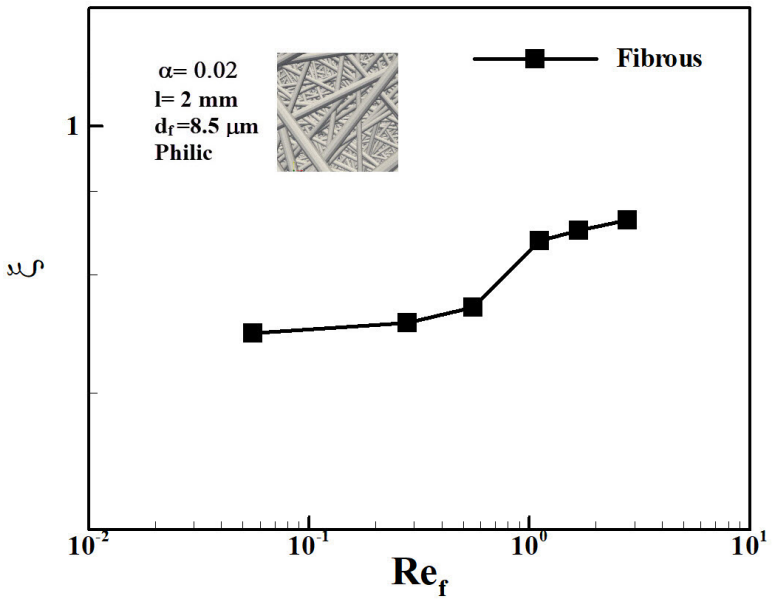

Figure 7.4: Retained oil final steady state centre of mass position at different Reynolds numbers in philic fibrous media.

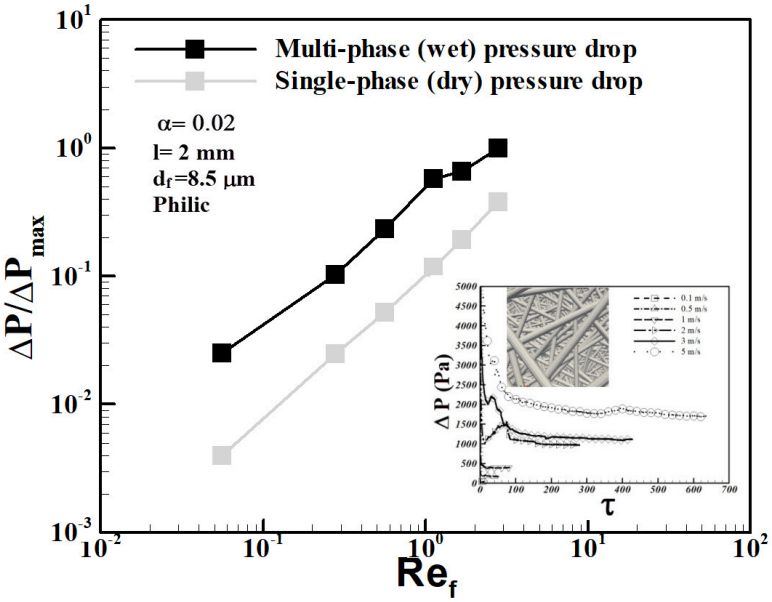

Figure 7.5: Effect of Reynolds number on multi-phase (wet) and single-phase (dry) pressure drop in philic fibrous filter media.

was discussed earlier, it is possible an optimum working condition from pressure drop perspective is present in philic media due to contrary effects of saturation reduction against dry pressure drop caused by increasing velocity.

For evaluating the influence of Reynolds number on performance of the philic fibrous filter, the Quality factor is calculated and illustrated by Figure 7.6.

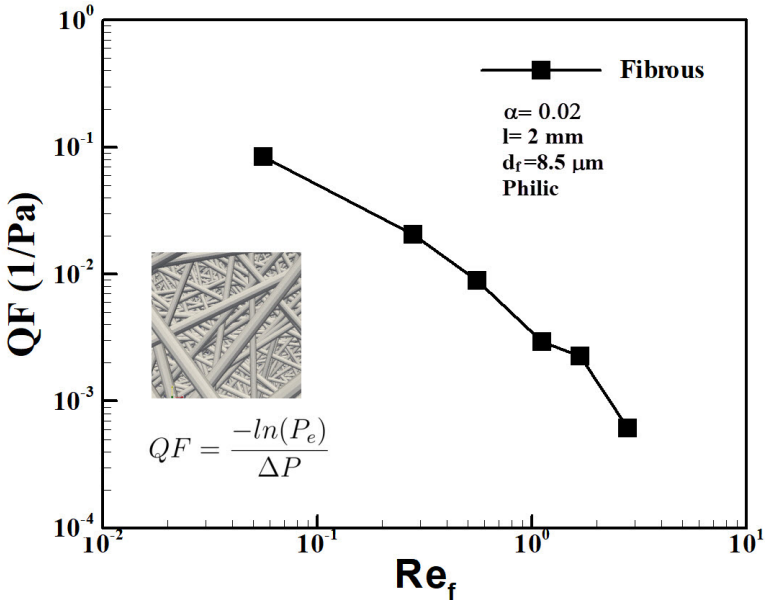

Figure 7.6: Effect of Reynolds number on quality factor in philic fibrous filter media.

It is evident form Figure 7.6 that the quality factor reduces by increasing in Reynolds number (inlet velocity rise). The quality factor values suggest that there is a 99% reduction in the performance from the lowest inlet velocity to the highest. It was shown earlier that the residual saturation drops by 35%, which reduces the wet pressure drop by 22%. On the other hand, the filter structure (dry pressure drop) enhances by 99% from the lowest to the highest inlet velocity. Investigating the quality factor results in fibrous filter proves the negative effect of pressure drop growth on performance which is significantly increases by climbing the inlet velocity.

7.1.3 Knitted Filter

The saturation profile against Reynolds number in philic knitted media is presented by Figure 7.7.

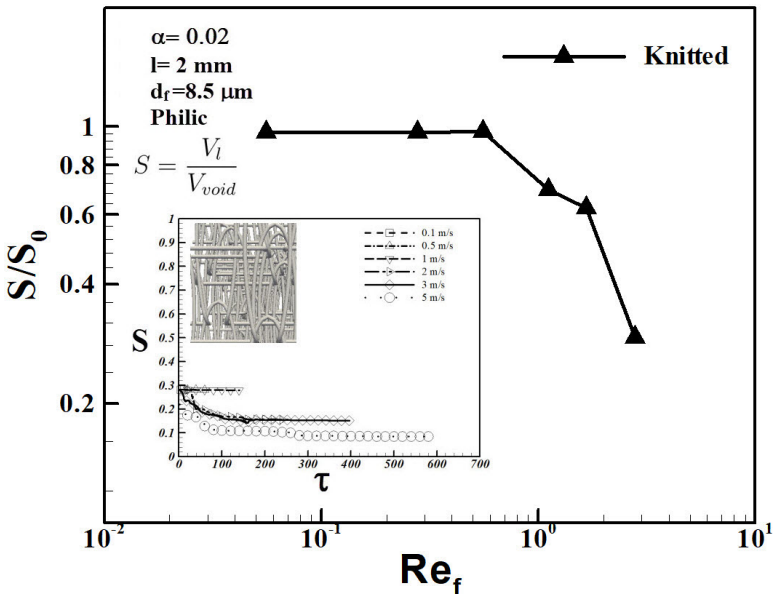

Figure 7.7: Effect of Reynolds number on equilibrium saturation in philic knitted filter.

It can be seen that the re-entrainment from the philic knitted filter starts in $R_f > 0.56$ (velocities above 1 m/s). The numerical results show that approximately 40 and 46 % saturation reduction take place in cases with $R_f = 1.11$ and 1.67 (2 and 3 m/s), respectively, while 68% residual oil saturation reduction occurs at the highest Reynolds number case (5 m/s inlet velocity). This profile can be better demonstrated by the final snapshots of the philic knitted media presented in Figure 7.8.

By comparing final position of droplets in knitted media presented in Figure 7.8, it is seen that at lower velocity cases ($\leq 1m/s$) the residual oil saturation form a continuous and stretched oil channel along the filter thickness, while higher inlet velocities causes higher sparse residual oil distribution which create more small dispersed fluid distribution. This is the same event that was explained in research work by Contal et al. (2004) which higher velocity reduces the flow resistance. Similar to fibrous media simulations, all the attached liquids in the rear face of the filter is included in the saturation profile calculations. It is also evident from Figure 7.8 that the residual saturation moves towards the rear face of the filter with increase in velocity. This can be confirmed by Figure 7.9 which the final steady state position of the residual oil centre of mass against Reynolds number in philic knitted media is presented.

It is evident from this graph that by increasing in Reynolds number (inlet velocity), the residual oil transfer toward the rear face of the filter. This condi-

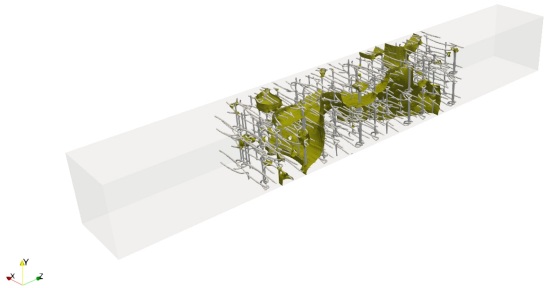

(a) 0.1 m/s

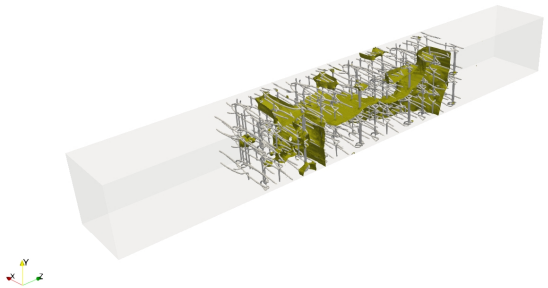

(b) 0.5 m/s

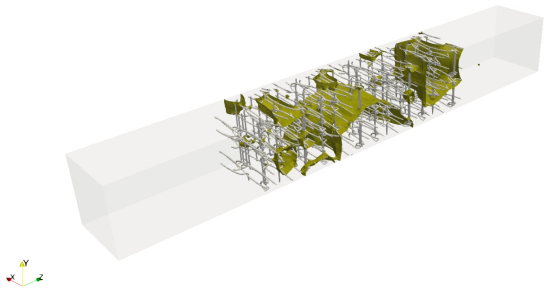

(c) 1 m/s

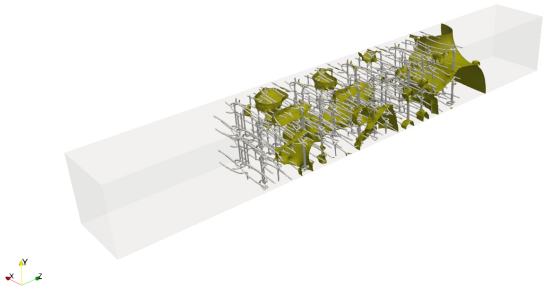

(d) 2 m/s

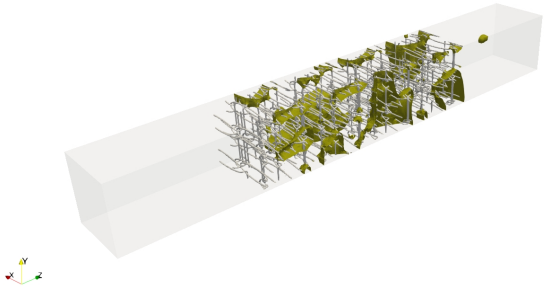

(e) 3 m/s

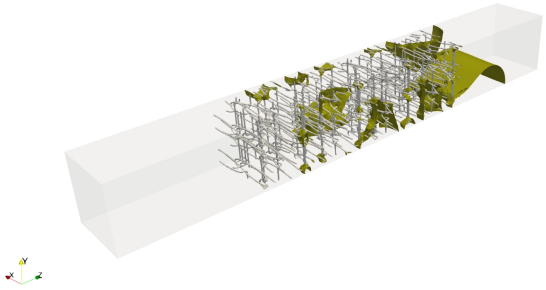

(f) 5 m/s

Figure 7.8: Retained oil droplets in philic knitted filter at final time step.

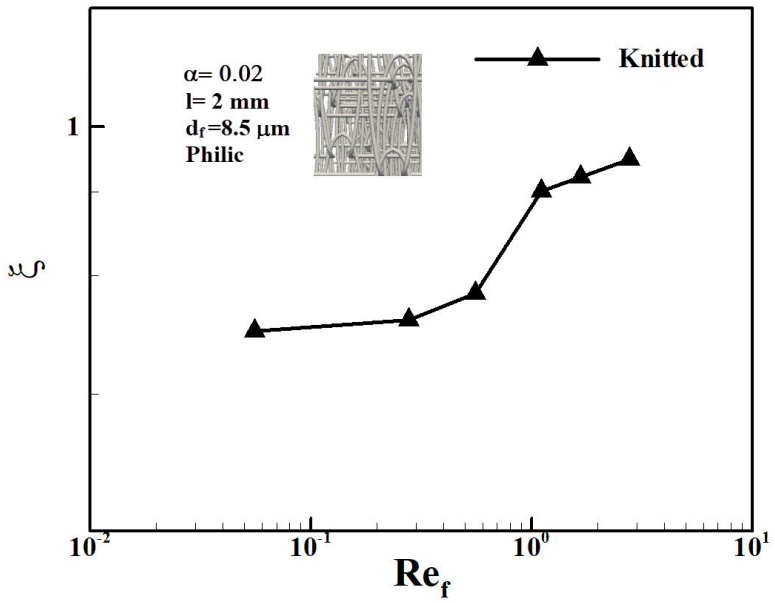

Figure 7.9: Reynolds number effect on retained oil final steady state centre of mass position in philic knitted media.

tion is already explained and attributed to the higher sheer forces in higher inlet velocities which are able to push the residual oil through the filter.

The influence of Reynolds number on multi-phase (wet) pressure drop profile in philic knitted media is shown by Figure 7.10. It is observable that multi-phase (wet) pressure drop soars by increasing in Reynolds number. The CFD results reveal that the wet pressure drop deviates from the linear dry pressure drop profile by increasing from 64%, which is the portion of wet pressure drop in total pressure drop at the lowest inlet velocity, to 77% in $Re_f = 1.11$ (2 m/s) case.

In higher Reynolds number cases (3 and 5 m/s inlet velocity) two important events occur which should be explored further. First, the wet pressure drop portion from total pressure drop in the domain declines from 52% to 47% which shows a shift compared to lower Reynolds numbers discussed earlier. This can be reasoned by reduction of residual oil saturation and also flow resistance (dispersing residual oil in the domain). The second point from Figure 7.10 is the reduction in the multi-phase pressure drop evolution profile in higher Reynolds numbers (between 2 and 3 m/s). This can be explained by looking at the final steady position of the residual oil (Figure 7.8) in those two cases. As discussed before, higher velocity causes more dispersion of residual oil in the domain, so the carrier flow has more ways for passing through the filter which reduces the pressure drop. Moreover, the saturation is decreasing as shown by Figure 7.7 which helps in pressure drop reduction. This local optimum region will be discussed in

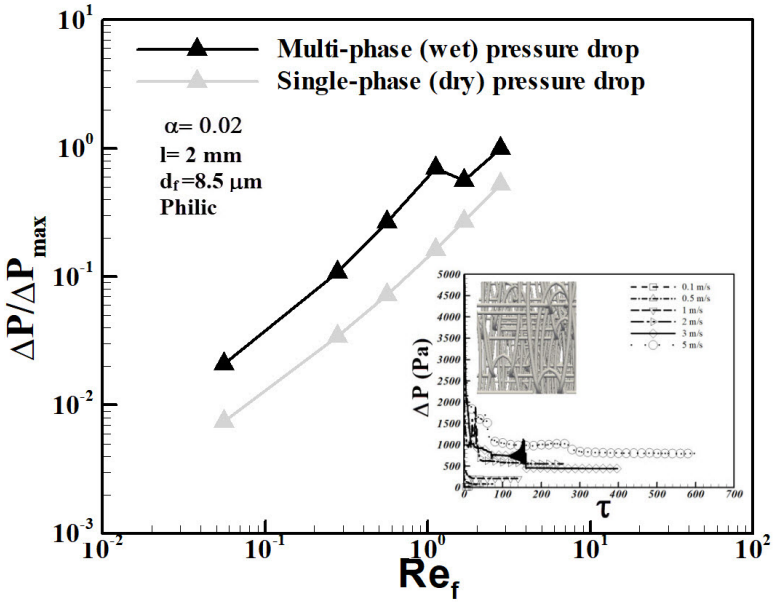

Figure 7.10: Effect of Reynolds number on multi-phase (wet) and single-phase (dry) pressure drop in philic knitted filter media.

more detain in Chapter 9.

For the purposes of performance evaluation, the quality factor of the philic knitted media is presented by Figure 7.11. Similar to fibrous filter media, the quality factor in philic knitted media drops by increasing in Reynolds number. This can be justified by knitted media's capability in holding oil in low velocities, while the re-entrainment occurs in higher velocities associated with higher pressure drop, consequently affects the quality factor adversely.

7.1.4 Open-cell Foam Filter

The saturation profile of the philic foam filter media is represented by the Figure 7.12. Similar general reduction in residual saturation with Reynolds number takes place in philic foam media as well. It is visible from the graph that re-entrainment starts in flows with $R_f > 0.5$. Moreover, CFD results shows a reduction of residual saturation at Reynolds numbers 1.11 and 1.67 (2 and 3 m/s cases) by 40 and 52%, respectively. The major saturation drop appears at the highest Reynolds number where 76% of the residual oil are pushed out from the filter media. The mentioned events can be visually confirmed by the final time step snapshots of the simulations presented by Figure 7.13.

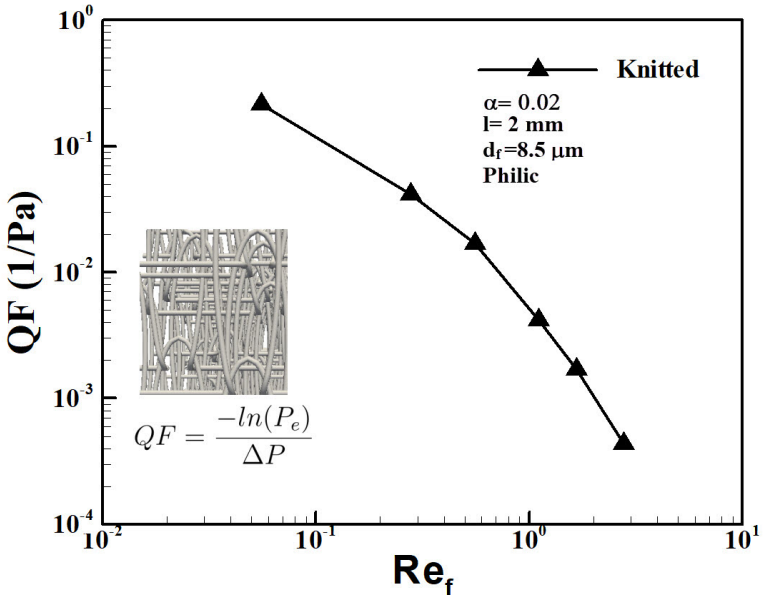

Figure 7.11: Effect of Reynolds number on quality factor in philic knitted filter media.

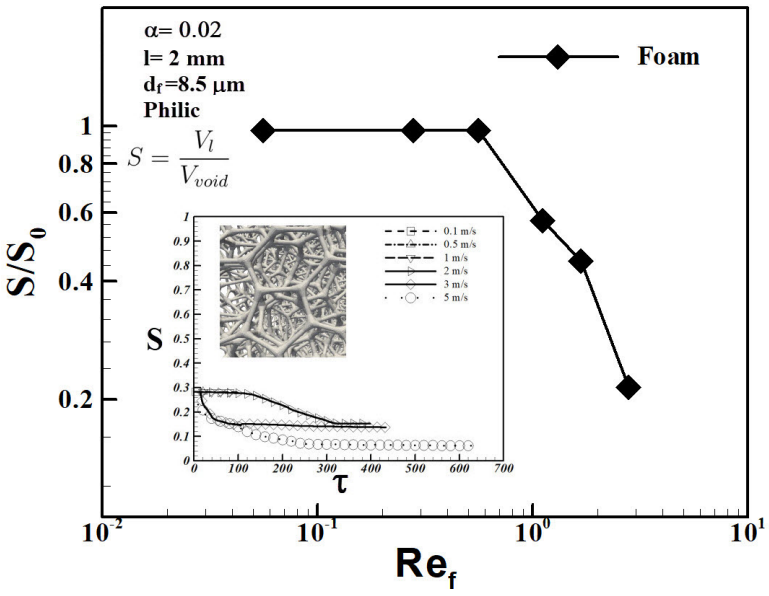

Figure 7.12: Effect of Reynolds number on equilibrium saturation in philic foam filter.

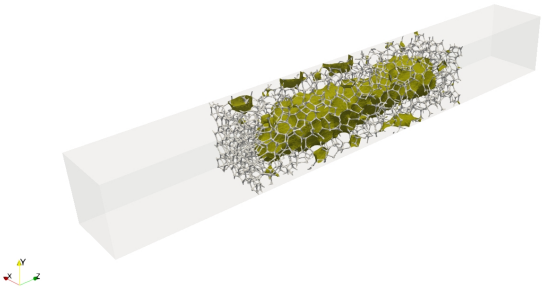

(a) 0.1 m/s

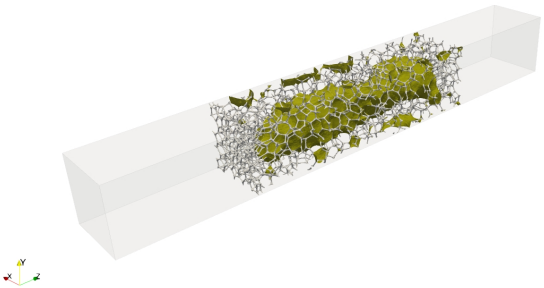

(b) 0.5 m/s

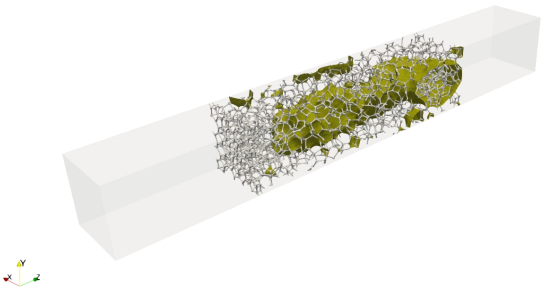

(c) 1 m/s

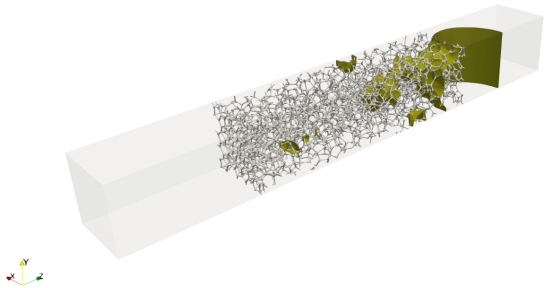

(d) 2 m/s

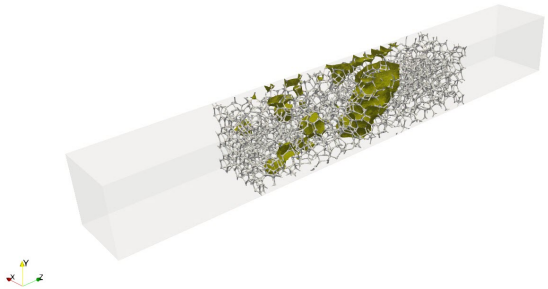

(e) 3 m/s

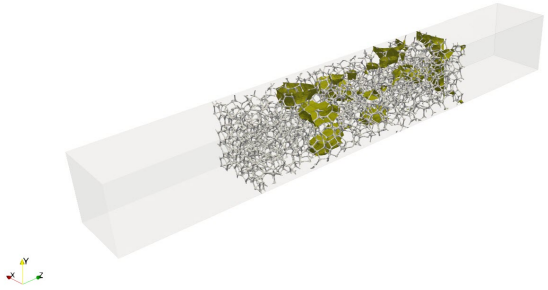

(f) 5 m/s

Figure 7.13: Retained oil droplets in philic foam filter at final time step.

As seen in initial low velocity cases in Figure 7.13, the residual oil coalesce which forms a contiguous shape along the filter thickness. This condition can be explained by low shear forces at low velocity cases which provides the residual oil with higher residence time. It is noticeable by increasing in inlet flow velocity, the residual oil becomes more disperse as expected and transport the saturation towards the rear face of the filter. The other point that should be discussed here is the position of the residual oil in 2 and 3 m/s cases. It is seen that the final position of the residual oil center of mass in 3 m/s case is closer to the inlet face compered to lower velocity case. This event can be justified by larger dispersion of residual oil in higher velocity which produces smaller droplets attached to the fibre elements, reduces the overall flow resistance and consequently the pressure drop which decreases the shear force on the droplets. It means that air flow has enough space in the filter domain to flow pass through. The other reason is the re-entrainment from the rear face of the filter which are not considered in centre of mass calculation when they leave the computation domain. The mentioned occurrence is shown by Figure 7.14 for a better demonstration.

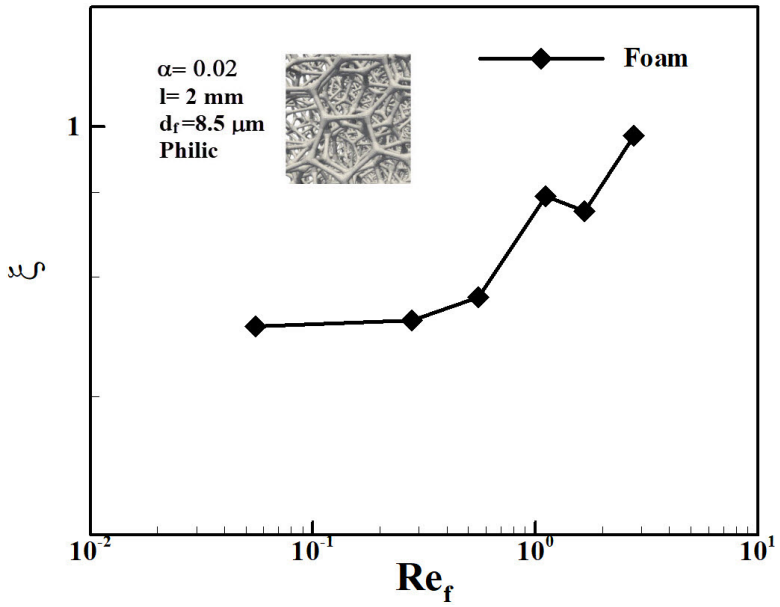

Figure 7.14: Effect of Reynolds number on retained oil final steady state centre of mass position in philic foam media.

Figure 7.14 illustrates that the overall residual centre of mass is moving toward the rear face of the filter. The explanation given in the preceding paragraph can be confirmed visually in Figure 7.14 where a decline in residual oil centre of mass can be seen at $Re_f > 1$, and increase in centre of mass vector for highest inlet velocity case as a result of higher shear force.

The multi-phase pressure drop profile in foam media is presented by the Figure 7.15.

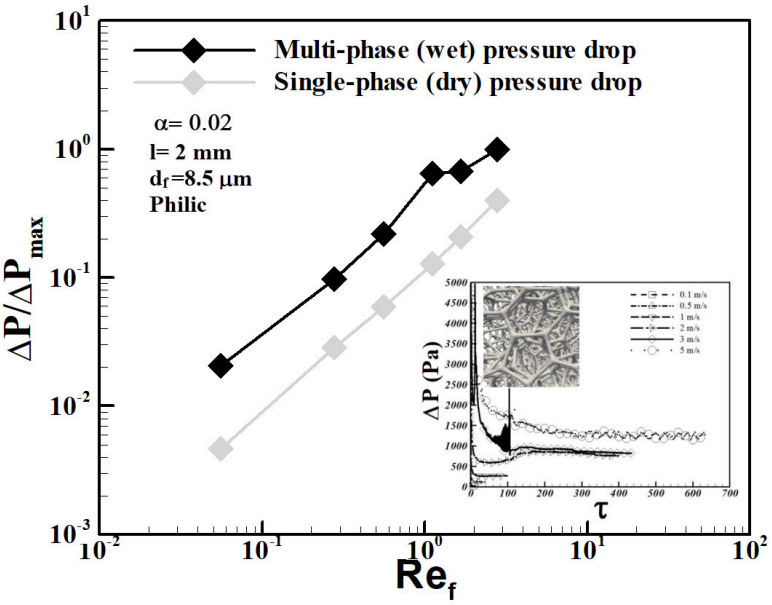

Figure 7.15: Effect of Reynolds number on multi-phase (wet) and single-phase (dry) pressure drop in philic foam filter media.

Similar to the knitted media discussed earlier, in philic foam media the wet pressure drop portion is 77% which increases by the growth in carrier flow Reynolds number to 80% in Reynolds with 1.11 (2 m/s) case. After this point, due to reduction in residual oil saturation the wet pressure drop share from the total pressure drop (wet+dry) drops to 69 and then 60%. An important point in this graph is the pressure drop difference between the case with $Re_f = 1.11$ and 1.67 (2 and 3 m/s) which shows only a marginal pressure drop increase fro the lower velocity to the higher. This event reiterates the presence of an optimum working condition from a pressure drop perspective due to opposing effects of residual oil saturation reduction and increase of pressure drop due to filter structure.

Figure 7.16 illustrates the performance of the philic foam media at different Reynolds numbers by plotting the corresponding quality number. Similar to other filter media investigated earlier, it is clearly observed that the quality factor declines by increasing in Reynolds number (increasing inlet flow velocity). This can be explained based on the poor capability of philic foam filter in holding the residual saturation and also imposing higher pressure drop to the system. The quality factor results show that the performance of the foam media drops by 80%

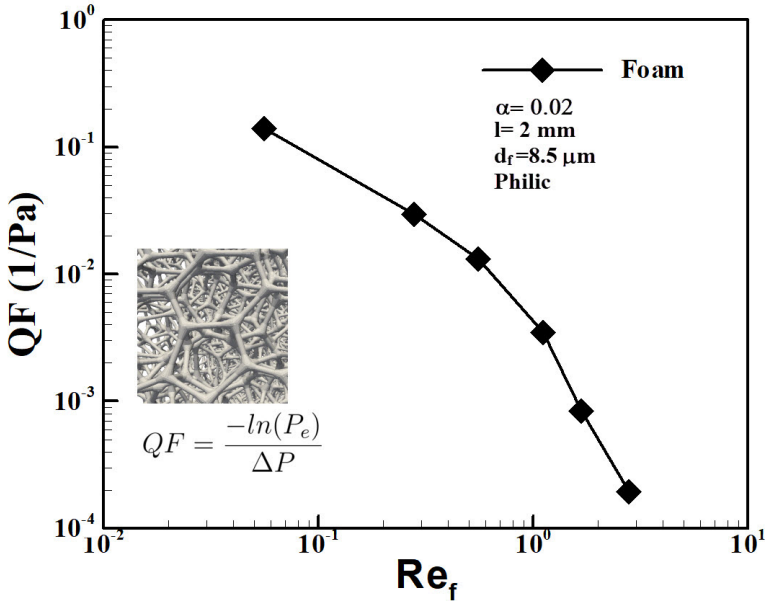

Figure 7.16: Effect of Reynolds number on quality factor in philic foam filter media.

for the second Reynolds number inlet flow case, and almost 99% for the highest Reynolds number.

7.1.5 Comparison of Performance of Three Philic Media With Different Structures

In this section, the quality factor calculations of all studied filter media are represented again in order to provide a better perspective for evaluation. Initially, the saturation profile of the fibrous, knitted and foam filter media are plotted in Figure 7.17 in order to compare these filters from saturation view point with similar initial conditions.

It is seen from the Figure 6.17 that all filters hold the initial oil saturation at low Reynolds number flows (inlet velocity $\leq$1 m/s). By viewing the saturation graph, it is visible that fibrous filter has the best holding capability among studied filter media. Foam and knitted media shows similar trend, although knitted media has higher retaining ability compared to foam media at higher Reynolds numbers. As explained in Chapter 6, this condition can be explained due to the differences in the structure of these media. As Contal et al. (2004) indicated that at filters with more intersections and also lower void spaces the residual oil can be trapped between fibers with narrower distance due to capillary force and also the

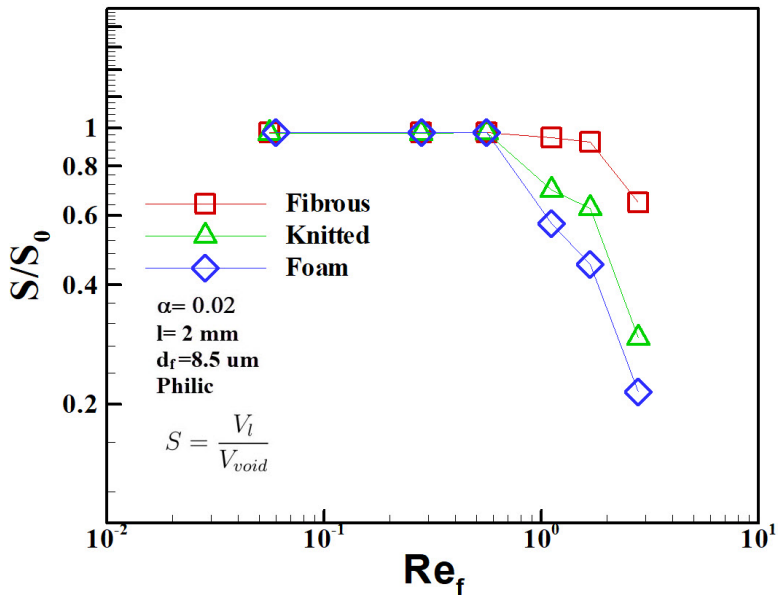

Figure 7.17: Effect of Reynolds number on equilibrium saturation in philic fibrous, knitted, and foam media filters.

effect of lower energy surface in philic media. As explained before, this narrow spaces are not present in knitted and foam filter media which causes lower holding ability in their saturation profile. Moreover, fibrous media showed less penetration through filter thickness due to better dispersion of the residual saturation in the domain. CFD results revealed that at the highest Reynolds number, fibrous filter hold 65% of the initial oil content inside the filter, while this value drops to 30 and 21% for knitted and foam media, respectively.

Figure 7.18 compares the multi-phase (wet) pressure drop profile in all studied filter media. It is worth mentioning that all pressure drop values are non-dimensionalised by the maximum wet pressure drop value (in fibrous filter) in order to be comparable.

It is observable from Figure 7.18 that the fibrous filter media produces the highest wet pressure drop in the studied systems, while knitted media shows the lowest value in all Reynolds numbers. The effects of structure pressure drop in different filters was discussed in Section 6.2.4, but the dry filter pressure drop depicted here again since the study carried out in higher velocities in philic media.

Figure 7.19 demonstrates the single-phase pressure drop profile in all three media at different Reynolds numbers. CFD results show that at the lowest Reynolds number, the filters with different structures almost produces similar pressure drop which the maximum difference is 15%. The differentiation between

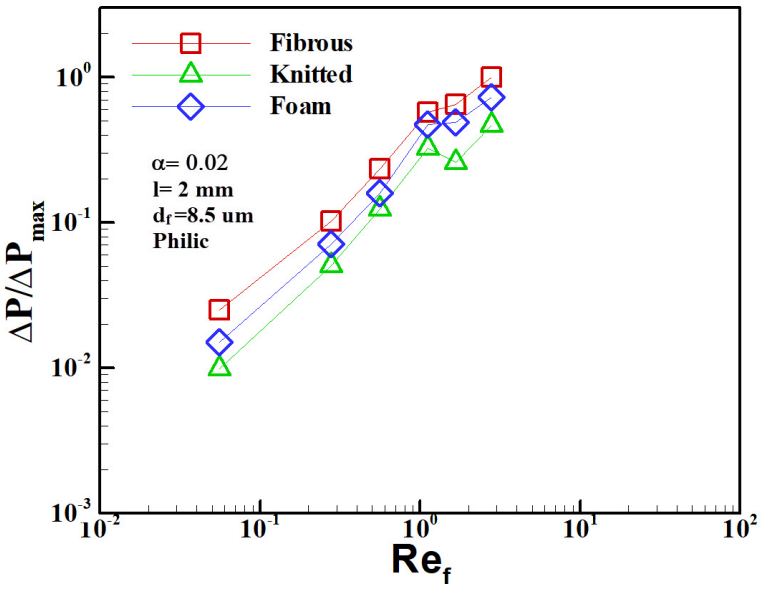

Figure 7.18: Effect of Reynolds number on multi-phase pressure drop in philic fibrous, knitted, and foam media filters.

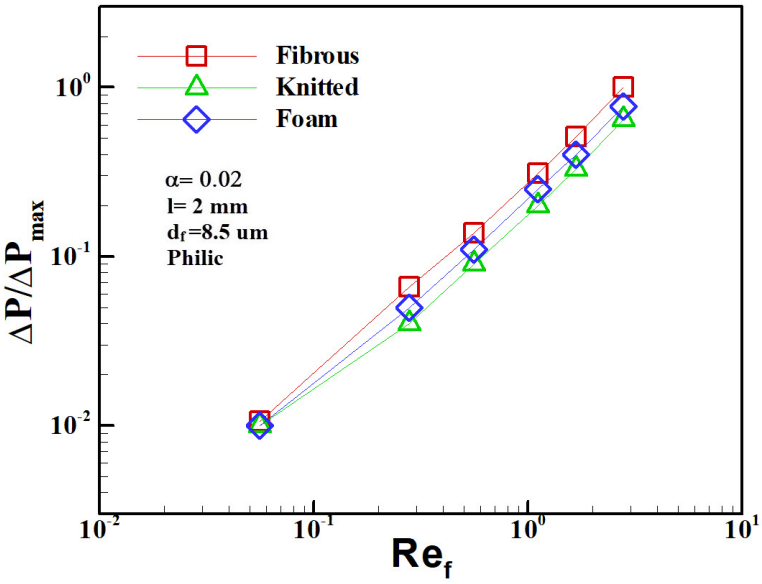

Figure 7.19: Effect of Reynolds number on single-phase pressure drop in fibrous, knitted, and foam media filters at higher Reynolds numbers.

different structures dry pressure drop at the highest Reynolds number is 35%. By reviewing the numerical wet pressure drop simulation results, it is found that the initial wet pressure drop difference between the highest pressure drop value (in fibrous media) and the lowest pressure drop value (in knitted media) is 61%, while it was shown earlier that the dry pressure drop difference in these filters when they operate dry is only 15%. This confirms the influence of the residual saturation and how they modify the packing density of the philic filters. It is found that by increasing in Reynolds number the difference reduces to 46% (was 35% when operated dry) which shows the influence of retained droplets in higher velocity is lower. These results corroborate the other researchers (Contal et al. (2004); Charvet et al. (2008)) findings which higher inlet velocities reduce the flow resistance and adverse effects of residual saturation in coalescing filters.

Figure 7.20 compares the quality factor with Reynolds number in all filter media studied . It is noticeable that in low Reynolds number case where $R_f \leq 1$ which resembles the inlet velocity up to 2 m/s, knitted media has the best performance among all studied filter media which support the finding of Sheng et al. (2020)'s recent research. It should be mentioned that in that study carried out in velocity ranges from 1 to 2 m/s, and there is no discussion about the wettability of the filter media, therefore it is not clear if the filters are philic or phobic.

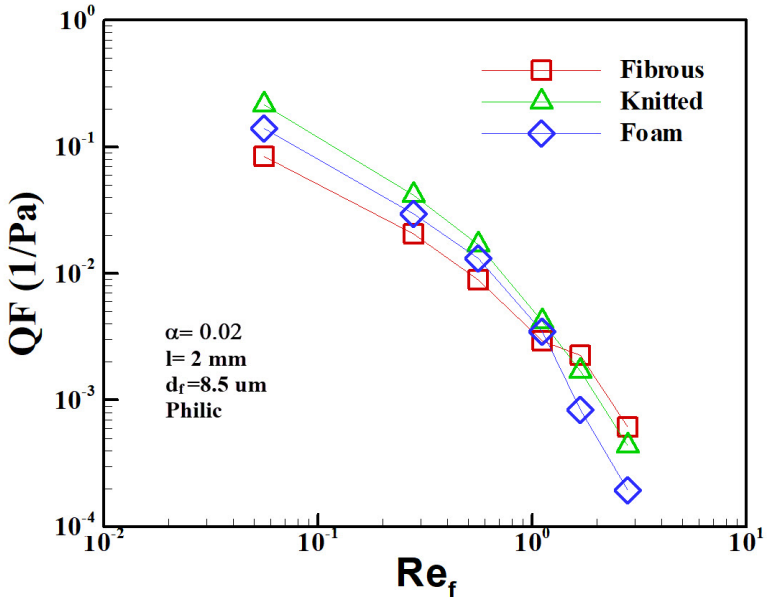

Figure 7.20: Effect of Reynolds number on quality factor in philic fibrous, knitted, and foam media filters.

The crucial point that should be addressed in Figure 7.20 is the change in quality factor graph trend which occurs at higher Reynolds numbers (inlet velocities

$>$ 2 m/s). This phenomenon has not been explored in any previous research. It is evident from the graph the fibrous filter shows a higher performance capability in higher inlet velocities which is mainly due to its higher residual saturation holding compared to other filters studied in this research. The calculations show that the difference between fibrous and knitted media quality factor is 3 and 29% in the last two Reynolds numbers, respectively while it is 70% for philic foam media.

7.2 Conclusion

In this chapter, CFD approach was applied to carry out multi-phase flow modeling in three different philic filter structures (fibrous, knitted, and foam) with contact angle equal to 20° at various inlet velocities (0.1, 0.5, 1, 2, 3 and 5 m/s) which were equally pre-saturated with 30 % of their void spaces by DEHS oil. The physical properties of all filters such as packing density, fibre element diameter, filter thickness, and filter cross section area were identical. Therefore it provided a perfect equivalent basis in order to investigate their performance against each other.

Numerical simulations showed that residual oil saturation reduces with increase in inlet velocity (due to increase in flow forces) as the general trend in all philic filter media. It was found that foam media has the lowest saturation holding capability among all philic filters, while it was found that fibrous filter has the best holding ability for higher velocities due to its structure difference which causes more distribution of residual oil inside the filter and reduces the flow resistance and pressure drop.

Multi-phase (wet) pressure drop results showed that residual oil saturation has a major influence on pressure drop profile in low Reynolds number cases and contributed to a strong deviation form the dry pressure drop trend, while its effect declines by increasing in inlet flow velocity due to reduction in residual oil and also flow resistance. Numerical modeling results showed that fibrous filter causes the highest pressure drop in all Reynolds number study cases, while the knitted media imposed the lowest pressure drop to the system. The results indicated that by increasing in inlet flow velocity, the influence of the residual saturation declines which suggested a possibility in presence of a local optimum region in pressure drop profile in all studied filter media.

Finally, the performance analysis of three philic media with different structures suggested that knitted media performed the best among all filters in lower Reynolds range ($0.05 \leq Re_f \leq 1.1$), while a turning point occurred in higher

Reynolds number which showed fibrous filter to have higher quality factor compared to other filter media studied.

Chapter 8

Effects of Contact Angle on Saturation, Pressure Drop and Quality Factor in Different Filter Structures

As mentioned in Chapters 1 and 2, the aim of this research project is to investigate coalescence filtration in different types of filter media. In this regard, three filters with different structures such as fibrous, knitted, and foam media with equivalent physical properties such as packing density, fibre diameter, filter thickness, and cross section area are considered. These filters are pre-saturated equally with DEHS oil and tested for a range of different velocities. Moreover, the effects of contact angle are considered by conducting separate simulations on two different contact angles ($\theta = 20^\circ$ (philic media) and 120° (phobic media)) for evaluation. The validity and accuracy of the generated filters and the methodology applied are verified in Chapter 5. The influence of inlet velocity variation on residual saturation, multi-phase pressure drop profile, and quality factor on different filter structures are studied in Chapters 6 and 7 for phobic and philic media, respectively.

In this chapter, the results from Chapters 6 and 7 are compared in order to evaluate the effect of contact angle on saturation, pressure drop profile, and quality factor in three filters with different structures.

8.1 Effect of Contact Angle on Saturation in Fibrous, Knitted and Foam Media

For the purpose of examining the influence of contact angle on saturation profile, the saturation results from phobic and philic media are re-presented in Figure 8.1. It is evident that reducing contact angle increases the saturation retaining ability of all the filters with different structures. It is seen from the graph that at low Re_f no change in saturation level takes place which literally shows both philic and phobic media holds the saturation level equally. This event can be seen in the lowest Reynolds number (0.1 m/s inlet velocity) for the foam filter media, and $Re_f \leq 0.55$ (inlet velocities ≤ 1 m/s) for knitted and fibrous filters. It can be seen that reducing the contact angle has the most effect on foam media which increased its holding capability by almost 100%. It is visible that by increasing in Reynolds number, the influence of contact angle on the foam filter holding capability reduces which is expected as more re-entrainment occurs by increasing in inlet velocity in both philic and phobic media (Manzo et al. (2016)). From Figure 8.1 it can be deduced that similar trend presents in both fibrous and knitted media, but at higher Reynolds numbers as their holding capability is higher than foam media which is discussed and verified in previous chapters. It is noticeable that reducing contact angle enhances the saturation level in fibrous media by 50% which was observed in Chen et al. (2019b) study as well.

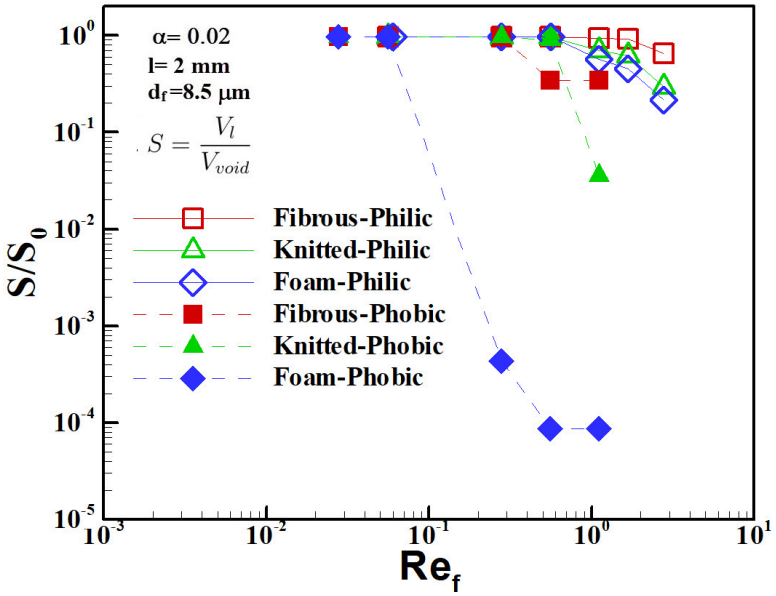

Figure 8.1: Effect of contact angle on saturation level and onset of re-entrainment in fibrous, knitted, and foam filter media.

Overall, it can be deduced that reducing contact angle (surface energy of the filter media) increases the saturation level in coalescence filters with equal initial and operating conditions (Patel et al. (2013); Chen et al. (2019b)). This event ws found in Mullins et al. (2014) work, as they tested different combination of philic and phobic fibrous media. The results suggested that there is more saturation in the philic layers in their filter combinations, while the saturation decreased in filters with using phobic media at the last layer. In another research conducted by Letts et al. (2003), it was found that fibrous filters with lower contact angle (glass fibres) contain 60% more liquid compared to fibrous filters with higher contact angle (polyaramid fibres) in similar operating condition. The underlying reason for this effect is the weaker droplet fibre adhesion forces associated with clamshell droplets (Minor et al. (1959); Mead-Hunter et al. (2014)) which formed in phobic media (Mead-Hunter et al. (2012); Mullins et al. (2014)), therefore re-entrainment occurs in phobic media with higher rate and at lower velocities as the hydro-static forces required for moving these droplets are lower (Mullins et al. (2014)). In order to investigate the influence of contact angle on the onset of re-entrainment in different filter structures, Figure 8.1 presents the saturation profiles in all filters with different contact angle.

It is observable in Figure 8.1 that in both foam and fibrous media the onset of re-entrainment take place at higher Reynolds with decreasing contact angle (Agranovski et al. (2001); Mullins et al. (2014)), while in the knitted media it is not very significant. It is seen that for knitted media, the saturation reduction occurs at $Re_f = 1.1$ (2 m/s inlet velocity) with higher reduction ratio (steep decline) in phobic case compared to philic knitted media which suggests that the start of re-entrainment is happening at higher velocity in philic media.

8.2 Effect of Contact Angle on Multi-phase Pressure Drop in Fibrous, Knitted and Foam Media

For investigating the effect of contact angle on multi-phase pressure drop, the wet pressure drop results from Chapters 6 and 7 are employed. In order to isolate the influence of contact angle, the parameter ΔP_θ is used to calculate the pressure drop difference between philic and phobic media, and is defined by the following equation:

$$\Delta P_\theta = \Delta P_{Philic} - \Delta P_{Phobic} \tag{8.1}$$

Where in Equation 8.1, ΔP_{Philic} and ΔP_{Phobic} are the final steady state multi-phase pressure drop values in philic and phobic media, respectively. From Equation 8.1, it can be concluded that when $\Delta P_\theta > 0$, reducing contact angle increases the wet pressure drop and vice versa. It should be re-stated again that the comparison is conducted only on common velocities between philic and phobic simulations. To provide a better demonstration, the ΔP_θ is normalised by pressure drop in phobic media and illustrated by Figure 8.2.

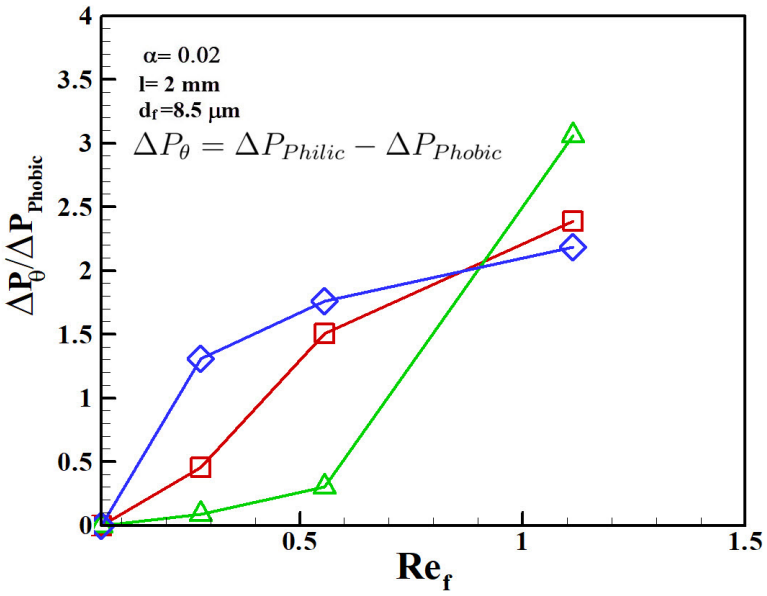

Figure 8.2: Effect of contact angle on multi-phase pressure drop in fibrous, knitted, and foam filter media.

It is obvious from Figure 8.2 that reducing the contact angle (shifting from phobic to philic) increases the wet pressure drop in all filter media. It is in clear view that foam filter produces almost 200% pressure drop increase at higher Reynolds number. It is seen that in low Reynolds number, the difference between philic and phobic media is marginal, while by increasing in Reynolds number the difference rises. It can be explained by the fact that lower surface energy fibre has higher droplet-fibre adhesion force (Mead-Hunter et al. (2012); Hotz et al. (2015)) which resulted in a higher saturation level (Letts et al. (2003)) and consequently increases the flow resistance and pressure drop inside the filter (Contal et al. (2004); Kampa et al. (2014); Liu et al. (2019)). Moreover, residual oil in phobic media form larger droplets (was visually observed from snapshots) which transport easier through the filter and reduce the flow resistance (Manzo et al. (2016)).

It is seen that the pressure drop difference curve is flattening in both foam and fibrous filters which is due to saturation reduction at higher Reynolds numbers.

In the case of knitted media, similar to foam and fibrous filters, the effect of reducing contact angle is obviously enhancing the wet pressure drop. It is seen that the pressure drop difference soars in knitted media at higher Reynolds number which can explained by the difference in saturation level and also higher velocity related pressure loss. It was shown previously that phobic knitted media's holding capability reduced significantly after $Re_f = 1.1$, but by reducing the contact angle the saturation level increased by 40% which caused higher pressure drop due to drag force on residual oil droplets.

8.3 Effect of Contact Angle on Quality Factor in Fibrous, Knitted and Foam Media

Gas-liquid coalescence filtration is a complex process in which the filter performance is influenced by a range of parameters including liquid properties, filter structure, liquid-fibre contact angle, and operating conditions. The effect of velocity variation on the performance of filters with different structure was discovered in Chapters 6 and 7. In this section, the effect of contact angle on quality factor in the mentioned filter structures is investigated by re-presenting quality factor results. Figure 8.3 compares the quality factor for both philic and phobic media results at common inlet velocity cases.

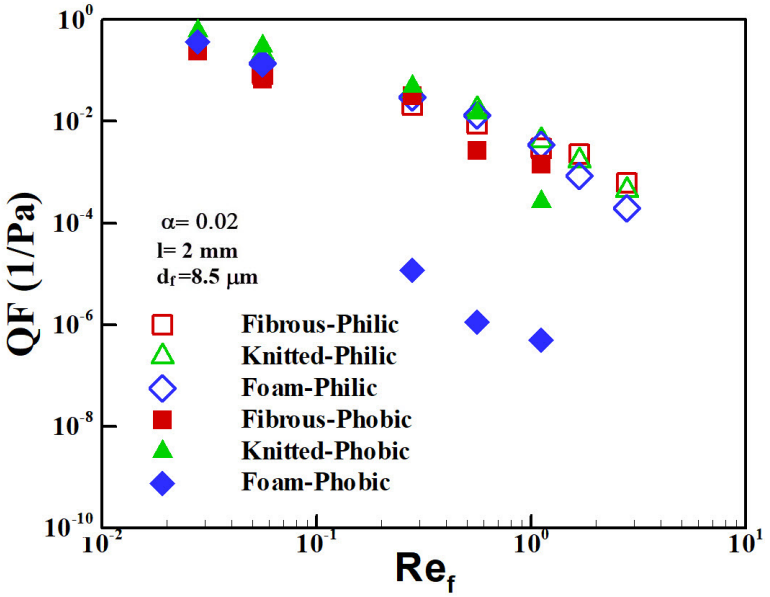

Figure 8.3: Effect of contact angle on quality factor in fibrous, knitted, and foam filter media.

It is clearly observed from Figure 8.3 that phobic filters have the highest quality factor compared to philic media in low Reynolds numbers. This results suggest that increasing contact angle improves the performance of the coalescence filters in low inlet velocity cases which has been reported by researchers previously (Manzo et al. (2016); Letts et al. (2003); Chen et al. (2019a,b)). Reviewing the present CFD results suggest that phobic knitted media has the highest quality factor among all phobic media with different structures and also outperform philic filters up to flow rate $Re_f < 1$ (u< 2 m/s). It can be associated with the structure difference in knitted media which produces the lowest pressure drop among all studied filter media in the range of $Re_f \leq 1$. Moreover, its hold-on capability is comparable or higher than other filters in that inlet velocity range as well.

The knitted media was only tested in research work by Sheng et al. (2020) which was only compared to fibrous filter at a range of velocities between 1 to 2.5 m/s with no information in regard to wettability of the media. The results showed that knitted media performs better than fibrous filter in all tested velocities. In the literature survey which is conducted in this research (Section 2.4.2), it is found that all the studies which found high energy surface filters (phobic media) has higher quality factor compared to low surface energy filters were carried out only in a low single or a limited range of inlet velocity.

The important point which is found in the present study is the turning point in quality factor graph which demonstrate that philic fibrous filter performs better (even compared to its phobic counterparts) at higher Reynolds numbers (inlet velocities). This event can be explained due to saturation retaining ability of fibrous filter at higher velocities. It was shown that at higher velocities phobic media affects by shear flow forces which causes transport of residual saturation toward the rear face of the filter and re-entrainment happens (Mullins et al. (2014)). This reduces the efficiency of the phobic media at higher velocities, while it was shown in Section 8.1 that decreasing the contact angle improves the hold-on capability of all studied filters including fibrous media significantly. It was discussed earlier that presence of the saturation inside the filter media attribute to 80% of the pressure drop in the system (Charvet et al. (2008)), but it should be mentioned that higher velocity in fibrous media causes more dispertion of the residual oil which helps to decline the flow resistance inside the filter (Contal et al. (2004)).

8.4 Conclusion

The objective of this chapter was to evaluate the effect of contact angle on residual saturation, multi-phase pressure drop profile, and the performance of different filters with different structures. Equivalent initial and operating conditions are considered for fibrous, knitted , and foam filter media for conducting numerical simulations.

The CFD results indicate that contact angle has a significant effect on the residual saturation level in coalescence filters with different structure. It is found that the major influence occurs in foam filter media which reducing the contact angle from 120° (phobic media) to 20° (philic media) increases its saturation level up to 100%. It is sown that both knitted and fibrous media affected by reducing contact angle by holding higher level of saturation. CFD results suggests that increasing in flow Reynolds number will reduce the difference between that saturation level of filters with high and low energy surface due to stronger shear flow forces at higher inlet velocities. Moreover, it is revealed that reducing contact angle lead to occurring the re-entrainment at higher inlet velocities in all filter media.

Reviewing the numerical results indicate that reducing contact angle enhances the wet pressure drop profile extensively in all filter media studied. It is shown that all filter media develops higher pressure drop by increasing in Reynolds number, although it is found that this influence will be declined ultimately as the saturation level decreases.

The performance analysis shows that phobic media has a better quality factor in low Reynolds numbers. It is revealed that phobic knitted media outperform all the phobic and philic counterparts by flow rate $Re_f < 1$. The investigations suggest that at higher Reynolds numbers, low surface energy filters (philic) has higher quality factor which is a turning point in quality factor graph.

Chapter 9

Investigating the Presence of Local Optimum in the pressure drop Profile in Different Filter Media

As explained in Chapter 1 and 2, the principal of this research is to develop a methodology for a rigorous evaluation and comparison of different filter media with different structures. As such, fibrous, knitted, and foam filters are generated virtually and the accuracy and validity of them are verified in Chapter 5. CFD method is employed, which is fully explained in Chapter 4, in this research in order to calculate the quality factor in different filters. To achieve this, all filters are loaded with 30% DEHS initially and has equivalent physical properties (packing density, thickness, fibre diameter, and cross section area). Simulations are carried out with different inlet velocities and contact angles to calculate residual saturation and pressure drop profile inside filters for evaluating the filters performance.

During the analysis of the wet pressure drop profiles, it was revealed that filters at certain inlet velocities deviate from the original pressure drop curve. By further research it is found that it is due to opposing effects of saturation reduction and dry pressure drop (due to filter structure) increase by rising filtration Reynolds number (inlet velocity enhancement in our research). This phenomena was suggested by Charvet et al. (2008) and Contal et al. (2004) that reduction in saturation at higher velocities may resulted in forming optimum working condition for filters as the flow resistance declines by increasing in inlet velocity. In order to investigate this possibility, multi-phase and single-phase pressure drop difference is calculated by the following equation:

$$\Delta P_e = \Delta P_{multi-phase} - \Delta P_{single-phase} \tag{9.1}$$

ΔP_e is normalised by the maximum pressure difference and plotted versus Reynolds number. Moreover, the saturation profile versus ΔP_e is presented in all study cases. For verifying the accuracy of numerical results, sets of experiments are conducted and the results are qualitatively validated.

It should be mentioned that previous research (Gac (2015); Chen et al. (2009); Payen et al. (2012); Lamb and Costanza (1979); Naim and Ismail (2013)) have indicated that fibre diameter, packing density, filter structure and wettability in addition to liquid aerosol physiochemical (viscosity, surface tension) significantly influence the filter behaviour. In this section, initially the possibility of optimum region presence in the pressure drop profile is examined in phobic and philic media separately. In the next step, the effect of contact angle is investigated, and finally a qualitative hypothesis is proposed for explaining the new findings in this research.

9.1 Local Optimum Pressure Drop Region in Phobic Media

In order to investigate the local optimum pressure drop in different phobic filters, Figures 9.1 to 9.4 present the normalised pressure drop difference, ΔP_e, against Reynolds number and also pressure drop difference, ΔP_e, versus residual saturation.

It is observed from Figure 9.1 (a) that a local optimum region presents between $0.5 \leq Re_f \leq 1$ (1 to 2 m/s) in the pressure drop profile of the phobic fibrous filter. Figure 9.1 (b) provides a better demonstration of the affecting parameters. As can be seen, in the higher Reynolds number cases (0.5 to 2 m/s) the saturation decreases by increasing Reynolds number (was discussed in Section 6.2.1) which resulted in a less obstruction against the airflow (decrease in flow resistance). On the other hand, the single phase pressure drop increases by increasing in inlet velocity (Figure 6.19). The optimum which is happening in this case causes the curve in Figure 9.1 (b) to shift toward the left (lower pressure) although velocity is increasing. In other words, the amount of residual oil saturation in $Re_f = 0.55$ (1 m/s) case and $Re_f = 1.11$ (2 m/s) case are very close values, but causes further pressure drop at the higher flow Reynolds number cases.

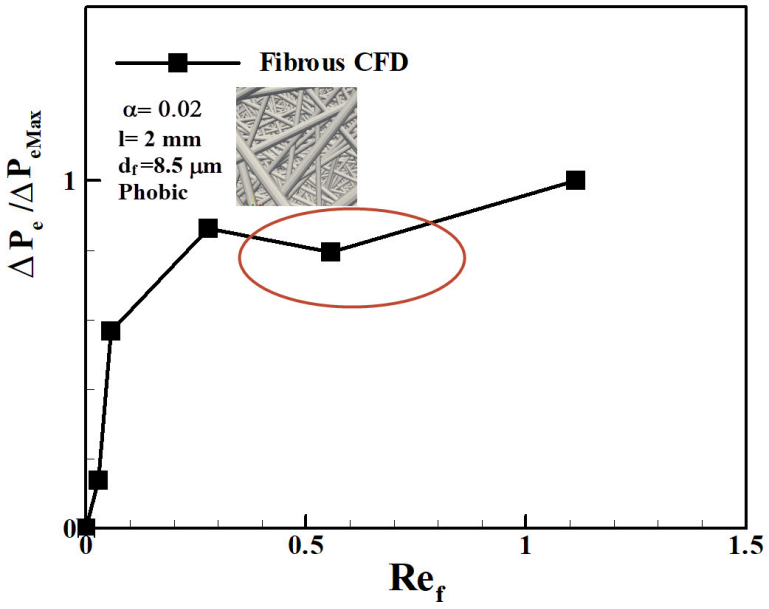

(a)

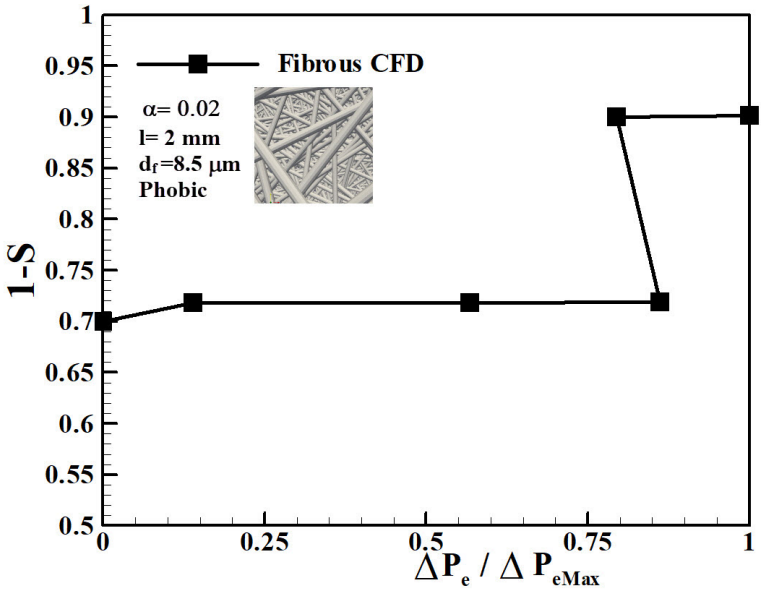

(b)

Figure 9.1: Numerical simulation results for phobic fibrous media: (a) Pressure drop difference versus Reynolds number, (b) Residual saturation versus pressure drop difference.

Figure 9.2 demonstrates the pressure drop difference versus Reynolds number and saturation in phobic knitted media. It is seen that the local optimum region in the pressure drop profile takes place at higher flow Reynolds number compared to fibrous media in phobic knitted filter. The underlying reason is similar to the phobic fibrous filter explained before, and the trend in 9.2 (b) is similar as well which shows reduction in saturation and decrease in the pressure drop difference while increasing the inlet flow Reynolds number.

It should be mentioned that in phobic knitted media case, the simulations continued to higher inlet velocity (3 m/s) since it was found that this media has a higher saturation hold-up capacity compared to other filters (explained in Section 6.2.2). The final saturation level is compared against 2 m/s case, and it is presented by Figure 9.3.

It can be deduced from Figure 9.3 that there is a marginal reduction in saturation in 3 m/s case in knitted media, but higher velocity case produces higher pressure drop in similar saturation level. Furthermore, lower velocity in this case (1 m/s) retained more liquid which resulted in high flow resistance and consequently higher pressure drop. Therefore, it is the main reason that the optimum occurs between $1 < Re_f < 1.5$ (1 to 3 m/s) in knitted media.

Figure 9.4 presents the pressure drop difference versus Reynolds number and saturation in phobic foam media in order to investigate for presence of possible optimum region in the pressure drop profile. It is visible form the Figure 9.4 (a) that the local optimum in the pressure drop profile is present in phobic foam media (similar to knitted and fibrous filters) as well, but at lower Reynolds number $Re_f, 0.5$. It can be explained due to lower residual hold-up capacity of phobic foam media which was discussed in Chapter 6. By viewing at Figure 9.4 (b) it is seen that the saturation reduces by increasing in Reynolds number which decreases the flow resistance in phobic foam media. On the contrary, the dry pressure drop (filter structure effect) is increasing by growing flow Reynolds number which two opposing events causes this optimum formation in the pressure drop profile.

In order to verify the optimum occurrence experimentally, a set of experiments conducted according to the methodology explained in section 4.3 on the Fibrous-ME1 filter from the Table 4.4. Figure 9.5 presents the pressure drop difference versus Reynolds number and residual saturation in Fibrous-ME1 experimental case. It is visible in Figure 9.5 (a) that the optimum region found in numerical results is present in the experiment as well. It is clearly seen that this region takes place in $0.5 < Re_f < 1$ (between 1 and 1.5 m/s inlet velocity) which is

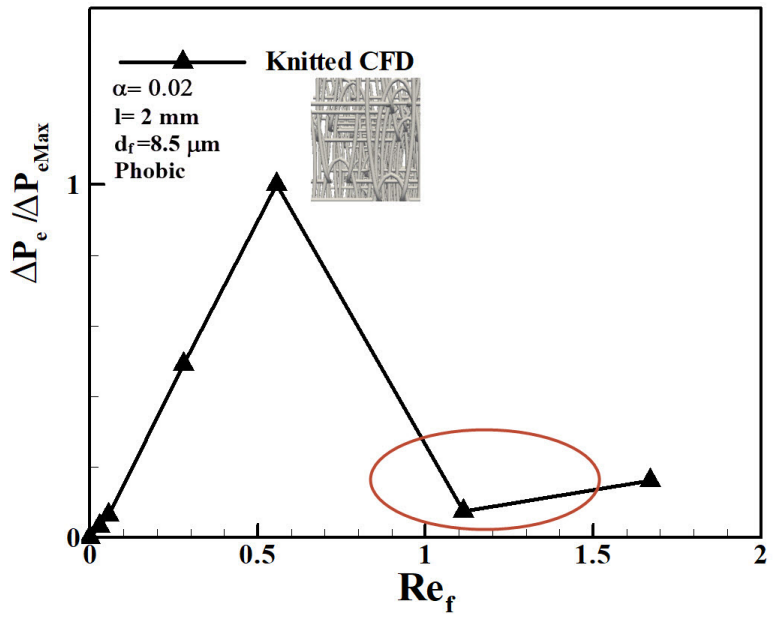

(a)

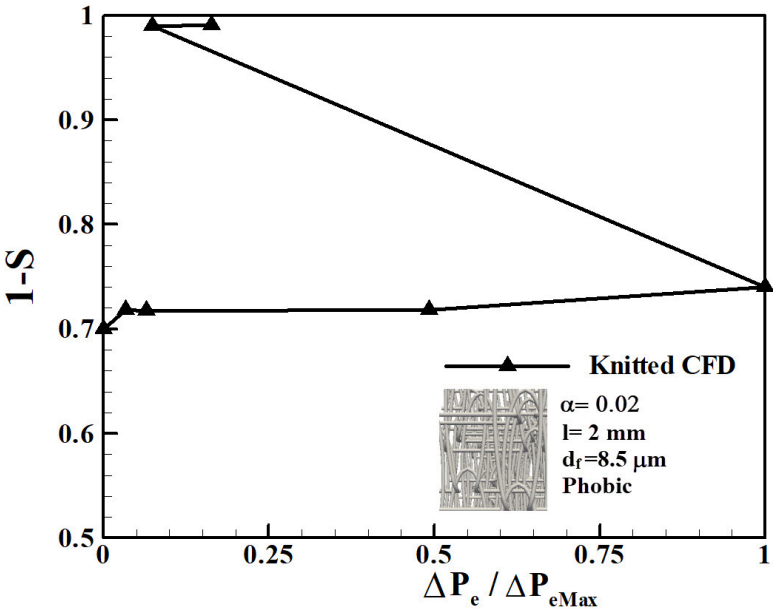

(b)

Figure 9.2: Numerical simulation results of phobic knitted media: (a) Pressure drop difference versus Reynolds number, (b) Residual saturation versus pressure drop difference.

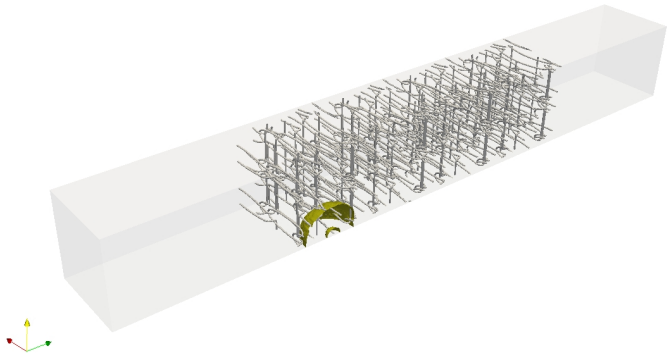

(a)

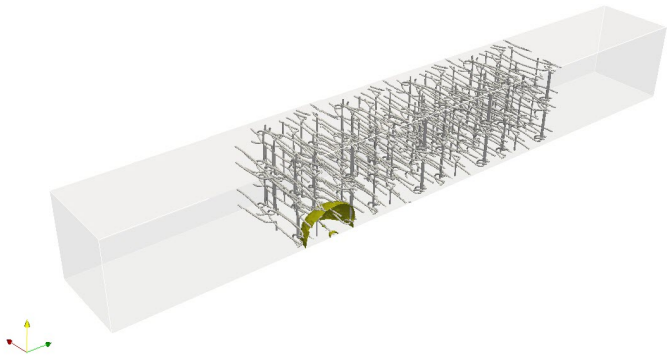

(b)

Figure 9.3: Residual oil saturation in phobic knitted filter at final steady state: (a) 2 m/s inlet velocity, (b) 3 m/s inlet velocity.

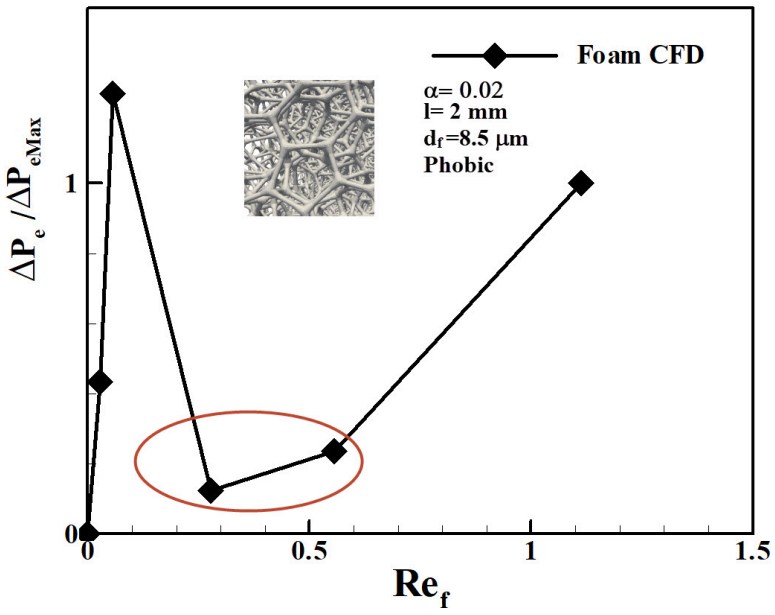

(a)

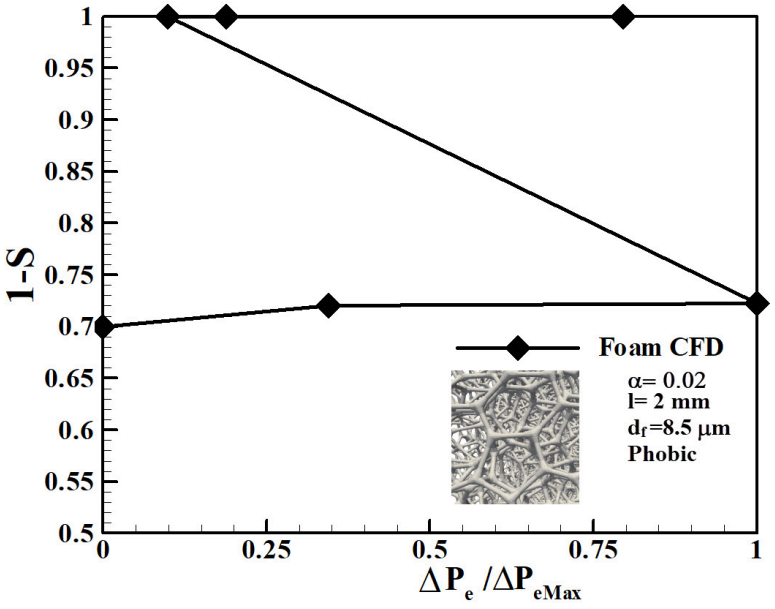

(b)

Figure 9.4: Numerical simulation results for phobic foam media: (a) Pressure drop difference versus Reynolds number, (b) Residual saturation versus pressure drop difference.

happening at higher Reynolds number range compared to numerical fibrous case in the present study. Since these two filters are not identical, it is very hard to identify the underlying reason for this difference, although most probably it can be attributed to the higher packing density in phobic fibrous experimental case (Fibrous-ME1). Moreover, the residual saturation trend is similar specially when a close attention goes toward Figure 9.5 (b). It is observed that the trend in captured liquid saturation is decreasing by increasing in flow Reynolds number, and a reduction in the pressure drop at higher Reynolds number.

In contrary to solid particle filtration, all numerical simulations and experimental studies suggest to operate liquid filtration at higher velocities as higher velocity causes more distribution of droplets through the filters and reduces the flow resistance (Contal et al. (2004); Frising et al. (2005); Charvet et al. (2008)). On the other hand, by increasing the inlet velocity in the filters the single phase pressure drop (mainly depends on the filter structure) increases which these two opposing phenomena form an optimum region in phobic filters. It is expected by increasing the inlet flow velocity, the multi-phase pressure drop and single-phase pressure drop difference tends to zero by expelling all the residual saturation.

Figure 9.6 presents all the experimental and numerical results. It should be mentioned that all the results have been normolised by the maximum pressure drop (in each case) to provide a condition for comparison.

It can be seen in Figure 9.6 that all the filter media which were studied numerically and experimentally has an optimum region due to combination of different parameters such as packing density, inlet flow velocity, surface energy and liquid properties. The region occurs at different Reynolds numbers in different filters, and it is mainly related to structural differences in the media. This is the case especially in numerical cases which they all have similar physical properties such as fibre diameter, packing density, thickness, and they all loaded with the same liquid particle droplets initially.

The interesting point in the graph is experimental and CFD results of fibrous case which have a similar trend as both have similar structures. It can be seen that the optimum region is happening at higher Reynolds number in the experimental test which can be reasoned by the fact that packing density in the experimental case is higher than the CFD simulations in this research, although another significant factor is contact angle which will be evaluated in this research by conducting numerical studies on philic filters. In this research, the experimental filters were selected carefully in order to cover a wider range of study. As such, the packing density of the selected experimental filter has a higher packing

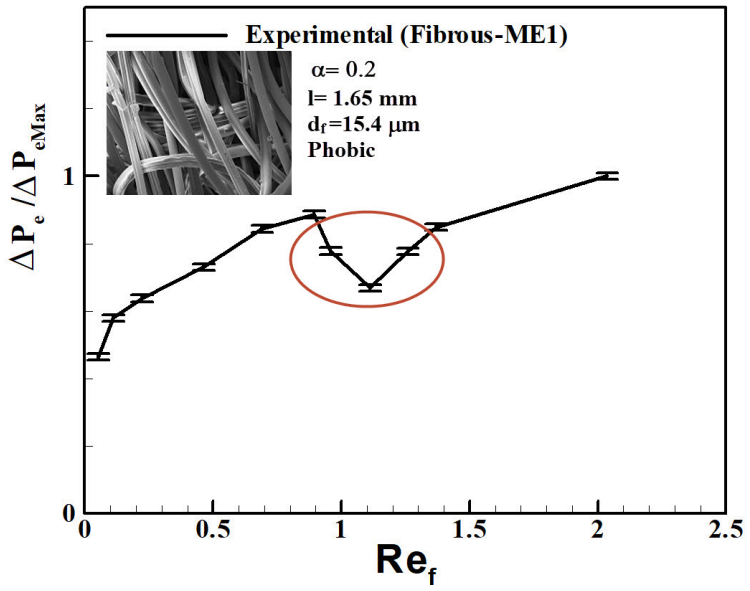

(a)

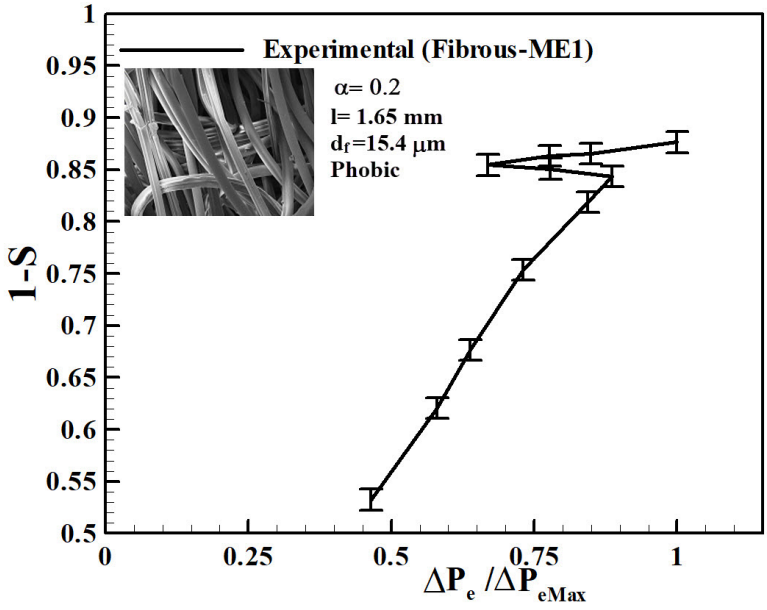

(b)

Figure 9.5: Experimental results in phobic fibrous media (Fibrous-ME1): (a) Pressure drop difference versus Reynolds number, (b) Residual saturation versus pressure drop.

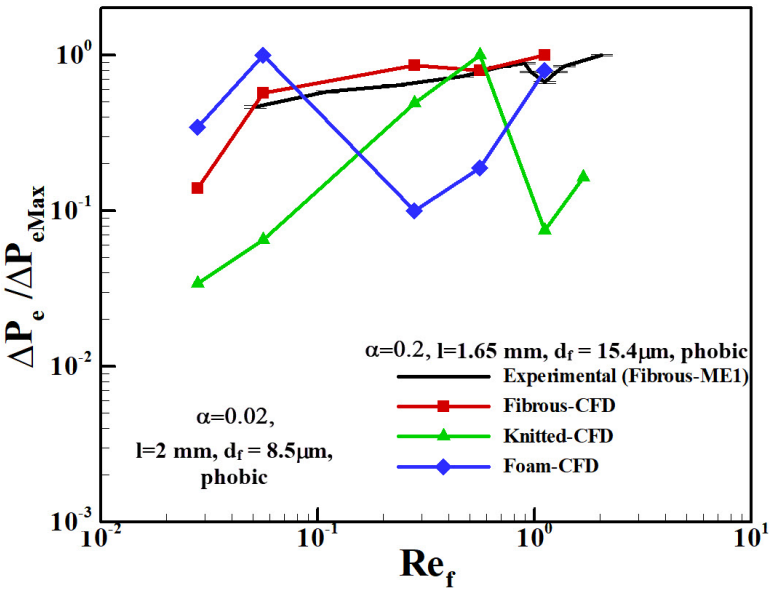

Figure 9.6: Non-dimensional pressure drop versus Reynolds number in phobic experimental case (Fibrous-ME1) and phobic CFD cases

density in phobic case, while in the next stage (philic media) a filter with lower packing density is considered for experimental study.

This optimum region has not been reported in previous works which studied phobic media (Chen et al. (2018); Chang et al. (2018); Chen et al. (2019a); Wurster et al. (2015); Chen et al. (2019b)). Likely due to the fact that most of the previous research focused on the filter efficiency and accordingly did not conduct study on pressure drop and saturation at higher velocities. More importantly, majority of studies in coalescing filtration mainly evaluate the filters from saturation hold-up, pressure drop, efficiency, quality factor globally. Therefore, there is no study to investigate different stages of filtration locally. Furthermore, many studies carried out based on operation velocities in industry which is based on the process constraints, where a high pressure drop in the system is not desirable, consequently mostly the operating velocities never go higher to prevent significant pressure drop. For instance, it can be seen from Figure 9.6 that in experimental case the pressure drop rises by increasing velocity, but after 1.3 m/s the pressure drop declines. In the industry operation, increasing velocity will be stopped as it is deduced that by improving velocity only the pressure drop increases, which is shown that it is not true. To provide a better demonstration on comparing the previous studies in phobic media and their operating conditions with the present study, Figure 9.7 indicates the non-dimensional pressure drop (in form of Eu) which is divided by packing density function to provide an equivalent basis for comparing the results.

It is observable from Figure 9.7 that all studies in phobic media filtration are conducted at low velocities which it can be seen that the gap between research -with respect to Reynolds numbers or inlet velocity- is filled by the current study. It is worth mentioning that only studies which provided enough information is considered and the details of their cases are listed in the Table 2.1.

9.2 Local Optimum Pressure Drop Region in Philic Media

In this section, the possibility of presence of an optimum region in the pressure drop profile in three types of philic filter media is investigated by plotting the pressure drop difference (ΔP_e) versus Reynolds number, and also residual saturation versus pressure drop difference which is presented by Figures 9.8 to 9.10.

Figure 9.8 illustrates the pressure drop difference against Reynolds number, and residual saturation versus pressure drop difference in philic fibrous media. As it can be seen in Figure 9.8 (a), an optimum region in the pressure drop profile is present in fibrous media when $1 < Re_f < 3$ (around $3m/s$) in this study. It should be stated that the optimum is not very significant (compared to phobic media) which can be associated to the inlet velocities selected for the philic media simulations which intervals were higher to capture the actual region. Figure 9.8 (b) shows the residual saturation, and it indicates that with decreasing the saturation level, the pressure drop is still increasing which is mainly due to strong adhesion forces between the residual saturation (which spreads on the fibres in philic media) and the effect of dry pressure drop. By having an overall view at Figure 9.8 (a), it can be deduced that the pressure drop curve is flattening which is showing the effect of re-entrainment and reduction of residual saturation level inside the filter (explained in Chapter 7). Therefore, the opposing effect of saturation reduction and increase of pressure drop by rising flow Reynolds number resulted in forming of a local optimum in the pressure drop profile of the philic fibrous media.

Figure 9.9 presents the pressure drop difference versus Reynolds number and the residual saturation against pressure drop difference in the philic knitted media. It is visible from Figure 9.9 (a) that the local optimum pressure drop presents in philic media which occurs in $1 < Re_f < 3$ (inlet velocity between 2 and 5 m/s). It can be seen from 9.9 (b) that residual saturation reduces and the local optimum appears when the saturation decreased between the last two simulation cases with highest Reynolds number.

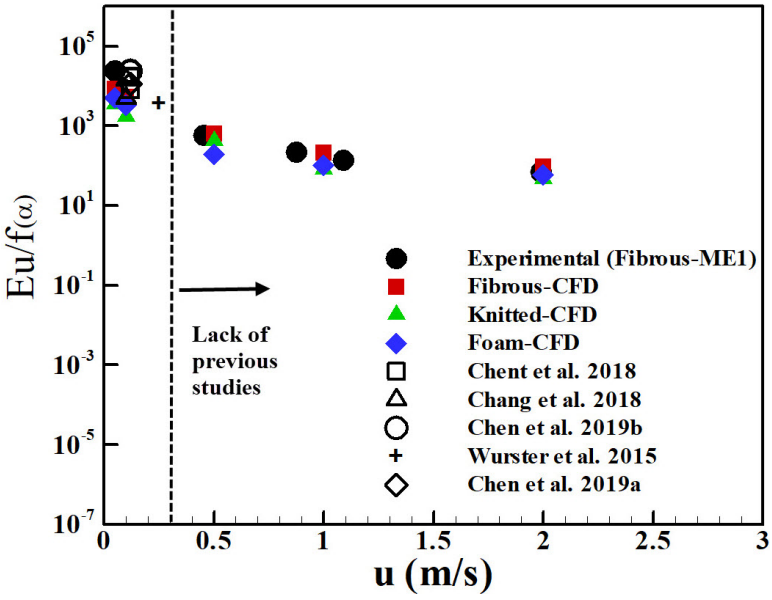

(a)

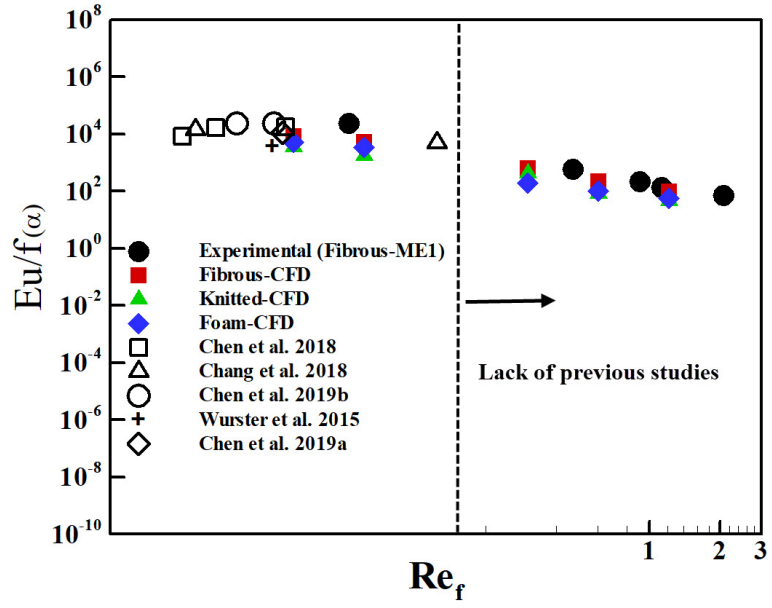

(b)

Figure 9.7: Numerical simulation results for all phobic filter media compared to previous studies: (a) All previous studies similar to this research based on flow velocities, (b) All previous studies similar to this research based on fibre Reynolds number.

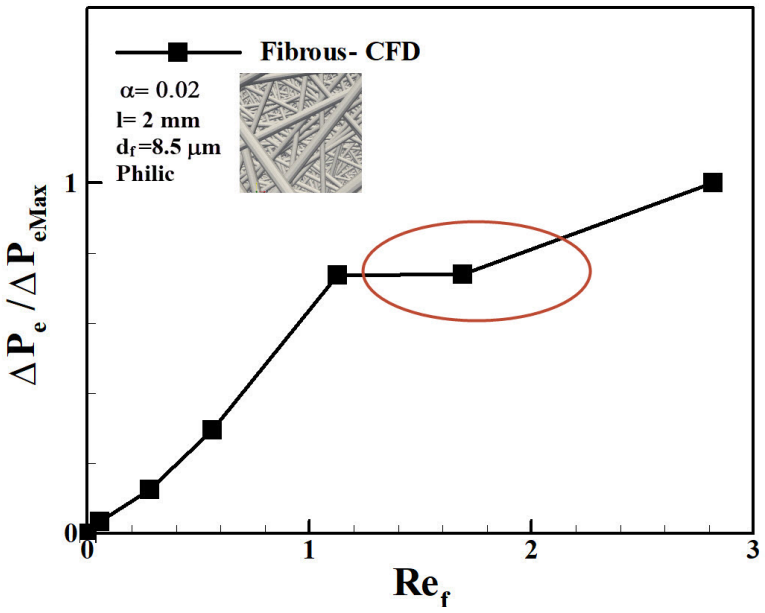

(a)

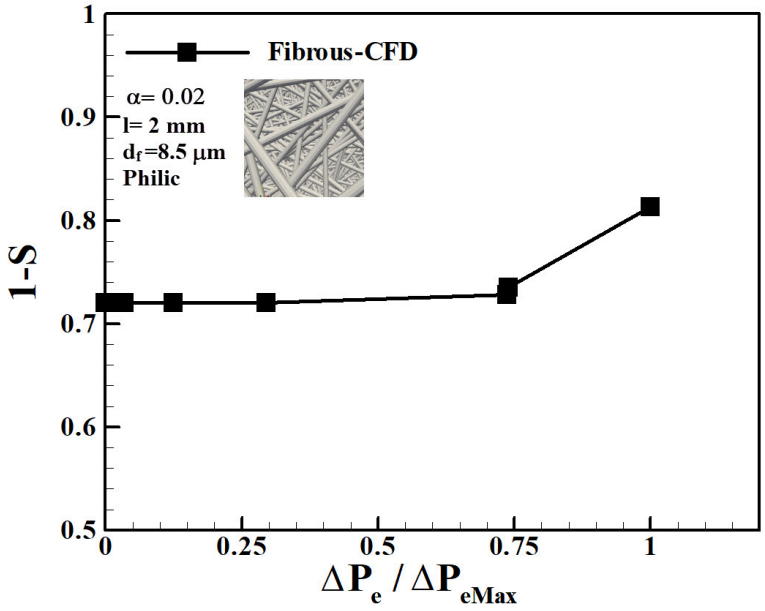

(b)

Figure 9.8: Numerical simulation results for philic fibrous media: (a) Pressure drop difference versus Reynolds number, (b) Residual saturation versus pressure drop difference.

Figure 9.10 indicates the pressure drop difference versus Reynolds number and residual saturation against pressure drop difference in philic foam filter. It is clearly observable from Figure 9.10 (a) that the trend is similar to philic knitted media, and the local optimum presents in $1 < Re_f < 3$ (inlet velocity between 2 and 5 m/s). Similar to all previous cases, the saturation decreases (by increasing in flow Reynolds number) which reduces the flow resistance in the foam media, and on contrary, the dry pressure drop soars by increasing in Reynolds number.

For the purpose of qualitative validation of the optimum region in the pressure drop profile of a philic media, sets of experiments conducted based on the methodology explained in section 4.3 on the Fibrous-ME2 which is a philic fibrous media, and its physical properties are listed in Table 4.4. Figure 9.11 presents the pressure drop difference versus Reynolds number and saturation against pressure drop difference in the Fibrous-ME2 case.

It can be deduced from this graph that the local optimum region in the pressure drop profile found in numerical studies philic filters is present in experimental investigation on a philic fibrous media as well. As it was discussed before, due to the combination of some contrary effects in liquid filtration (saturation reduction by increasing velocity and dry pressure drop increase by increasing velocity), a local optimum region from pressure drop prospective is possible which in this research has investigated.

Figure 9.12 presents the non-dimensional pressure drop across all numerical simulations for philic filter media plus the experimental study in one graph. It can be seen that all the case studies show an optimum region in their pressure drop profile. It is seen from this graph that the optimum region in the pressure drop profile is happening similarly in all CFD cases while in experimental case it occurs at lower velocities probably due to the low packing density of the tested filter compared to numerical cases.

In the following, the evaluation of the current investigations versus the previous studies in the literature (Zhang et al. (2017); Chen et al. (2018); Chang et al. (2018); Chen et al. (2019a); Wurster et al. (2015); Chen et al. (2019b); Letts et al. (2003); Jankowski (2009); Frising et al. (2005); Agranovski and Shapiro (2001); Agranovski and Braddock (1998b); Agranovski et al. (2002)) which conducted their research on philic media is presented. Figure 9.13 presents the comparison of the numerical and experimental studies in this research versus previous investigations in this field. It should be noted that all these studies used fibrous filter and investigated philic filters.

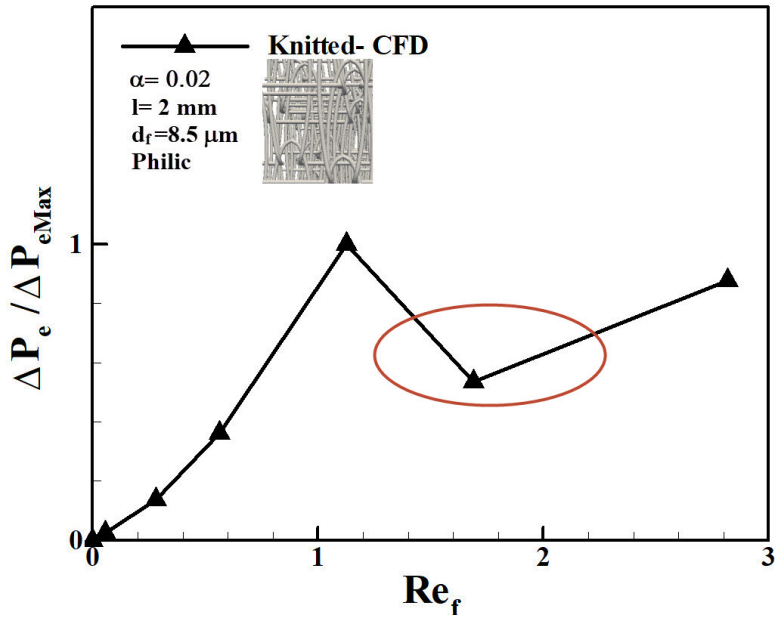

(a)

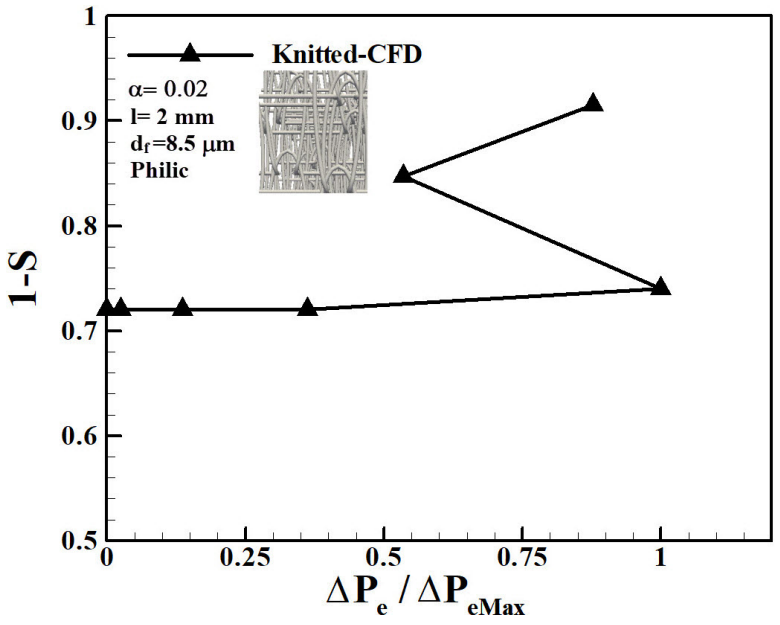

(b)

Figure 9.9: Numerical simulation results for philic knitted media: (a) Pressure drop difference versus Reynolds number, (b) Residual saturation versus pressure drop.

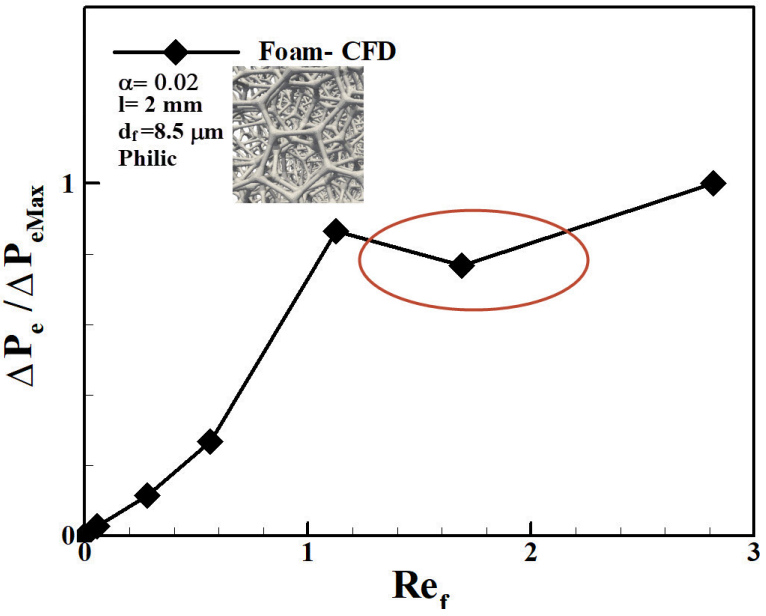

(a)

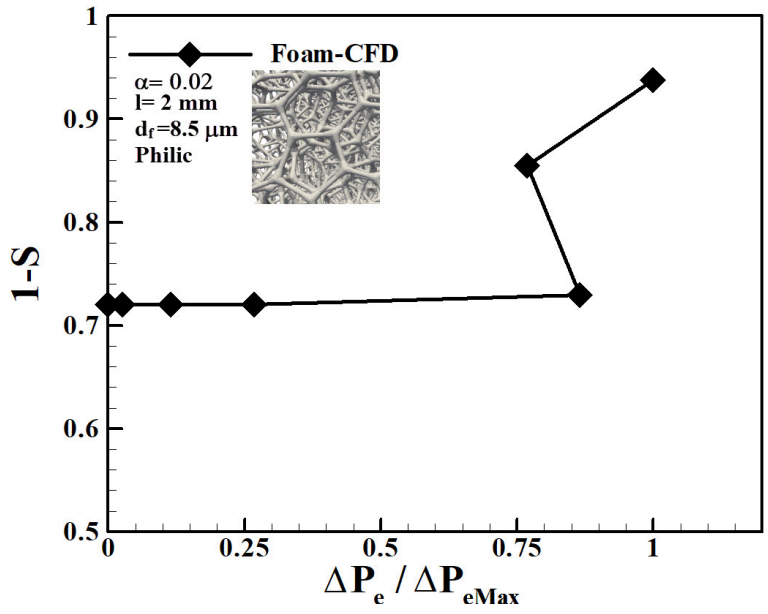

(b)

Figure 9.10: Numerical simulation results for philic foam media: (a) Pressure drop difference versus Reynolds number, (b) Residual saturation versus pressure drop.

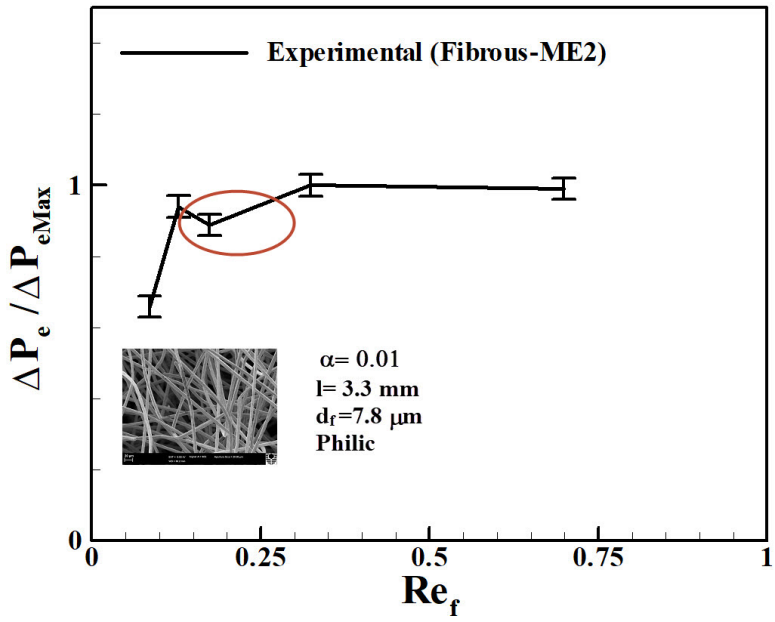

(a)

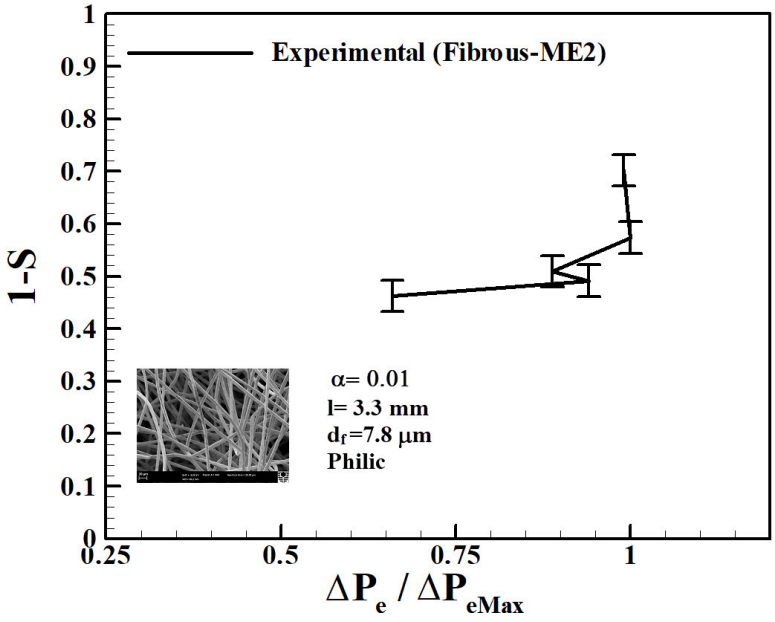

(b)

Figure 9.11: Experimental results in phobic fibrous media (Fibrous-ME1): (a) Pressure drop difference versus Reynolds number, (b) Residual saturation versus pressure drop.

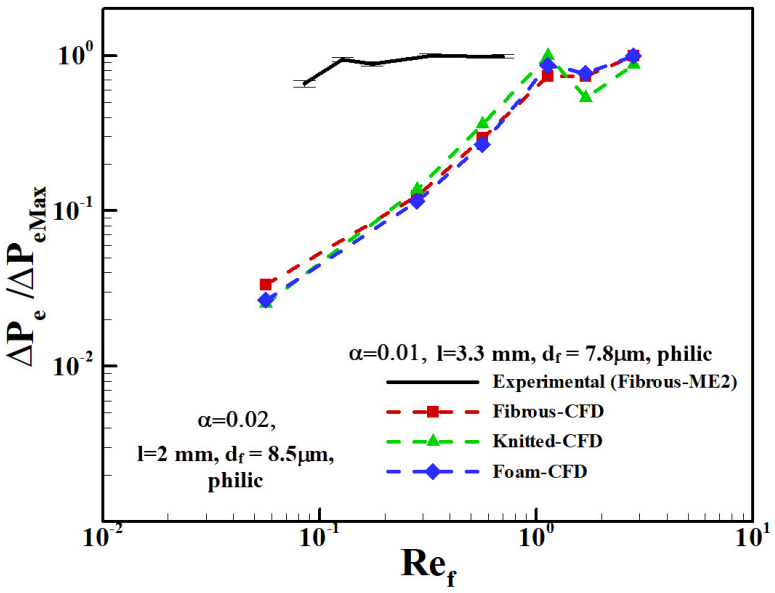

Figure 9.12: Non-dimensional Pressure Drop Versus Velocity in Experimental and CFD Cases for philic Media

Figures 9.13-(a) and (b) compare studies in philic filtration field against the experimental and numerical results carried out in this research. To provide an equivalent condition for comparing the results, the effect of packing density is normolaised with a packing density function ($Eu/f(\alpha)$).

It can be seen in Figure 9.13 that there is a lack of studies at higher velocity in philic media. As it is visible in the both graphs, there is only one study that experimented a fibrous media at high velocity, but they applied water as the liquid in their filtration tests, and Agranovski and Braddock (1998a) did not report any optimum in the pressure drop profile. Recent research by Chen et al. (2019a) indicated that pressure drop profile and also efficiency in coalescing filters are greatly affected by liquid surface tension, therefore it is concluded that using water with very different surface tension (compared to DEHS employed in experiments and CFD) in Agranovski and Braddock (1998a)'s study is the reason for not seeing any optimum in the pressure drop profile. Moreover, as mentioned earlier, majority of the research in coalescence field mainly focused on global filtration and pressure drop which seems to be the case in Agranovski and Braddock (1998a)'s work as well. It should be noted that Mead-Hunter et al. (2013)'s research results supports the findings in this research, although the objective of their research was to present a capillary based saturation model. Mead-Hunter et al. (2013) reported the "dip" in the pressure drop was possibly regarded in experimental variation.

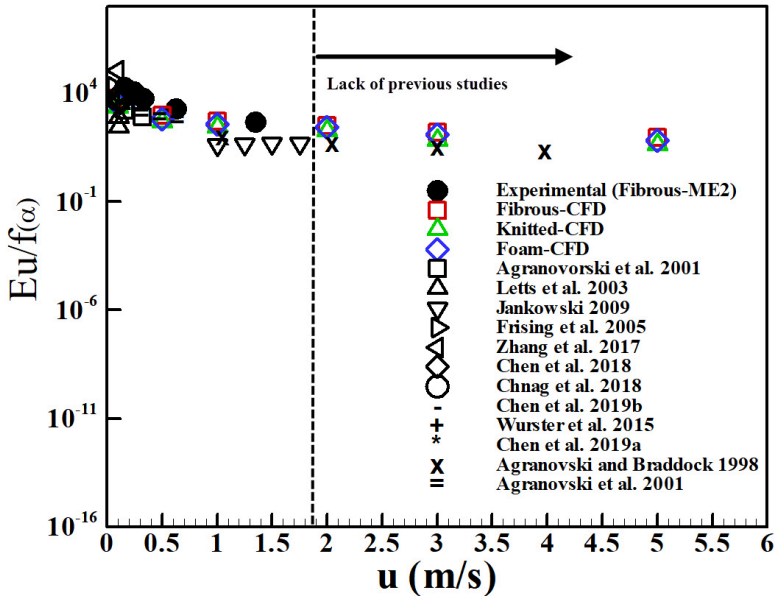

(a)

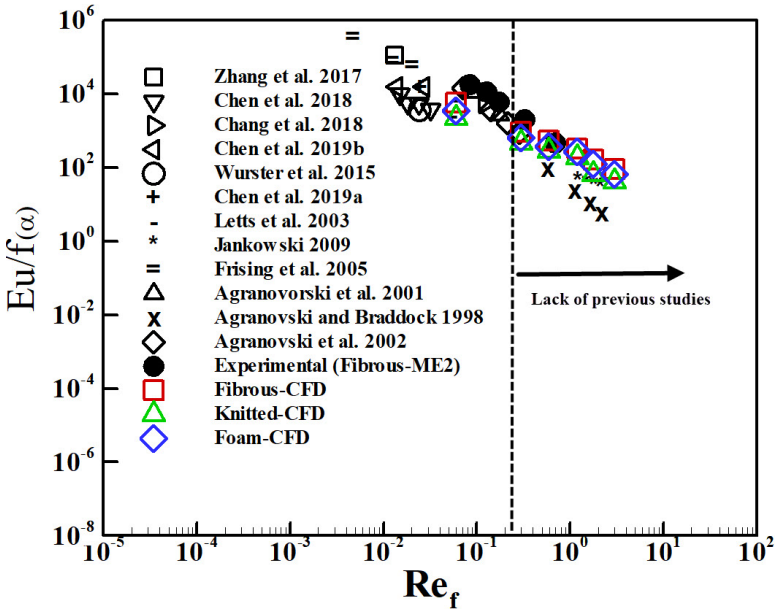

(b)

Figure 9.13: Numerical simulation results for all philic filter media compared to previous studies: (a) All previous studies similar to this research based on flow velocities, (b) All previous studies similar to this research based on fibre Reynolds number.

9.3 Effect of Contact Angle on the Local Optimum Pressure Drop Region in Coalescing Filter Media

It was shown in Chapter 8 that contact angle affect the coalescing filtration significantly by changing the residual saturation, wet pressure drop profile, and quality factor in different filter media. The results indicate that reducing contact angle resulted in improving coalescing filters saturation hold-up capability and increases the wet pressure drop in all filter media studied with different structures. In this section, the influence of changing contact angle on the discovered local optimum region is examined by comparing the results in previous sections in all CFD and experimental cases. In order to provide a comparable situation, the pressure drop curves are non-dimensionalised by the maximum pressure drop value in the graph.

Figure 9.14 demonstrates the effect of reducing contact angle on the local optimum region in the pressure drop profile in different filter media. It is clearly seen that reducing contact angle (from 120° to 20° in present study) affected the emerging region of local optimum in the pressure drop profile by shifting that to the higher Reynolds numbers in all CFD study cases. As it was shown before, all the physical properties of these different filters such as packing density, fibre diameter, thickness, and cross section area are identical, therefore, the investigated effect is merely the influence of contact angle which is one of the great advantages of employing CFD in this study as such an ideal comparison is not achievable by conducting experiments.

Analysing the results from contact angle effect suggests that decreasing contact angle improves all filters saturation retaining ability which is mainly due to improving the droplet-fibre adhesion forces (Mullins et al. (2014)). Therefore, transporting residual liquid throughout the filter require higher shear forces which is happening at higher Reynolds number. By reducing the residual saturation (which is happening at higher Reynolds number by reducing contact angle) the flow resistance declines and the opposing influence of dry pressure drop (due to filter structure) acts against each other and forms this local optimum at higher Reynolds number.

Figure 9.15 shows the effect of changing contact angle on the local optimum in the pressure drop profile of experiential fibrous cases. It is visible from the graph

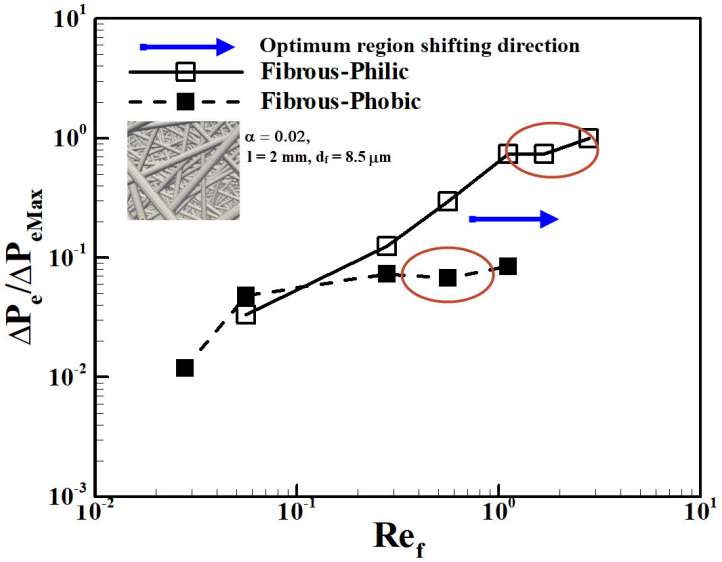

(a) Fibrous-CFD

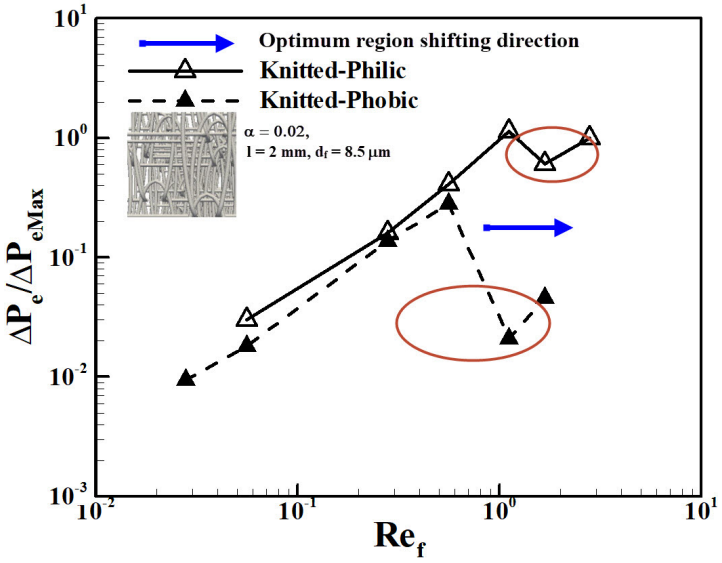

(b) Knitted-CFD

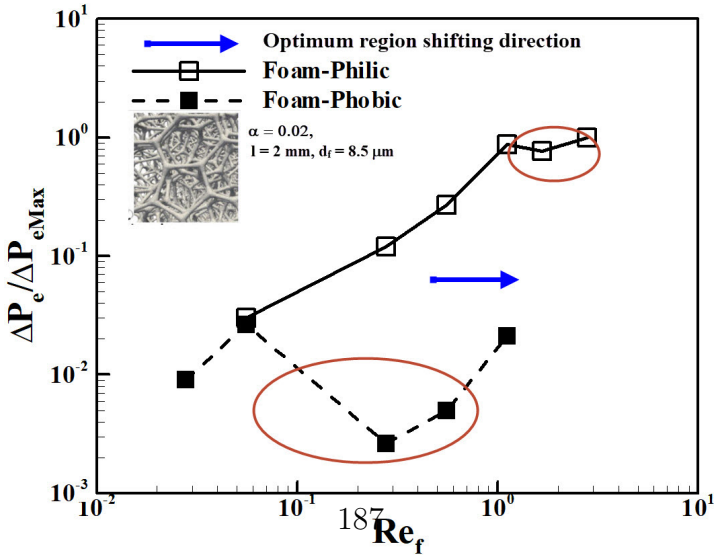

(c) Foam-CFD

Figure 9.14: Effect of contact angle on local optimum in the pressure drop profile region presence in different filter media.

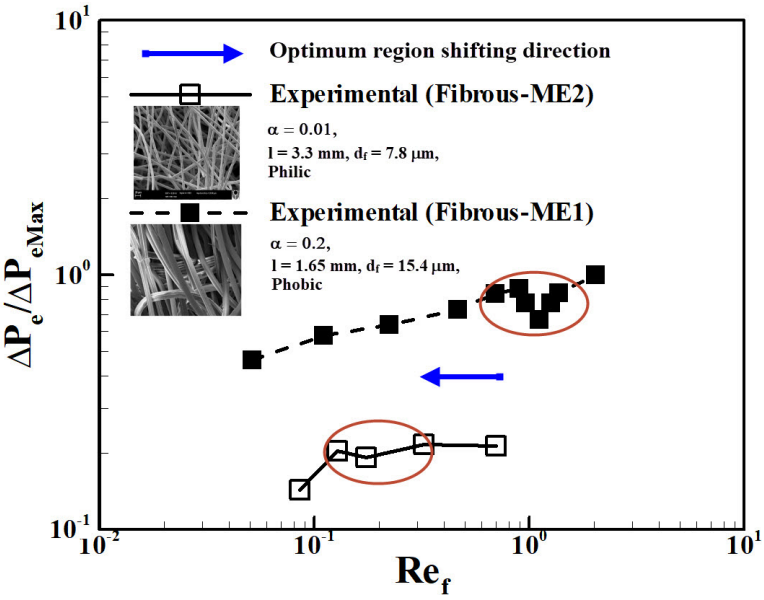

Figure 9.15: Effect of contact angle on local optimum in the pressure drop profile region presence in experimental cases.

that the local optimum shifting direction is opposite of the CFD results discussed earlier. It should be mentioned that the two experimental cases Fibrous-ME1 and Fibrous-ME2 (details are listed in Table 4.4) has different physical properties which make understanding of the underlying reason harder compared to ideal situation of CFD cases. By further look at different data (comparing Fibrous-ME2 with phobic Fibrous-CFD in Figure 9.6) it suggests that increasing packing density can shift the local optimum occurring at higher Reynolds numbers. It should be mentioned that the phobic fibrous CFD case and Fibrous-ME1 are not identical for a solid conclusion, but further analysis will be done in the next section where the hypothesis is proposed.

9.4 Qualitative Hypothesis in Forming a Local Optimum in the Pressure Drop Profile of Coalescing Filters

The numerical and experimental studies conducted during this research suggest that there are two main factors which play a significant role in forming of the local optimum region in the pressure drop curve. These two factors are contact angle and packing density which following Figures 9.16 and 9.17 presents their effects on possible optimum, respectively.

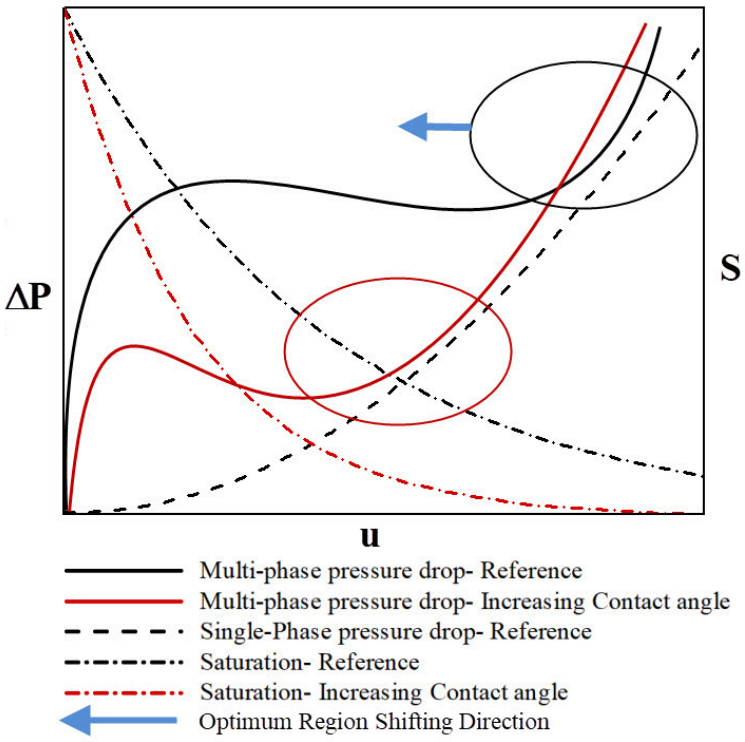

Figure 9.16: The proposed hypothesis of increasing contact angle effect on optimum pressure drop profile.

It can be deduced from Figure 9.16 that by increasing the contact angle in filter media, the single phase pressure drop remain constant, although the holding-up capability of a filter will reduce which resulted in saturation reduction (Contal et al. (2004); Charvet et al. (2008); Mead-Hunter et al. (2014)). These effects can be confirmed by the CFD results presented in Chapter 8 as well. The effect of contact angle is evaluated in this research by studying philic and phobic media by keeping all other parameters (fibre diameter, packing density, filter thickness, and cross section area) constant, therefore it provides an equivalent condition to isolate only the contact angle effects for the evaluation.

As discussed earlier in this chapter, the opposing effects of saturation reduction and rising the dry pressure drop (due to filter structure) by increasing in inlet flow velocity form a local optimum in the pressure drop profile. As shown by Figure 9.16, the reference line for the single-phase pressure drop is not affected by changing in contact angle, and it increases with inlet velocity because of higher flow resistance at higher flow velocities (Davies (1953)). On the other hand, growing the inlet velocity reduces the saturation level inside the filter and consequently decreases the wet pressure drop and also flow resistance (Contal

et al. (2004)). It means the opposing events are happening at lower velocity by increasing contact angle, therefore the local optimum in the pressure drop curve occurs at lower inlet velocities.

The other parameter mentioned before is packing density which the hypothesis of its effects in the filters is presented by Figure 9.17. It is observable from Figure 9.17 that single-phase pressure drop increases with increasing in inlet velocity and also packing density which was expected as it rises the flow resistance (Davies (1953); Spielman and Goren (1968)). It is seen that the saturation expected to increase compared to the lower packing density. This can be concluded from the research of Contal et al. (2004) who shows higher packing density filters tend to have a higher hold-up ability due to higher fibres intersections inside the filter. It was shown by Hotz et al. (2015) that trapped droplets on intersections in a filter require 77% and 32% higher forces to detach the droplets in philic an phobic media, respectively. Consequently, holding more saturation increase the flow resistance and increase the wet pressure drop which is considered in the Figure 9.17.

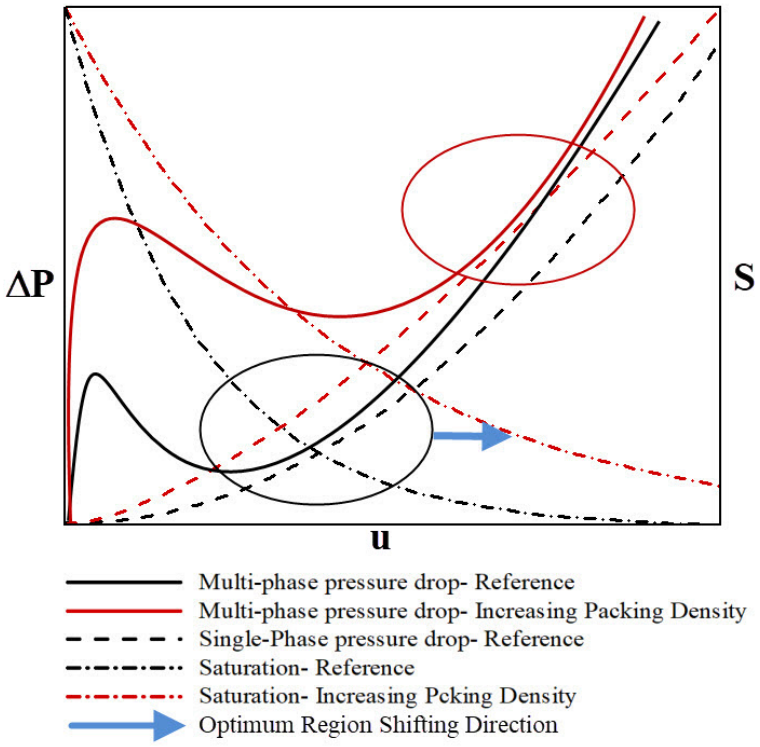

Figure 9.17: The proposed hypothesis of increasing packing density effect on optimum pressure drop profile.

According to Figure 9.17, it is suggested that the local optimum in the pressure drop profile shifts to occur at higher velocities by increasing in packing density.

This phenomena is observed when compared the CFD results in phobic fibrous with experimental phobic case (Fibrous-ME1). It is shown in Figure 9.6 that the local optimum presents at higher velocity for the experimental case with about 10 times higher packing density. It should be noted that the other difference between the CFD case and experimental one is the fibre diameter which is about two times larger in experimental case. In regard to effect of fibre diameter on detachment from filters and also pressure drop profile, although this effect is not studied in this research, but the Hotz et al. (2015)'s research shows that increase in fibre diameter resulted in increase in required detachment force which is explained by the fact that increase in fibre diameter rises the contact line length between droplet and fibre element. In order to provide a better demonstration of the proposed hypothesis, the Re_f where the local optimum has occurred in fibrous CFD cases and also two experimental ones are depicted by Figure 9.18.

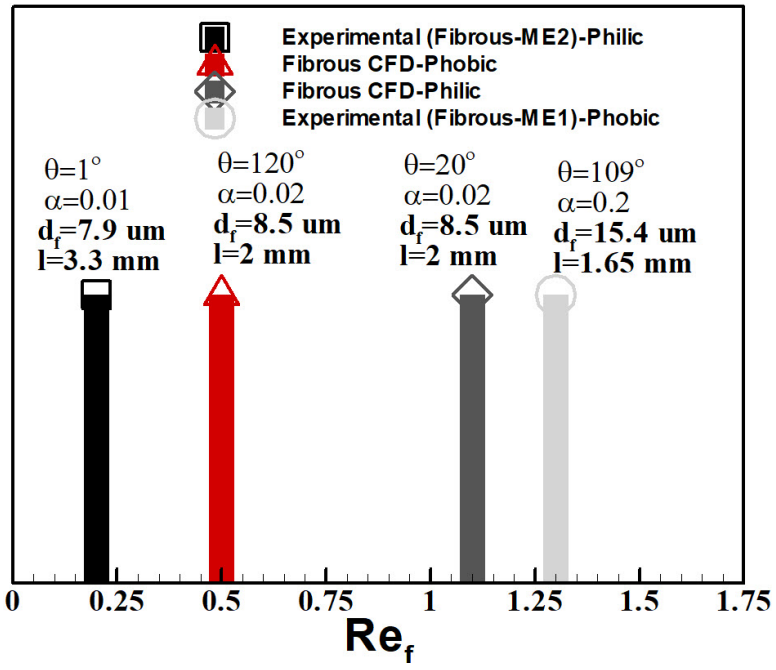

Figure 9.18: Comparison of local optimum pressure drop occurrence Re_f in fibrous CFD and experimental cases.

By comparing "Fibrous CFD-Philic" case to "Experimental (Fibrous-ME2)-Philic" case, it is seen that the values of d_f are similar, but packing density value is greater in "Fibrous CFD-Philic" (although the contact angle is higher in CFD case and has an opposite effect), and it has shifted the optimum pressure drop to higher Reynolds number. This shows that the effect of packing density can be higher than contact angle. Moreover, by comparing "Fibrous CFD-Phobic" case to "Experimental (Fibrous-ME2)-Philic", it is seen that the optimum is still

taking place at a higher Reynolds number, although the contact angle in phobic CFD case is much higher, therefore it corroborate the previous finding. In the case of contact angle effect, as discussed earlier, it has its effects and shift the occurrence of optimum pressure drop to a lower Reynolds number. This can be confirmed clearly by comparing two CFD cases which ideally isolate the influence of contact angle. It is seen that increasing in contact angle shifts the optimum pressure drop to a lower Reynolds number.

Comparison between "Experimental (Fibrous-ME1)-phobic" case and "Experimental (Fibrous-ME2)-philic" confirms the aforementioned hypothesis. It is visible from Figure 9.18 that there is a great difference between the contact angle in these two experimental cases, but the higher packing density (and also larger d_f) has shifted the local optimum in the pressure drop curve to happen at a higher Reynolds number.

There are other parameters which has a potential influence on the local optimum in the pressure drop curve which require further study. These factors are fibre diameter, filter thickness, filter cross section area, operating temperature, liquid surface tension, flow direction, flow viscosity, and filter pore size.

9.5 The Importance of the Local optimum in the pressure drop Curve

Higher efficiency and lower pressure drop have always been the main goal of coalescing filters with high performance. Pressure drop in filters which defined as the difference in total pressure between the feed and rear face of a filter during the filtration process is a principal index parameter directly related to the lifetime and energy consumption of a filter (Zaatari et al. (2014); Liu et al. (2003)). It is reported that higher pressure drop in the system is associated with higher energy consumption. Nassif (2012) calculated that 1 Pa increase in the pressure drop of a filter in the system can be resulted in 1.8 to 3.2 KWh higher power consumption. Moreover, filters operating under high pressure drop condition apt to damage, resulting in fault of filtration.

Apart from all the disadvantages of the high pressure drop in the system, reducing pressure drop can be beneficial for filter design and filter sizing. In regard to filter sizing criteria, generally if a coalescing filter equipment is sized in standard cubic feet per minute (SCFM), filter is selected for a particular application based on the airflow and allowable pressure drop. Process design engineers size

the filters according to allowable pressure drop in the system. This means that if the calculated pressure drop according to a filter dimension is high, the flow should be reduced, and if it is not practical, larger filters are required which increase the cost. Moreover, in some cases it is not possible to go to a higher surface area in filter for reducing the flow rate and consequently decreasing the pressure drop in the system. From this, it can be concluded that reducing pressure drop in filters is an important factor which can resulted in a better performance.

To provide a better demonstration of local optimum in the pressure drop curve application, Figure 9.19 indicates the net pressure drop with the optimum in the pressure drop curve for the experimental case from present study (Fibrous-ME1) versus the inlet velocity to the filter.

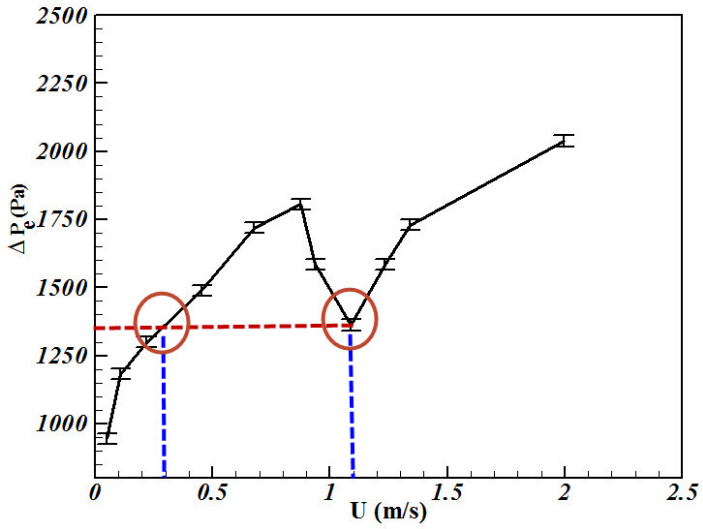

Figure 9.19: Applying the optimum in the pressure drop curve in sizing the filters.

If the maximum allowable pressure drop to a system assumed to be 1300 Pa, it is seen from the Figure 9.19 that there are two velocities which can produce such a pressure drop. At first, the flow can be calculated to be 0.3 m/s which require a filter with surface area of A1. After locating the optimum in the pressure drop curve, it is seen that the similar pressure drop can be produced at a higher velocity which can be measured from the graph as 1.1 m/s which needs a filter with A2 cross section area. By comparing the size A2 against A1, it can be calculated that the filter with A2 size can be 3.6 times smaller which can save on the manufacturing and maintenance costs. All these simple calculations conducted in this example are only for demonstration of a bench scale filter and advantage of finding the optimum in the pressure drop curve.

9.6 Conclusion

In this chapter, the possibility of presence of a local optimum region in the pressure drop curve in different coalescing filter media with different structures was investigated numerically and experimentally. In order to achieve this, the difference between multi-phase and single-phase pressure drop was calculated and plotted against Reynolds number and also saturation profile. It was found that the saturation reduction by increasing Reynolds number and enhancing the dry pressure drop (accosted with the filter structure) acts as opposing parameters which can form a local optimum in the pressure drop profile.

The investigations revealed that this local optimum was present in all filter media with different structures in both philic and phobic cases. The CFD results were verified by a qualitative validation of two fibrous experimental cases. The results from experiments confirmed the presence of a local optimum in the pressure drop curve. In the next stage, the effect of contact angle was examined by comparing the results from phobic and philic media CFD simulations which was found that contact angle can affect the occurring flow rate of the optimum in the pressure drop curve.

According to the conducted investigations in both CFD and experimental cases, a qualitative hypothesis was proposed which provided an understanding on the presence of the local optimum in the pressure drop curve. It was indicated that contact angle and packing density had a significant influence on the forming of the optimum in local pressure drop curve. It was found that increasing contact angle tends to shift the occurring of the local optimum in the pressure drop curve at lower Reynolds numbers, while increasing in packing density of the filter had an opposite effect.

It was shown that finding the local optimum region in the pressure drop curve had significant advantages to reduce the energy consumption cost and improved the flexibility with filter sizing and design, and also reduced the manufacturing and maintenance cost of the coalescing filters.

Chapter 10

Conclusions

This work has presented a general approach for comparing the performance of different coalescing filters such as fibrous, knitted, and foam structures with equivalent physical and initial conditions; packing density, fibre element diameter, thickness, cross section area, contact angle, initial saturation level, and inlet velocities. The effects of velocity and contact angle on different filter structures performance have studied which was not possible to be done systematically and ideally by conducting experiments. In the end, a qualitative hypothesis has proposed in regard to forming a local optimum in the pressure drop curve.

In Chapter 4, the methodology employed for generating different coalescing filters with different structures was described. In the present study, CFD method was applied for investigations and single-phase, multi-phase solution techniques, and their setup in OpenFOAM software were explained. Moreover, the experimental approach and apparatus design for conducting single and multi-phase were elaborated. The validation of generated filter media, single-phase and multi-phase CFD solver, mesh generation techniques, and mesh sensitivity study were conducted in Chapter 5. After presenting the mesh generation techniques and mesh quality improving procedure, it was found that filter geometry packing density was independent from mesh refining process ($\pm 5\%$) for 'number of cells $> 1.8\times 10^6$' in the given geometry size. The mesh sensitivity analysis for single-phase flows indicated that all geometries produced independent pressure drop value for 'number of cells $>2 \times 10^6$'. The single-phase (dry) pressure drop results were used for evaluating the accuracy of the generated virtual filter media. It was shown that the dry pressure drop results in all generated filter media (fibrous, knitted, and foam) had a good agreement with established theoretical models and experimental data which could be concluded that all generated filters with different structures are suitable and accurate for further investigations. It was shown in the literature review (Chapter 2) that the majority of the research

works in filtration focused on fibrous filters and used various imaging techniques for the fibrous geometry with a very limited geometry validation discussion. It was demonstrated that this study could fill this gap by applying rigorous techniques in order to generate realistic virtual filters with different structures. This study extended the filter investigation to other structures such as knitted and foam media which have been subject of fewer studies.

The mesh sensitivity analysis for multi-phase simulations was conducted, and the results suggested that 'number of cells $> 2\times 10^6$' resulted in accurate equilibrium saturation results ($\pm 10\%$) in all filter media considered in this research. The validity of the multi-phase simulations were demonstrated in Chapter 5 by comparing the numerical results with experimental data from this research and from literature. It was shown that the equilibrium saturation and wet (multi-phase) pressure drop results agreed well with experimental data which corroborate the validity of the applied numerical techniques. It was discussed that empirical models were only applicable to a narrow range of fibrous filters which reinforced the necessity of the current research. From Chapters 4 and 5, it could be concluded that the methodology presented in this research could provide an equivalent basis for further filtration investigations and be able to isolate a specific parameter effect which was not possible by only conducting experiments.

In Chapter 6, the quality factor in three phobic filter media (fibrous, knitted, and foam) with contact angle of $\theta = 120^\circ$ was investigated. The saturation and pressure drop of these filters at different inlet velocities were measured by using CFD. The results indicated that the saturation decreased by increasing in inlet velocity which was attributed to higher shear forces at higher velocities. It was found that phobic foam filter media had the lowest saturation retaining capability which its re-entrainment started at 0.1 to 0.5 m/s velocity range. On the other hand, phobic knitted media had the highest saturation hold-up capacity which its re-entrainment started at u>1 m/s. The results suggested that fibrous filter had a higher saturation retaining capability at higher velocities compared to other filters. Analysis of the pressure drop results revealed that residual saturation had a significant influence on the wet pressure drop in the filters which its effect declined by increasing in inlet velocity. Pressure drop results showed that fibrous filter had the highest value compared to other filters which produced 5 times higher than knitted media at low velocities. The performance analysis showed that phobic knitted media had the highest quality factor among all filter media in $0.05 \leq u \leq 1$ m/s, but fibrous had the best performance for velocity above 2 m/s which was reasoned due to its high hold-up ability at higher velocities. Quality factor results indicated that phobic foam media had the lowest value among all studied filters. It was shown in literature review (Chapter 2) that phobic me-

dia is the subject of fewer studies which the current research aimed to fill this gap especially by extending the research to the filter media structures including knitted media. The performance analysis results corroborate the necessity of this research as it was shown that knitted media had the best quality factor among all filter structures studied. Moreover, due to empirical models limitation to fibrous filter and specific filter physical conditions, CFD investigations in this research provided a better understanding of other filter structures filtration and performance.

In Chapter 7, the performance of philic fibrous, knitted, and foam filters at different inlet velocities were evaluated. It was discussed that the higher velocity range was considered for philic filters as greater forces are required for detaching droplets from low energy surfaces. The initial condition was set similar to phobic media, but the contact angle was considered as $\theta = 20°$. The CFD saturation results demonstrated a decreasing trend by increasing in inlet flow velocity. It was found that foam filter had the lowest residual saturation compared to other filters at all velocities above 1 m/s, while fibrous filter indicated the highest retaining ability in all inlet velocity cases. It was shown that high dispersion ability of the residual oil saturation in fibrous filter reduced the flow resistance and caused higher saturation level in this filter. The CFD pressure drop values indicated that fibrous filter imposed up to 61 % more pressure drop to the system compared to the knitted media which had the lowest wet pressure drop among philic filters. It was shown that this difference declined to 46 % by increasing in inlet velocity which was reasoned due to lower saturation level at higher inlet velocities. Investigating the quality factor results showed that philic knitted media outperformed all other philic filters in the range of $0.1 \leq u \leq 2$ m/s, while philic fibrous filter had higher quality factor value at $u > 3$ m/s as a result of its high oil retaining capability at higher inlet velocities.

Reviewing the numerical results in Chapters 6 and 7 showed that studying higher inlet velocity range in filtration is necessary as benefits of liquid filtration at higher velocities for fibrous filters were observed. Moreover, this research filled the gap in literature by an ideal quality factor comparison of different filter media structures by applying CFD techniques which was not possible through experiment.

Analysis of the contact angle results indicated that reducing contact angle had the most influence on foam media saturation hold-up which was improved by 100 % in some velocities. This caused the onset of its re-entrainment shifted from $u < 0.5$ m/s in media with $\theta = 120°$ to $u > 1$ m/s in media with contact angle of $\theta = 20°$. In general, it was found that reducing the contact angle improved the residual saturation level significantly in all filter media, and the re-

entrainment occurred at higher velocities. In terms of wet pressure drop all filter media imposed higher pressure drop to the system which was attributed to enhanced adhesion force between oil droplets and fibre elements by reducing contact angle. The quality factor results from all the filter media suggested that phobic filters had a better performance at low inlet velocity cases ($u \leq 2$ m/s), while philic filters had higher quality factor values at $u > 2$ m/s. In summary, phobic knitted media outperformed all its counterparts and philic fibrous at higher inlet velocities. By reviewing the Chapter 8 results, it can be concluded that the current research study has successfully investigated the effect of contact angle in different filter structures. Furthermore, the combination effects of contact angle and inlet flow velocity provided a better insight of the coalescence filtration in different filter media which has not been reported in literature. It can be concluded that the developed methodology for evaluating different filter media in the present research produced reliable results, and effect of a single parameter on performance has been isolated and investigated perfectly.

In Chapter 9, investigation was conducted to evaluate the possibility of a local optimum in the pressure drop curve. By deducting the dry pressure drop results (due to filters structure) from the wet pressure drop values, it was revealed that an optimum region in the pressure drop curve existed. Further analysis of the results indicated that the residual saturation reduction inside the filter by increasing in inlet velocity and growing the dry pressure drop acted as opposing factors which resulted in forming the local optimum in pressure drop trend. This occurrence was observed in both philic and phobic media which was validated qualitatively by sets of experiments with different contact angles. Based on the numerical and experimental observations, a qualitative hypothesis was suggested. It was shown that packing density and contact angle had the most influence on the location of the optimum in the pressure drop curve. It was deduced that the effect of packing density was higher than the contact angle in the location of the optimum in the pressure drop curve. It was suggested that increasing the contact angle was resulted in forming the optimum at lower inlet velocities, while increasing packing density had the opposite influence. Reviewing the quality factor results from Chapters 6 and 7 suggested that operating coalescence filters at lower inlet velocities mainly due to lower pressure drop in these flow rates. In high volumetric flow rate processes, this means a larger cross section area for the filter in order to reduce the inlet velocity. The local optimum in the pressure drop curve can be significantly helpful as indicated the possibility of a region with lower pressure drop at higher velocities. This can lead to the need for smaller cross section area of a filter which reduces the manufacturing and operating costs markedly. This phenomena has not been reported previously for two reasons. First, the majority of the research in coalescence filtration were limited to narrow inlet velocity

ranges as it was believed lower velocities reduce re-entrainment and increase the quality factor of the filter. Second, all the studies focused on the global efficiency or pressure drop in coalescence filters which considered all the filtration stages. In this research, an intensive research on the last filtration stage (steady state and also the stage where the filters typically operate the longest) with higher inlet velocity range resulted in finding the possibility of an local optimum in the pressure drop curve.

In conclusion, this work was used an approach for studying coalescing filters in micro-scale which could compare different filters with different structures. In this study, the effects of inlet velocity variation and contact angle were investigated in details by CFD. The numerical results were validated against experimental tests conducted in this study, experimental data in literature, and empirical models. Finally, a qualitative hypothesis was proposed in order to evaluate the location of a local optimum region in the pressure drop curve.

10.1 Recommendations For Further Work:

- Applying the methodology developed and used in the present study to conduct a systematic study isolating further parameters which potentially affect coalescing filtration such as fibre diameter, packing density, cross section area of the filter, temperature, and surface tension;
- Further studies of knitted media to develop a correlation for estimating the dry pressure drop by conducting a systematic numerical study on virtual knitted media;
- Carrying out further numerical and experimental studies on forming the local optimum in the pressure drop curve by investigating the effect of other parameters such as fibre diameter, filter thickness, filter cross section area, humidity, temperature, and surface tension;
- Using CFD to develop a saturation model for predicting the equilibrium saturation level related to identified key parameters in each virtually generated filter type;
- Using CFD to develop a wet pressure drop model to predict the multi-phase pressure drop in the coalescing filter according to inlet velocity, contact angle, saturation level and other identified key parameters in each virtually generated filter type;

- Developing quality factor estimation correlation based on the equilibrium saturation and pressure drop results by using CFD in different filter structures.

Statement of Contribution

S. Abishek, A.J.C. King, R. Mead-Hunter, V. Golkarfard, W. Heikamp, B.J. Mullins (2017) Generation and Validation of Virtual Nonwoven, Foam and Knitted Filter (Separator/ Coalescer) Geometries for CFD Simulations, Separation and Purification Technology, 188, 493-507.

Co-author	Conception & design	Acquisition of data & methodology	Analysis & statistical method	Interpretation & discussion	Final approval
Abishek Sridhar	×	×	×	×	×
I acknowledge that these represent my contribution to the above research output.					
Andrew.J.C King	×			×	
I acknowledge that these represent my contribution to the above research output.					
Ryan Mead-Hunter				×	×
I acknowledge that these represent my contribution to the above research output.					
Wolfgang Heikamp					
I acknowledge that these represent my contribution to the above research output.					
Benjamin.J Mullins	×			×	×
I acknowledge that these represent my contribution to the above research output.					

V. Golkarfard , A.J.C. King, S. Abishek, R. Mead-Hunter , G. Kasper , B.J. Mullins (2019) Optimisation of wet pressure drop in nonwoven fibrous, knitted, and open-cell foam filters, Separation and Purification Technology, 213, 45-55, Elsevier.

Co-author	Conception & design	Acquisition of data & methodology	Analysis & statistical method	Interpretation & discussion	Final approval
Andrew.J.C King	×			×	×
I acknowledge that these represent my contribution to the above research output.					
Abishek Sridhar	×			×	×
I acknowledge that these represent my contribution to the above research output.					
Ryan Mead-Hunter				×	×
I acknowledge that these represent my contribution to the above research output.					
Gerhard Kasper					
I acknowledge that these represent my contribution to the above research output.					
Benjamin.J Mullins	×			×	×
I acknowledge that these represent my contribution to the above research output.					

Vahid Golkarfard, Ramanathan Subramaniam, Jonathan Broughton, Andrew King, and Benjamin Mullins (2018) Comparative Performance of 12 Crankcase Oil Mist Separators, SAE International, 12(1), 03-12-01-0001.

Co-author	Conception & design	Acquisition of data & methodology	Analysis & statistical method	Interpretation & discussion	Final approval
Ramanathan Subramaniam					
I acknowledge that these represent my contribution to the above research output.					
Jonathan Broughton					
I acknowledge that these represent my contribution to the above research output.					
Andrew King					×
I acknowledge that these represent my contribution to the above research output.					
Benjamin Mullins	×	×	×	×	×
I acknowledge that these represent my contribution to the above research output.					

Copyright Permission

The following pages contain the right granted by Elsevier to the author of the publications (Golkarfard et al. (2019) and Abishek et al. (2017)) to represent the contribution in this thesis as well as granted by SAE International to the first author of the publication (Golkarfard et al. (2018)).

Generation and validation of virtual nonwoven, foam and knitted filter (separator/coalescer) geometries for CFD simulations

Author: S. Abishek,A.J.C. King,R. Mead-Hunter,V. Golkarfard,W. Heikamp,B.J. Mullins

Publication: Separation and Purification Technology

Publisher: Elsevier

Date: 29 November 2017

Optimisation of wet pressure drop in nonwoven fibrous, knitted, and open-cell foam filters

Author: V. Golkarfard,A.J.C. King,S. Abishek,R. Mead-Hunter,G. Kasper,B.J. Mullins

Publication: Separation and Purification Technology

Publisher: Elsevier

Date: 15 April 2019

Copyright Clearance Center Marketplace™

SAE International - License Terms and Conditions

This is a License Agreement between Vahid Golkar Fard ("You") and SAE International ("Publisher") provided by Copyright Clearance Center ("CCC"). The license consists of your order details, the terms and conditions provided by SAE International, and the CCC terms and conditions.

All payments must be made in full to CCC.

Order Date	28-Apr-2020	Type of Use	Republish in a thesis/dissertation
Order license ID	1031395-1		
ISSN	1946-3936	Publisher	SAE International
		Portion	Abstract

LICENSED CONTENT

Publication Title	SAE International journal of engines	Country	United States of America
		Rightsholder	SAE International
Author/Editor	Society of Automotive Engineers.	Publication Type	Journal
Date	01/01/2009		
Language	English		

REQUEST DETAILS

Portion Type	Abstract	Distribution	Worldwide
Format (select all that apply)	Electronic	Translation	Original language of publication
Who will republish the content?	Author of requested content	Copies for the disabled?	No
		Minor editing privileges?	No
Duration of Use	Life of current edition	Incidental promotional use?	No
Lifetime Unit Quantity	Up to 499		
Rights Requested	Main product	Currency	AUD

NEW WORK DETAILS

Title	Comparative Performance of 12 Crankcase Oil Mist Separators	Institution name	Curtin University
		Expected presentation date	2020-05-30
Instructor name	Vahid Golkar Fard		

ADDITIONAL DETAILS

Order reference number	N/A	The requesting person / organization to appear on the license	Vahid Golkar Fard

REUSE CONTENT DETAILS

Title, description or numeric reference of the portion(s)	Comparative Performance of 12 Crankcase Oil Mist Separators	Title of the article/chapter the portion is from	N/A
Editor of portion(s)	N/A	Author of portion(s)	Society of Automotive Engineers.

References

Abishek, S. (2013). *Department of Mechanical Engineering Single Phase and Boiling Heat Transfer under Steady and Pulsating Confined Jet Impingement Abishek Sridhar*. Ph. D. thesis.

Abishek, S., A. King, J. Schuler, G. Kasper, H.-J. Schmid, and B. Mullins (2018, dec). Representative domain size for the simulation of coalescence filtration in nonwoven and foam media. *Separation and Purification Technology 207*, 344–352.

Abishek, S., A. J. C. King, R. Mead-Hunter, V. Golkarfard, W. Heikamp, and B. J. Mullins (2017). Generation and validation of virtual nonwoven, foam and knitted filter (separator/coalescer) geometries for CFD simulations. *Separation and Purification Technology 188*, 493–507.

Abishek, S., R. Mead-Hunter, A. J. King, and B. J. Mullins (2019, oct). Capture and re-entrainment of microdroplets on fibers. *Physical Review E 100*(4), 042803.

Agranovski, I. E. and R. D. Braddock (1998a, dec). Filtration of liquid aerosols on nonwettable fibrous filters. *AIChE Journal 44*(12), 2784–2790.

Agranovski, I. E. and R. D. Braddock (1998b). Filtration of liquid aerosols on wettable fibrous filters. *AIChE Journal 44*(12), 2775–2783.

Agranovski, I. E., T. Myojo, R. D. Braddock, and D. Jarvis (2001). Combined wettable/non-wettable filter for mist purification. *Chemical Engineering and Technology 24*(3), 287–292.

Agranovski, I. E., T. Myojo, R. D. Braddock, and D. Jarvis (2002, oct). Inclined wettable filter for mist purification. *Chemical Engineering Journal 89*(1-3), 229–238.

Agranovski, I. E. and M. Shapiro (2001). Clogging of wet filters by dust particles. *Journal of aerosol science 32*(8), 1009–1020.

Ahn, Y., S. Park, G. Kim, Y. Hwang, C. Lee, H. Shin, and J. Lee (2006). Development of high efficiency nanofilters made of nanofibers. *Current Applied Physics 6*(6), 1030–1035.

Aitken, R. J., J. H. Vincent, and D. Mark (1993, apr). Application of Porous Foams as Size Selectors for Biologically Relevant Samplers. *Applied Occupational and Environmental Hygiene 8*(4), 363–369.

Amin, Z., H. Z. Amin, L. Z. Amin, and F. A. Mutiksa (2017, apr). Air pollution and atherosclerosis. *Indian Journal of Public Health Research and Development 8*(2), 182–186.

Anand, S. C. and P. J. Lawton (1991, jan). The Development of Knitted Structures for Filtration. *Journal of the Textile Institute 82*(3), 297–308.

Andan, S., S. I. Hariharan, and G. G. Chase (2008, may). Continuum Model Evaluation of the Effect of Saturation on Coalescence Filtration. *Separation Science and Technology 43*(8), 1955–1973.

Andrade, J. S., U. M. Costa, M. P. Almeida, H. A. Makse, and H. E. Stanley (1999). Inertial effects on fluid flow through disordered porous media. *Physical Review Letters 82*(26), 5249–5252.

Ardekhani, A. and R. Raiszadeh (2012, jul). Removal of double oxide film defects by ceramic foam filters. *Journal of Materials Engineering and Performance 21*(7), 1352–1362.

Bagheri, G. H., M. Salmanzadeh, V. Golkarfard, and G. Ahmadi (2012). Simulation of solid particles behavior in a heated cavity at high Rayleigh numbers. *Aerosol Science and Technology 46*(12), 1382–1391.

Basha, N. (2016). Cfd Study of Filtration Process in Moulded Filters. *research.tees.ac.uk* (October).

Belforte, G., T. Raparelli, and A. Trivella (2011). EFFICIENCY MEASURES OF COALESCING FILTERS FOR PNEUMATIC EQUIPMENT. In *Proceedings of the 8th JFOS International*, pp. 4–9.

Bell, S. (2001). Good Practice Guide No. 11 The Beginner's Guide to Uncertainty of Measurement. Technical report.

Bensaid, S., D. L. Marchisio, and D. Fino (2010, jan). Numerical simulation of soot filtration and combustion within diesel particulate filters. *Chemical Engineering Science 65*(1), 357–363.

Billiet, M., S. De Schampheleire, H. Huisseune, M. De Paepe, M. Billiet, S. De Schampheleire, H. Huisseune, and M. De Paepe (2015, oct). Influence of Orientation and Radiative Heat Transfer on Aluminum Foams in Buoyancy-Induced Convection. *Materials 8*(10), 6792–6805.

Bonnet, J. P., F. Topin, and L. Tadrist (2008, jun). Flow laws in metal foams: Compressibility and pore size effects. *Transport in Porous Media 73*(2), 233–254.

Brackbill, J., D. Kothe, and C. Zemach (1992). A continuum method for modeling surface tension. *Journal of computational physics 100*(2), 335–354.

Bredin, A. (2012). *The Influence of Contaminant Particles and Filtration Regime on Fibrous Mist-Filter Performance*. Ph. D. thesis.

Bredin, A. and B. J. Mullins (2012). Influence of flow-interruption on filter performance during the filtration of liquid aerosols by fibrous filters. *Separation and purification technology 90*, 53–63.

Bredin, A., R. A. O'Leary, and B. J. Mullins (2012, aug). Filtration of soot-in-oil aerosols: Why do field and laboratory experiments differ? *Separation and Purification Technology 96*, 107–116.

Brinkman, H. C. (1949, dec). A calculation of the viscous force exerted by a flowing fluid on a dense swarm of particles. *Flow, Turbulence and Combustion 1*(1), 27.

Brown, P. and C. L. Cox (2017). *Fibrous Filter Media*. Woodhead Publishing.

Brown, R. C. (1993). *Air filtration: an integrated approach to the theory and applications of fibrous filters*. Pergamon.

Brunazzi, E. and A. Paglianti (1998, mar). Design of wire mesh mist eliminators. *AIChE Journal 44*(3), 505–512.

Brunazzi, E. and A. Paglianti (2000, jun). Design of complex wire-mesh mist eliminators. *AIChE Journal 46*(6), 1131–1137.

Carpenter, C. L. and D. F. Othmer (1955, dec). Entrainment removal by a wire-mesh separator. *AIChE Journal 1*(4), 549–557.

Ceken, F., O. Kayacan, A. Ozkurt, and S. S. Ugurlu (2012, sep). The electromagnetic shielding properties of some conductive knitted fabrics produced on single or double needle bed of a flat knitting machine. *Journal of the Textile Institute 103*(9), 968–979.

Chang, C., Z. Ji, and J. Liu (2018, apr). The effect of a drainage layer on saturation and liquid distribution of oleophobic coalescence filters. *Separation and Purification Technology 194*, 355–361.

Chapman, R. E. (1981). Geology and water: an introduction to fluid mechanics for geologists. *THE HAGUE, THE NETHERLANDS, MARTINUS NIJHOFF/DR. W. JUNK PUBLISHERS B.V., 1981 1) (ISBN.*

Charvet, A., Y. Gonthier, A. Bernis, and E. Gonze (2008). Filtration of liquid aerosols with a horizontal fibrous filter. *Chemical Engineering Research and Design 86*(6), 569–576.

Charvet, A., Y. Gonthier, E. Gonze, and A. Bernis (2010, mar). Experimental and modelled efficiencies during the filtration of a liquid aerosol with a fibrous medium. *Chemical Engineering Science 65*(5), 1875–1886.

Charvet, A., S. Rolland Du Roscoat, M. Peralba, J. Bloch, and Y. Gonthier (2011, feb). Contribution of synchrotron X-ray holotomography to the understanding of liquid distribution in a medium during liquid aerosol filtration. *Chemical Engineering Science 66*(4), 624–631.

Chaudhuri, J., A. Baukelmann, K. Boettcher, and P. Ehrhard (2019, jul). Pressure drop in fibrous filters. *European Journal of Mechanics, B/Fluids 76*, 115–121.

Chen, C. Y. (1955). Filtration of aerosols by fibrous media. *Chemical Reviews 55*(3), 595–623.

Chen, F., Z. Ji, and Q. Qi (2018, aug). Effect of pore size and layers on filtration performance of coalescing filters with different wettabilities. *Separation and Purification Technology 201*, 71–78.

Chen, F., Z. Ji, and Q. Qi (2019a). Effect of liquid surface tension on the filtration performance of coalescing filters. *Separation and Purification Technology 209*, 881–891.

Chen, F., Z. Ji, and Q. Qi (2019b, dec). Effect of surface wettability on filtration performance of gas-liquid coalescing filters. *Powder Technology 357*, 377–386.

Chen, X., P. Vroman, M. Lewandowski, A. Perwuelz, and Y. Zhang (2009). Study of the Influence of Fiber Diameter and Fiber Blending on Liquid Absorption Inside Nonwoven Structures. *Textile Research Journal 79*(15), 1364–1370.

Cheng, Y.-H. and C.-J. Tsai (1998). Factors Influencing Pressure Drop through a Dust Cake during Filtration. *Aerosol Science and Technology 29*(4), 315–328.

Choi, K. and T. Lo (2003, aug). An Energy Model of Plain Knitted Fabric. *Textile Research Journal 73*(8), 739–748.

Clark, N., E. Tatli, R. Barnett, W. S. Wayne, and D. L. McKain (2006). Characterization and abatement of diesel crankcase emissions. Technical report, SAE Technical Paper.

Clarke, A. and R. Issa (1997, may). A numerical model of slug flow in vertical tubes. *Computers & Fluids 26*(4), 395–415.

Contal, P., J. Simao, D. Thomas, T. Frising, S. Callé, J. C. Appert, and D. Bémer (2004, mar). Clogging of fibre filters by submicron droplets. Phenomena and influence of operating conditions. *Journal of Aerosol Science 35*(2), 263–278.

Courant, R., K. Friedrichs, and H. Lewy (1928). Über die partiellen Differenzengleichungen der mathematischen Physik. *Mathematische annalen 100*(1), 32–74.

Daly, B. J. (1967). Numerical Study of Two Fluid Rayleigh-Taylor Instability. *Physics of Fluids 10*(2), 297.

Darcy, H. (1856). Les fontaines publiques de la ville de Dijon : exposition et application des principes à suivre et des formules à employer dans les questions de distribution d'eau. *Recherche*, 647.

Davies, C. N. (1953). The separation of airborne dust and particles. *Proceedings of the Institution of Mechanical Engineers, Part B: Management and engineering manufacture 1*(1-12), 185–213.

De Schampheleire, S., P. De Jaeger, K. De Kerpel, B. Ameel, H. Huisseune, M. De Paepe, S. De Schampheleire, P. De Jaeger, K. De Kerpel, B. Ameel, H. Huisseune, and M. De Paepe (2016, feb). How to Study Thermal Applications of Open-Cell Metal Foam: Experiments and Computational Fluid Dynamics. *Materials 9*(2), 94.

Decoufle, P. (1978). Further analysis of cancer mortality patterns among workers exposed to cutting oil mists. *Journal of the National Cancer Institute 61*(4), 1025–1030.

Degennes, P. G. (1987). WETTING-STATICS AND DYNAMICS. *Uspekhi Fizicheskikh Nauk 151*(4), 619–681.

Dehkordi, S. S. H., M. Ghane, S. B. Abdellahi, and M. B. Soultanzadeh (2017, sep). Numerical modeling of the air permeability of knitted fabric using computational fluid dynamics (CFD) method. *Fibers and Polymers 18*(9), 1804–1809.

Della Torre, A., G. Montenegro, G. R. Tabor, and M. L. Wears (2014, dec). CFD characterization of flow regimes inside open cell foam substrates. *International Journal of Heat and Fluid Flow 50*, 72–82.

Dervieux, A. and F. Thomasset (1980). A finite element method for the simulation of a Rayleigh-Taylor instability. In *Approximation methods for Navier-Stokes problems*, pp. 145–158. Springer, Berlin, Heidelberg.

Deshpande, S. and L. Anumolu (2012). Evaluating the performance of the two-phase flow solver interFoam. *Computational science & 5*(1), 14–16.

Deuschle, T., U. Janoske, and M. Piesche (2008, jan). A CFD-model describing filtration, regeneration and deposit rearrangement effects in gas filter systems. *Chemical Engineering Journal 135*(1-2), 49–55.

Diani, A., K. K. Bodla, L. Rossetto, and S. V. Garimella (2014, jan). Numerical Analysis of Air Flow through Metal Foams. *Energy Procedia 45*, 645–652.

Diani, A., K. K. Bodla, L. Rossetto, and S. V. Garimella (2015, sep). Numerical investigation of pressure drop and heat transfer through reconstructed metal foams and comparison against experiments. *International Journal of Heat and Mass Transfer 88*, 508–515.

Dickenson, C. (1995, jan). Filters and Filtration-Handbook 3rd Edition (1994). *Drying Technology 13*(4), 1047–1048.

Diedericks, G. P. J., J. P. DU PLESSIS, A. MONTILLET, J. COMJTI, and J. EGRAND (1998, jan). FLOW THROUGH A HIGHLY POROUS ANISOTROPIC MULTIFILAMENT KNIT. *Chemical Engineering Communications 167*(1), 21–49.

Dietrich, B., W. Schabel, M. Kind, and H. Martin (2009). Pressure drop measurements of ceramic sponges-Determining the hydraulic diameter. *Chemical Engineering Science 64*(16), 3633–3640.

Dukhan, N. (2006, oct). Correlations for the pressure drop for flow through metal foam. *Experiments in Fluids 41*(4), 665–672.

El-Dessouky, H. T., I. M. Alatiqi, H. M. Ettouney, and N. S. Al-Deffeeri (2000, mar). Performance of wire mesh mist eliminator. *Chemical Engineering and Processing: Process Intensification 39*(2), 129–139.

Ergun, S. and A. A. Orning (1949, jun). Fluid Flow through Randomly Packed Columns and Fluidized Beds. *Industrial & Engineering Chemistry 41*(6), 1179–1184.

Fairs, G. (1958). High Efficiency Fibre Filters for the Treatment of Fine Mists.

Forchheimer, P. (1901). Wasserbewegung durch boden. *Z. Ver. Dtsch. Ing., 45,*, 1736–1741, 1781–1788.

Fotovati, S., H. Tafreshi, B. Pourdeyhimi, H. Vahedi Tafreshi, and B. Pourdeyhimi (2010, sep). Influence of fiber orientation distribution on performance of aerosol filtration media. *Chemical Engineering Science 65*(18), 5285–5293.

Frising, T., D. Thomas, J. Appert-Collin, S. Calle-Chazelet, and P. Contal (2005). Influence of liquid aerosol stop-and-go on the performance of fibrous filters. *Filtration Solutions 5*(4), 286–294.

Frising, T., D. Thomas, D. Bemer, and P. Contal (2005). Clogging of fibrous filters by liquid aerosol particles: Experimental and phenomenological modelling study. *Chemical Engineering Science 60*(10), 2751–2762.

Gac, J. M. (2015, mar). A simple numerical model of pressure drop dynamics during the filtration of liquid aerosols on fibrous filters. *Separation Science and Technology 50*(13), 2015—-2022.

Gac, J. M. and L. Gradon (2012, nov). Modeling of axial motion of small droplets deposited on smooth and rough fiber surfaces. *Colloids and Surfaces A: Physicochemical and Engineering Aspects 414*, 259–266.

Gallou, G., J. B. Sirven, C. Dutouquet, O. L. Bihan, and E. Frejafon (2011, aug). Aerosols Analysis by LIBS for Monitoring of Air Pollution by Industrial Sources. *Aerosol Science and Technology 45*(8), 918–926.

Gervais, P.-C., N. Bardin-Monnier, and D. Thomas (2012, may). Permeability modeling of fibrous media with bimodal fiber size distribution. *Chemical Engineering Science 73*, 239–248.

Gibson and Ashby (1989). Cellular solids: Structure & properties, Oxford: Pergamon Press, ISBN: 0-08-036607-4, 1988, 357 + ix pages, $35.00. *Advances in Polymer Technology 9*(2), 165–166.

Goldstein, D. H., J. N. Benoit, H. A. Tyroler, and C. Hill (1970). An epidemiologic study of an oil mist exposure. *Archives of Environmental Health 21*(5), 600–603.

Golkarfard, V., A. J. King, S. Abishek, R. Mead-Hunter, G. Kasper, and B. J. Mullins (2019, apr). Optimisation of wet pressure drop in nonwoven fibrous, knitted, and open-cell foam filters. *Separation and Purification Technology 213*, 45–55.

Golkarfard, V., R. Subramaniam, J. Broughton, A. King, and B. Mullins (2018, oct). Comparative Performance of 12 Crankcase Oil Mist Separators. *SAE International Journal of Engines 12*(1), 03–12–01–0001.

Gougeon, R., D. Boulaud, and A. Renoux (1994, may). 15.P.01 Theoretical and experimental study of fibrous filters loading with liquid aerosols in the inertial regime. *Journal of Aerosol Science 25*(SUPPL. 1), 189–190.

Greenshields, C. (2011). The OpenFOAM Foundation User Guide.

Gregor, E. C. (2009). Primer on Nonwoven Fabric Filtration. *Textile World 159*(2).

Guo, W., Q. Zhang, H. Xiao, J. Xu, Q. Li, X. Pan, and Z. Huang (2014). Cu mesh's super-hydrophobic and oleophobic properties with variations in gravitational pressure and surface components for oil/water separation applications. *Applied Surface Science 314*, 408–414.

Gurreri, L., A. Tamburini, A. Cipollina, G. Micale, and M. Ciofalo (2016). Pressure drop in woven-spacer-filled channels for reverse electrodialysis: CFD prediction and experimental validation. *Desalination and Water Treatment*.

Hajra, M. G., K. Mehta, and G. G. Chase (2003). Effects of humidity, temperature, and nanofibers on drop coalescence in glass fiber media. *Separation and Purification Technology 30*(1), 79–88.

Hasan, R. and Raisul (2016). Approach of Computational Fluid Dynamics of VOF Model in Two Phase flow through Porous Medium under Microgravity Condition. *41st COSPAR Scientific Assembly, abstracts from the meeting that was to be held 30 July - 7 August at the Istanbul Congress Center (ICC), Turkey, but was cancelled. See http://cospar2016.tubitak.gov.tr/en/, Abstract id.# G0.1-10-16. 41.*

Heim, M., B. J. Mullins, H. Umhauer, and G. Kasper (2008). Performance evaluation of three optical particle counters with an efficient "multimodal" calibration method. *Journal of Aerosol Science 39*(12), 1019–1031.

Helsor, T., H. Svendsen, and L. H. Gjertsen (2005). Experimental characterisation of wire mesh demisters. In *AIChE Annual Meeting, Conference Proceedings*, pp. 2581–2586.

Hendy, M. S., B. E. Beattie, and P. S. Burge (2016). Occupational asthma due to an emulsified oil mist. *British Journal of Industrial Medicine 42*(1), 51–54.

Heywood, J. (1988). *Internal combustion engine fundamentals*. McGraw-Hill Education.

Hinds, W. C. (1999a). Aerosol Technology, J.

Hinds, W. C. (1999b). Properties, Behavior, and Measurement ofAirborne Particles. *Journal of Aerosol Science 14*(2), 175.

Hlushkou, D. and U. Tallarek (2006). Transition from creeping via viscous-inertial to turbulent flow in fixed beds.

Hoover, B. (2019, jul). Analyzing the Effect of Air Pollution Regulations on Aerosol Concentrations in Urban Areas. In *Purdue Undergraduate Research Conference*.

Hosseini, S. and H. V. Tafreshi (2010a, aug). Modeling particle filtration in disordered 2-D domains: A comparison with cell models. *Separation and Purification Technology 74*(2), 160–169.

Hosseini, S. and H. V. Tafreshi (2010b, mar). Modeling permeability of 3-D nanofiber media in slip flow regime. *Chemical Engineering Science 65*(6), 2249–2254.

Hosseini, S. and H. V. Tafreshi (2012, aug). Modeling particle-loaded single fiber efficiency and fiber drag using ANSYS–Fluent CFD code. *Computers & Fluids 66*, 157–166.

Hotz, C. J., R. Mead-Hunter, T. Becker, A. J. C. King, S. Wurster, G. Kasper, and B. J. Mullins (2015, may). Detachment of droplets from cylinders in flow using an experimental analogue. *Journal of Fluid Mechanics 771*, 327–340.

Huang, H., K. Wang, and H. Zhao (2016, may). Numerical study of pressure drop and diffusional collection efficiency of several typical noncircular fibers in filtration. *Powder Technology 292*, 232–241.

Hutten, I. M. (2007). *Handbook of nonwoven filter media*. Butterworth-Heinemann.

Inayat, A., J. Schwerdtfeger, H. Freund, C. Körner, R. F. Singer, and W. Schwieger (2011). Periodic open-cell foams: Pressure drop measurements and modeling of an ideal tetrakaidecahedra packing. *Chemical Engineering Science 66*(12), 2758–2763.

Ince, M. E. and H. Yildirim (2019, jul). Air permeability and bursting strength of weft-knitted fabrics from glass yarn. Part II: knit architecture effect. *The Journal of The Textile Institute 110*(7), 1072–1084.

Incera Garrido, G., F. C. Patcas, S. Lang, and B. Kraushaar-Czarnetzki (2008). Mass transfer and pressure drop in ceramic foams: A description for different pore sizes and porosities. *Chemical Engineering Science 63*(21), 5202–5217.

Innocentini, M. D., V. R. Salvini, A. Macedo, and V. C. Pandolfelli (1999). Prediction of ceramic foams permeability using Ergun's equation. *Materials Research 2*(4), 283–289.

Jaganathan, S., H. Vahedi Tafreshi, and B. Pourdeyhimi (2008, jan). A realistic approach for modeling permeability of fibrous media: 3-D imaging coupled with CFD simulation. *Chemical Engineering Science 63*(1), 244–252.

Jankowski, T. (2009). Influence of structural characteristics on liquid aerosol filtration in multilayer nonwoven fabrics of the spunlace type. *Fibres & Testiles in Eastern Europe 17*, 87–92.

Jeddi, A. A. and H. Dabiryan (2008). Ideal stitch model for interlock-knitted fabric. *Journal of the Textile Institute 99*(4), 369–374.

Ka Fai Choi, K. F. and T. Y. Tin Yee Lo (2006, oct). The Shape and Dimensions of Plain Knitted Fabric: A Fabric Mechanical Model. *Textile Research Journal 76*(10), 777–786.

Kampa, D., J. Meyer, B. J. Mullins, and G. Kasper (2009). A model for steady-state oil transport and saturation in a mist filter. In *Proceedings of the 18thWorld IMACS and MODSIM09 International Congress on Modellingand Simulation: Interfacing Modelling and Simulation with Mathemat-ical and Computational Sciences*.

Kampa, D., S. Wurster, J. Buzengeiger, J. Meyer, and G. Kasper (2014). Pressure drop and liquid transport through coalescence filter media used for oil mist filtration. *International Journal of Multiphase Flow 58*, 313–324.

Kang, Y., J. Wang, G. Yang, X. Xiong, X. Chen, L. Yu, and P. Zhang (2011). Preparation of porous super-hydrophobic and super-oleophilic polyvinyl chloride surface with corrosion resistance property. *Applied Surface Science 258*(3), 1008–1013.

Kennard, E. H. (1938). *Kinetic theory of gases, : With an introduction to statistical mechanics*, Volume 57.

Khalili, M., H. Yahyazadeh, M. Gorji-Bandpy, and D. Ganji (2016, jun). Application of volume of fluid method for simulation of a droplet impacting a fiber. *Propulsion and Power Research 5*(2), 123–133.

Klouda, G. A., R. A. Fletcher, J. G. Gillen, and J. R. Verkouteren (2011, feb). Aerosol Collection Efficiency of a Graded Metal-Fiber Filter at High Airflow Velocity (10 m s –1). *Aerosol Science and Technology 45*(3), 336–342.

Kolb, H. E., J. Meyer, and G. Kasper (2017). Flow velocity dependence of the pressure drop of oil mist filters. *Chemical Engineering Science 166*, 107–114.

Kumar, P. and F. Topin (2014, sep). Micro-structural Impact of Different Strut Shapes and Porosity on Hydraulic Properties of Kelvin-Like Metal Foams Foam-Morphology & Transport properties View project Analytical AC losses model developement View project Micro-structural Impact of Different. *Transp Porous Med 105*(1), 57–81.

Kuwabara, S. (1959). The forces experienced by randomly distributed parallel circular cylinders or spheres in a viscous flow at small Reynolds numbers. *Journal of the physical society of Japan 14*(4), 527–532.

Lacent (1990). Health risks of oil mist. *The Lancet 336*(8725), 1246.

Lacroix, M., P. Nguyen, D. Schweich, C. Pham Huu, S. Savin-Poncet, and D. Edouard (2007). Pressure drop measurements and modeling on SiC foams. *Chemical Engineering Science 62*(12), 3259–3267.

Lamb, G. E. and P. A. Costanza (1979). Influences of Fiber Geometry on the Performance of Nonwoven Air Filters: Part II : Fiber Diameter and Crimp Frequency. *Textile Research Journal 49*(2), 79–87.

Lammermann, M., W. Schwieger, and H. Freund (2016, sep). Experimental investigation of gas-liquid distribution in periodic open cellular structures as potential catalyst supports. *Catalysis Today 273*, 161–171.

Lee, K. W. and B. Y. Liu (1982, jan). Theoretical study of aerosol filtration by fibrous filters. *Aerosol Science and Technology 1*(2), 147–161.

Lehmann, M. J., J. Weber, A. Kilian, and M. Heim (2016, mar). Microstructure Simulation as Part of Fibrous Filter Media Development Processes - From Real to Virtual Media. *Chemical Engineering & Technology 39*(3), 403–408.

Letts, G. M., P. C. Raynor, and R. L. Schumann (2003, nov). Selecting fiber materials to improve mist filters. *Journal of Aerosol Science 34*(11), 1481–1492.

Leung, W. W. F., C. H. Hung, and P. T. Yuen (2010). Effect of face velocity, nanofiber packing density and thickness on filtration performance of filters with nanofibers coated on a substrate. *Separation and Purification Technology 71*(1), 30–37.

Liew, T. and J. Conder (1985, jan). Fine mist filtration by wet filters—I. Liquid saturation and flow resistance of fibrous filters. *Journal of Aerosol Science 16*(6), 497–509.

Liu, B. Y. H. and K. L. Rubow (1990). Efficiency, pressure drop and figure of merit of high efficiency fibrous and membrane filter media. In *Vth World Filtration Congress*, pp. 112–119.

Liu, J., H. Zhou, X. Wu, H. Wang, Z. Ji, Y. Xing, J. Lu, X. Wei, and T. Lin (2020, jan). Superoleophobic Filters: Improvement of Filtration Performance by Front Attachment of Oil-Guiding Fabric. *Advanced Materials Interfaces 7*(2).

Liu, J. F., W. T. Wu, W. C. Chiu, and W. H. Hsieh (2006). Measurement and correlation of friction characteristic of flow through foam matrixes. *Experimental Thermal and Fluid Science 30*(4), 329–336.

Liu, K., Y. Zhao, L. Jia, R. Hao, and D. Fu (2019, jul). A novel CFD-based method for predicting pressure drop and dust cake distribution of ceramic filter during filtration process at macro-scale. *Powder Technology 353*, 27–40.

Liu, M., D. E. Claridge, and S. Deng (2003, may). An air filter pressure loss model for fan energy calculation in air handling units. *International Journal of Energy Research 27*(6), 589–600.

Liu, Z., Z. Ji, J. Zhang, and L. Li (2015, jan). Influence of processing parameters on gas-liquid filtration performance of fibrous filter cartridge. In *Procedia Engineering*, Volume 102, pp. 911–920. Elsevier Ltd.

Lorimier, C., L. Le Coq, A. Subrenat, and P. Le Cloirec (2008, feb). Indoor air particulate filtration onto activated carbon fiber media. *Journal of Environmental Engineering 134*(2), 126–137.

Luan, Y. and H. Sun (2010). Simplification model for prediction of pressure drop in wire mesh mist eliminator by CFD. In *Applied Mechanics and Materials*, Volume 26-28, pp. 297–302.

Madani, B., F. Topin, F. Rigollet, and L. Tadrist (2007). Flow laws in metallic foams: Experimental determination of inertial and viscous contributions. *Journal of Porous Media 10*(1), 51–70.

Maddineni, A. K., D. Das, and R. M. Damodaran (2018, mar). Air-borne particle capture by fibrous filter media under collision effect: A CFD-based approach. *Separation and Purification Technology 193*, 1–10.

Manzo, G. M., Y. Wu, G. G. Chase, and A. Goux (2016, apr). Comparison of nonwoven glass and stainless steel microfiber media in aerosol coalescence filtration. *Separation and Purification Technology 162*, 14–19.

Matteson and A. S. Ward (2018, sep). Liquid Filtration Theory. In *Filtration*, pp. 133–161. Routledge.

McFee, D. R. and J. Sedlet (1968, nov). Plutonium-uranium-molybdenum fume characteristics and sand filtration. *Journal of Nuclear Energy 22*(11), 641–650.

McHale, G., M. I. Newton, and B. J. Carroll (2001). The shape and stability of small liquid drops on fibers. *Oil & Gas science and technology 56*(1), 47–54.

McMurry, P. H. (2000, jan). A review of atmospheric aerosol measurements. *Atmospheric Environment 34*(12-14), 1959–1999.

Mead-Hunter, R. (2013, aug). *Modelling micro-scale coalescence and transport-processes in liquid aerosol filtration*. Ph. D. thesis, Department of Chemical Engineering.

Mead-Hunter, R., T. Bergen, T. Becker, R. A. O'Leary, G. Kasper, and B. J. Mullins (2012, feb). Sliding/rolling phobic droplets along a fiber: Measurement of interfacial forces. *Langmuir 28*(7), 3483–3488.

Mead-Hunter, R., R. Braddock, D. Kampa, N. Merkel, G. Kasper, and B. J. Mullins (2013). The relationship between pressure drop and liquid saturation in oil-mist filters–Predicting filter saturation using a capillary based model. *Separation and Purification Technology 104*, 121–129.

Mead-Hunter, R., A. Bredin, A. J. King, A. V. Larcher, T. Becker, and B. J. Mullins (2012). The influence of soot nanoparticles on the micro/macro-scale behaviour of coalescing filters. *Chemical Engineering Science 84*, 113–119.

Mead-Hunter, R., A. J. King, G. Kasper, and B. J. Mullins (2013, jul). Computational fluid dynamics (CFD) simulation of liquid aerosol coalescing filters. *Journal of Aerosol Science 61*, 36–49.

Mead-Hunter, R., A. J. King, and B. J. Mullins (2017). Fibrous filtration of liquid aerosols. In *Fibrous Filter Media*, pp. 51–93.

Mead-Hunter, R., A. J. C. King, and B. J. Mullins (2012). Plateau Rayleigh Instability Simulation. *Langmuir 28*(17), 6731–6735.

Mead-Hunter, R., A. J. C. King, and B. J. Mullins (2014). Aerosol-mist coalescing filters–a review. *Separation and Purification Technology 133*, 484–506.

Mezarcioz, S., S. Mezarcioz, and R. T. Ogulata (2014). Prediction of air permeability of knitted fabrics by means of Computational Fluid Dynamics. *Tekstil ve Konfeksiyon 24*(2), 202–211.

Minor, F., A. Schwartz, E. Wulkow, L. B. I. T. R. J., and U. 1959 (1959). Part III: The Behavior of Liquids on Single Textile Fibers. *Textile Research Journal 29*(12), 940–949.

Moghadam, A., S. H. Yousefi, H. V. Tafreshi, and B. Pourdeyhimi (2019, mar). Characterizing nonwoven materials via realistic microstructural modeling. *Separation and Purification Technology 211*, 602–609.

Monfared, M. A., N. Kasiri, and T. Mohammadi (2016, jul). Microscopic modeling of critical pressure of permeation in oily waste water treatment via membrane filtration. *RSC Advances 6*(75), 71744–71756.

Mullins, B. J., I. E. Agranovski, R. D. Braddock, and C. M. Ho (2004, jan). Effect of fiber orientation on fiber wetting processes. *Journal of Colloid and Interface Science 269*(2), 449–458.

Mullins, B. J., R. D. Braddock, and I. E. Agranovski (2004, nov). Particle capture processes and evaporation on a microscopic scale in wet filters. *Journal of Colloid and Interface Science 279*(1), 213–227.

Mullins, B. J., R. D. Braddock, I. E. Agranovski, R. A. Cropp, and R. A. O'Leary (2005). Observation and modelling of clamshell droplets on vertical fibres subjected to gravitational and drag forces. *Journal of Colloid and Interface Science 284*(1), 245–254.

Mullins, B. J., R. D. Braddock, and G. Kasper (2007). Capillarity in fibrous filter media: Relationship to filter properties. *Chemical Engineering Science 62*(22), 6191–6198.

Mullins, B. J. and G. Kasper (2006). Comment on: "Clogging of fibrous filters by liquid aerosol particles: Experimental and phenomenological modelling study" by Frising et al. *Chemical Engineering Science 61*(18), 6223–6227.

Mullins, B. J., A. J. King, and R. D. Braddock (2011). Modelling the influence of filter structure on efficiency and pressure drop in knitted filters. In *MODSIM 2011 - 19th International Congress on Modelling and Simulation - Sustaining Our Future: Understanding and Living with Uncertainty*, pp. 579–585.

Mullins, B. J., A. J. King, R. Mead-Hunter, and W. Heikamp (2017, jan). Knitted fibrous filter media. In *Fibrous Filter Media*, pp. 125–132. Woodhead Publishing.

Mullins, B. J., R. Mead-Hunter, R. N. Pitta, G. Kasper, and W. Heikamp (2014, aug). Comparative performance of philic and phobic oil-mist filters. *AIChE Journal 60*(8), 2976–2984.

Mullins, B. J., A. Pfrang, R. D. Braddock, T. Schimmel, and G. Kasper (2007). Detachment of liquid droplets from fibres-Experimental and theoretical evaluation of detachment force due to interfacial tension effects. *Journal of Colloid and Interface Science 312*(2), 333–340.

Murshed, S. M., K. C. Leong, and C. Yang (2008, may). Investigations of thermal conductivity and viscosity of nanofluids. *International Journal of Thermal Sciences 47*(5), 560–568.

Naim, R. and A. F. Ismail (2013, aug). Effect of fiber packing density on physical CO2 absorption performance in gas-liquid membrane contactor. *Separation and Purification Technology 115*, 152–157.

Nakamura, K., T. Suda, and K. Matsumoto (2018, may). Characterization of pore size distribution of non-woven fibrous filter by inscribed sphere within 3D filter model. *Separation and Purification Technology 197*, 289–294.

Nassif, N. (2012, dec). The impact of air filter pressure drop on the performance of typical air-conditioning systems. *Building Simulation 5*(4), 345–350.

Nazarboland, M. A., X. Chen, J. W. Hearle, R. Lydon, and M. Moss (2008). Modelling and simulation of filtration through woven media. *International Journal of Clothing Science and Technology 20*(3), 150–160.

Nichols, B. and C. Hirt (1973, feb). Calculating three-dimensional free surface flows in the vicinity of submerged and exposed structures. *Journal of Computational Physics 12*(2), 234–246.

Nie, Z., Y. Lin, and Q. Tong (2018, dec). Numerical simulations of two-phase flow in open-cell metal foams with application to aero-engine separators. *International Journal of Heat and Mass Transfer 127*, 917–932.

Nishio, G., S. Kitani, and K. Takahashi (1974). Thermophoretic Deposition of Aerosol Particles in a Heat-Exchanger Pipe. *Industrial & Engineering Chemistry Process Design and Development 13*(4), 408–415.

Noman, R. and Z. Kalam (1990). Transition from laminar to non-Darcy flow of gases in porous media. *Advances in Core Evaluation: Accuracy and Precision in Reserves Estimation*, 447–462.

Novick, V., P. Monson, and P. Ellison (1992, sep). The effect of solid particle mass loading on the pressure drop of HEPA filters. *Journal of Aerosol Science 23*(6), 657–665.

Oggiano, L., F. Pierella, T. A. Nygaard, J. De Vaal, and E. Arens (2017, oct). Reproduction of steep long crested irregular waves with CFD using the VOF method. *Energy Procedia 137*, 273–281.

Okolo, P. N., K. Zhao, J. Kennedy, and G. J. Bennett (2019, jul). Numerical assessment of flow control capabilities of three dimensional woven wire mesh screens. *European Journal of Mechanics, B/Fluids 76*, 259–271.

Orlov, A. S., A. V. Minakov, and A. V. Proshkin (2015, aug). Mathematical Modeling of Electrolyte Filtration through the Porous Cathode Blocks during Aluminum Electrolysis with Regard Interblock Seams. *MATEC Web of Conferences 23*, 01032.

Osher, S. and J. A. Sethian (1988, nov). Fronts propagating with curvature-dependent speed: Algorithms based on Hamilton-Jacobi formulations. *Journal of Computational Physics 79*(1), 12–49.

Paik, J. and C. Shin (2015). Multiphase flow modeling of landslide induced impulse wave by VOF method. *American Geophysical Union, Fall Meeting 2015, 2015*, NG23A–1764.

Palakurthi, N. K., S. Konangi, U. Ghia, and K. Comer (2015, dec). Micro-scale simulation of unidirectional capillary transport of wetting liquid through 3D fibrous porous media: Estimation of effective pore radii. *International Journal of Multiphase Flow 77*, 48–57.

Palakurthi, N. K., S. Konangi, A. Kishore, K. Comer, and U. Ghia (2018, jan). Prediction of capillary pressure-saturation relationship for primary drainage in a 3D fibrous porous medium using volume-of-fluid method. *European Journal of Mechanics, B/Fluids 67*, 357–365.

Patankar, S. and D. Spalding (1972, oct). A calculation procedure for heat, mass and momentum transfer in three-dimensional parabolic flows. *International Journal of Heat and Mass Transfer 15*(10), 1787–1806.

Patel, S. U., P. S. Kulkarni, S. U. Patel, and G. G. Chase (2013, jan). Coalescence Filter Media with Drainage Channels. *Drying Technology 31*(2), 185–192.

Payen, J., P. Vroman, M. Lewandowski, A. Perwuelz, S. Callé-Chazelet, and D. Thomas (2012, nov). Influence of fiber diameter, fiber combinations and solid volume fraction on air filtration properties in nonwovens. *Textile Research Journal 82*(19), 1948–1959.

Payet, S., D. Boulaud, G. Madelaine, and A. Renoux (1992, oct). Penetration and pressure drop of a HEPA filter during loading with submicron liquid particles. *Journal of Aerosol Science 23*(7), 723–735.

Penner, T., J. Meyer, G. Kasper, and A. Dittler (2019, mar). Impact of operating conditions on the evolution of droplet penetration in oil mist filters. *Separation and Purification Technology 211*, 697–703.

Perry, R. M. H. (1986). *Handbook of Air Pollution Analysis*. Springer Netherlands.

Pich, J. (1971). Pressure characteristics of fibrous aerosol filters. *Journal of Colloid And Interface Science 37*(4), 912–917.

Pich, J. (2017, nov). Gas Filtration Theory. In *Filtration*, pp. 1–132. Routledge.

Podgorski, A., A. Bałazy, and L. Gradon (2006). Application of nanofibers to improve the filtration efficiency of the most penetrating aerosol particles in fibrous filters. *Chemical Engineering Science 61*(20), 6804–6815.

Pohanish, R. P. (2011). *Sittig's Handbook of Toxic and Hazardous Chemicals and Carcinogens.* Elsevier Science.

Poon, W. W. S. and B. Y. H. Liu (1999). Interception and impaction collection efficiency for fibrous media in moderate Reynolds number regime. In *Fall Topical Conference of the American Filtration and Separations Society. Minneapolis*, Minneapolis, pp. 135–141.

Purchas, D.B., S. (2002). *Handbook of Filter Media* (2nd ed ed.). Elsevier Advanced Technology, Oxford.

Puszkarz, A. K. and I. Krucińska (2018). Modeling of Air Permeability of Knitted Fabric Using the Computational Fluid Dynamics. *Autex Research Journal 18*(4), 364–376.

Qian, F., J. Zhang, and Z. Huang (2009). Effects of the operating conditions and geometry parameter on the filtration performance of the fibrous filter. *Chemical Engineering and Technology 32*(5), 789–797.

Rahimi, R. and D. Abbaspour (2008). Determination of pressure drop in wire mesh mist eliminator by CFD. *Chemical Engineering and Processing: Process Intensification 47*(9-10), 1504–1508.

Rakhimov, F., Z. Yunusova, and P. S. I. J. of Advanced (2018). Industrial Knitted Sleeve Filters. *International Journal of AdvancedResearch in Science, Engineering and Technology 5*(10).

Ray, S., B. Milligan, and N. Keegan (2005). Measurement of filtration performance, filtration theory and practical applications of ceramic foam filters. *Aluminium Cast House Technology*, 1–12.

Raynor, P. C. P. and D. Leith (2000, jan). The influence of accumulated liquid on fibrous filter performance. *Journal of Aerosol Science 31*(1), 19–34.

Reed, C. M. and N. Wilson (1993, sep). The fundamentals of absorbency of fibres, textile structures and polymers. I. The rate of rise of a liquid in glass capillaries. *Journal of Physics D: Applied Physics 26*(9), 1378–1381.

Rice, W. K. M., P. J. Armitage, K. Wood, and G. Lodato (2006). Dust filtration at gap edges: implications for the spectral energy distributions of discs with embedded planets. *Monthly Notices of the Royal Astronomical Society 373*(4), 1619.

Richardson, J. T., Y. Peng, and D. Remue (2000). Properties of ceramic foam catalyst supports: Pressure drop. *Applied Catalysis A: General 204*(1), 19–32.

Rief, S., E. Glatt, E. Laourine, D. Aibibu, C. Cherif, and A. Wiegmann (2011). Modeling and CFD-simulation of woven textiles to determine permeability and retention properties. *Autex Research Journal 11*(3), 78–83.

Roe, R.-J. (1975, jan). Wetting of fine wires and fibers by a liquid film. *Journal of Colloid and Interface Science 50*(1), 70–79.

Rozy, M. I. F., M. Ueda, T. Fukasawa, T. Ishigami, and K. Fukui (2020, feb). Direct numerical simulation and experimental validation of flow resistivity of nonwoven fabric filter. *AIChE Journal 66*(2).

Rudolph, C., U. Schillinger, A. Ortiz, K. Tabatt, C. Plank, R. H. Müller, and J. Rosenecker (2004). Application of Novel Solid Lipid Nanoparticle (SLN)-Gene Vector Formulations Based on a Dimeric HIV-1 TAT-Peptide in Vitro and in Vivo. *Pharmaceutical Research 21*(9), 1662–1669.

Rueden, C. T., J. Schindelin, M. C. Hiner, B. E. DeZonia, A. E. Walter, E. T. Arena, and K. W. Eliceiri (2017, dec). ImageJ2: ImageJ for the next generation of scientific image data. *BMC Bioinformatics 18*(1), 529.

Run, Z., Z. Yi, S. Tiexiong, and X. Songling (2015). Design of Engine Crankcase Oil Separator. *Design and Manufacture of Diesel Engine 3*, 4.

Saleem, M. and G. Krammer (2007, jun). Effect of filtration velocity and dust concentration on cake formation and filter operation in a pilot scale jet pulsed bag filter. *Journal of Hazardous Materials 144*(3), 677–681.

Saleh, A., S. Hosseini, H. Vahedi Tafreshi, and B. Pourdeyhimi (2013, aug). 3-D microscale simulation of dust-loading in thin flat-sheet filters: A comparison with 1-D macroscale simulations. *Chemical Engineering Science 99*, 284–291.

Sanchez, J. R., J. M. Rodriguez, A. Alvaro, and A. M. Estevez (1997, jul). Comparative study of different fabrics in the filtration of an aerosol using more complete filtration indexes.

Sauter, H., K. Brodesser, and D. Brüggemann (2003). Highly effective oil mist separator for crankcase ventilation. *MTZ worldwide 64*(3), 6–8.

Scheidegger, A. E. (1974). The physics of flow through porous media. *journals.lww.com* ((THIRD EDITION: 1974)).

Schmierer, E. N. and A. Razani (2006). Self-consistent open-celled metal foam model for thermal applications. *Journal of Heat Transfer 128*(11), 1194–1203.

Schweers, E. and F. Löffler (1994, sep). Realistic modelling of the behaviour of fibrous filters through consideration of filter structure. *Powder Technology 80*(3), 191–206.

Semal, S., T. D. Blake, V. Geskin, M. J. De Ruijter, G. Castelein, and J. De Coninck (1999). Influence of surface roughness on wetting dynamics. *Langmuir 15*(25), 8765–8770.

Seveno, D., A. Vaillant, R. Rioboo, H. Adao, J. Conti, and J. De Coninck (2009). Dynamics of wetting revisited. *Langmuir 25*(22), 13034–13044.

Sheng, Y., L. Zhang, Y. Wang, and Z. Miao (2020). Exploration of a novel three-dimensional knitted spacer air filter with low pressure drop on cooking fume particles removal. *Building and Environment 177*.

Siegel, J. A. and W. W. Nazaroff (2003). Predicting particle deposition on HVAC heat exchangers. *Atmospheric Environment 37*(39), 5587–5596.

Skibinski, J., K. Cwieka, T. Kowalkowski, B. Wysocki, T. Wejrzanowski, and K. J. Kurzydlowski (2015, dec). The influence of pore size variation on the pressure drop in open-cell foams. *Materials & Design 87*, 650–655.

Soleimani-Gorgani, A. and Z. Karami (2016, apr). The effect of biodegradable organic acids on the improvement of cotton ink-jet printing and antibacterial activity. *Fibers and Polymers 17*(4), 512–520.

Soltani, P., M. S. Johari, and M. Zarrebini (2014). Effect of 3D fiber orientation on permeability of realistic fibrous porous networks. *Powder Technology 254*, 44–56.

Sozumert, E., Y. Kiyak, E. Demirci, and V. V. Silberschmidt (2020). Effect of microstructure on porosity of random fibrous networks. *The Journal of The Textile Institute*, 1–11.

Spielman, L. and S. L. Goren (1968, apr). Model for predicting pressure drop and filtration efficiency in fibrous media. *Environmental Science & Technology 2*(4), 279–287.

Spielman, L. A. (1977, jan). Particle Capture from Low-Speed Laminar Flows. *Annual Review of Fluid Mechanics 9*(1), 297–319.

Spurny, K. (1998). *Advances in aerosol filtration.* Lewis Publishers.

Stechkina, I. B., A. A. Kirsch, and N. A. Fuchs (1969). Studies on fibrous aerosol filters-iv calculation of aerosol deposition in model filters in the range of maximum penetration. *Annals of Occupational Hygiene 12*(1), 1–8.

Sutherland, K. (2008). Section 4 - Liquid Filtration. In K. Sutherland (Ed.), *Filters and Filtration Handbook (Fifth Edition)* (Fifth Edit ed.)., pp. 209–293. Oxford: Elsevier.

Tabor, G., O. Yeo, P. Young, and P. Laty (2008, may). CFD SIMULATION OF FLOW THROUGH AN OPEN CELL FOAM. *International Journal of Modern Physics C 19*(05), 703–715.

Tafreshi, H. V., M. S. A Rahman, S. Jaganathan, Q. Wang, B. Pourdeyhimi, H. Tafreshi, M. Rahman, and S. Jaganathan (2009, mar). Analytical expressions for predicting permeability of bimodal fibrous porous media. *Chemical Engineering Science 64*(6), 1154–1159.

Takizawa, A., S. Koshizuka, and S. Kondo (1992, nov). Generalization of physical component boundary fitted co-ordinate (PCBFC) method for the analysis of free-surface flow. *International Journal for Numerical Methods in Fluids 15*(10), 1213–1237.

Thomas, D., P. Penicot, P. Contal, D. Leclerc, and J. Vendel (2001). Clogging of fibrous filters by solid aerosol particles Experimental and modelling study. *Chemical Engineering Science 56*(11), 3549–3561.

Thornburg, J. and D. Leith (2000). Size Distribution of Mist Generated During Metal Machining. *Applied Occupational and Environmental Hygiene 15*(8), 618–628.

Topin, F., J. P. Bonnet, B. Madani, and L. Tadrist (2006, sep). Experimental analysis of multiphase flow in metallic foam: Flow laws, heat transfer and convective boiling. *Advanced Engineering Materials 8*(9), 890–899.

Tung, K. L., J. S. Shiau, C. J. Chuang, Y. L. Li, and W. M. Lu (2002, mar). CFD analysis on fluid flow through multifilament woven filter cloths. *Separation Science and Technology 37*(4), 799–821.

Ubbink, O. (1997). Numerical prediction of two fluid systems with sharp interfaces. *Splash* (January 1997), 69.

Ubbink, O. and R. Issa (1999, jul). A method for capturing sharp fluid interfaces on arbitrary meshes. *Journal of Computational Physics 153*(1), 26–50.

Vasudevan, G. and G. G. Chase (2004, jan). Performance of B-E-glass fiber media in coalescence filtration. *Journal of Aerosol Science 35*(1), 83–91.

Wang, Q., B. Maze, H. Vahedi Tafreshi, and B. Pourdeyhimi (2007, sep). On the pressure drop modeling of monofilament-woven fabrics. *Chemical Engineering Science 62*(17), 4817–4821.

Wei, X., H. Zhou, F. Chen, H. Wang, Z. Ji, and T. Lin (2019, jan). High-Efficiency Low-Resistance Oil-Mist Coalescence Filtration Using Fibrous Filters with Thickness-Direction Asymmetric Wettability. *Advanced Functional Materials 29*(1), 1806302.

Whitaker, S. (1996, oct). The Forchheimer equation: A theoretical development. *Transport in Porous Media 25*(1), 27–61.

WHO (2016). Burden of disease from ambient air pollution for 2016 Description of method. Technical report.

Williams, J. A. (1977). The Action of Lubricants in Metal Cutting. *Journal Mechanical Engineering Science 19*(5), 202–212.

Wurster, S., J. Meyer, H. E. Kolb, and G. Kasper (2015). Bubbling vs. blow-off - On the relevant mechanism(s) of drop entrainment from oil mist filter media. *Separation and Purification Technology 152*, 70–79.

Xiao, F., S. Ii, and C. Chen (2011, aug). Revisit to the THINC scheme: A simple algebraic VOF algorithm. *Journal of Computational Physics 230*(19), 7086–7092.

Xu, W., H. Zhang, Z. Yang, and J. Zhang (2008, jul). Numerical investigation on the flow characteristics and permeability of three-dimensional reticulated foam materials. *Chemical Engineering Journal 140*(1-3), 562–569.

Yarin, A. L., G. G. Chase, W. Liu, S. V. Doiphode, and D. H. Reneker (2006, jan). Liquid drop growth on a fiber. *AIChE Journal 52*(1), 217–227.

Yeh, H. C. and B. Y. Liu (1974, mar). Aerosol filtration by fibrous filters-II. experimental. *Journal of Aerosol Science 5*(2), 205–217.

Yip, J. and S. P. Ng (2008, sep). Study of three-dimensional spacer fabrics:. Physical and mechanical properties. *Journal of Materials Processing Technology 206*(1-3), 359–364.

Yoshida, Y., Y. Inoue, A. Shimosaka, Y. Shirakaw, and J. Hidaka (2015, jul). Numerical simulation of flow resistivity of metal woven mesh. *Journal of Chemical Engineering of Japan 48*(7), 545–555.

Yue, C., Q. Zhang, and Z. Zhai (2016, nov). Numerical simulation of the filtration process in fibrous filters using CFD-DEM method. *Journal of Aerosol Science 101*, 174–187.

Yuksekkaya, M., M. Tercan, and G. Dogan (2010, nov). An experimental investigation of nonwoven filter cloth with and without reinforcement of woven fabric. *Journal of the Textile Institute 101*(11), 950–957.

Zaatari, M., A. Novoselac, and J. Siegel (2014, mar). The relationship between filter pressure drop, indoor air quality, and energy consumption in rooftop HVAC units. *Building and Environment 73*, 151–161.

Zhang, J., W. Pan, Z. Long, C. Wang, and Z. Feng (2017). Study of the Oil Mist Filtration Performance: Pressure Drop Characteristics and Filter Efficiency Model. *Aerosol and Air Quality Research 17*, 1063–1072.

Zhang, S., N. A. Rind, N. Tang, H. Liu, X. Yin, J. Yu, and B. Ding (2018, jan). Electrospun nanofibers for air filtration. In *Electrospinning: Nanofabrication and Applications*, pp. 365–389. Elsevier.

Zhou, Y., M. Li, X. Zhong, Z. Zhu, P. Deng, and H. Liu (2015). Hydrophobic composite coatings with photocatalytic self-cleaning properties by micro/nanoparticles mixed with fluorocarbon resin. *Ceramics International 41*(4), 5341–5347.

Zhu, M., R. Tian, Z. Xing, and Y. Liu (2015). Experimental research on flow resistance characteristic of Wire Mesh demister. In *International Conference on Nuclear Engineering, Proceedings, ICONE*, Volume 2015-Janua.

Appendix A

Transient Simulation Results in Phobic and Philic Filter Media

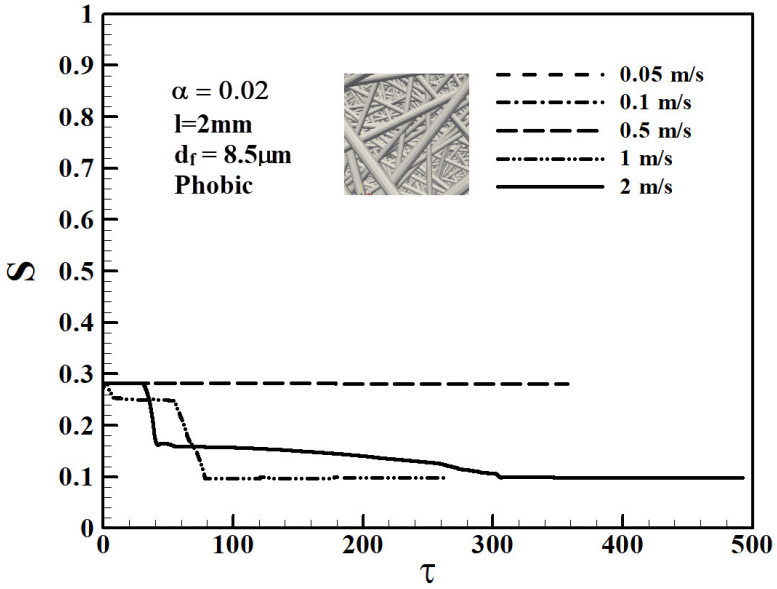

(a) Saturation

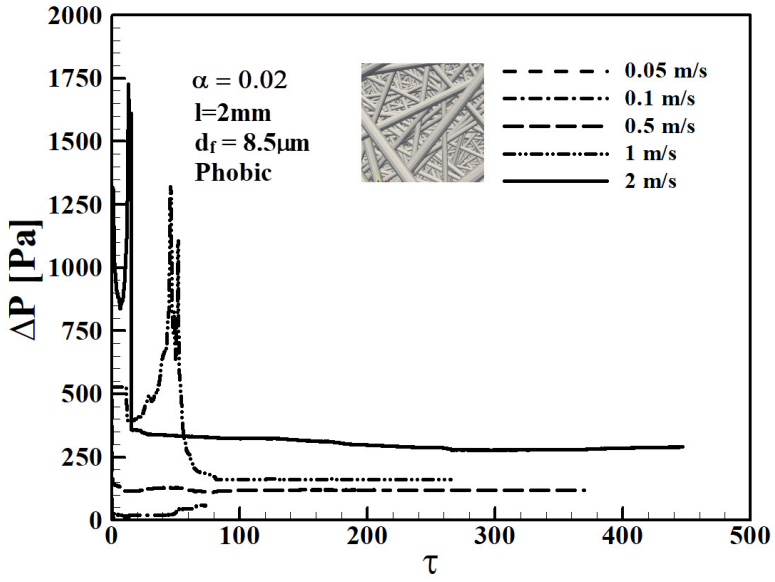

(b) Pressure Drop

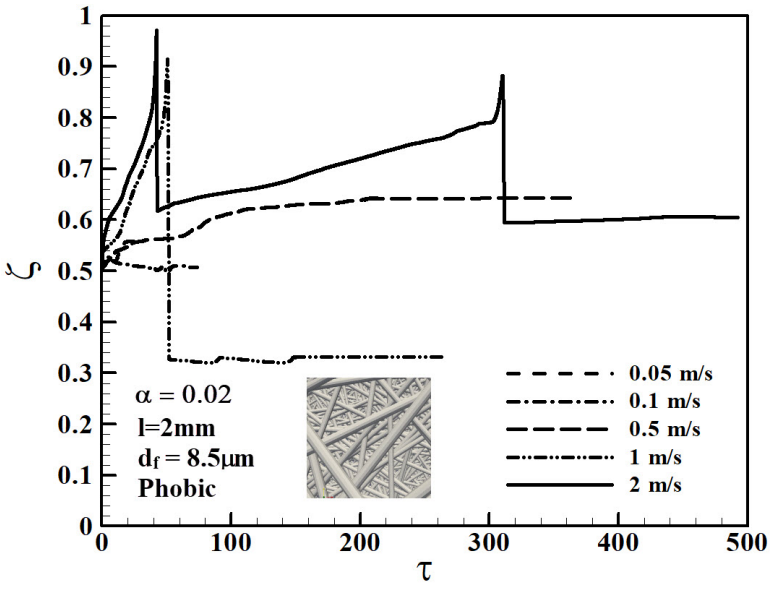

(c) Centre of Mass

Figure A.1: Transient variation in the saturation, pressure drop, and liquid centre of mass at different inlet velocities in phobic fibrous media.

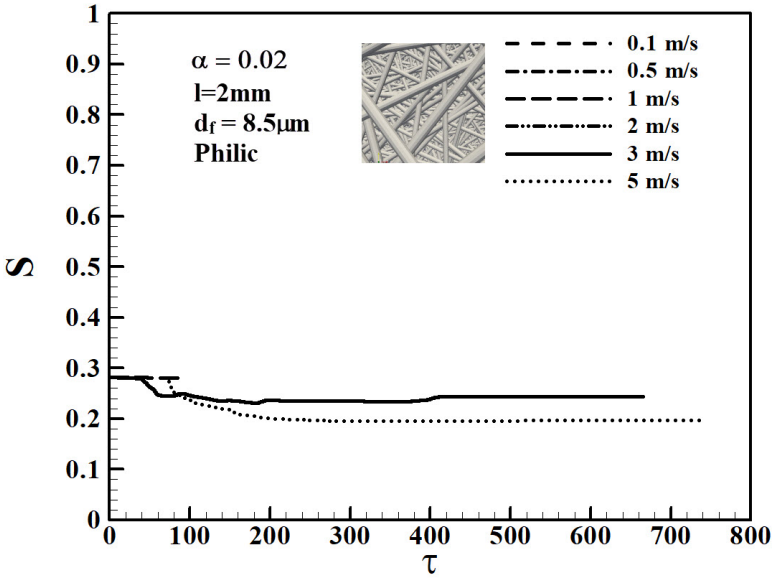

(a) Saturation

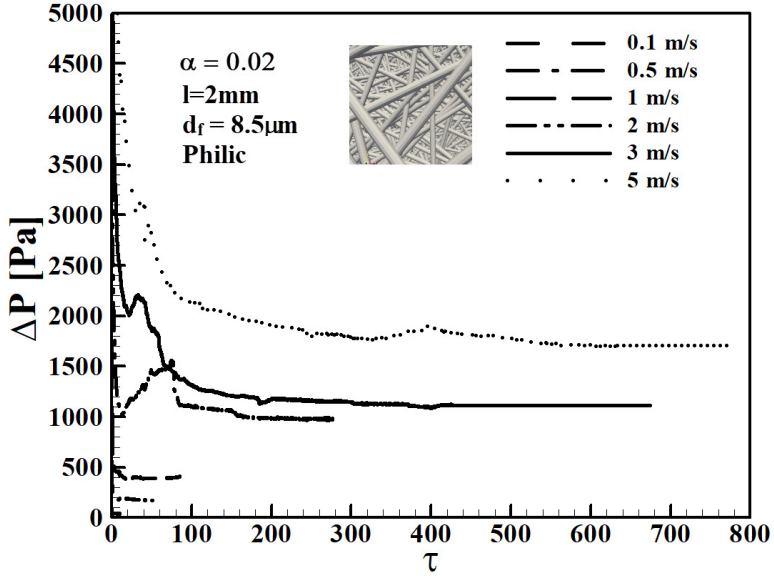

(b) Pressure Drop

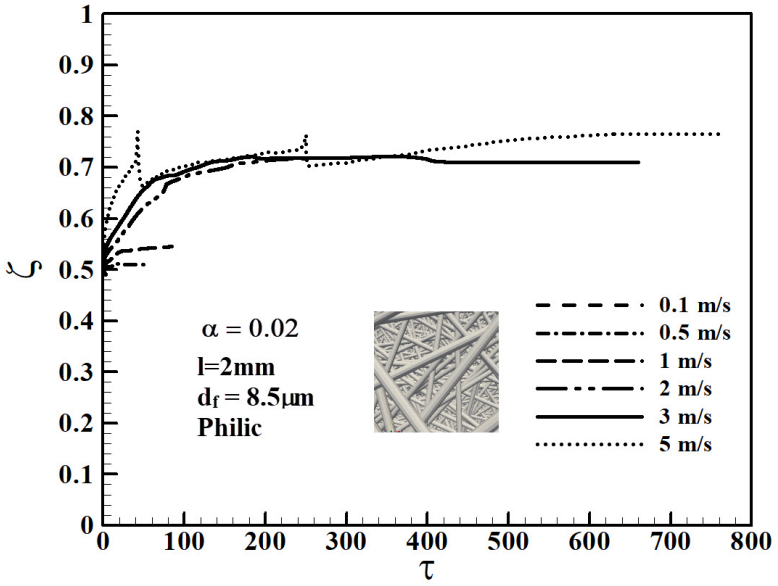

(c) Centre of Mass

Figure A.2: Transient variation in the saturation, pressure drop, and liquid centre of mass at different inlet velocities in philic fibrous media.

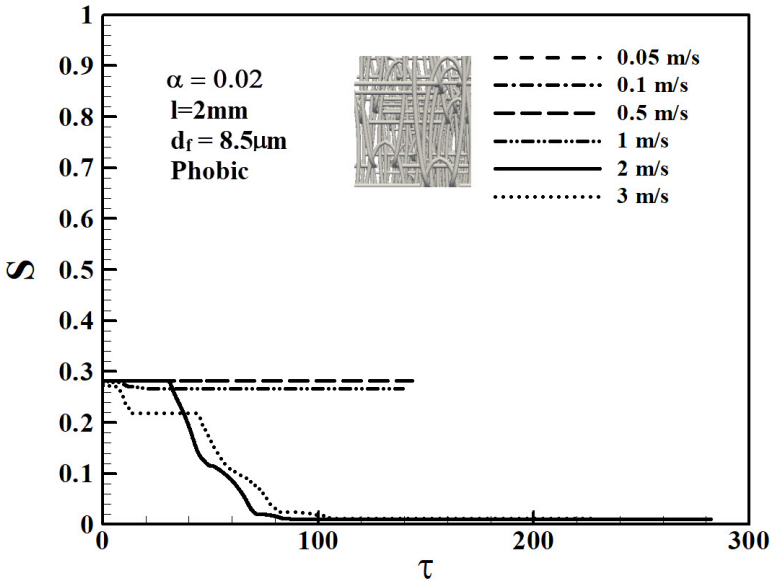

(a) Saturation

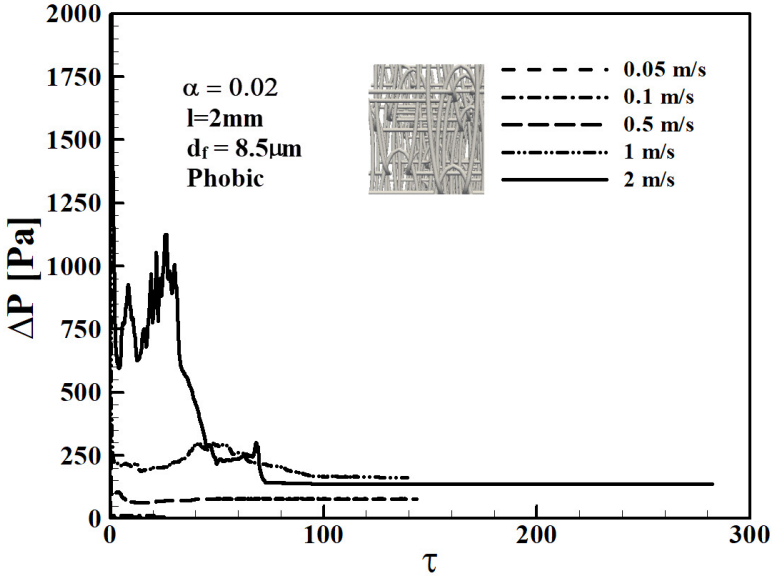

(b) Pressure Drop

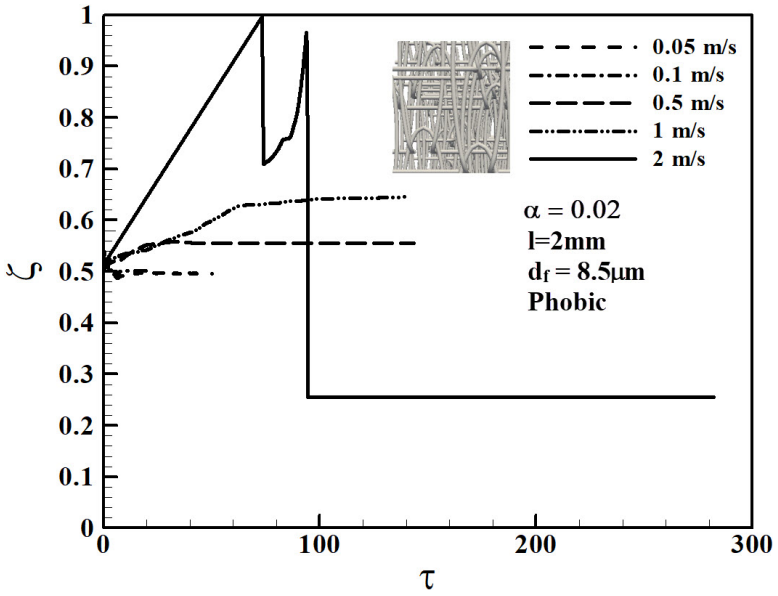

(c) Centre of Mass

Figure A.3: Transient variation in the saturation, pressure drop, and liquid centre of mass at different inlet velocities in phobic knitted media.

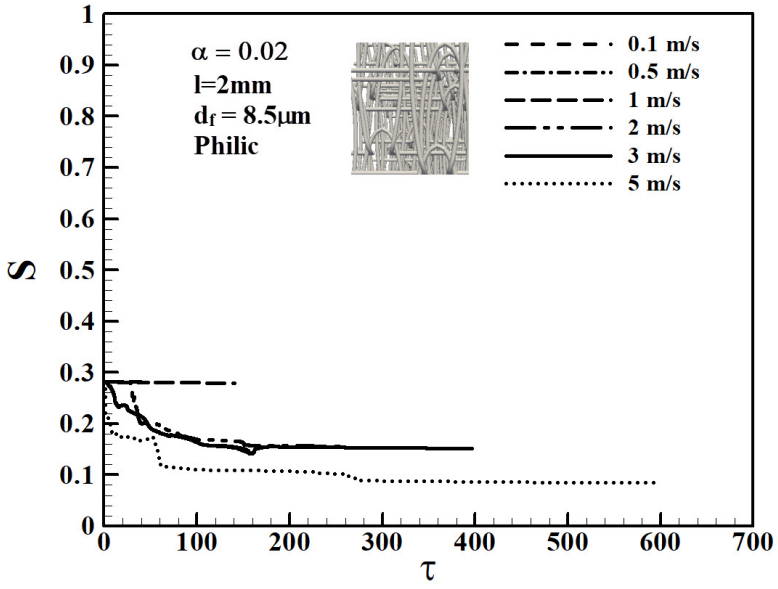

(a) Saturation

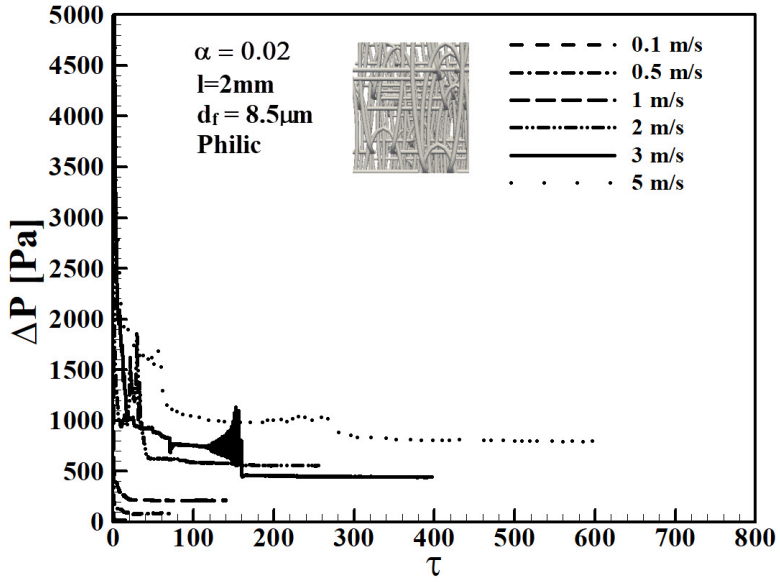

(b) Pressure Drop

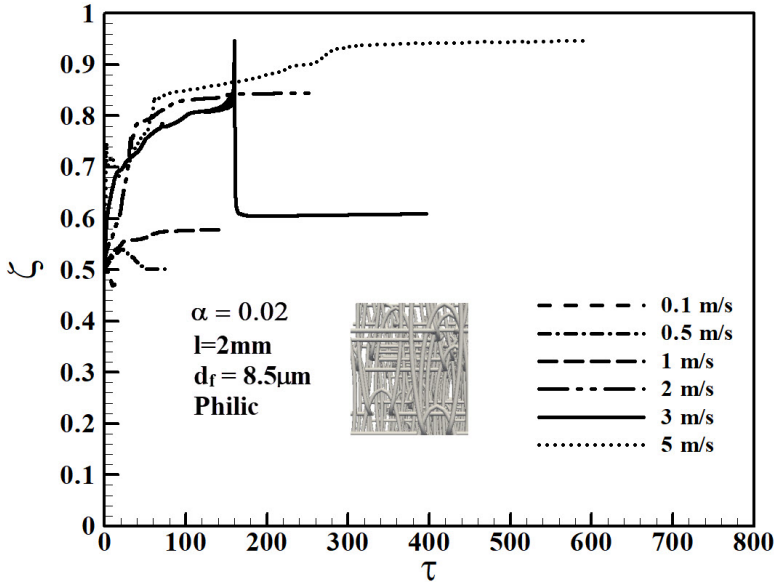

(c) Centre of Mass

Figure A.4: Transient variation in the saturation, pressure drop, and liquid centre of mass at different inlet velocities in philic knitted media.

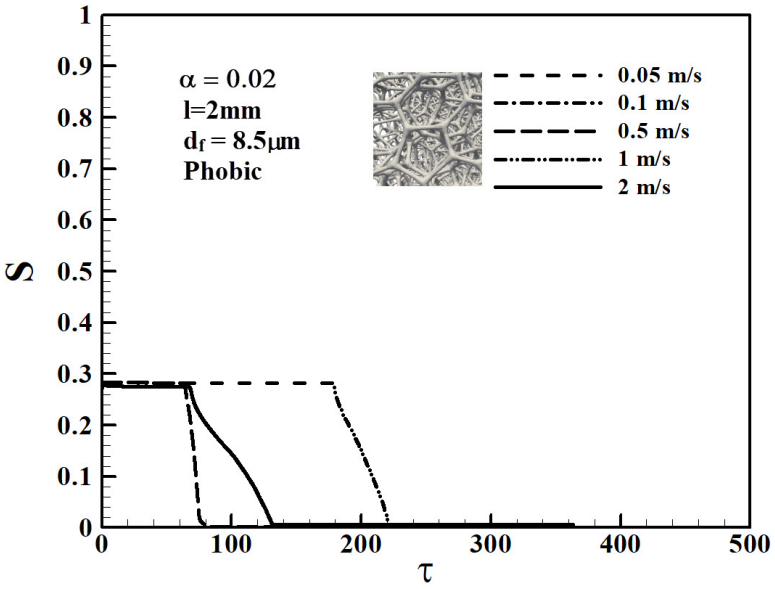

(a) Saturation

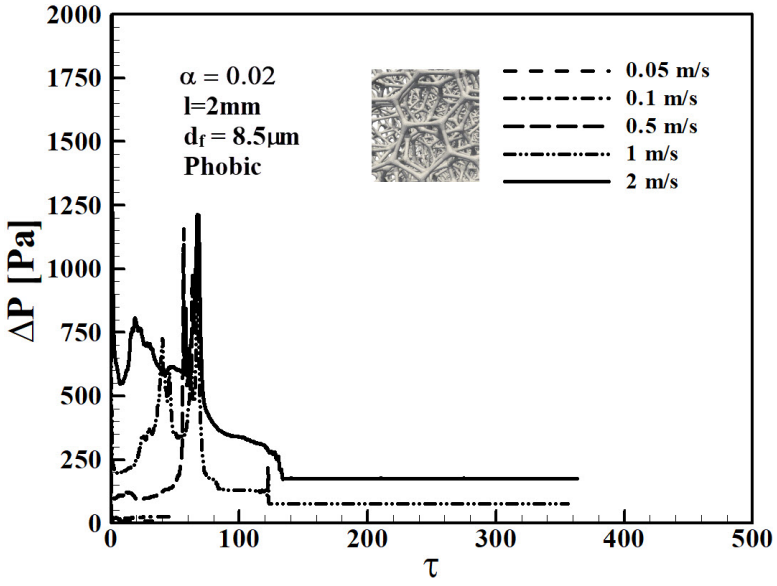

(b) Pressure Drop

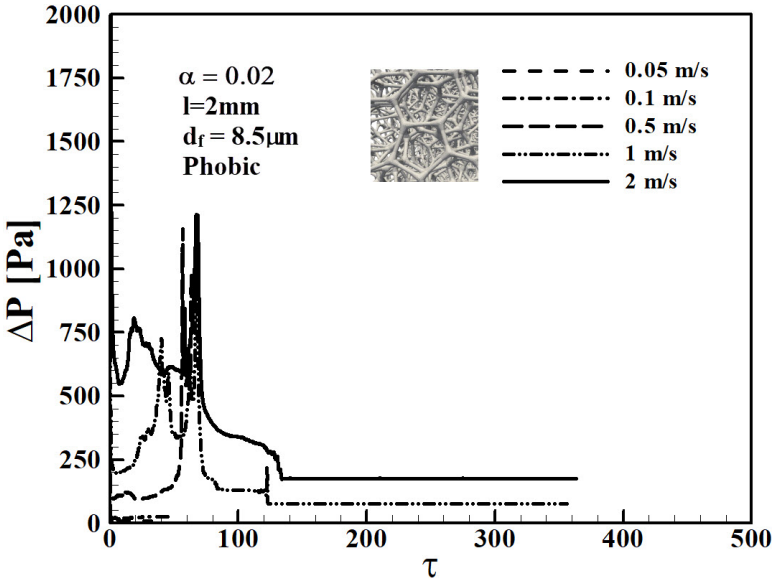

(c) Centre of Mass

Figure A.5: Transient variation in the saturation, pressure drop, and liquid centre of mass at different inlet velocities in phobic foam media.

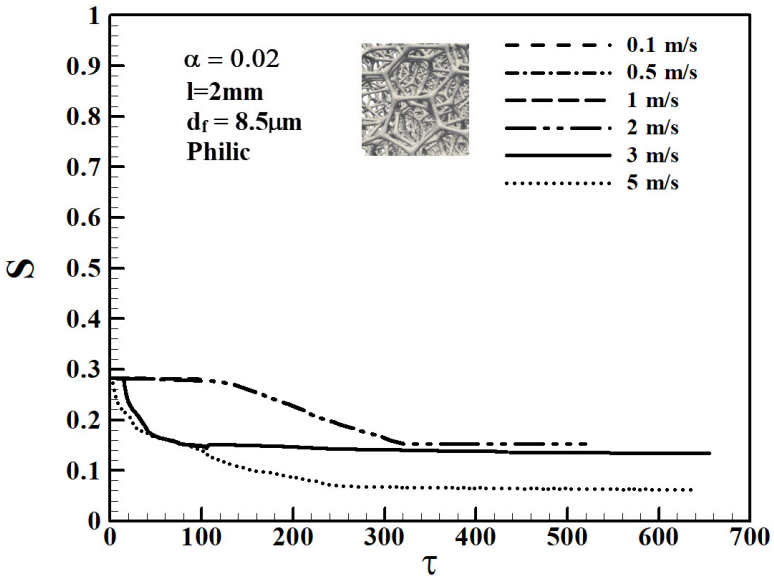

(a) Saturation

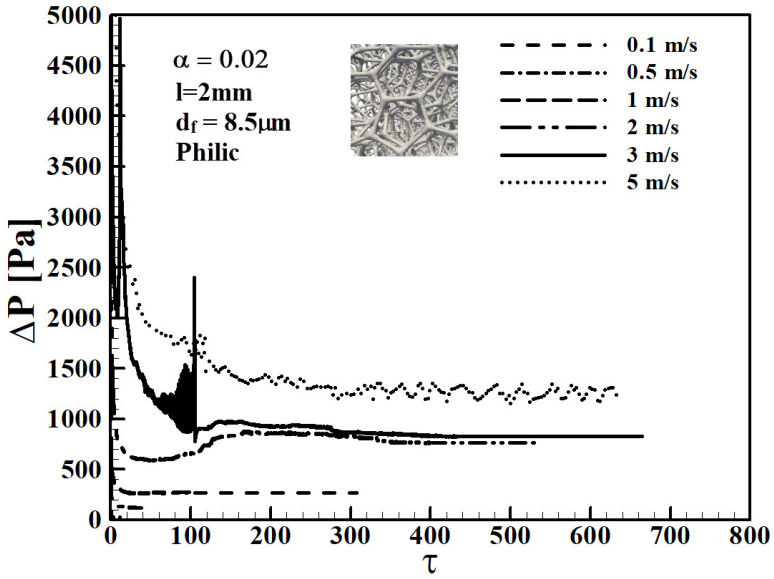

(b) Pressure Drop

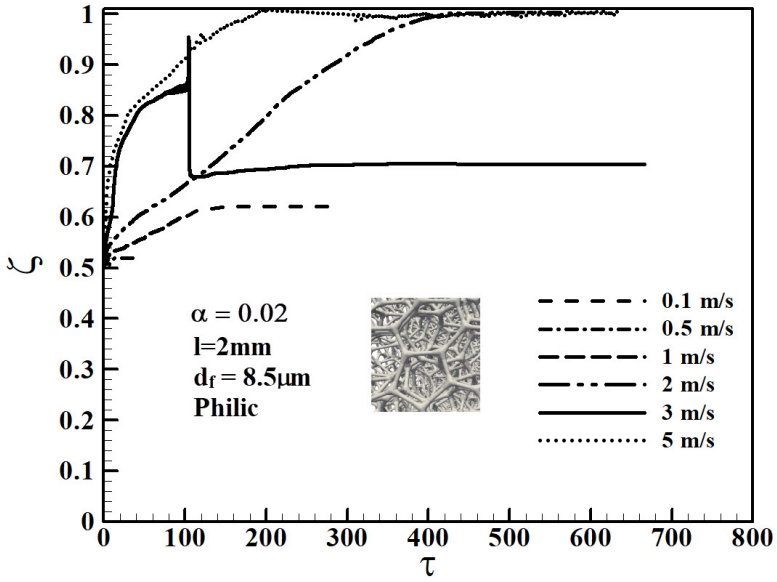

(c) Centre of Mass

Figure A.6: Transient variation in the saturation, pressure drop, and liquid centre of mass at different inlet velocities in philic foam media.

Appendix B

Knitted Media Validation

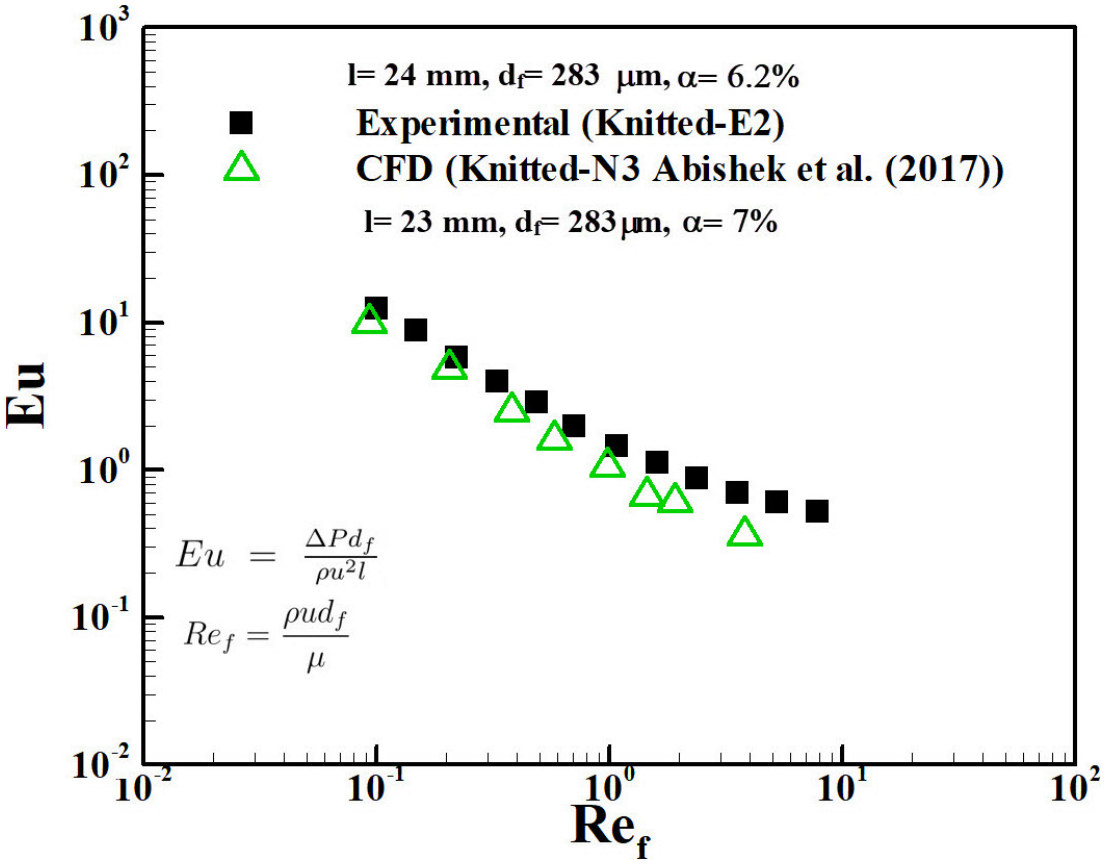

Figure B.1: Abishek et al. (2017) CFD simulation (Kitted-N3) against experimental data (Knitted-E1).